UNIVERSITY OF OKLAHOMA

GRADUATE COLLEGE

POTENTIAL SOURCES OF OIL FROM HUGOTON EMBAYMENT RESERVOIRS

A THESIS

SUBMITTED TO THE GRADUATE FACULTY

in partial fulfillment of the requirements for the

Degree of

MASTER OF SCIENCE

By

BRITTNEY LYNN TAMBORELLO

Norman, Oklahoma

2020

Downloaded from SHAREOK. Persistent Handle URL: https://hdl.handle.net/11244/323319

POTENTIAL SOURCES OF OIL FROM HUGOTON EMBAYMENT RESERVOIRS

A THESIS APPROVED FOR THE
SCHOOL OF GEOSCIENCES

BY THE COMMITTEE CONSISTING OF

Dr. Xiaolei Liu, Chair

Dr. R. Paul Philp

Dr. Roger M. Slatt

© Copyright by BRITTNEY LYNN TAMBORELLO 2020

All Rights Reserved.

To my parents,

To my family,

To my friends,

Thank you for the encouragement and red wine

ACKNOWLEDGEMENTS

The completion of my thesis was made possible because of my fantastic advisor, Dr. R. Paul Philp. Dr. Philp generously supported my research, provided invaluable guidance in this project, and was extremely patient in helping me to write this manuscript. I would like to thank Dr. Xiaolei Liu and Dr. Roger Slatt for serving on my committee and taking the time to review my thesis and provide valuable feedback for this study. I am also very thankful to the excellent faculty and staff in the School of Geoscience at the University of Oklahoma for their help and guidance throughout my master's degree.

I would like to thank Suemarur Exploration & Production, LLC, Matthew Totten, and Joe Hatch for the donation of the oils that were used and analyzed in this research. I would also like to thank the USGS Core Research Center for providing core samples that were used in this project.

Others that were instrumental in the completion of this thesis were all the students, faculty, and staff associated with the Organic Geochemistry Group. I would have stumbled much more than I did without the guidance of Carl Symcox, Jon Allen, Larry Hyde, and all the others. Thank you for taking the time to show me the ropes in the lab.

I would also like to thank all the friends I have met in my two years here at Sarkeys Energy Center. Your support, encouragement, friendship, and willingness to put up with my complaining and procrastination was instrumental to my success. I deeply value our friendships and hope to continue those friendships for years to come.

Lastly, I want to take the time to thank my parents, Paul and Cheri, my brother, and all of my family. Your love and encouragement mean the world to me; I would not be here without you.

Thank you all for everything!

TABLE OF CONTENTS

LIST OF FIGURES……..……..ix

LIST OF TABLES……...…xix

ABBREVIATIONS …….……xxi

ABSTRACT…...……xxiii

CHAPTER 1: INTRODUCTION…….……...……1

1.1. Objectives ……...……..1

1.2. Biomarkers…….……..…..……1

Saturate Hydrocarbons…….……..……4

Aromatic Hydrocarbons……..……6

Heteroatomic Molecules…….…8

1.3. Study Area……..…….…….…9

1.4. Previous Research…….…….…….…10

CHAPTER 2: GEOLOGICAL SETTING……..……...…14

2.1. Kansas Geology…….….…15

Structural Influences in Kansas…….…..……16

Kansas Stratigraphy……..……..……18

Kansas Oil Production…….……..……19

Migration Pathways…….....……21

2.2. Anadarko Basin Structure, Stratigraphy, and Woodford Shale……..…….……22

Anadarko Basin Structures…….…..…23

Stratigraphy of the Anadarko Basin and the Woodford Shale…….……24

Woodford Shale v. SCOOP/STACK Oil Geochemistry ……26

CHAPTER 3: METHODS……28

3.1. Sample Selection and Collection……28

3.2. Fractionation Methods……30

Rock-Eval Pyrolysis and TOC……31

Source Rock Extraction ……32

Bitumen Fractionation……33

Column Chromatography……34

Molecular Sieving……34

Nitrogen Compound Separation ……34

3.3. Analytical Methods……35

Whole Oil Gas Chromatography (WOCG)……35

Gas Chromatography (GC) ……36

Gas Chromatography – Mass Spectrometry (GCMS) ……36

Gas Chromatography – Mass Spectrometry- Mass Spectrometry (GCMS-MS)…37

Bulk Isotope Analysis……38

Biomarker Identification……38

CHAPTER 4: RESULTS AND DISCUSSION……40

4.1. Whole Oil Geochemistry……40

4.2. Compositional Geochemistry……43

4.3. Biomarker Analysis……46

Depositional Environment and Organic Matter Source……46

Depositional Environment and Source Rock Lithology……57

Thermal Maturity……65

Water Column Stratification……70

Migration……77

4.4. Source Rock Evaluation……89

Thermal Maturity……90

Organofacies……91

Production Potential……92

4.5. Isotope Analysis……93

CHAPTER 5: CONCLUSIONS……95

5.1. Source and Nature of Kansas Oils……95

5.2. Migration of Kansas Oils……97

5.3. Future Work……97

REFERENCES……98

APPENDIX I: BIOMARKER RATIOS……121

APPENDIX II: STRUCTURES……123

APPENDIX III: FORMULAS……128

APPENDIX IV: CHROMATOGRAMS……129

A. Whole Oil GC Chromatograms……129

B. Saturate GC Chromatograms……135

C. Maltene GCMS Chromatograms……149

D. Saturate GCMS Chromatograms……160

E. Aromatic GCMS Chromatograms……183

F. Low Polarity Compound GCMS Chromatograms……206

LIST OF FIGURES

Figure 1. Breakdown of organic matter from a source rock into insoluble kerogen, soluble bitumen, and molecular biomarkers (Tissot and Welte, 1984). ……2

Figure 2. Structure of pristane (Pr) and phytane (Ph) (**APPX. II;** Dembicki, 2017). ……..……..……4

Figure 3. Typical GC chromatogram of a Pennsylvanian Kansas oil, Schroeder 1-26 from the Lansing-Kansas City (LKC) Formation, Kansas. ……4

Figure 4. Common structures of saturate hydrocarbons: (**a**) triterpanes, (**b**) steranes, and (**c**) diamondoids (**APPX. II**; Burns et al., 1978; Waples and Machihara, 1990; Hays et al., 2007)……..……...…...5

Figure 5. Common aromatic compounds: (**a**) the phenanthrene series, (**b**) aryl isoprenoids/carotenoids, and (**c, d**) the mono- and tri-aromatic steroidal hydrocarbons (**APPX. II**; Peters et al., 2004b; Dembicki, 2017)……..7

Figure 6. Water column stratification during photic zone euxinia. Hydrogen sulfide (H2S) rich waters are in the photic zone, and the color of the bacteria depends on the amount of sunlight received and creates the various carotenoids (Connock, 2015). ……..……7

Figure 7. Common heteroatomic molecules: (**a**) the thiophene series and (**b**) the carbazole series (Hughes, 1984; Larter, 1996)……..….8

Figure 8. Kansas study area: 20 counties in Kansas where oil samples were taken and their relation to the main structures of Kansas. Oklahoma correlation area: 2 counties in the Anadarko Basin,

Pauls Valley Area, Oklahoma that are true Woodford oils and are used to compare biomarker signatures and their relation to the main structures in Oklahoma. ……..……9

Figure 9. Map of all oil and gas fields in Kansas; the focus of this study, in red, is in the west-central, oil-rich area of Kansas (Kansas Geological Survey, 2009; Mpanje, 2016). ……10

Figure 10. To the left, Pennsylvanian oil samples from Kansas and Oklahoma and to the right, the relative migration distance showing a range of 0-350 miles for the migrated oils using a ratio of toluene/(n-heptane+methylcyclohexane+toluene) vs. the distance to the depocenter of the Anadarko Basin, proposed by Burrus and Hatch, 1989 (**APPX. I**)……..……...……..…11

Figure 11. Oils in five petroleum reservoirs show an increasing relative migration distance and a decreasing BC ratio (Larter et al., 1996). ……..……12

Figure 12. Major tectonic elements in Kansas and Oklahoma showing the extent and general thermal maturity of the Woodford Shale (modified from GeoMark, 2013; Mpanje, 2016)……..14

Figure 13. Structural features in Kansas in: (**a**) Early Mississippian showing the initial uplift of the Central Kansas Uplift; and (**b**) Early Pennsylvanian times showing the progression of uplifting events that have resulted in the main modern subsurface features (modified from Merriam, 1963). …..……..……15

Figure 14. Paleotopographic map at the end of the Mississippian time (i.e. top of the Mississippian formation) showing the present structures. A-A' is a line for the cross-section in **Fig. 15** (modified from Gerhard, 2004; Kansas Geological Survey, 2009). ……..……17

Figure 15. Cross-section running east to west across Kansas with county names labeled on the top of the cross-section. The Hugoton Embayment is in the West, the Central Kansas Uplift and the Nemaha Ridge in Central Kansas, and the Forest City Basin in the East (modified from Gerhard, 2004). ……17

Figure 16. Stratigraphic column of the Paleozoic rock formations in Kansas (Newell et al., 1987). The Woodford Shale equivalent in Kansas is referred to as both the Kinderhook and Chattanooga formation. ……...……19

Figure 17. Oil and gas fields in Kansas by decade of discovery, from the early 1900s to 2009 (Kansas Geological Survey, 2009). ……...……20

Figure 18. Migration pathways out of the Anadarko Basin and into the Hugoton Embayment of Kansas via lateral migration through Arbuckle strata and vertical migration up the major faults and uplifts. Pathways such as these may account for the abundance of hydrocarbons found throughout Kansas even with a lack of prominent source rock in the area (Gerhard, 2004). …….……22

Figure 19. Structural influences in the Anadarko Basin, showing the tectonic events in Oklahoma. The major sediment accumulation occurs north of the Wichita Mountains in the heart of the Anadarko Basin where sediment thickness reaches 40,000 feet (Perry, 1989; Northcutt and Campbell, 1996; Cardott, 2012; Mitchell, 2012). ……..……23

Figure 20. North-south cross-section through Oklahoma, leading into Kansas showing the depositional pinch-out over the northern Anadarko Basin as it enters the Hugoton Embayment of western Kansas (modified from Johnson, 1989; Gallardo and Blackwell, 1999.) ……24

Figure 21. General stratigraphic column of the Paleozoic Anadarko Basin showing major unconformities in time (Johnson, 1989). ……25

Figure 22. Location of oils and cores for this study in map view with the corresponding stratigraphic section above in **Fig. 23**. ……...……28

Figure 23. Location of oils and cores for this study within the general stratigraphic section that is representative of the formations in the Greater Anadarko Basin. The oils from the Hugoton Embayment are green, Pauls Valley conventional Woodford oils are yellow, and the core samples from Kansas are purple (modified from Merriam, 1963). ……..…29

Figure 24. Schematic fractionation method starting from either crude oils or source rocks (green) showing the various steps (orange), and fractions (white, pink, red, and blue) as well as the different types of analyses used on the different fractions (yellow) (modified from Romero and Philp, 2012). ……..……31

Figure 25. Chromatogram from Rock-Eval pyrolysis (Peters and Cassa, 1994)……..32

Figure 26. Whole oil chromatogram of HE-L10 showing the C_7 peaks (**APPX. II**; Canipa-Morales et al., 2003). ……..……40

Figure 27. Aromaticity (toluene/n-heptane; **APPX. I**) verses paraffinicity (n-heptane/methylcyclohexane; **APPX. I**) are used to determine the effects on a normal oil. This plot shows that many of the oils have been strongly affected by water washing, as is seen by the low aromaticity in the red circle (modified from Thompson, 1987; Hakimi and Al-Sufi, 2018). ……42

Figure 28. A ternary diagram modified from Tissot and Welte (1984) showing that the relative composition of the crude oils characterized in this study plot close to the normal crude oil zone. Isofrequency contour lines were determined from a study of 636 crude oil samples: oils in the normal crude oil contour are enriched in saturate compounds, oils in the aromatic crude oil contour are enriched in aromatic compounds when compared to the normal oils, and the oils in the heavy oil contour indicated biodegraded oils enriched in NSO and asphaltene compounds (Tissot and Welte, 1984)……...44

Figure 29. Saturate GC chromatogram of HE-L10 identifying n-C_{17}, n-C_{18}, pristane, and phytane (**APPX. II**). ……..……..…46

Figure 30. Redox conditions of most of the oils in the Hugoton Embayment group well with the conventional Woodford oils (red outline) and plot in the mixed organic matter and show a mixed to reducing environment. The extracts from core samples in this study are also plotted here and show a mixed organic matter input (modified from Shanmugam, 1985; **APPX. I**).……..49

Figure 31. Regular sterane distribution of HE-L5. The top panel, the total ion chromatogram (TIC), shows the entire distribution of regular steranes. The descending panels show the C_{27}, C_{28}, C_{29}, and C_{30} steranes (**APPX. II**) from parent-daughter relationships on the GCMS-MS. ……50

Figure 32. Ternary plot showing Woodford and Hugoton Embayment oils and rock extracts enriched in C_{29} steranes which indicates that the organic matter input is a marine algae (Volkman, 1986; Wang, 2016; plot modified from Moldowan et al., 1985). ……51

Figure 33. Plot of the $C_{27}/(C_{27}+C_{29})$ steranes vs. the Pr/Ph ratio that indicates an anoxic depositional environment and an algal rich organic matter input of the oils and rock extracts in this study where the Hugoton Embayment oils (HE) are have been separated from the conventional Woodford oils (WF) (plot modified from Hossain et al., 2009; **APPX. I**)..……..55

Figure 34. The plot of the homohopane index ($C_{35}/[C_{31}+C_{32}+C_{33}+C_{34}+C_{35}]$ homohopanes) against the sterane index ($C_{30}/[C_{27}+C_{28}+C_{29}+C_{30}]$ steranes) shows that the source rock for these samples was deposited in an open marine setting (modified from Moldowan et al., 1985; Wang, 2016; **APPX. I**). ……..……....57

Figure 35. Sample HE-L5 showing the phenanthrene series compounds (**APPX. II**) on a mass chromatogram of the summed m/z 178+192+206 and the dibenzothiophene series compounds (**APPX. II**) on a summed mass chromatogram of m/z 184+198+212. See **Table 7** for peak identification. ……58

Figure 36. Analysis of conventional Woodford oils, Hugoton Embayment oils and rock extracts, and Chattanooga (Woodford) core use MDBT compounds for oil/source correlation. This plot shows that the circled oils and extracts are likely related (Wang and Fingas, 1995)……..60

Figure 37. The samples show that the major lithology of the source rock is a mixed lacustrine/marine shale as seen by the low Pr/Ph and low DBT/PHEN ratios. The Chattanooga/Woodford Shale source rock samples also plot in the same area, inferring that this ratio is accurate (modified from Hughes et al., 1995; **APPX. I**)……61

Figure 38. GCMS chromatogram of m/z 191 showing the terpanes and hopanes with the identified peaks in sample HE-L5 (**APPX. II**). ……..……62

Figure 39. The source rock lithology of the oils from the Woodford Shale and the Hugoton Embayment show either a marine shale or carbonate lithology from the ratios of the $C_{31}R$ hopane/C_{30} hopane to the C_{26}/C_{25} tricyclic terpanes. The Chattanooga/Woodford source rock samples also plot in the same area, inferring that this ratio is accurate (modified from Hays et al., 2007; **APPX. I**)……..63

Figure 40. A plot of C_{24}/C_{23} tricyclic terpane verses C_{22}/C_{21} tricyclic terpane which indicated that the oils from the conventional Woodford Shale and the Hugoton Embayment are marine shales. The Chattanooga/Woodford source rock samples also plot in the marine shale area, as expected, inferring that this ratio is accurate (Zumberge, 1987; modified from Peters et al., 2004b; **APPX. I**)……..……64

Figure 41. The %Rc from MPI-1 of oils and rock extracts are plotted on this map. The oils in the Hugoton Embayment show an overall decrease in thermal maturity from the SE to NW which could be the result of multi-stage migration that has not equilibrated (Radke and Welte, 1983; England, 2007). …….……67

Figure 42. Conventional Woodford oils and Hugoton Embayment oils are all mature oils as they plot in the main oil window of the C_{30} moretane/C_{30} hopane (**APPX. I**; **APPX. II**) ratio vs. maturity (%Rc) from the MPI-1. This is due to the depletion of moretane relative to hopane as the oil samples become more mature (modified from van Graas, 1990; **APPX. I**)……69

Figure 43. Top: unstratified water column, bottom: stratified water column showing photic zone euxinia (modified from Connock, 2015). ……..……71

Figure 44. Gammacerane index verses pristane/phytane ratio indicates a low level of water stratification and a low salinity environment (Peng et al., 2004; **APPX. I**; **APPX. II**). ……71

Figure 45. Chromatograms showing the aryl isoprenoids (**APPX. II**) and carotenoids (**APPX. II**) in the maltene fraction at m/z 133+134. The carotenoids, due to varying concentrations, are found near the baseline of most samples and may be seen as small peaks. ……..……..……74

Figure 46. Plot of the ratio of paleoreineratane to isorenieratane vs. the MPI-1 based maturity value (%Rc) showing that the paleoreineratane/isorenieratane ratio in the oil and rock extract samples is not affected by maturity. ……..……76

Figure 47. The paleoreineratane/isorenieratane ratio vs. pristane/phytane ratio shows the reducing nature of the anoxic depositional environment in which carotenoids are found (modified from Schwark and Frimmel, 2004). ……76

Figure 48. Mass chromatogram of the LPC fraction, from the NSOs, showing carbazole (m/z 167; **APPX. II**) and the benzocarbazoles (m/z 217; **APPX. II**) over the time range of 30-50 minutes in samples HE-L2 and WF-H1 (**APPX. IVF**). ……..……79

Figure 49. The BC ratio (**APPX. I**; **APPX. III**) shows no variation in the Woodford oils (crosses), some variation in the Hugoton Embayment oils from the Lansing-Kansas City (inverted triangles),

and an unusually low sample in the Lansing-Kansas City cores (left triangles). This demonstrates that Larter's BC ratio (1996) does not apply to these oils that were analyzed. ……81

Figure 50. Chromatogram of sample HE-L5 showing the identification of the thiophene compounds. DBT: Dibenzothiophene; MDBT: Methyldibenzothiophene; DMDBT: Dimethyldibenzothiophene, BNT: Benzo[b]naphthothiophene. ……...……82

Figure 51. Contour map showing the distribution of the 4-/1-MDBT ratio (**APPX. I**) identifying filling trends of oils out of the Woodford source and into the reservoirs of the Hugoton Embayment. …….85

Figure 52. Contour map showing the distribution of the 4,6/(1,4+1,6)-DMDBT ratio (**APPX. I**) identifying filling trends of oils out of the Woodford source and into the reservoirs of the Hugoton Embayment. ……...……86

Figure 53. Contour map showing the distribution of the (2,3+3,6)/(1,4+1,6)-DMDBT ratio (**APPX. I**) identifying filling trends of oils into the Woodford source from the reservoirs of the Hugoton Embayment. ……..…….87

Figure 54. Contour map showing the distribution of the 2,1/(2,1+1,2)-BNT ratio (**APPX. I**) identifying filling trends of oils out of the Woodford source and into the reservoirs of the Hugoton Embayment. …….88

Figure 55. Zones of petroleum generation showing the top and bottom of the %Ro range (0.57-1.09 %Ro) from the samples in this study. All samples plot in the oil zone (plot modified from Robertson Research Inc., 1983). ……91

Figure 56. Pseudo van Krevelen diagram, using the HI against the OI, showing that Chattanooga core samples plot in the same kerogen type II range and the Lansing-Kansas City cores plot in both the type II and type III range (plot modified from Baudin et al., 1990). ……92

Figure 57. Hydrocarbon potential of the evaluated core samples. This plot of S2 peak and the TOC% show how the Chattanooga cores are considered very good source rocks while the Lansing-Kansas City core samples are more variable (plot modified from Peters et al., 2004b; Wang, 2016). ……93

Figure 58. Isotope values for three of the samples, HE-L6, HE-L10, and HE-M2, display a light isotope composition which is characteristic of the Woodford oils. The Woodford Shale samples from the Burrus and Hatch study "X" show this same light isotope signature (Burrus and Hatch 1989; plot modified from Sofer, 1984)……..…94

Figure 59. Hierarchal cluster analysis of all oil and rock extract samples using the following variables: MPI-1 %Rc, DBT/PHEN, 4/1MDBT, paleorenieratane/isorenieratane, Pr/C_{17}, Ph/C_{18}, Pr/Ph, C_{27}/C_{29} sterane, hopane index, H_{31}R/H_{30}, C_{26}/C_{25} tricyclic terpanes, C_{24}/C_{23} tricyclic terpanes, C_{22}/C_{21} tricyclic terpanes, C_{26} tricyclic terpane/C_{24} tetracyclic terpane, C_{29}/C_{30} hopanes, C_{19}/C_{23} tricyclic terpanes, C_{23}/C_{28} tricyclic terpanes, gammacerane/C_{30} hopane, C_{23} tricyclic terpane/C_{30} hopane, and the homohopane index (**APPX. I**)……..……96

LIST OF TABLES

Table 1. Oil and core samples from the Hugoton Embayment and oils from the conventional Woodford, with their associated formation, location, and county name that have been used in this study…….……..30

Table 2. C_7 peaks identification by name and abbreviation (Canipa-Morales et al., 2003). ……41

Table 3. Aromaticity and paraffinicity ratios calculated from whole oil chromatograms. ……..……..……42

Table 4. Values of the saturate, aromatic, and NSO + asphaltene fractionations of oils as percentage of the whole oil. …….. ……45

Table 5. Values of n-C_{17}, n-C_{18}, pristane, and phytane ratios determined from saturate GC chromatograms used for inferring the depositional environment (**APPX. I**)……47

Table 6. Peak identification of steranes found above in **Fig. 31**. ……52

Table 7. Values of the C_{27}, C_{28}, and C_{29} steranes for the oil and rock extract samples in this study plotted in **Fig. 32**. ……..……53

Table 8. Peak identification for the phenanthrene (A-F) and dibenzothiophene (a-e) series chromatograms (**Fig. 35**). ……..59

Table 9. Maturity values of the oil samples in this study: MPI-1, MPI-1 %Rc, and C_{30} moretane/C_{30} hopane (**Fig. 44**). ……...68

Table 10. Thirty-five maltene samples showing the ratio of paleorenieratane to isorenieratane (**Fig. 46** and **Fig. 47**)……..…… 75

Table 11. BC ratio values for the conventional Woodford oils (WF), Hugoton Embayment oils (HE), and Lansing-Kansas City rock extract (HEC-L) evaluated, also shown below in **Fig. 49**.....…80

Table 12. Values used to infer the migration filling pathways. MDBT = Methyldibenzothiophene, DMDBT = Dimethyldibenzothiophene, BNT = Benzo[b]naphthothiophene…….84

Table 13. Rock-Eval data of the two core samples from the Chattanooga (Woodford) Shale and the three Lansing-Kansas City shales in Kansas (Formulas found in **APPX. III**). ……..…….89

Table 14. Kerogen types with their corresponding depositional environments and biomass composition (modified from Pepper and Corvi, 1995). ……..92

ABBREVIATIONS

%Ro	Measured Vitrinite Reflectance
B/C	Branched and Cyclic Alkanes
BBO	Billion Barrels of Oil
BC	Benzocarbazole Ratio
BNT	Benzo[b]naphthothiophene
$\delta^{13}C$	Stable Carbon Isotope Ratio
DBT	Dibenzothiophene
DCM	Dichloromethane
DMDBT	Dimethyldibenzothiophene
EOM	Extractable Organic Matter
FID	Flame Ion Detection
GC	Gas Chromatography
GC-IRMS	Gas Chromatography-Isotope Ratio Mass Spectrometry
GCMS	Gas Chromatography-Mass Spectrometry
GCMS-MS	Gas Chromatography-Mass Spectrometry-Mass Spectrometry
HI	Hydrogen Index
HPC	High Polarity Compounds
IRMS	Isotope Ratio Mass Spectrometry
LKC	Lansing-Kansas City
LPC	Low Polarity Compounds
m/z	Mass to Charge Ratio

MDBT	Methyldibenzothiophene
MPI	Methylphenanthrene Index
MPI-1 %Rc	Calculated Vitrinite Reflectance from MPI-1
NSO	Nitrogen-Sulfur-Oxygen Compounds
OI	Oxygen Index
PAH	Polyaromatic Hydrocarbons
Ph	Phytane
PHEN	Phenanthrene
PI	Production Index
Pr	Pristane
PZE	Photic Zone Euxinia
SCOOP	South Central Oklahoma Oil Province
SIM	Selected Ion Monitoring
STACK	Sooner Trend Anadarko Basin Canadian and Kingfisher Country Province
T_{max} %Rc	Calculated Vitrinite Reflectance from T_{max}
TCF	Trillion Cubic Feet
TOC	Total Organic Carbon
WOGC	Whole Oil Gas Chromatography
Wt%	Weight Percent

ABSTRACT

Oil has been produced in the Hugoton Embayment in western Kansas since the early 1900s, but the primary source rock for these oils has not definitively been determined. Thirty-two oils from the Middle Pennsylvanian to the Ordovician and three Middle-Pennsylvanian shales are compared to conventional Woodford sourced oils in the Anadarko Basin as well as to local Chattanooga (Woodford) Shale core in Kansas. The oil and core samples were characterized using various geochemical techniques to understand the variations in source rock lithology, organic matter, depositional environment, thermal maturity, and secondary migration. Instruments used in the characterization of oils and source rock extracts include gas chromatography (GC), gas chromatography-mass spectrometry (GCMS), bulk isotope analysis, and Rock-Eval pyrolysis. Several biomarker families were investigated, including steranes, terpanes, and aryl isoprenoids. Diamondoids, C_7 compounds, and various aromatic compounds, while not true biomarkers, have also been studied for use as diagenetic derivatives.

It has been proposed previously that the majority of oils produced in the Hugoton Embayment originated from the Early Mississippian-Late Devonian Woodford Shale in the Anadarko Basin and underwent long distance migration into the reservoirs of the Hugoton Embayment. The geochemical characteristics of the oils from these reservoirs are relatively consistent throughout the Hugoton Embayment – both laterally and vertically – and are very similar to those found in Woodford derived oils from the Anadarko Basin in Oklahoma which supports the concept of long distance migration that was proposed by Burrus and Hatch in 1989.

Using oil/oil and oil/source rock correlation techniques, data from this work has shown that the source of oils from the Hugoton Embayment has been determined to be the Woodford Shale. Knowing this, the variability of fill patterns into the Hugoton Embayment may be better

understood, and the risk of overestimating hydrocarbon accumulations in these reservoirs may be prevented.

CHAPTER 1: INTRODUCTION

1.1. Objectives

The main objective of this thesis is to determine the composition, source(s), and potential migration pathways of Paleozoic West-Central Kansas oils through the use of oil/oil and oil/source rock organic geochemistry. The composition of the Paleozoic Hugoton Embayment oils was determined using multiple geochemical biomarkers, which in turn could be used to visualize lateral and vertical changes in source rock lithology, organic matter, depositional environment, and thermal maturity. The source of these oils has been understudied, and the likely sources include migrated Devonian-Mississippian Woodford/Chattanooga oil, migrated Late Cretaceous Niobrara oil, and self-sourced oil from various organic rich shales in Kansas. Based on these geochemical analyses and potential sources, generalizations could be made to compare and contrast the Paleozoic Hugoton Embayment oils with the conventional Woodford oils derived from the Anadarko Basin in Southern Oklahoma, a local Woodford shale in Eastern Kansas, and local organic rich shales in Central Kansas. Finally, following the determination of the potential source rock, migration distances can be inferred, and migration pathways can be hypothesized. Understanding the oil migration pathways may help predict hydrocarbon accumulations in these reservoirs and increase the general understanding of the secondary migration pathways of Woodford sourced oils.

1.2. Biomarkers

Biomarkers are organic molecular fossils that have parent molecules formed from living organisms and do not change much during deposition. These biomarkers are composed of the

elements carbon and hydrogen, but other useful molecular compounds may contain elements such as nitrogen, sulfur, and oxygen (Waples and Machihara, 1990). These molecules, in the scope of organic geochemistry, are essential because they can be used to infer the organic matter input, depositional environment, degree of maturity and biodegradation, and oil/oil and oil/source rock relationships (Waples and Machihara, 1990). Biomarkers are usually found in sedimentary rocks, they are abundant in hydrocarbon rich source rocks, and a small percentage of those biomarkers can be extracted from the organic matter in the source rock (Tissot and Welte, 1984). The organic matter is composed of insoluble kerogen, soluble bitumen, and some hydrocarbon gasses, **Fig. 1** (Tissot and Welte, 1984; Peters et al., 2004a). In bitumen, other families of compounds can be separated and analyzed. The primary families are saturate hydrocarbons, aromatic hydrocarbons, heavy resins, and asphaltenes that all contain a unique chemical fingerprint that can be used for correlation (Moustafa and Morsi, 2012).

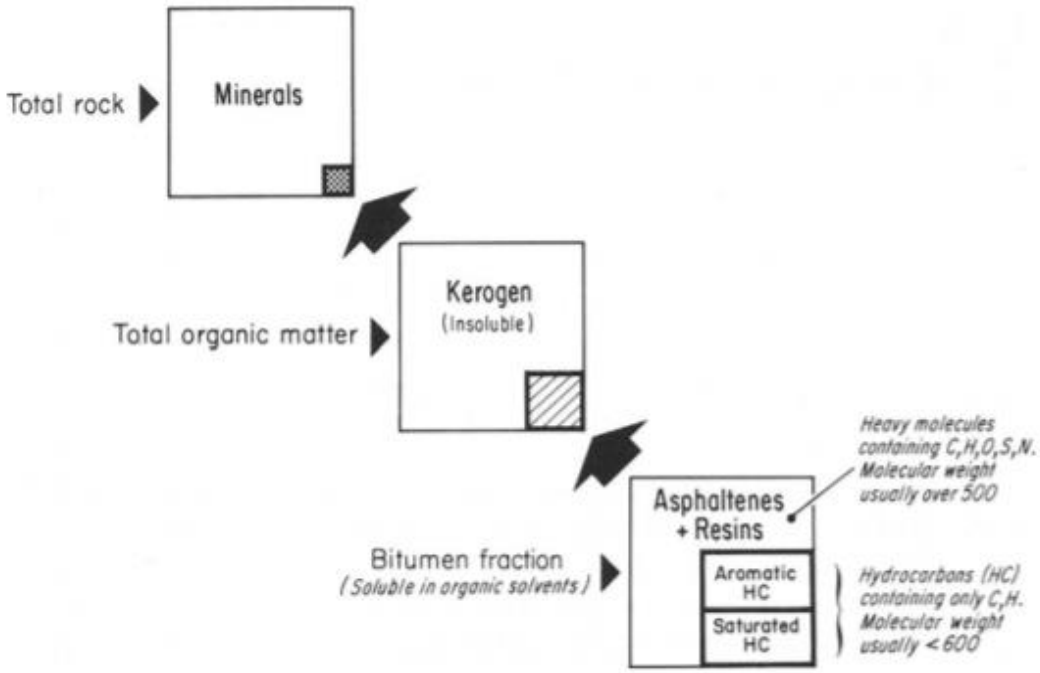

Figure 1. Breakdown of organic matter from a source rock into insoluble kerogen, soluble bitumen, and molecular biomarkers (Tissot and Welte, 1984).

Biomarkers are extremely useful compounds that can help determine the geologic history and petroleum potential of a basin and may be used to create a more efficient exploration plan for petroleum companies (Peters and Fowler, 2002). Biomarkers are most helpful when other data are available for comparing the results as there are potential pitfalls when working only with biomarker data. These challenges include a low concentration of samples, some ubiquitous characteristics, oil mixing, high levels of biodegradation, and possible contamination from processed petroleum products (Waples and Machihara, 1990; Fahl and Stein, 1999).

Biomarkers are identified on multiple types of instruments that are described in detail in **Chapter 3**. The most basic of these instruments is gas chromatography (GC) that uses flame ion detection (FID) to resolve organic compounds such as the saturate hydrocarbons by their abundance and retention time (McWilliam and Dewar, 1958; Zimmerman and Thurman, 1999). Another instrument that is widely used for biomarker characterization is the gas chromatograph-mass spectrometer (GCMS). The use of the GCMS was able to provide higher accuracy (Grayson, 2016) as it provided a detailed look at the structures of the various families of organic compounds found in oils and rock extracts using a technique called selected ion monitoring (SIM). SIM records the mass⁄charge (m⁄z) of an ion that is thought to be characteristic of a particular family of compounds (Zimmerman and Thurman, 1999). Another instrument that has revolutionized the study of biomarkers is the gas chromatograph–mass spectrometer–mass spectrometer (GCMS-MS). The GCMS-MS uses a triple quadrupole mass spectrometer that is able to separate oils and rock extracts into parent molecules and daughter fragments within various families of compounds (Philp et al., 1988; Futrell, 2000).

Saturate Hydrocarbons

Saturate hydrocarbons are "true biomarkers" as they only contain hydrogen and carbon in their atomic structures which range from straight-chain alkanes like n-C_{17} and n-C_{18}, to branched and cyclic isomers, such as pristane (Pr), and phytane (Ph) (**Fig. 2**, **APPX. II**; **APPX. IVB**; Peters et al., 2004a). The families of saturate hydrocarbons identified in this research include triterpanes, steranes, and diamondoids that can be found on various m/z chromatograms (**APPX. IVB**). The isoprenoids, Pr and Ph are identified on the GC chromatogram (**Fig. 3**) and can be used to indicate the redox conditions at the time of deposition (Shanmugam, 1985, Wang, 2016).

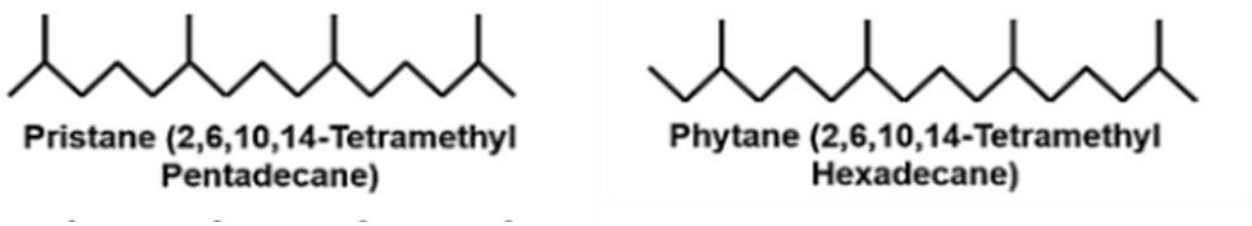

Figure 2. Structure of pristane (Pr) and phytane (Ph) (**APPX. II;** Dembicki, 2017).

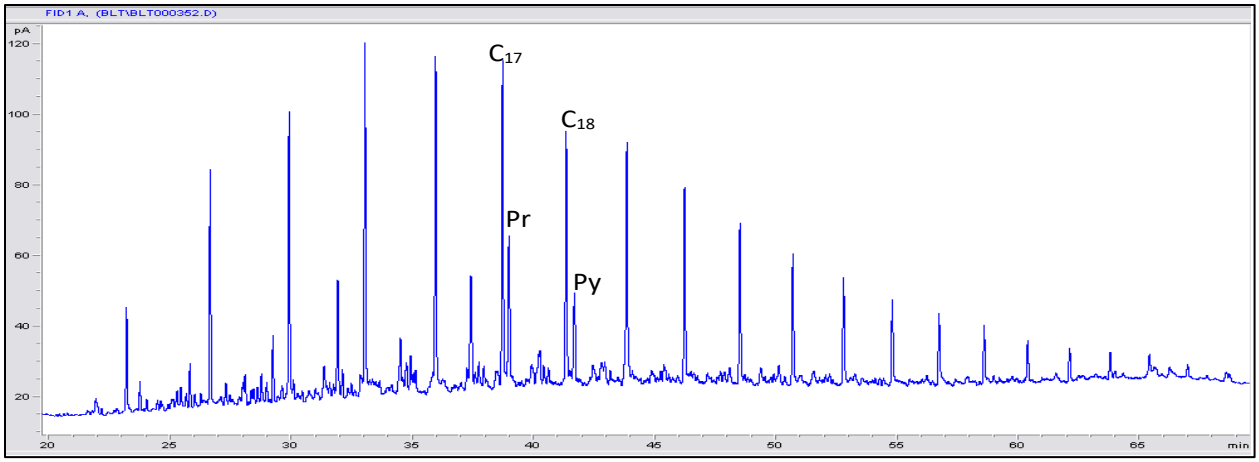

Figure 3. Typical GC chromatogram of a Pennsylvanian Kansas oil, Schroeder 1-26 from the Lansing-Kansas City (LKC) Formation, Kansas.

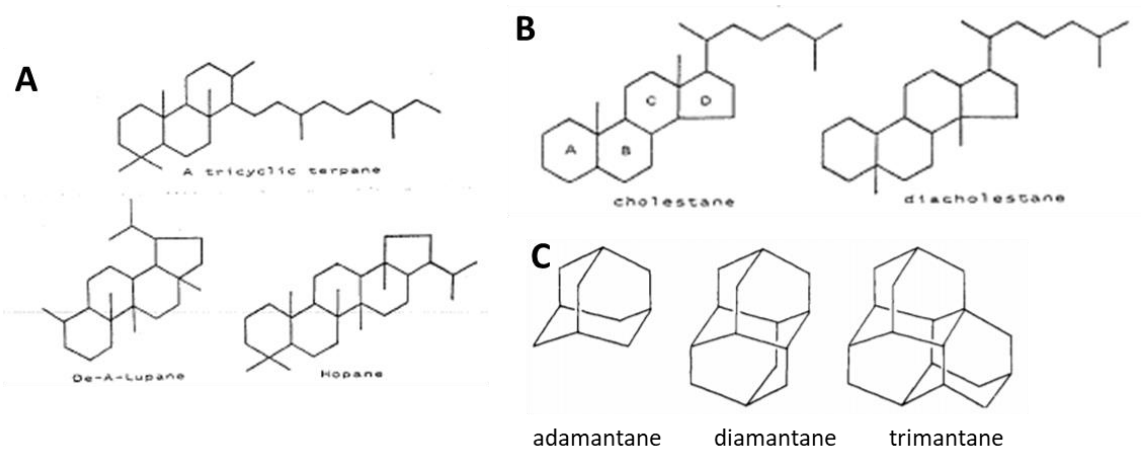

Figure 4. Common structures of saturate hydrocarbons: (**a**) triterpanes, (**b**) steranes, and (**c**) diamondoids (**APPX. II**; Burns et al., 1978; Waples and Machihara, 1990; Hays et al., 2007).

Triterpanes (**Fig. 4a, APPX. II**) are resolved using GCMS and SIM of the characteristic ion at m/z 191 chromatogram (**APPX. IVD**) and are generally thought to be derived from living precursors, such as terpenoids that are present in bacteria and algae and have various structures depending on the precursor organism (Waples and Machihara, 1990). Triterpanes have three rings (tricyclic), four rings (tetracyclic), or five rings (pentacyclic), and of these groups the pentacyclic terpanes, hopanes, are the most prominent in common oils/source rocks (Waples and Machihara, 1990; El-Sabagh et al., 2018). The abundance of certain hopanes can help infer maturity or type of organic matter in oils and rock extracts (Waples and Machihara, 1990). Steranes (**Fig. 4b, APPX. II**), however, are formed from steroids found in both algae and higher plants. These compounds have a tetracyclic structure with carbon numbers ranging from C_{20} to C_{30} and are determined from the m/z 217 and m/z 218 chromatograms. A common method used to interpret the sterane data is based on a C_{27}-C_{28}-C_{29} ternary diagram that can be used to infer depositional environments and whether oils are derived primarily from algal vs. higher plant source materials (Waples and Machihara, 1990; Moustafa and Morsi, 2012). The ternary diagram also becomes a

very useful approach for determining oil/oil and oil/source rock relationships. The diamondoids, unlike the triterpanes and steranes, can be used to evaluate thermal degradation and microbial oxidation as determined by the degree of diamondoid methylation (Dahl et al., 1999; Jalees et al., 2011) because they are derived from more stable polycyclic precursors and their structures (**Fig. 4d, APPX. II**) are diamond-like fused-ring alkanes (Jalees et al., 2011).

Aromatic Hydrocarbons

Aromatic hydrocarbons (**Fig. 6, APPX. II**), like saturate hydrocarbons, contain hydrogen and carbon, but they also have an aromatic ring that creates unsaturated bonds. The most common aromatic molecules are naphthalenes, phenanthrenes (**APPX. IVE)**, the aromatic steroidal hydrocarbons, and aryl isoprenoids/carotenoids. Phenanthrenes have three fused benzene rings (**Fig. 6a, APPX. II**) and may be formed from the dehydrogenation of molecular fossils (Kashirtsev et al., 2018). The phenanthrene series includes various methylated compounds that can be used to infer the thermal maturity of an oil-based on varying stability of the different methyl isomers. This maturity parameter is called the methylphenanthrene index (MPI, **APPX. III**) which has been shown to correlate closely with measured vitrinite reflectance (Radke et al., 1982). Aryl isoprenoids are fragments of carotenoids derived from sulfur reducing bacteria (**Fig. 4c, APPX. II**) and are extremely useful in verifying environmental conditions. The carotenoids and aryl isoprenoids (**APPX. IVC**) are indicative of photic zone euxinia (PZE) in high concentrations (**Fig. 5**) – a phenomenon where anoxic waters are present in the photic zone and have created water column stratification (Hays et al., 2007; Connock, 2015).The mono- and tri- aromatic steroidal hydrocarbons (**Fig. 6c, APPX. II**) are highly resistant to biodegradation and useful, like regular steranes, for oil/source rock correlations (Wang et al., 2007).

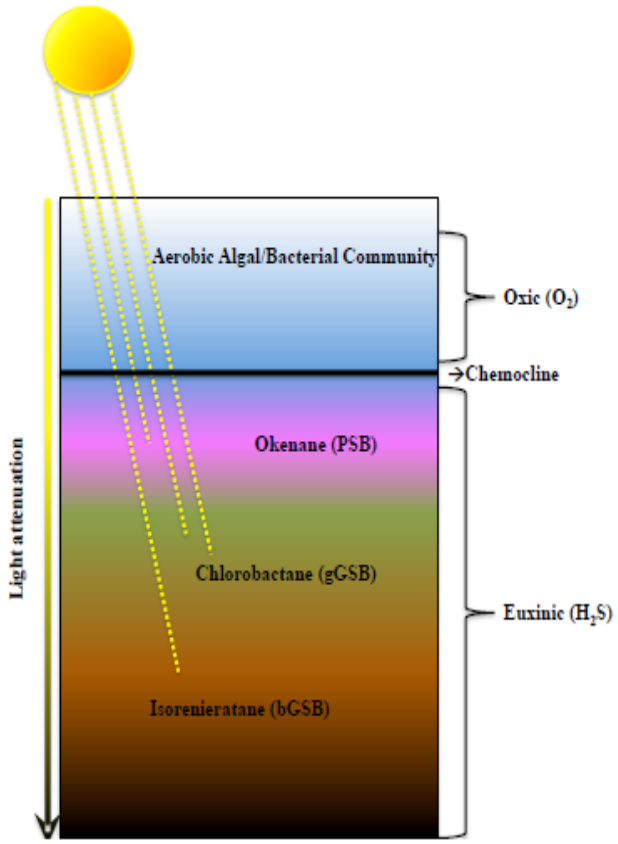

Figure 5. Water column stratification during photic zone euxinia. Hydrogen sulfide (H2S) rich waters are in the photic zone, and the color of the bacteria depends on the amount of sunlight received and creates the various carotenoids (Connock, 2015).

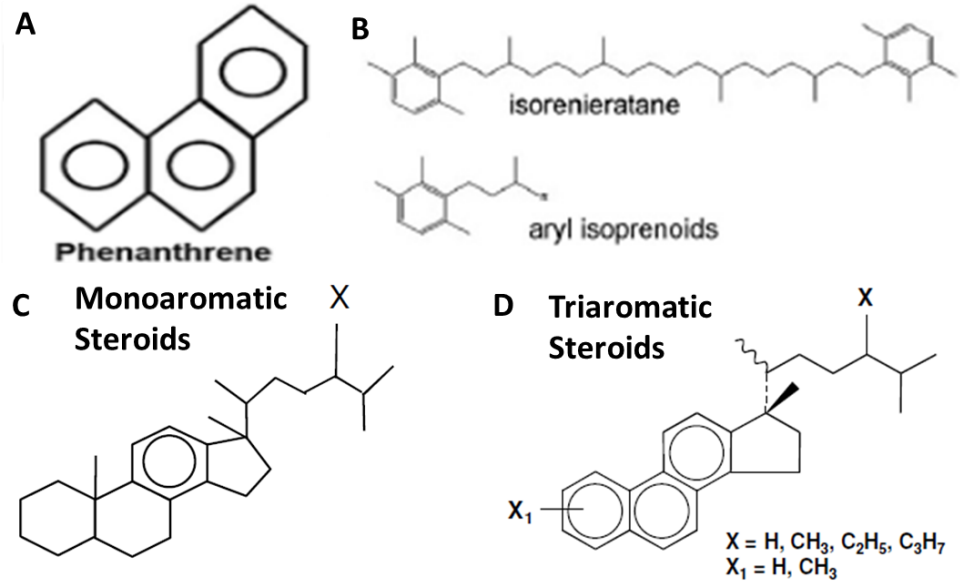

Figure 6. Common aromatic compounds: (**a**) the phenanthrene series, (**b**) aryl isoprenoids/carotenoids, and (**c, d**) the mono- and tri-aromatic steroidal hydrocarbons (**APPX. II**; Peters et al., 2004b; Dembicki, 2017).

Heteroatomic Molecules

Molecules that have more than just hydrogen and carbon are considered heteroatomic molecules. When these molecules interact with microbial organisms, chemicals in the source rock, or air the molecules react to and absorb nitrogen, oxygen, sulfur or other elements (Bragg et al., 1994; Hunt, 1996). The common heteroatomic molecules in this study include benzo-, dibenzo-, methyldibenzo-, and benzonaphthothiophene (**APPX. IVE)** and carbazoles (**APPX. IVF;** Wang et al., 2007) The thiophene series is a group of heteroatomic, aromatic molecules which contains a sulfur atom (**Fig. 7a, APPX. II**) can be found in the aromatic fraction. The thiophene series can be used to infer maturity, like the phenanthrenes, as well as an indication of biodegradation and depositional environment (Ho et al., 1974; Hughes, 1984). Carbazoles (**Fig. 7b, APPX. II**), which are found in the low polarity compounds (LPC) of the resins fraction, are nitrogen-bearing heteroatomic, aromatic molecules that have been utilized to give some indication of relative migration distances (Li et al., 1992). Carbazole and benzocarbazole can be seen on the m/z 167 and m/z 217, respectively (**APPX. IVF**) in the LPC fraction.

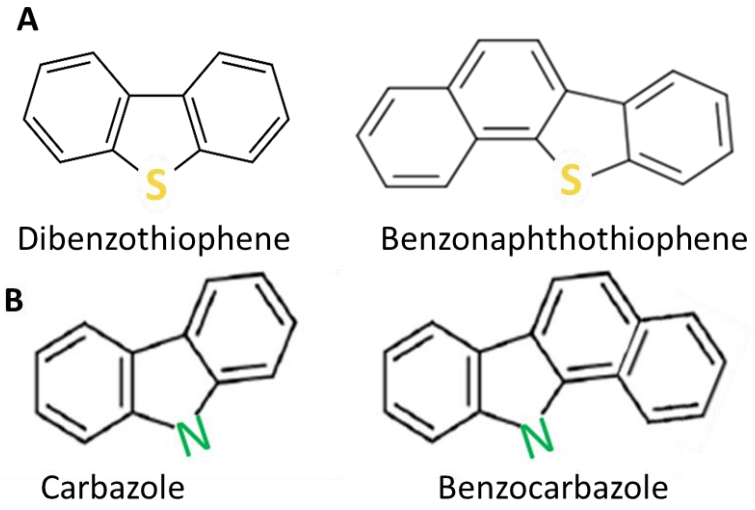

Figure 7. Common heteroatomic molecules: (**a**) the thiophene series and (**b**) the carbazole series (Hughes, 1984; Larter, 1996).

1.3. Study Area

Oils produced in the Hugoton Embayment of western Kansas have not been extensively studied, so the study area of this project encompasses most of western Kansas (**Fig. 8**). The samples in this study area include multiple oils and source rock cores in 20 counties in Kansas, as well as a Woodford core in the area. The location of original Woodford oil samples from two counties in Pauls Valley, southern Oklahoma have been used to compare the oils on the Hugoton Embayment to (**Fig. 8**). This process of oil/oil and oil/source rock correlation using these samples will provide a robust study and improve the understanding of the migration of oils and filling of reservoirs in the area.

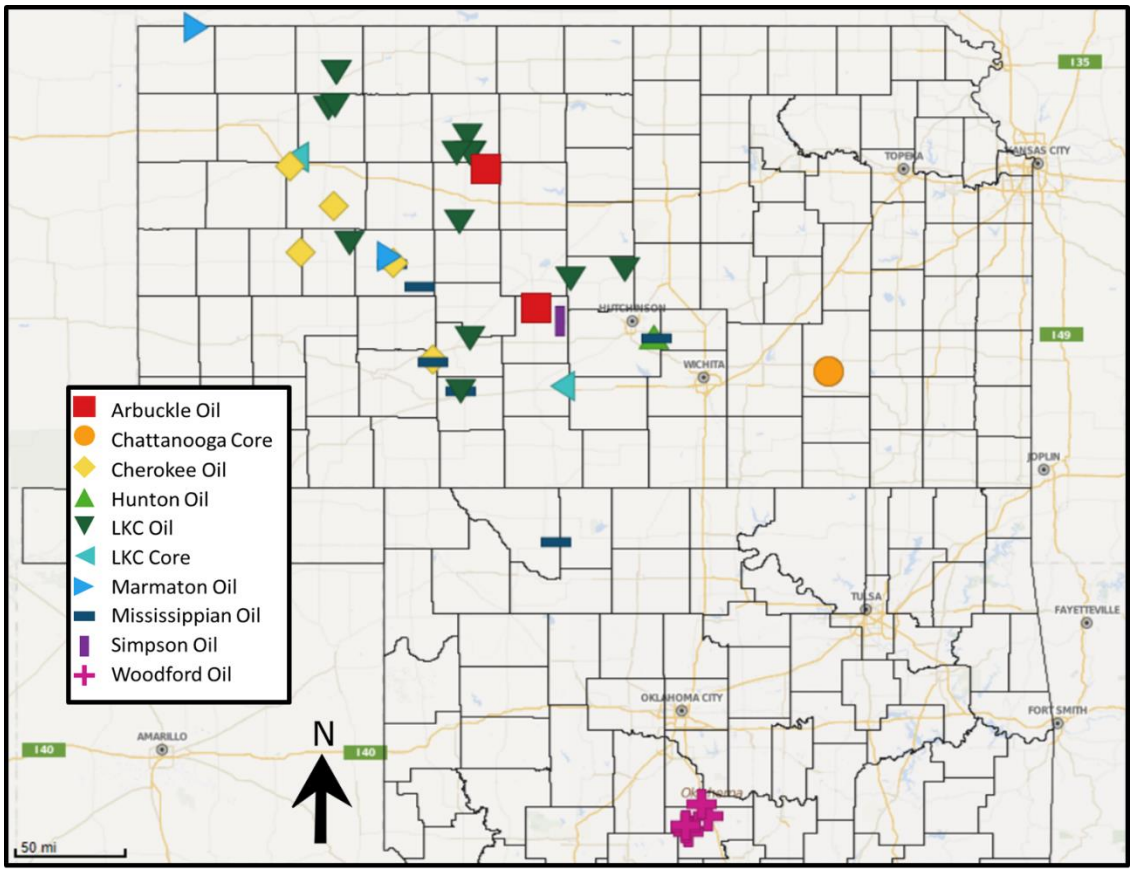

Figure 8. Kansas study area: 20 counties in Kansas where oil samples were taken and their relation to the main structures of Kansas. Oklahoma correlation area: 2 counties in the Anadarko Basin, Pauls Valley Area, Oklahoma that are true Woodford oils and are used to compare biomarker signatures and their relation to the main structures in Oklahoma.

The oils that have been produced in Kansas are typically found in and around major structural controls, as seen in **Fig. 9** (Baars and Watney, 1991). The main area that is studied here – where the majority of the oil and source rock samples have come from – is the Hugoton Embayment of the Anadarko Basin in Kansas and Oklahoma.

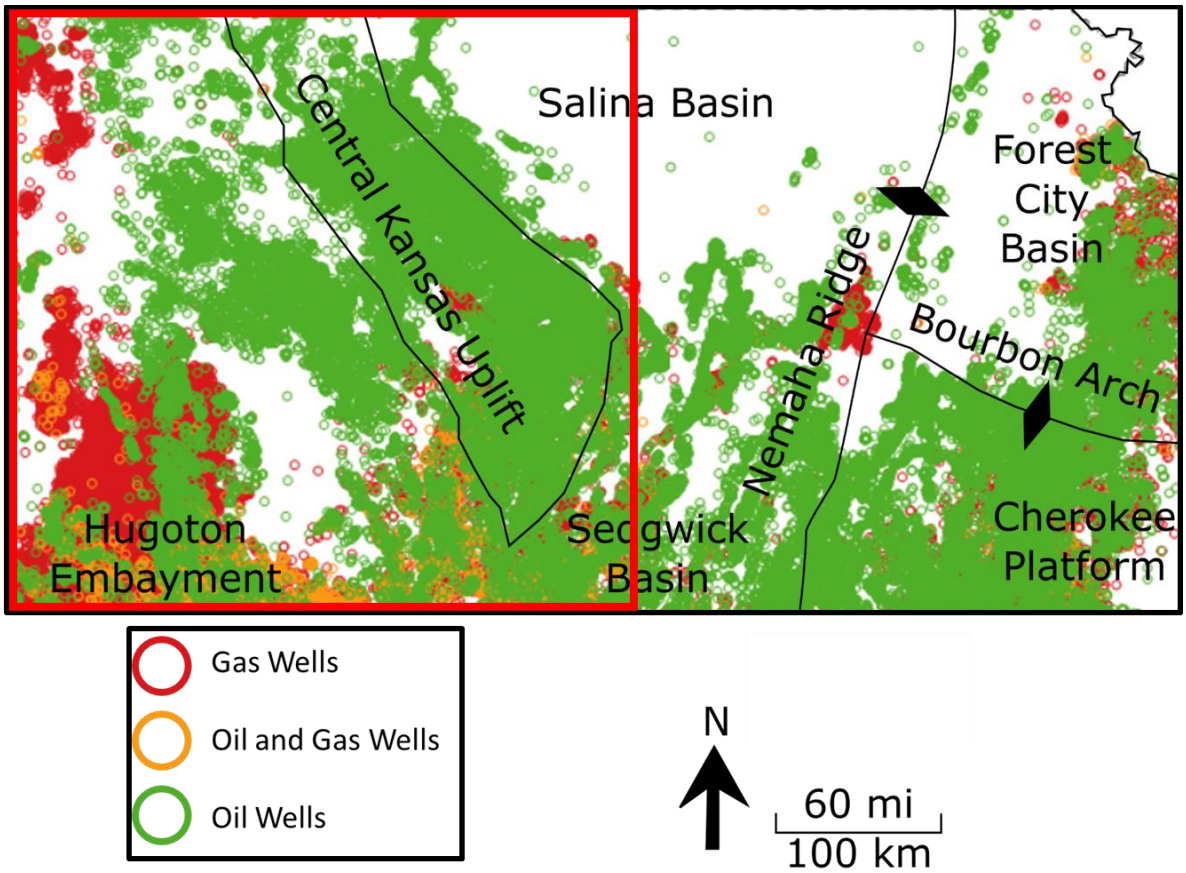

Figure 9. Map of all oil and gas fields in Kansas; the focus of this study, in red, is in the west-central, oil-rich area of Kansas (Kansas Geological Survey, 2009; Mpanje, 2016).

1.4. Previous Research

In 1989, Burrus and Hatch conducted a study similar to this one in order to determine the origin of oils found in the greater Anadarko Basin. Using whole oil chromatograms, saturate chromatograms and bulk isotope data to genetically type Pennsylvanian oils to Woodford oils, it

was noticed that the oils from the Hugoton Embayment of Kansas had only trace amounts of toluene, an aromatic C_7 hydrocarbon, as compared to Woodford oils and there seemed to be a general decrease in toluene the further away from the depocenter of the Anadarko Basin. These compounds tend to be preferentially removed by water washing during migration through water wet reservoirs. In **Fig. 10**, it can be seen that the toluene concentration, relative to a sum of toluene+n-heptane+methylcyclohexane (**APPX. I**), is inversely related to the distance from the depocenter of the Anadarko Basin to the oil sample. The use of these parameters determined that oils produced from Kansas reservoirs may have migrated up to 350 miles.

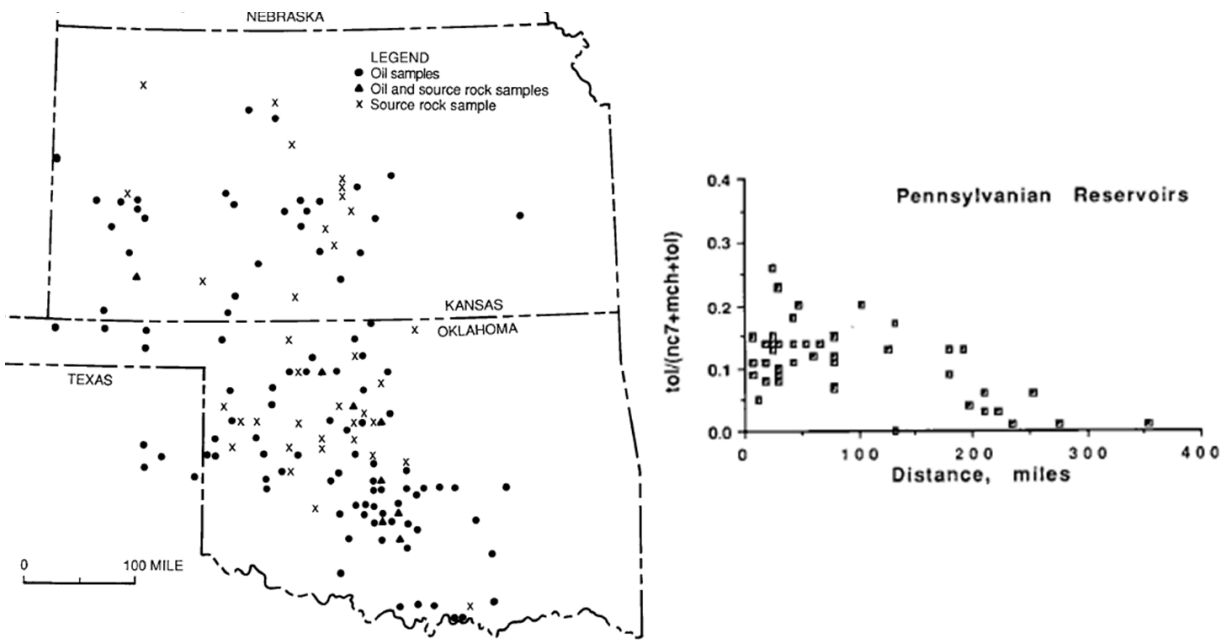

Figure 10. To the left, Pennsylvanian oil samples from Kansas and Oklahoma and to the right, the relative migration distance showing a range of 0-350 miles for the migrated oils using a ratio of toluene/(n-heptane+methylcyclohexane+toluene) vs. the distance to the depocenter of the Anadarko Basin, proposed by Burrus and Hatch, 1989 (**APPX. I**).

In 1996, Larter et al. published a paper that proposed a new way to measure migration distance. Benzocarbazoles, a family of nitrogen-bearing compounds, were analyzed in various oils

to determine how far an oil had migrated from the source rock via secondary migration. The benzocarbazoles are used as migration tracers – which ideally would not vary with thermal maturity or other factors – that stay in the oil and can appear as quantitative indicators of relative migration distance. This is done by using two isomers of the benzocarbazole compound (**APPX. II**) in the benzocarbazole (BC) ratio: benzo[a]carbazole/(benzo[a]carbazole + benzo[c]carbazole) as there is thought to be a preferential sorption of the benzo[a]carbazole compound during migration due to its elongated shape (**APPX. I**). In an experiment that measured the BC ratio of oils with a similar thermal maturity from five petroleum reservoirs, it was discovered that the lower the BC ratio, the further an oil had migrated as the benzocarbazoles are absorbed onto clay mineral surfaces and are left behind in the carrier bed (**Fig. 11**).

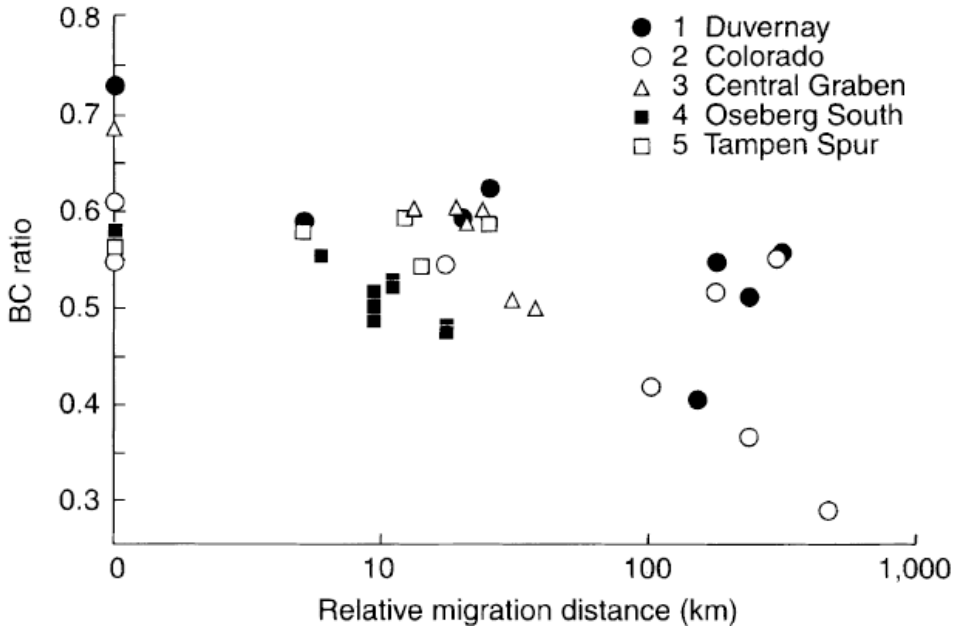

Figure 11. Oils in five petroleum reservoirs show an increasing relative migration distance and a decreasing BC ratio (Larter et al., 1996).

In another study on migration, Fang et al. (2016) used methyldibenzothiophenes (MDBT), dimethyldibenzothiophenes (DMDBT), and benzo[b]naphthothiophene (BNT, **APPX. II**) to

determine the direction of oil migration. These compounds are all sulfur-bearing compounds that have been shown to reflect little to no maturity, lithology, or organic matter input influences on migration direction within geochemically related oils. Migration pathways are determined using the same principle defined in Larter et al. (1996), where rod-shaped compounds adsorb onto the clay minerals and get left behind (Fang et al., 2016).

It is the goal of this research to provide a more in depth confirmation of the oil/oil and oil/source rock work done by Burrus and Hatch in 1989 with the use of GCMS analysis of a broader range of biomarkers and organic compounds. The work done by Larter et al. (1996) using benzocarbazoles to determine migration distance and the work done by Fang et al. (2016) using various thiophene compounds to determine migration pathways, along with the work of other researchers, may help confirm the migration distances and directions previously suggested.

CHAPTER 2: GEOLOGICAL SETTING

Many tectonic events, i.e. the Central Kansas Uplift and Anadarko Basin, and depositional events, i.e. the extent and burial history of the Woodford Shale, have shaped Kansas and Oklahoma (**Fig. 12**). The timing of these structures controlled sedimentation accumulation, production of hydrocarbons, and the eventual migration/trapping of hydrocarbons.

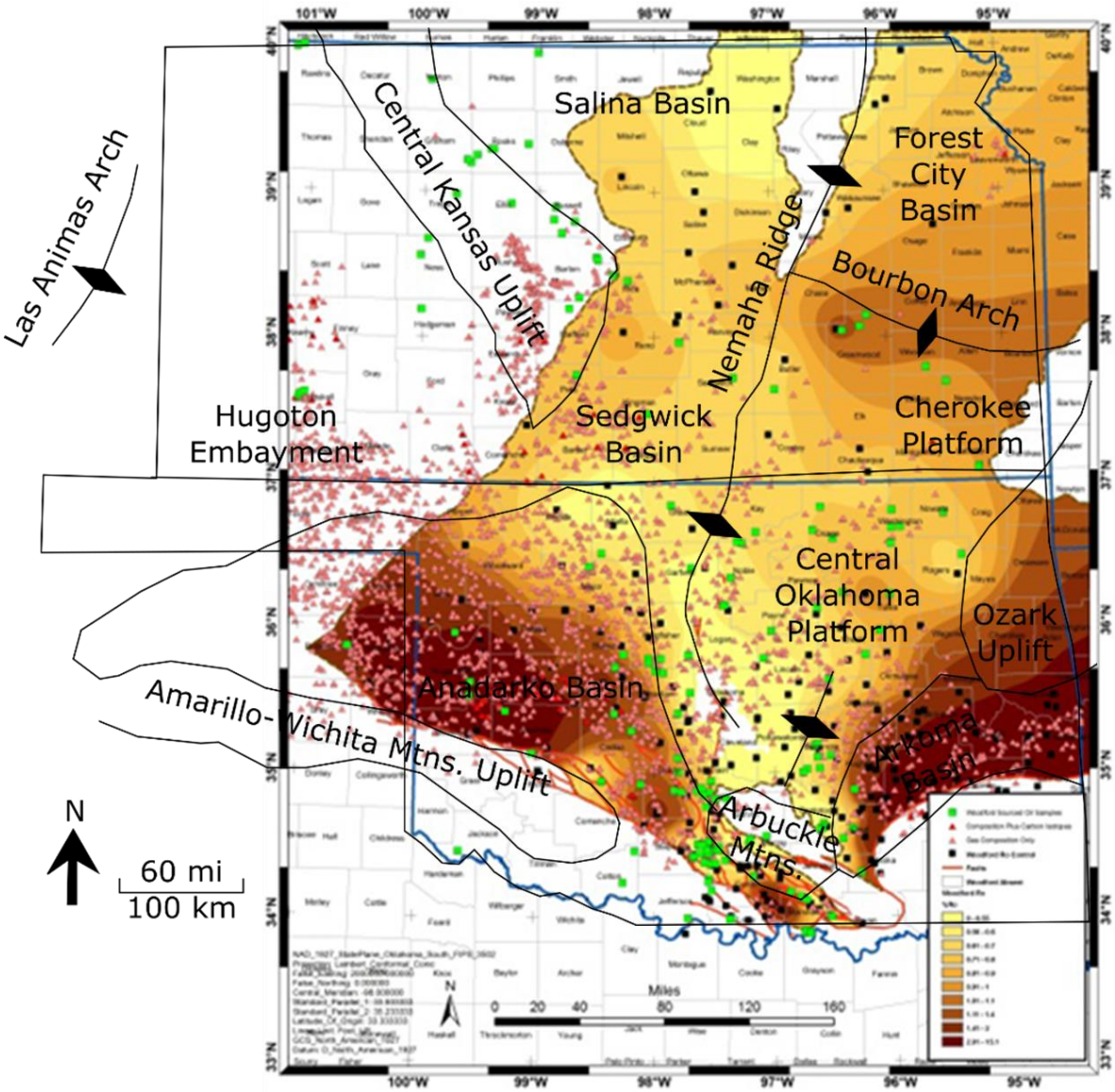

Figure 12. Major tectonic elements in Kansas and Oklahoma showing the extent and general thermal maturity of the Woodford Shale (modified from GeoMark, 2013; Mpanje, 2016).

2.1. Kansas Geology

The main formations that have been analyzed in this study area include the Lansing-Kansas City (LKC), Cherokee, Marmaton, Mississippian, Hunton, Simpson, and Arbuckle – arranged in stratigraphic order – that fill the Hugoton Embayment of the Anadarko Basin and cover the Central Kansas Arch (Newell et al., 1987). The main structural elements in this area are the Central Kansas Uplift and the Nemaha Ridge that bound the multiple basins in Kansas (**Fig. 13**).

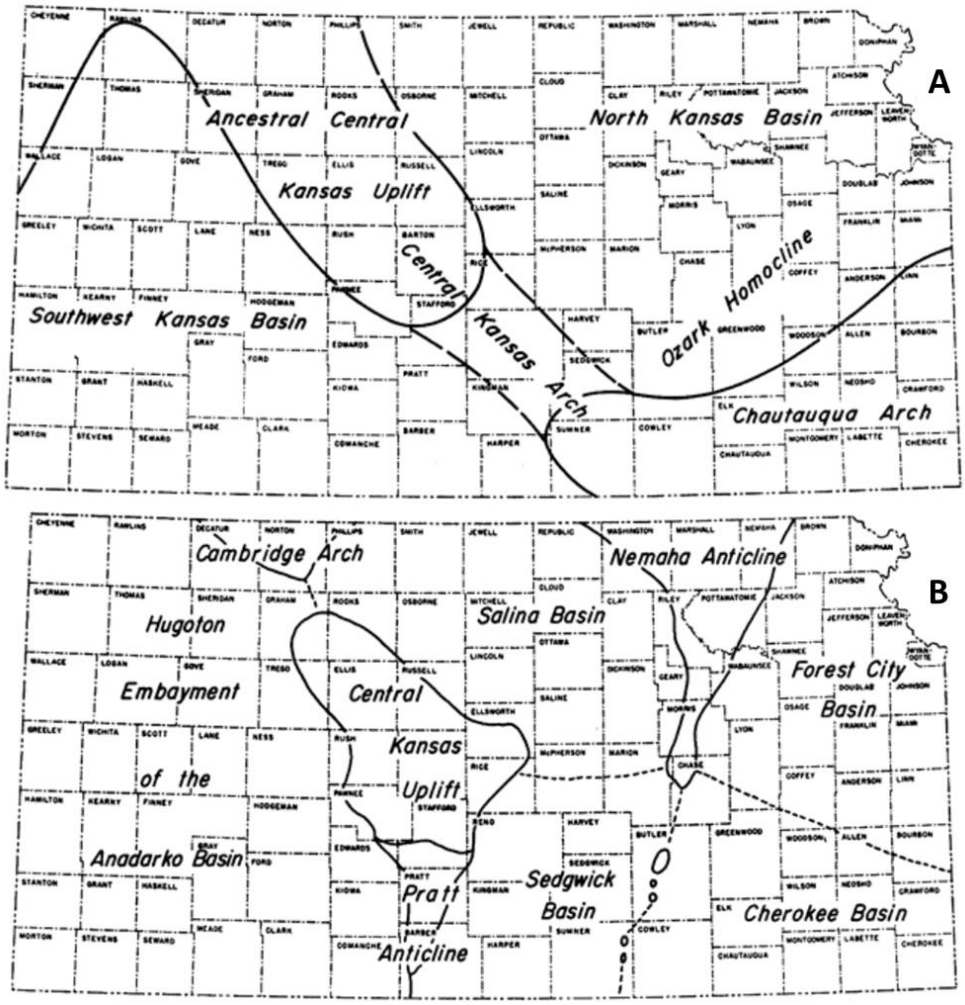

Figure 13. Structural features in Kansas in: (**a**) Early Mississippian showing the initial uplift of the Central Kansas Uplift; and (**b**) Early Pennsylvanian times showing the progression of uplifting events that have resulted in the main modern subsurface features (modified from Merriam, 1963).

Structural Influences in Kansas

In the northwest Anadarko Basin, the main structures that controlled deposition are the central Kansas uplift, a large shelf area, and a deep basin area. The sediments from the Anadarko Basin from Arbuckle Permian time onlapped onto positive tectonic features that were exposed in the early Pennsylvanian and eroded (Beebe, 1956). The Central Kansas Uplift that the Lansing-Kansas City was deposited on was created by geologic deformation in the Late Mississippian to Early Permian, according to Merriam (1963).

The basin of interest in this study is the Hugoton Embayment, also known as the Southwest or Western Kansas Basin, which is bound by the Central Kansas Uplift in the northeast and the Las Animas Arch in eastern Colorado (**Fig. 13**). The Hugoton Embayment dips to the south along the basinal axis, toward the Anadarko Basin and has up to 9,500 feet of sediment overlying the Precambrian basement rocks. The Central Kansas Uplift is a northwest-trending structure that was uplifted in the early Paleozoic and later deformed in the Early Pennsylvanian. This structure separates the Hugoton Embayment from the basins in north and east Kansas and can be seen in a paleotopographic map of the Mississippian formation (**Fig. 14**). The majority of the sediments that have accumulated in Kansas are Paleozoic and Mesozoic in age and the thickness does not exceed 5,000 feet (**Fig. 15**; Gerhard, 2004). In the west, the Cretaceous Las Animas Arch (**Fig. 14**) separates the Hugoton Embayment from the Denver-Julesburg Basin in eastern Colorado and has a general northeastern dip that intersects the Central Kansas Uplift in northwest Kansas and prevents hydrocarbon flow to the north (Merriam, 1963; Newell et al., 1987).

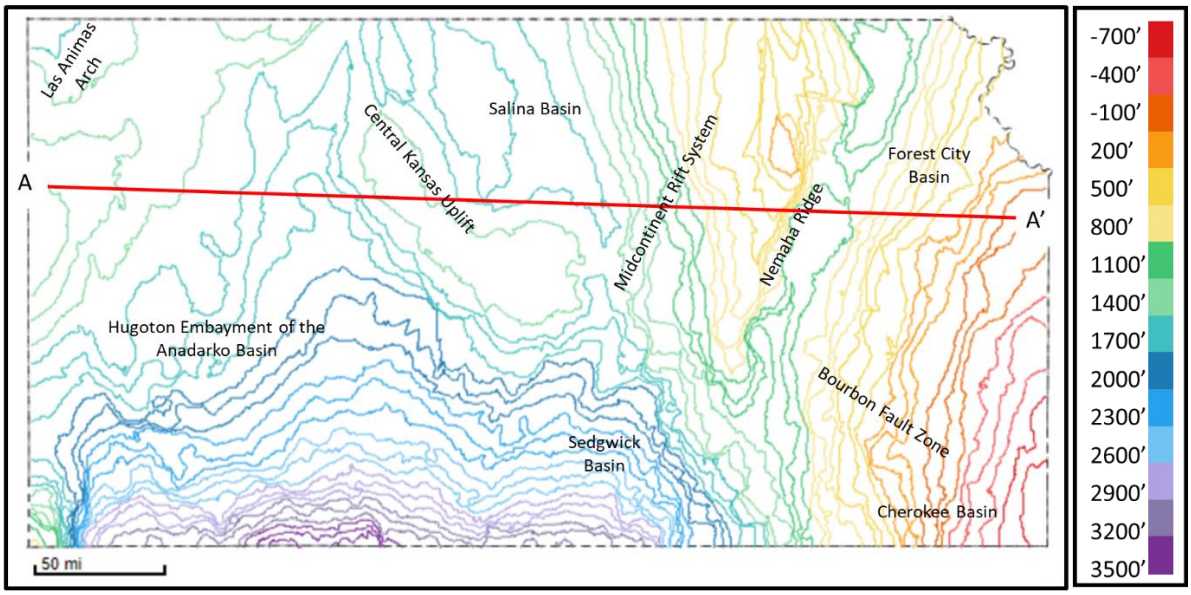

Figure 14. Paleotopographic map at the end of the Mississippian time (i.e. top of the Mississippian formation) showing the present structures. A-A' is a line for the cross-section in **Fig. 15** (modified from Gerhard, 2004; Kansas Geological Survey, 2009).

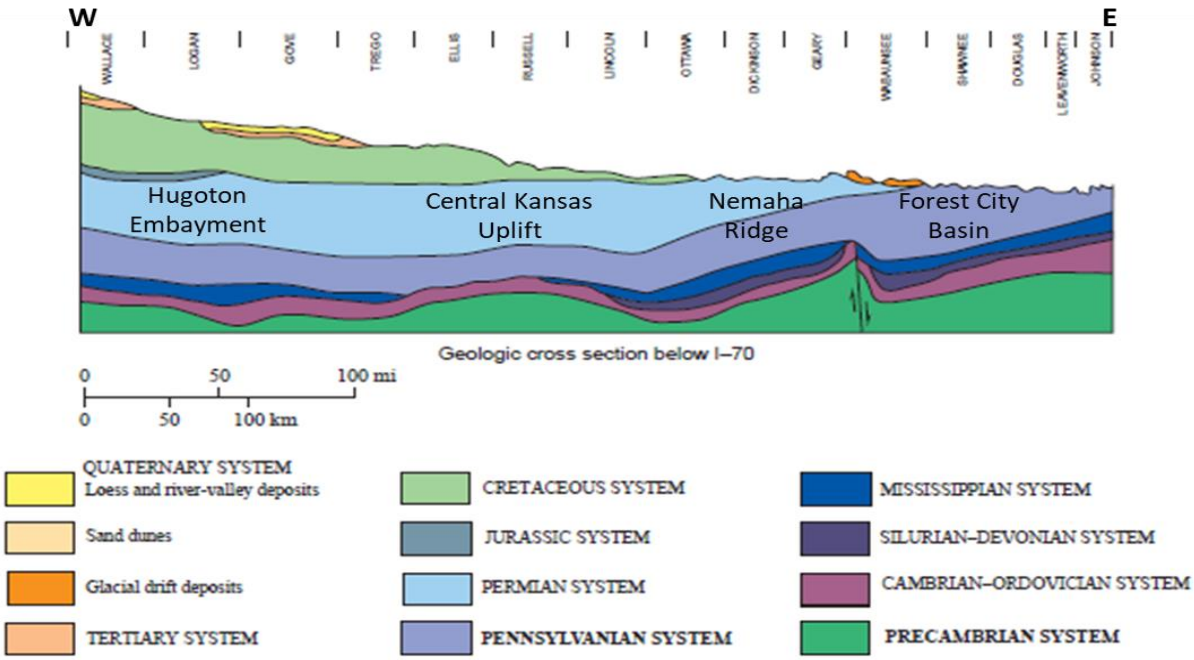

Figure 15. Cross-section running east to west across Kansas with county names labeled on the top of the cross-section. The Hugoton Embayment is in the West, the Central Kansas Uplift and the Nemaha Ridge in Central Kansas, and the Forest City Basin in the East (modified from Gerhard, 2004).

Kansas Stratigraphy

The stratigraphic intervals of interest are the producing units of the Late Pennsylvanian Lansing-Kansas City through the Cambrian Arbuckle formation (**Fig. 16**). The thickness of the Lansing-Kansas City ranges from 370 to 600 feet throughout Kansas and is comprised of major cyclothem events that dominate the deposition in the Pennsylvanian to Permian times and are laterally continuous throughout Kansas and into Oklahoma. The lithologies of the Lansing-Kansas City reflect this cyclic nature as there are both marine and nonmarine algal, cross-bedded and oolitic limestones interbedded with shale units that reflect the rise and fall of sea level across the intercontinental epeiric shelf (Merriam, 1963; Watney, 1980). These changes in deposition and freshwater diagenesis greatly affect the porosity in the limestone units (Watney, 1980).

The other Pennsylvanian formations of interest are the Cherokee, Marmaton, and the Morrow – which all have alternating sandstone, limestone, shale, and coal beds as the epeiric shelf became more restricted in the late Pennsylvanian. The Mississippian strata are generally grouped together and classified as mostly marine carbonates that are up to 1,700 feet thick. Below the massive Mississippian limestone unit is the Lower Mississippian-Upper Devonian unit, the Chattanooga Shale or Kinderhook Limestone. The Chattanooga Shale is the Kansas extension of the Woodford Shale in Oklahoma and it grades from organic rich and silty in the south to organic poor in the north. However, it is not present in the Hugoton Embayment. The Silurian Hunton Group and Ordovician Simpson and Arbuckle Groups are mostly dolomitic, have a thickness of up to 1,500 feet, and are laterally extensive throughout all of Kansas (Zeller et al., 1968).

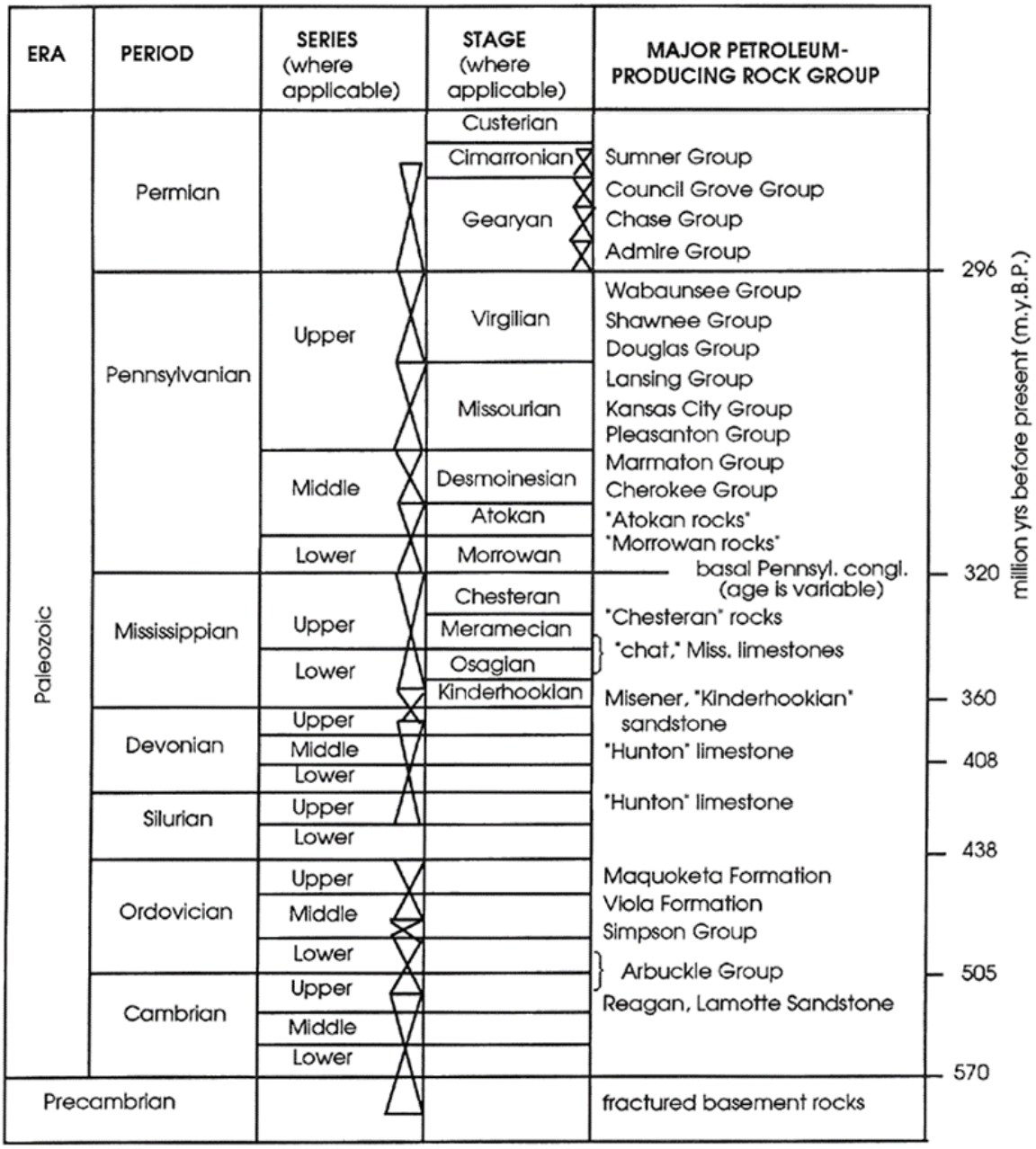

Figure 16. Stratigraphic column of the Paleozoic rock formations in Kansas (Newell et al., 1987). The Woodford Shale equivalent in Kansas is referred to as both the Kinderhook and Chattanooga formation.

Kansas Oil Production

Oil production is most abundant in the Hugoton Embayment on the Central Kansas Uplift, but it is also scattered to the east and west. The Upper Pennsylvanian Lansing-Kansas City

formation produces oil and some dissolved gas from between 3,000 and 5,000 feet (Price, 1980; Newell et al., 1987). The production through time by decade, starting in the early 1900s to the 1980s, is shown in **Fig. 17** (Kansas Geological Survey, 2009). The distribution of the oil production shows the productive reservoir locations become more scattered, most likely because production is Kansas has had a history of non-uniform hydrocarbon fill in reservoirs (Newell et al., 1987; personal communication, 2015).

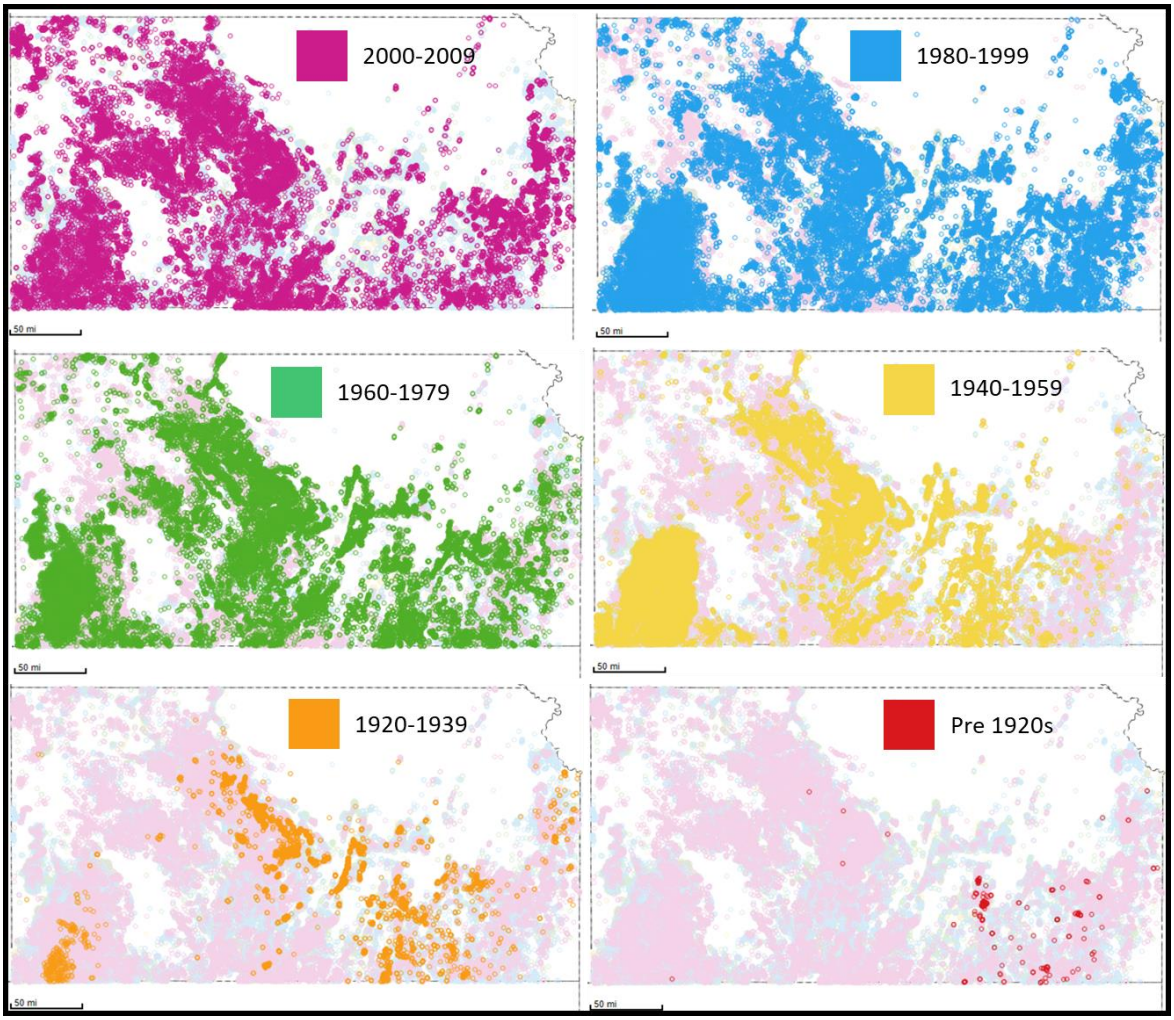

Figure 17. Oil and gas fields in Kansas by decade of discovery, from the early 1900s to 2009 (Kansas Geological Survey, 2009).

Migration Pathways

The most likely migration pathways out of the Anadarko Basin are horizontal porous beds leading out of the basin that move up-dip as well as the vertical fractures and faults from tectonic activity (**Fig. 18**). The Hugoton Embayment is a shallow basin that does not have any prolific source rocks. The Hugoton Embayment is located on the shelf of the Anadarko Basin; therefore the oil found in the Hugoton Embayment has likely undergone long distance migration from the deep, hot, petroleum-rich Anadarko Basin (Price, 1980). It was proposed by Price (1980) that oils found in the Hugoton Embayment migrated through permeable Arbuckle rocks that underlie the Woodford Shale in the south but, due to erosion, are juxtaposed in the north towards Kansas (Newell and Hatch, 1999; Gerhard, 2004). However, there is local petroleum generation in the Forest City Basin (**Fig. 12**) located in northeast Kansas. It is unlikely that the Forest City oils migrated into the Hugoton Embayment as there are two uplifts (the Nemaha Ridge and the Central Kansas Uplift) that separate the Forest City Basin from the Hugoton Embayment (Gerhard, 2004).

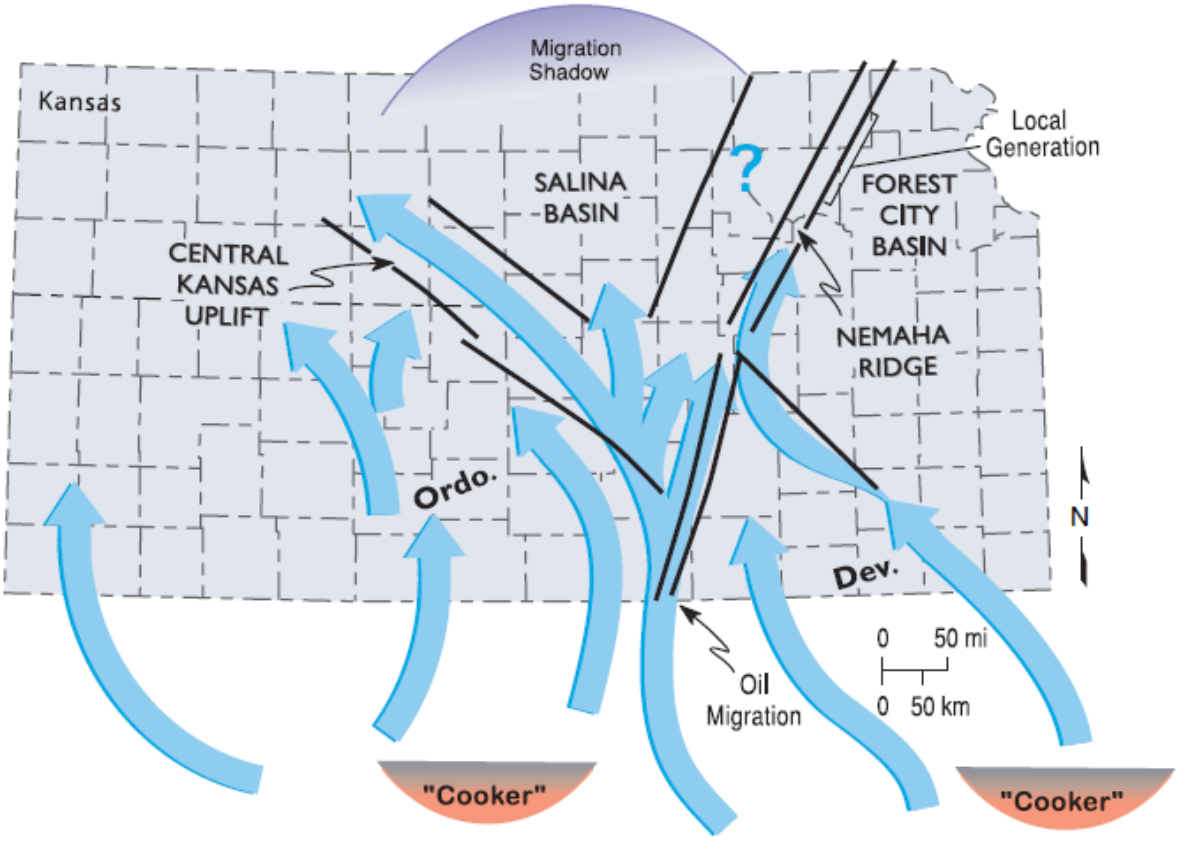

Figure 18. Migration pathways out of the Anadarko Basin and into the Hugoton Embayment of Kansas via lateral migration through Arbuckle strata and vertical migration up the major faults and uplifts. Pathways such as these may account for the abundance of hydrocarbons found throughout Kansas even with a lack of prominent source rock in the area (Gerhard, 2004).

2.2. Anadarko Basin Structure, Stratigraphy, and Woodford Shale

The Anadarko Basin is the deepest sedimentary basin in the North American craton. It is located at the northern foot of the Wichita Mountains in southeastern Oklahoma (**Fig. 19**) and extends into the Texas Panhandle, southeastern Colorado, and western Kansas (Perry, 1989, Mitchell, 2012). The Anadarko Basin has an area of roughly 70,000 square miles with up to 40,000 feet of sediment in the deepest part of the basin. It has been extensively studied and is estimated to contain 5.4 billion barrels of oil (BBO) and 125 trillion cubic feet (TCF) of gas, both produced and in reserve, which makes up 70-85% of the conventional hydrocarbons produced in this basin (Mitchell, 2012, Wang, 2016).

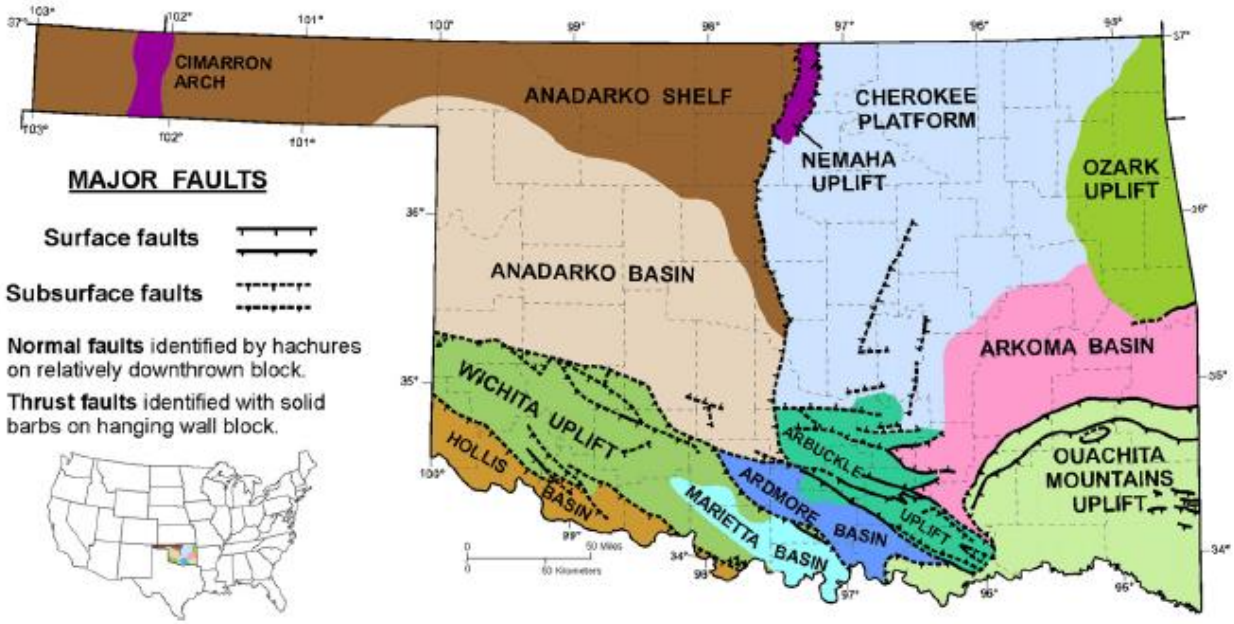

Figure 19. Structural influences in the Anadarko Basin, showing the tectonic events in Oklahoma. The major sediment accumulation occurs north of the Wichita Mountains in the heart of the Anadarko Basin where sediment thickness reaches 40,000 feet (Perry, 1989; Northcutt and Campbell, 1996; Cardott, 2012; Mitchell, 2012).

Anadarko Basin Structure

The Anadarko Basin is an asymmetrical foreland basin that is bound by the Cambrian Amarillo-Wichita Uplift in the southwest and the Late Mississippian Nemaha Ridge in the east. To the north, the basin grades into a shelf area that is known as the Hugoton Embayment of the Anadarko Basin (Dolton and Fin, 1989; Perry, 1989; Gallardo and Blackwell, 1999). The internal structure of the Anadarko Basin is a series of faults along the Amarillo-Wichita Uplift which created the subsiding depocenter for the basin (**Fig. 20**; Johnson, 1989; Gallardo and Blackwell, 1999; Liu, 2015).

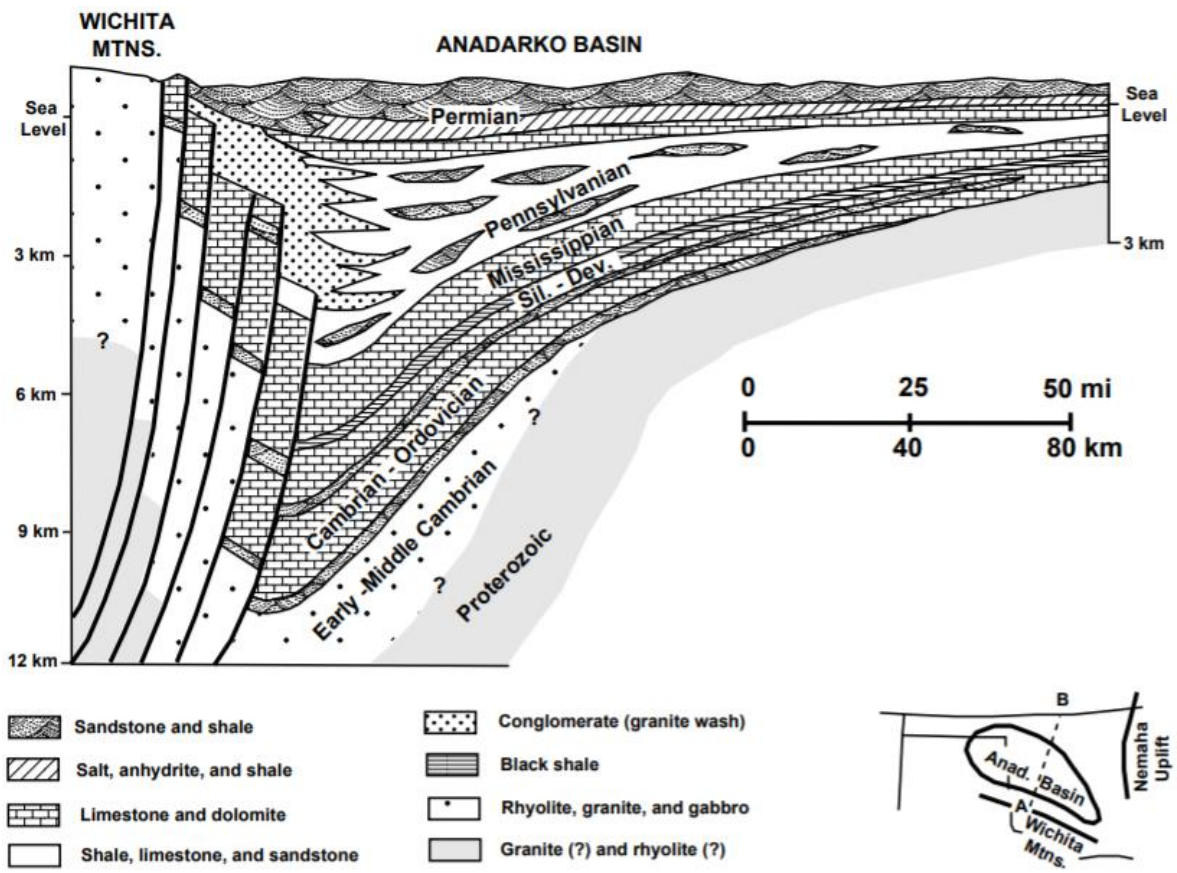

Figure 20. North-south cross-section through Oklahoma, leading into Kansas showing the depositional pinch-out over the northern Anadarko Basin as it enters the Hugoton Embayment of western Kansas (modified from Johnson, 1989; Gallardo and Blackwell, 1999.)

Stratigraphy of the Anadarko Basin and The Woodford Shale

The general stratigraphy of the Anadarko Basin (**Fig. 21**) is similar to that of west-central Kansas as the formations of the Hugoton Embayment and the Anadarko Basin were deposited at the same time.

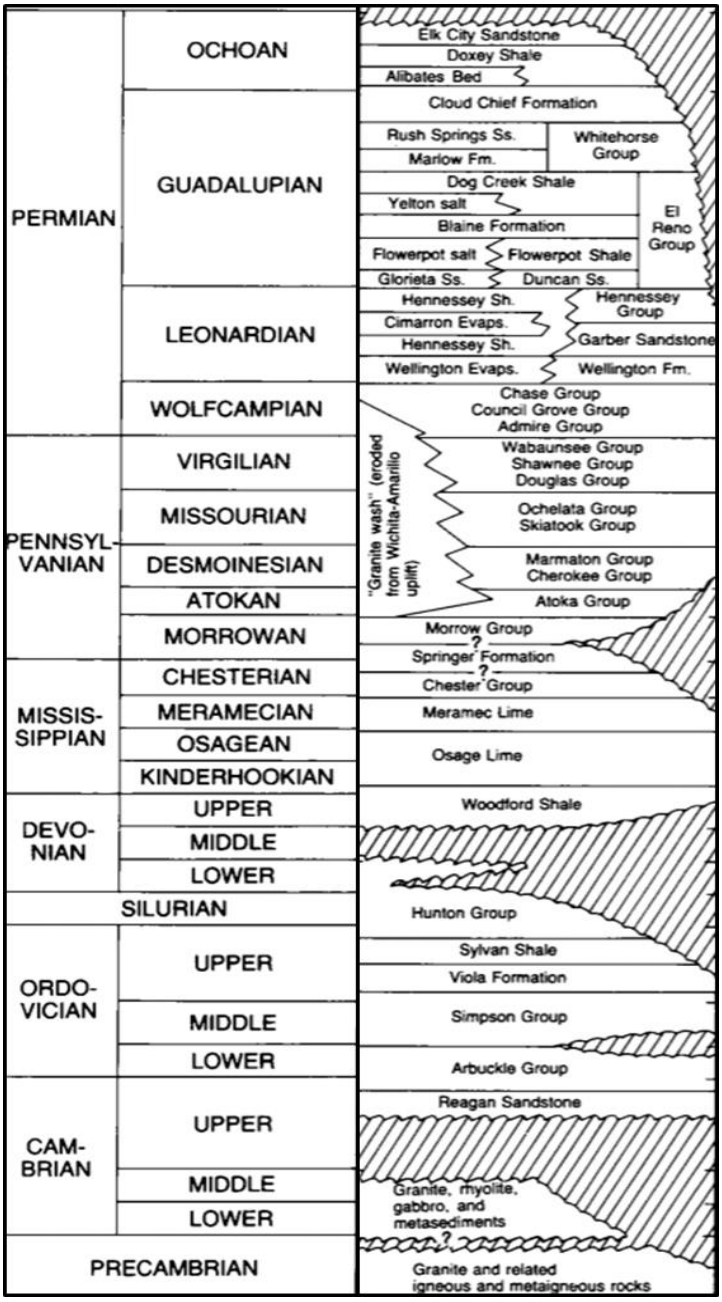

Figure 21. General stratigraphic column of the Paleozoic Anadarko Basin showing major unconformities in time (Johnson, 1989).

The primary producing formation of the Anadarko Basin is the Late Ordovician to Early Mississippian Woodford Shale which can be subdivided into the upper, middle, and lower Woodford members (Althoff, 2012; Slatt, et al., 2012). The Upper Woodford Shale shows a high

amount of chert and phosphate nodules that are from a regional regressive sequence (Hester et al., 1988; Jing, 2016); the Middle Woodford Shale shows the highest amount of organic matter and clay content, (Slatt and Rodriguez, 2012); the Lower Woodford Shale also has abundant clay and organic matter content – it also shows a widespread black shale that is indicative of a marine transgression (Hester et al., 1988). Within each of these members, it has been observed that the variability is significant as the thicker, clay rich, organic rich, ductile beds act as small scale source rocks and the thinner, quartz rich, brittle beds act as the reservoir (Slatt, 2019). These changes are due to cyclic transgressions and regressions that have been observed in all scales of the Woodford Shale (Romero and Philp, 2012; Ekwunife, 2017; Zhang, 2019; Slatt, 2019). Overall, the Woodford Shale is a TOC rich source rock with type II, oil-bearing, kerogen with up to 25% organic matter and can be brittle due to high inputs of biogenic silica and has a porous organic matter network and it unconformably overlies the Hunton Limestone. These components make the Woodford Shale a source rock of enormous capacity as well as a good reservoir rock (Cardott, 2013).

Woodford Shale v. SCOOP/STACK Oil Geochemistry

The conventional oil produced from Woodford Shale reservoirs is different from the oils currently being produced out of the relatively new plays: the South-Central Oklahoma Oil Province (SCOOP) and the Sooner Trend of the Anadarko Basin in Canadian and Kingfisher Counties (STACK). The conventional Woodford source rock from Pontotoc County, Oklahoma contains type II kerogen which has an organic matter content that ranges from TOC values of 5.01 to 14.81 wt. % (Romero and Philp, 2012), and conventional Woodford oils used in this study contain organic matter from source rocks that appear to have a marine source (Jones and Philp, 1990;

Wang, 2016). SCOOP/STACK source rocks contain kerogen type II or II/III and an average TOC value of 1.60 wt. % (Cardott, 2017; Symcox and Philp, 2019). Type II/III kerogen organic matter and the hydrocarbons produced are more gas rich and there has been evidence of oil cracking in STACK oils (Kvale and Bynum, 2014; Liborius and Sneddon, 2017). Also, SCOOP reservoirs show a presence of mature thermogenic methane gas (Kornacki and Dahl, 2016) which is different from what is found in conventional Woodford oils. In looking at the various plays in Oklahoma, the two main factors that play into the changes in the plays are thickness and thermal maturity, while facies variability may also be important (Kvale and Bynum, 2014).

CHAPTER 3: METHODS

3.1. Sample Selection and Collection

Thirty-two oil samples (**Table 1**) were acquired from the Lansing-Kansas City, Mississippian, and various other formations in the Hugoton Embayment (**Fig. 22**) that occur within the Paleozoic stratigraphic interval in Kansas (**Fig. 23**). Five core samples were collected from cored intervals of Kansas wells to determine whether the oils of the Hugoton Embayment had migrated into these reservoirs or were locally sourced. Two core samples were from a well that was drilled and cored in the Chattanooga Shale; the other three core samples were from wells drilled and completed in the Lansing-Kansas City. Also, eight conventional Woodford oils from the Pauls Valley area were used in this study for oil/oil correlation and estimating migration distance and direction.

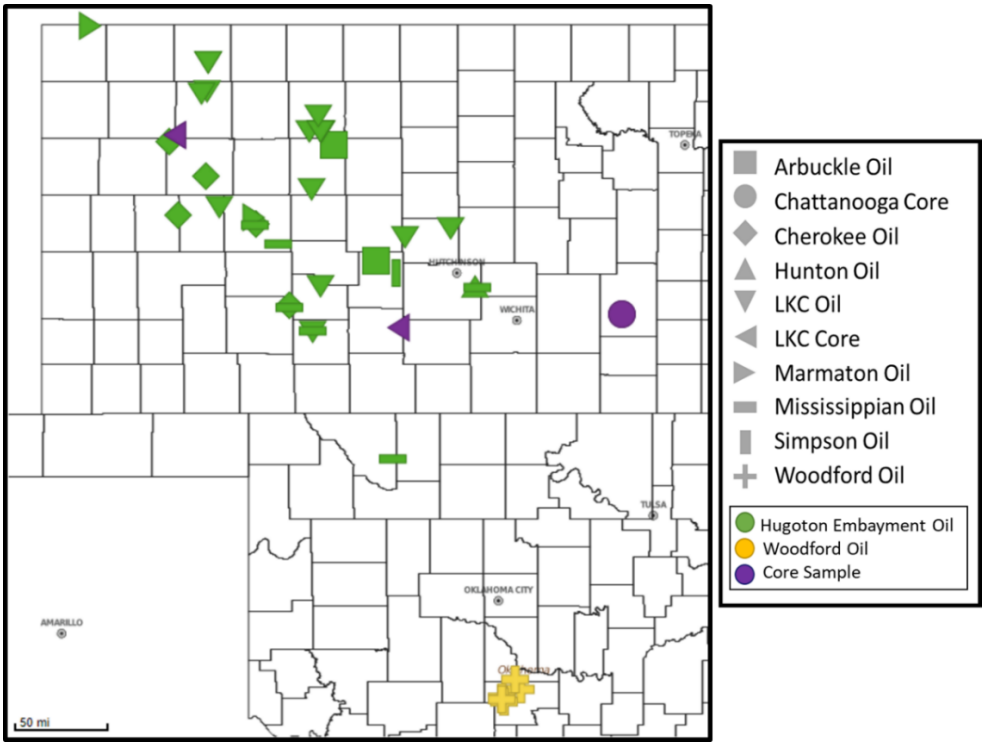

Figure 22. Location of oils and cores for this study in map view with the corresponding stratigraphic section above in **Fig. 23**.

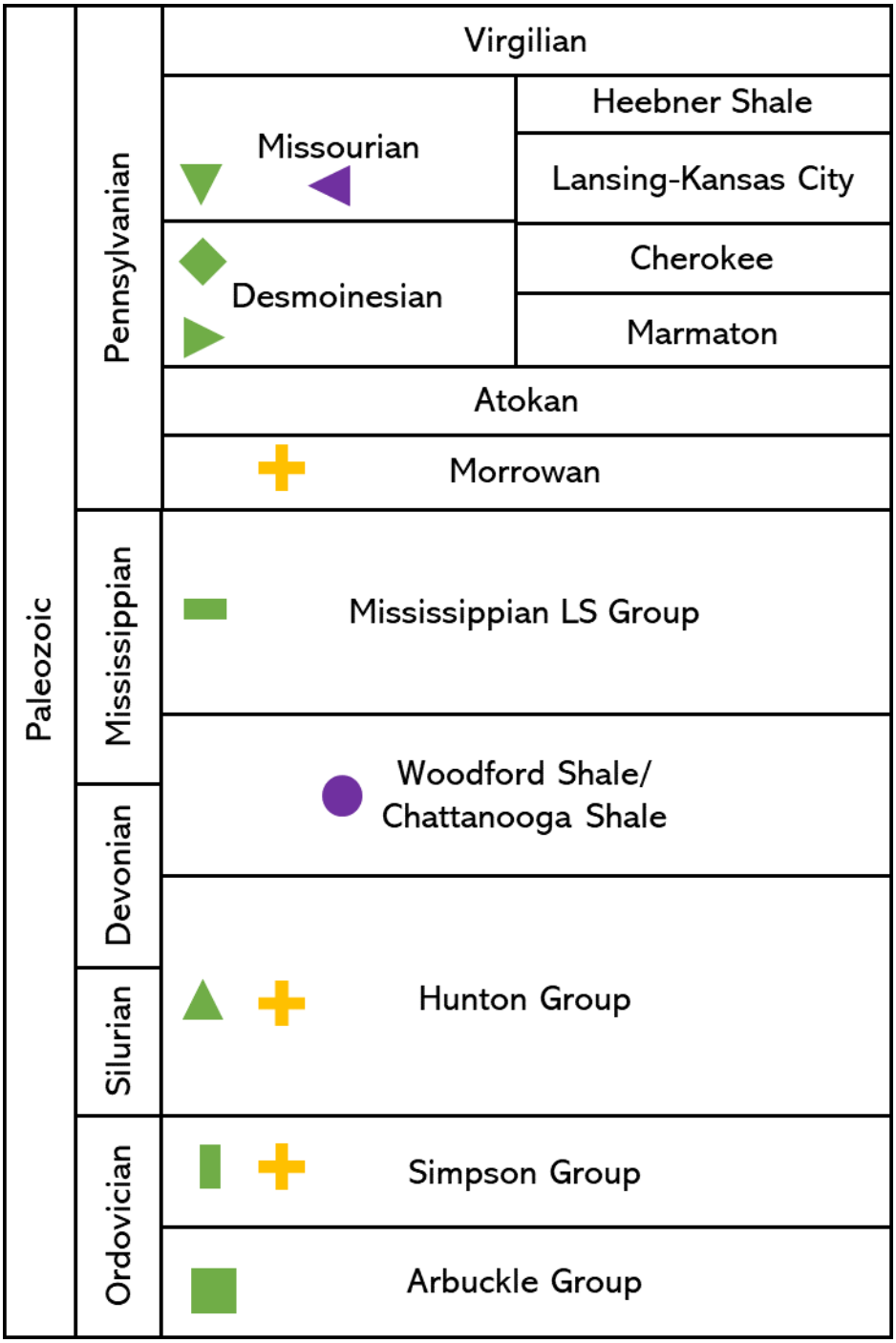

Figure 23. Location of oils and cores for this study within the general stratigraphic section that is representative of the formations in the Greater Anadarko Basin. The oils from the Hugoton Embayment are green, Pauls Valley conventional Woodford oils are yellow, and the core samples from Kansas are purple (modified from Merriam, 1963).

Hugoton Embayment Oil Sample	Sample Name	Formation	Section-Township-Range	County	State
Gates 2	HE-A1	Arbuckle	27-21S-13W	Stafford	KS
Slimmer Twin 1-X	HE-A2	Arbuckle	19-11S-16W	Ellis	KS
Burndgardt 1	HE-C1	Cherokee	26-25S-21W	Scott	KS
Herrmann 2-26	HE-C2	Cherokee	25-17S-31W	Ford	KS
Pfannenstiel 1	HE-C3	Cherokee	24-18S-24W	Ness	KS
Wieland 'A' 5	HE-C4	Cherokee	8-11S-31W	Gove	KS
Ziegebalg 1	HE-C5	Cherokee	10-14S-28W	Gove	KS
Collins 1	HE-H1	Hutton	22-26S-10E	Edwards	KS
Bowles 3-72	HE-L1	LKC	22-26S-10E	Rooks	KS
Britton Trust 1	HE-L2	LKC	25-10S-31W	Rooks	KS
Jones 2	HE-L3	LKC	25-10S-31W	Rooks	KS
Jones 3	HE-L4	LKC	22-27S-11W	Rooks	KS
Jones 4	HE-L5	LKC	3-1S-38W	Rice	KS
MM-MC-4A	HE-L6	LKC	35-17S-24W	Kiowa	KS
Odessa Field Unit 19	HE-L7	LKC	3-24S-4W	Sheridan	KS
Pyle Taylor Farms 1	HE-L8	LKC	3-17S-27W	Sheridan	KS
Schamberger 2-5	HE-L9	LKC	26-6S-28W	Rice	KS
Schroeder 1-26	HE-L10	LKC	29-19S-10W	Decatur	KS
Theodore Dueser 1	HE-L11	LKC	18-4S-27W	Decatur	KS
Vavroch Farms 1-18_C	HE-L12	LKC	18-4S-27W	Rooks	KS
Vavroch Farms 1-18_D	HE-L13	LKC	13-10S-19W	Rush	KS
Vohs 2	HE-L14	LKC	13-15S-19W	Cheyenne	KS
Wasinger 2	HE-L15	LKC	32-18S-6W	Ness	KS
Christensen 3-32	HE-F1	Marmaton	13-10S-18W	Reno	KS
Young 1-35	HE-F2	Marmaton	13-10S-18W	Lane	KS
Israel 2	HE-M1	Mississippian	13-10S-18W	Ford	KS
Joachim 1	HE-M2	Mississippian	3-9S-18W	Woods	OK
Pfannenstiel 'A' 1	HE-M3	Mississippian	3-24S-18W	Ness	KS
Pyle 1	HE-M4	Mississippian	2-28S-19W	Kiowa	KS
Stalcup-Rimbey 1	HE-M5	Mississippian	5-7S-28W	Reno	KS
Wittman 1	HE-M6	Mississippian	35-25S-21W	Ness	KS
Fritzemeir 1	HE-S1	Simpson	12-29S-12W	Stafford	KS
Hugoton Embayment Core Sample	**Sample Name**	**Formation**	**Section-Township-Range**	**County**	**State**
Huntington 22-12 A	HEC-C1	Chattanooga Core	24-18S-24W	Greenwood	KS
Huntington 22-12 B	HEC-C2	Chattanooga Core	2-28S-19W	Greenwood	KS
Bixenman 32-35 A	HEC-L1	LKC Core	2-24S-4W	Thomas	KS
Bixenman 32-35 B	HEC-L2	LKC Core	12-20S-22W	Thomas	KS
Preissner 1	HEC-L3	LKC Core	33-22S-11W	Pratt	KS
Woodford Oil Sample	**Sample Name**	**Formation**	**Section-Township-Range**	**County**	**State**
Hatcher 'C' 1	WF-B1	Bromide	28-4N-1S	Garvin	OK
Adams P 1	WF-B2	Bromide	22-3N-3W	Garvin	OK
Sharpe A 1	WF-B3	Bromide	15-3N-3W	Garvin	OK
Adams Q 1	WF-B4	Bromide	23-3N-3W	Garvin	OK
Gardenhire 'B' 1	WF-H1	Hunton	36-3N-3W	Garvin	OK
Gardenhire A 1	WF-H2	Hunton	36-3N-3W	Garvin	OK
Kay C 1	WF-H3	Hunton	22-3N-3W	Garvin	OK
Ruby Beam 1-25	WF-P1	Pennsylvanian UC	25-5N-2W	McClain	OK

Table 1. Oil and core samples from the Hugoton Embayment and oils from the conventional Woodford, with their associated formation, location, and county name, that have been used in this study.

3.2. Fractionation Methods

The method used for fractionating organic matter, either from crude oil or from source rocks, is illustrated in **Fig. 24** and is explained in greater detail below.

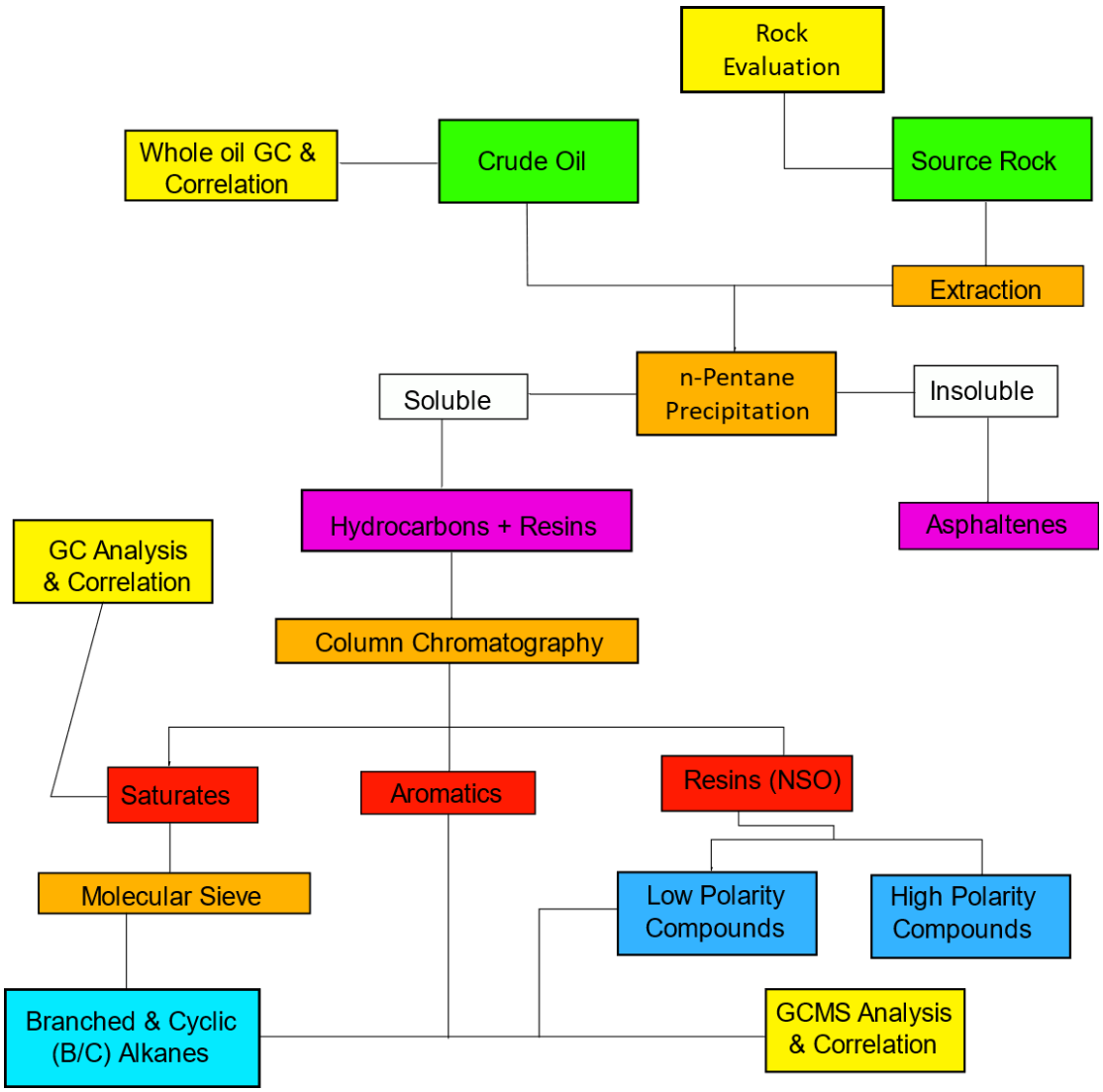

Figure 24. Schematic fractionation method starting from either crude oils or source rocks (green) showing the various steps (orange), and fractions (white, pink, red, and blue) as well as the different types of analyses used on the different fractions (yellow) (modified from Romero and Philp, 2012).

Rock-Eval Pyrolysis and TOC

Rock-Eval pyrolysis (**Fig. 25**) and total organic carbon (TOC) measurements can provide screening data related to thermal maturity and generation potential of a rock (Peters, 1986). In this study, one gram of each of the five core samples was sent to the GeoMark Research™ facility in Houston, TX for Rock-Eval and LECO TOC measurements. LECO TOC measurements are done

by crushing the sample into a fine powder and dissolving it in HCl to remove any carbonate material and then combusting 1mg of the crushed rock in a LECO TOC analyzer at 1000ºC to yield the weight percent (wt.%) of the total organic carbon in the sample. The Rock-Eval pyrolysis measurements were taken from the remaining sample (~90mg). The measurements obtained from Rock-Eval are S1 – produced hydrocarbons, S2 – potential hydrocarbons, and S3 – the amount (in mg) of carbon dioxide (CO_2) produced from kerogen due to thermal cracking simulated in the programmed pyrolysis, up to 390 ºC (Peters, 1986; Connock, 2015; Pearson, 2016). Other measurements that can be calculated include vitrinite reflectance from the T_{max} (T_{max} %Rc), the hydrogen and oxygen index (S2*100/TOC and S3*100/TOC), and production index (S1/[S1+S2]; Jones, 2017).

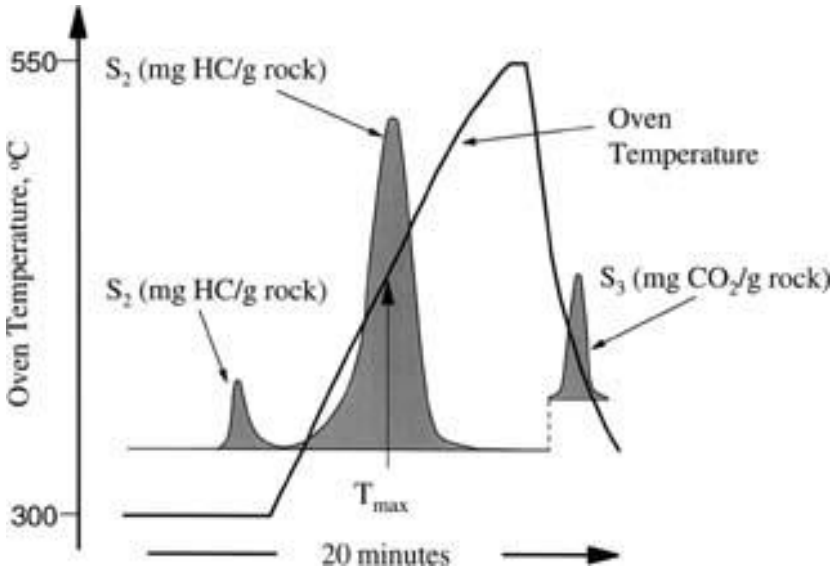

Figure 25. Chromatogram from Rock-Eval pyrolysis (Peters and Cassa, 1994).

Source Rock Extraction

The five source rock samples were crushed into a fine powder (~50g) and then extracted using a soxhlet extraction system to obtain the extractable organic matter (EOM). The soxhlet

system, including the thimble and glass wool, was cleaned using 1:1 dichloromethane(DCM):methanol solution (350ml). After cleaning, the powdered rock was added to the thimble and the glass wool was packed on top. The solvent was replaced with a fresh 1:1 DCM:methanol solution (350ml), and the extraction process was run for 24 hours to extract the organic matter. The solvent in the 500ml round bottom flask was removed using a rotary evaporator and the EOM from the soxhlet extraction is transferred to a weighed 4ml vial, dried under nitrogen, and weighed. The EOM was fractionated using the same deasphalting and fractionation methods that are used for oils (method modified from Connock, 2015.)

Bitumen Fractionation

A portion of each oil sample was removed from its collection container and stored in a refrigerator to preserve the volatile hydrocarbons in the oil. An aliquot of the oil sample (~450mg) was deasphaltened. The deasphalting process requires the aliquot to be put into a 50ml glass centrifuge tube with the excess volume filled with n-pentane. The centrifuge tube was put in a freezer for 1 hour and then centrifuged at 2500 RPM for 20 minutes. The asphaltenes precipitated to the bottom of the centrifuge tube and the maltene fraction remained in the n-pentane. The n-pentane solution was transferred to a 50ml round bottom flask and roto-vaped, the dried maltene fraction was transferred to a weighed 4ml vial. The asphaltene fraction was transferred from the centrifuge tube to a weighed 4ml vial using DCM. Both the maltene and asphaltene fractions were dried under nitrogen and weighed.

Column Chromatography

A 35mg portion of the maltene fraction was transferred to a 4ml vial for fractionation by column chromatography. A 50ml glass column with a valve was packed with glass wool and activated alumina (8g) and cleaned with hexane (15ml). The maltene fraction was loaded onto the alumina and the saturate fraction eluted with hexane (10ml) and collected in a 50ml round bottom flask. The aromatic fraction was eluted with hexane:dichloromethane (7:3; 16ml) and collected in a 50ml round bottom flask. The resins (NSOs) were eluted with DCM:methanol (1:1; 16ml) and collected in a 50ml round bottom flask. The three fractions were roto-vaped, transferred to weighed 4ml vials, dried under nitrogen, and weighed.

Molecular Sieving

Half of the saturate fraction was molecularly sieved to remove the n-alkanes using a pipette packed with glass wool and activated S115 zeolite (~5cm). The column was cleaned with n-pentane and then the saturate fraction was loaded onto the column and the branched and cyclic fraction (B/C) was eluted with n-pentane (2ml) and collected into a weighed 4ml vial, dried under nitrogen, and weighed. This fraction was diluted to a 4mg/ml solution with DCM and analyzed on the GCMS.

Nitrogen Compound Separation

Half of the NSO was dissolved in hexane and adsorbed on to silicic acid hydrate powder (0.5g) and the solvent allowed to evaporate overnight in a 4ml vial covered in foil. A 50ml glass column was filled with silicic acid hydrate powder (2g) and packed using hexane. The adsorbed NSOs were transferred into the column and the low polarity compounds (LPC) were eluted with

hexane:DCM (85:15; 50ml). The high polarity compounds (HPC) were eluted with DCM:methanol (95:5; 50ml). The LPCs were dried, weighed, and diluted to 4mg/1ml with DCM to elute carbazole and the benzocarbazoles on the GCMS (method modified from Larter et al., 1981 and Liu, 2015).

3.3. Analytical Methods

Whole Oil Gas Chromatography (WOGC)

Whole oil samples were initially analyzed by a whole oil GC (WOGC) in order to determine the distribution of the light hydrocarbons in the C_7 range. This process was done using the Agilent 6890 series gas chromatography with split capillary injection and a 100m x 0.25mm fused silica capillary column coated with a 0.5µm liquid film. The needle that was used to inject the whole oil into the GC was first washed in pentane and then heated to 300 ºC to remove the pentane from the needle and then 0.3µm of whole oil was injected into the GC. The helium carrier gas flow rate was 0.5ml/minute and the temperature program ramped up first to 130ºC at a rate of 2ºC/minute and then to 300ºC at a rate of 4ºC/minute with an isothermal period of 26 minutes which made the total run time 115 minutes. The GC was equipped with a flame ionization detector (FID) set at 310ºC using GC ChemStation software. Through this process, the C_7 compounds were resolved on the GC chromatogram. Unfortunately, a number of the samples could not be analyzed on the WOGC due to poor preservation where samples lost most of their light hydrocarbons.

Gas Chromatography (GC)

Whole oils, saturate and aromatic fractions from oils and rock extracts were initially analyzed by gas chromatography. The whole oils were diluted to 3mg/ml using DCM for sample screening and the saturate and aromatic fractions were diluted to 4mg/ml using DCM. For the analyses, 1µl of each fraction or whole oil was injected into the Agilent 6890 series gas chromatography equipped with splitless capillary injector and a 100m x 0.25mm fused silica capillary column coated with a 0.5µm liquid film (J&W Scientific 122-5544G DB-5MS). The inlet was set at 300ºC at the time of injection and the oven was heated to an initial 40ºC and held for 1.5 minutes. The helium carrier gas flow rate was 0.5ml/minute and the temperature program ramped up to 300ºC at a rate of 4ºC/minute. The isothermal period was 34 minutes which made the total run time 100.5 minutes. The GC was equipped with a flame ionization detector (FID) set at 310ºC using GC ChemStation software.

Gas Chromatography - Mass Spectrometry (GCMS)

The fractions analyzed using GCMS include the whole maltene fraction, the B/C fraction, aromatic fraction, and LPCs. All fractions were diluted to 4mg/ml with DCM and injected into the GCMS for peak identification and biomarker distributions which was used for oil/oil and oil/source rock correlations as well as to obtain information on the source input, depositional history, and thermal maturity from the oils. The GCMS system was an Agilent Technologies 7890A gas chromatograph equipped with a DB-5MS silica capillary column (60m x 250µm x 0.25µm) attached to an Agilent Technologies 5975C mass spectrometer. The mass spectrometer

operated in the single-stage mode and the ion source operated in electron impact mode with energy of 70eV.

The B/C hydrocarbons and aromatic hydrocarbons were analyzed using a GC program that, after injection, held the oven at 40ºC for 1.5 minutes and was then heated to 300ºC at 4ºC/minute and held for 34 minutes with a total run time of 100.5 minutes. The flow rate was 1.4ml/minute in splitless mode. The LPCs were analyzed using a similar method, with an isothermal period of 24 minutes. The maltenes were analyzed using a method where the oven was held at 40ºC for 1.5 minutes and programmed to 315˚C at 4ºC/minute and held at 315ºC for 50 minutes for a total run time of 120 minutes.

Gas Chromatography – Mass Spectrometry-Mass Spectrometry (GCMS-MS)

The GCMS-MS used selected samples to assist in the identification of specific compounds that were initially identified by GCMS on a Thermo Scientific TRACE 1310 GC with an 8000 Triple Quadrupole MS, similar to the GCMS in the previous section. The GCMS-MS uses a DB-5MS fused silica capillary column (60m x 250µm x 0.25µm) and the method uses helium gas as the carrier gas at a flow rate of 1.4ml/minute. After injection, the oven temperature was held at 40ºC for 1.5 minutes with a 4ºC/minute ramp-up to 300ºC and an isothermal hold for 34 minutes for a total run time of 100.5 minutes. The parent/daughter relationships that were analyzed at a scan time of 0.025 seconds were those for sterane identification: 358 → 217, 372 → 217, 386 → 217, 400 → 217, and 414 → 217. The ion source for the parent/daughter ions in the electron impact mode with an electron energy of 9eV and was set to a temperature of 250ºC (method modified from Wang, 2016).

Bulk Isotope Analysis

Saturate and aromatic bulk isotope data from the Hugoton Embayment were used to compare oil samples in this study to previously analyzed Woodford and other Devonian oils (Lewan, 1983; Wang, 2016). The fractions of the three samples were measured out to 250µg and then loaded on to an autosampler and analyzed by gas chromatography-isotope ratio mass spectrometry (GC-IRMS), the Costech 4010EA and Thermo Delta V Plus isotope mass spectrometer (Wang, 2016; Pedentchouk and Turich, 2017). Before entering the GC, the samples are heated in a furnace reactor packed with the reagents silvered cobalt oxide and chromium oxide at a set temperature of 1000ºC for flash combustion of organic matter (Philp, 2007; Wang, 2016). The remaining CO_2 is then pushed through a heat reduction column packed with reductive copper wire to drop the temperature down to 650ºC and analyzed in by GC where the temperature was set to 55 ºC and the helium flow rate was set to 100ml/min (Wang, 2016). The relative proportions of $^{13}CO_2$ and $^{12}CO_2$ were measured in the IRMS in and converted to $\delta^{13}C$ values using the Vienna Pee Dee Belemnite standard for both the saturate and aromatic fractions (Philp, 2007; Wang, 2016).

Biomarker Identification

Biomarker data from the GCMS was shown using the Qualitative Analysis Navigator (B.08.00) from MassHunter Workstation Software. This software displayed compound peaks that were later identified and integrated through the use of:

- [Canipa-Morales et al., 2003]
- [Cassani et al., 1987]
- [Clegg et al., 1998]
- [Hays et al., 2007]
- [Peters and Fowler, 2002]
- [Peters and Moldowan, 1991]
- [Pu et al., 1990]
- [Wang and Fingas, 1995]

among others. The publications on specific families of compounds showed and identified the peaks of biomarkers and other compounds that were used for oil/oil and oil/source rock correlation. The GCMS-MS was also used to confirm the sterane biomarkers by using parent/daughter relationships and the available literature.

CHAPTER 4: RESULTS AND DISCUSSION

4.1. Whole Oil Geochemistry

In this study, seventeen whole oil samples were characterized by WOGC (**APPX. IVA**). These samples had been preserved in air-tight glass containers and were refrigerated after collection and hence met the criteria to preserve the C_7 hydrocarbons and are amenable to WOGC. In the whole oil chromatograms, sixteen C_7 compounds shown in **Fig. 26** (**Table 2**) were identified and integrated. In many of the oils that were run, the samples show a very low abundance of toluene (peak P) compared to conventional Woodford oils. This low abundance is most likely a result of water washing, either in the reservoir or during the migration process (Burrus and Hatch, 1989; Mango, 1997).

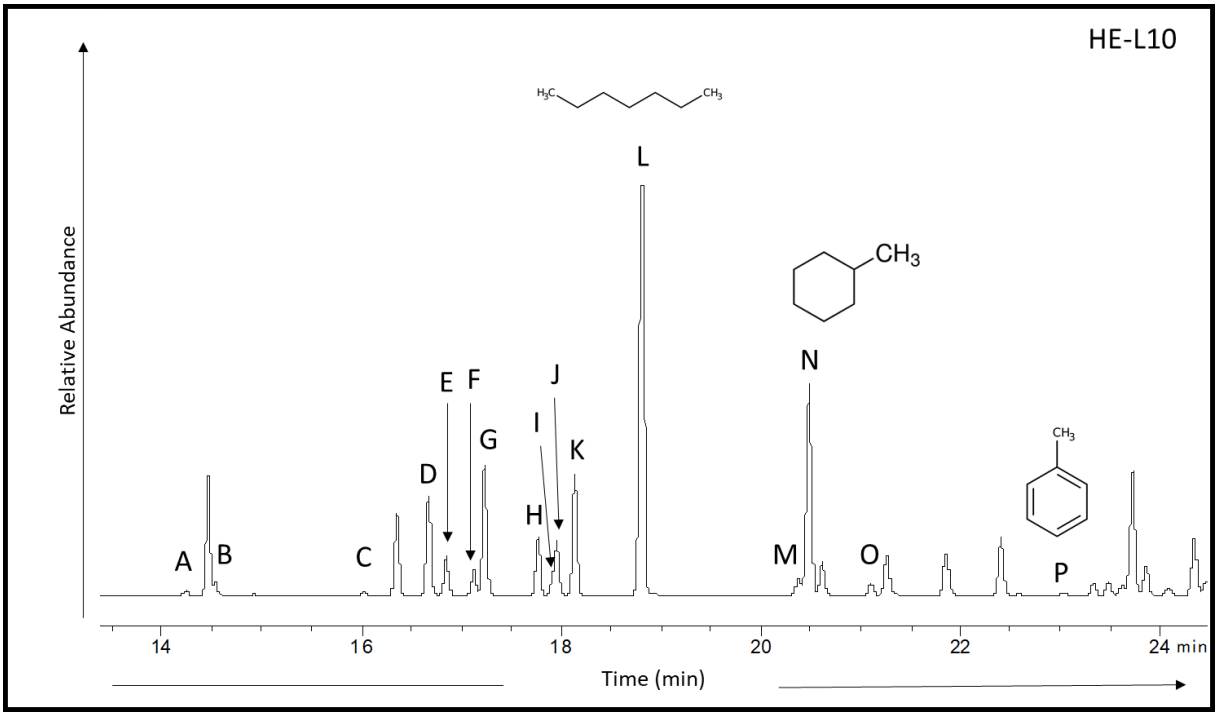

Figure 26. Whole oil chromatogram of HE-L10 showing the C_7 peaks (**APPX. II**; Canipa-Morales et al., 2003).

Peak	Compound	Abbreviation
A	2,2-Dimethylpentane	2,2-DMP
B	2,4-Dimethylpentane	2,4-DMP
C	3,3-Dimethylpentane	3,3-DMP
D	2-Methylhexane	2-MH
E	2,3-Dimethylpentane	2,3-DMP
F	1,1-Dimethylcyclopentane	1,1-DMCP
G	3-Methylhexane	3-MH
H	1c3-Dimethylcyclopentane	1c3-DMCP
I	3-Ethylpentane	3-EP
J	1t3-Dimethylcyclopentane	1t3-DMCP
K	1t2-Dimethylcyclopentane	1t2-DMCP
L	Normal Heptane	n-C7
M	1c2-Dimethylcyclopentane	1c2-DMCP
N	Methylcyclohexane	MCH
O	Ethylcyclopentane + 2,5-Dimethylcyclopentane	ECP+2,5-DMCP
P	Toluene	TOL

Table 2. C_7 peaks identification by name and abbreviation (Canipa-Morales et al., 2003).

When plotting the paraffinicity (n-heptane/methylcyclohexane) against aromaticity (toluene/n-heptane) normal, pristine oil samples would be seen in the grey area of **Fig. 27**. The majority of the oils in **Fig. 27** are either affected by water washing or evaporative fractionation. Evaporative fractionation, proposed by Thompson in 1987, is defined as the separation of oil to condensates/gases in the subsurface, while water washing is the removal of light aromatic hydrocarbons by migration (Thompson, 1987; Mango, 1997). It is more likely that these oils are showing the effects of water washing because their aromaticity ratio has been severely diminished (values found in **Table 3**; **APPX. I**) and the samples appear to follow a water washing trend, blue area, rather than a maturity trend. Whole oil samples may have also been affected by biodegradation (bottom left corner) or maturity, as seen on the maturity trendline.

Sample	Aromaticity Ratio	Paraffinicity Ratio
HE-A1	0.06	1.00
HE-A2	0.00	0.98
HE-C5	0.00	0.69
HE-H1	0.01	0.52
HE-L1	0.00	0.21
HE-L6	0.29	0.04
HE-L7	0.91	1.59
HE-L9	0.00	1.65
HE-L10	0.03	1.85
HE-L11	0.03	1.40
HE-L12	0.00	1.81
HE-L13	0.00	0.74
HE-L14	0.03	1.22
HE-M2	0.27	8.65
HE-M5	0.07	1.27
HE-M6	0.00	1.03
HE-S1	0.05	1.32

Table 3. Aromaticity and paraffinicity ratios calculated from whole oil chromatograms.

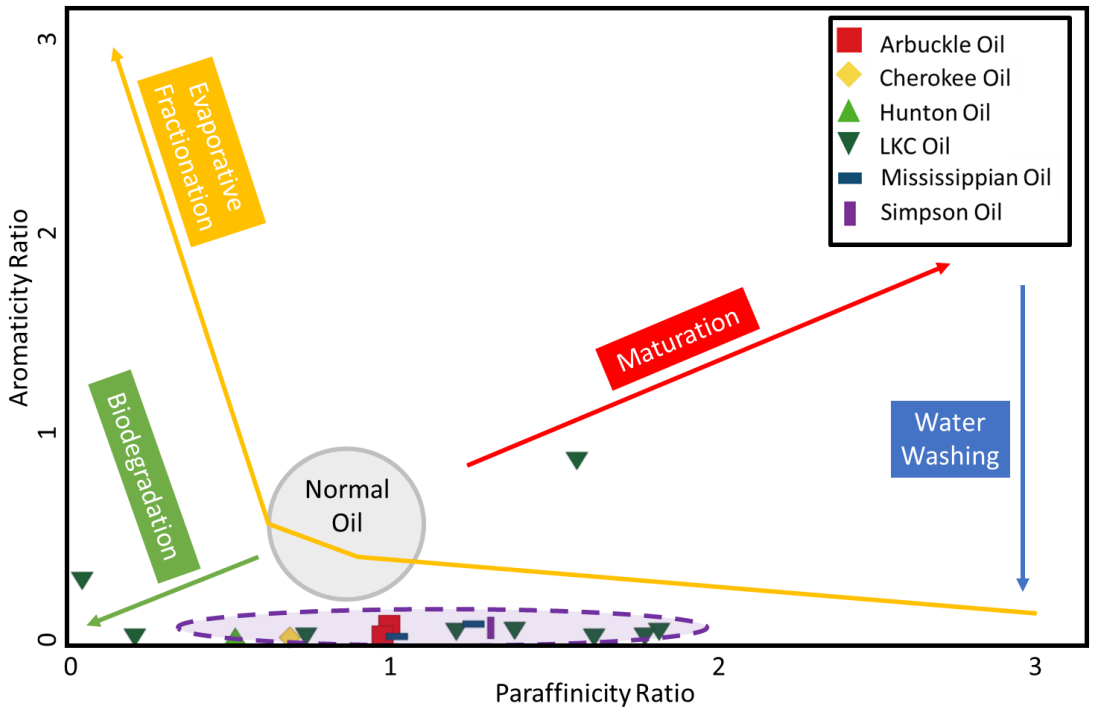

Figure 27. Aromaticity (toluene/n-heptane; **APPX. I**) verses paraffinicity (n-heptane/methylcyclohexane; **APPX. I**) are used to determine the effects on a normal oil. This plot shows that many of the oils have been strongly affected by water washing, as is seen by the low aromaticity in the purple area (modified from Thompson, 1987; Hakimi and Al-Sufi, 2018).

4.2. Compositional Geochemistry

After whole oil analysis, the oil was fractionated into: asphaltenes and maltenes (saturates, aromatics, and NSOs). By looking at the relative proportions of saturates, aromatics, NSOs, and asphaltene fractions for the oils in this study, the effects of migration and expulsion can be seen by the enrichment or depletion of these fractions as these four subdivisions of the whole oil work together which is able to indicate some correlation between oils (Tissot and Welte, 1984; Hunt, 1996). When there is an increase in the NSO+asphaltene composition, it is likely that there is some type of biodegradation occurring that degrades the existing hydrocarbons (Tissot and Welte, 1984). Variations in the composition of saturates, aromatics, NSOs, and asphaltene fractions is able to separate oils into genetic-based families and may also infer thermal maturity, depositional environment, and biodegradation as the changes in composition (Tissot and Welte, 1984; El-Sabagh et al., 2015).

The average values of the thirty-five fractionated oil samples show that saturates makeup 69.4% of the overall composition; aromatics makeup 20.8%; NSOs + asphaltenes makeup 9.8%. The compositional data for all of the oils (**Table 4**) are plotted on a ternary diagram based on earlier work by Tissot and Welte (1984) that identifies a compositional range for normal, aromatic and degraded oils. In the ternary diagram (**Fig. 28**), the Hugoton Embayment oils (circles) and conventional Woodford oils (diamonds) plot near the normal range for crude oils, as defined by Tissot and Welte (1984) showing that they are enriched in saturate and aromatic hydrocarbons (Hunt, 1996), as was expected. Overall, the crude oil samples cluster together and would appear to be related (Tissot and Welte, 1984).

The rock extracts were not plotted on the compositional ternary diagram because the hydrocarbons would have shown an enrichment in the NSO and asphaltene compounds. This is because the hydrocarbons that were extracted from the core samples (rock extracts) never left the source rock due to their low solubility, therefore they still retain all the heavier compounds (Tissot and Welte, 1984; Hunt, 1996).

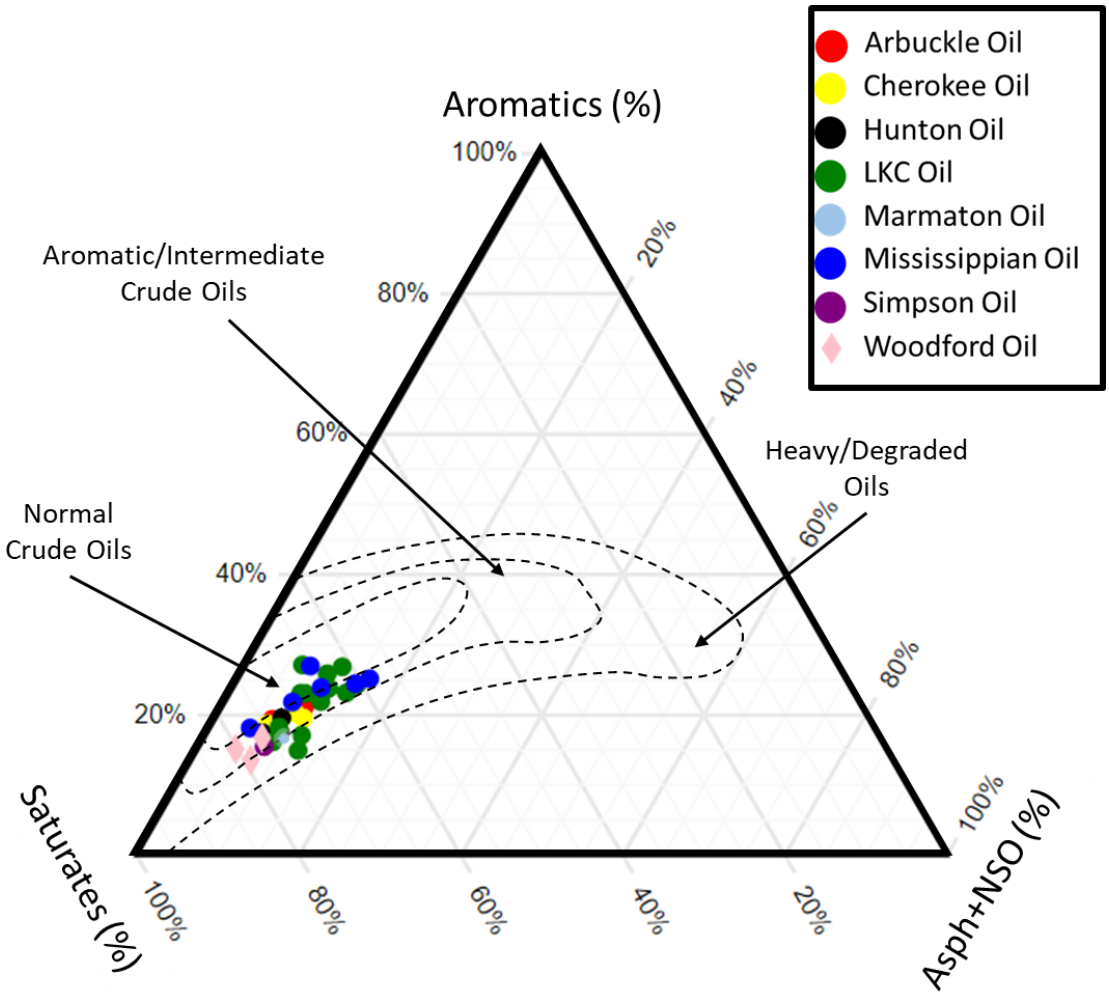

Figure 28. A ternary diagram modified from Tissot and Welte (1984) showing that the relative composition of the crude oils characterized in this study plot close to the normal crude oil zone. Isofrequency contour lines were determined from a study of 636 crude oil samples: oils in the normal crude oil contour are enriched in saturate compounds, oils in the aromatic crude oil contour are enriched in aromatic compounds when compared to the normal oils, and the oils in the heavy oil contour indicated biodegraded oils enriched in NSO and asphaltene compounds (Tissot and Welte, 1984).

Sample	Saturate (wt. %)	Aromatic (wt. %)	NSO+Asphaltene (wt. %)
HE-A1	73.6%	19.4%	7.0%
HE-A2	68.6%	21.2%	10.1%
HE-C1	70.3%	20.3%	9.5%
HE-C2	64.4%	24.3%	11.3%
HE-C3	75.0%	17.2%	7.8%
HE-C4	69.6%	19.6%	10.8%
HE-C5	74.5%	18.7%	6.8%
HE-F1	75.8%	17.5%	6.7%
HE-F2	73.5%	17.6%	8.9%
HE-H1	72.3%	19.6%	8.1%
HE-L1	73.3%	18.3%	8.4%
HE-L2	61.2%	26.9%	11.9%
HE-L3	62.5%	23.2%	14.3%
HE-L4	64.9%	23.6%	11.5%
HE-L5	60.7%	24.3%	15.0%
HE-L6	64.4%	23.8%	11.8%
HE-L7	71.1%	17.1%	11.8%
HE-L8	72.6%	15.0%	12.4%
HE-L9	67.7%	23.1%	9.2%
HE-L10	68.2%	23.1%	8.7%
HE-L11	75.1%	16.2%	8.7%
HE-L12	66.0%	27.1%	6.9%
HE-L13	63.5%	25.9%	10.6%
HE-L14	65.6%	23.3%	11.1%
HE-L15	66.3%	21.9%	11.8%
HE-M1	65.1%	27.0%	8.0%
HE-M2	58.7%	25.2%	16.2%
HE-M3	65.3%	23.9%	10.8%
HE-M4	60.8%	24.5%	14.8%
HE-M5	69.9%	21.8%	8.3%
HE-M6	76.9%	18.1%	4.9%
HE-S1	76.5%	15.5%	8.0%
WF-B1	76.1%	16.8%	7.1%
WF-H1	79.1%	13.6%	7.3%
WF-P1	80.2%	15.1%	4.6%

Table 4. Values of the saturate, aromatic, and NSO + asphaltene fractionations of oils as percentage of the whole oil.

4.3. Biomarker Analysis

Some of the main saturate biomarkers and diagnostic aromatic compounds were mentioned in **Chapter 1**. In this section, these biomarkers, aromatic compounds, and heteroatomic molecules were used to evaluate and correlate the depositional environment, organic matter source, source rock lithology, water column stratification, thermal maturity, and migration of Woodford oils into the Greater Anadarko Basin (biomarker ratios used in this study are found in APPX).

Depositional Environment and Organic Matter Source

The first molecules analyzed were the n-alkanes, n-C_{17} and n-C_{18}, and isoprenoids, pristane and phytane (**APPX. II**) to determine the redox conditions of the depositional environment during the time of deposition (**Fig. 29**). The ratio of pristane/n-C_{17}, has an average of 0.58 and ranges from 0.13 to 1.65 and the ratio of phytane/n-C_{18} shows similar values of 0.16 to 1.34 with an average of 0.51 (**Table 5**; **APPX. I**).

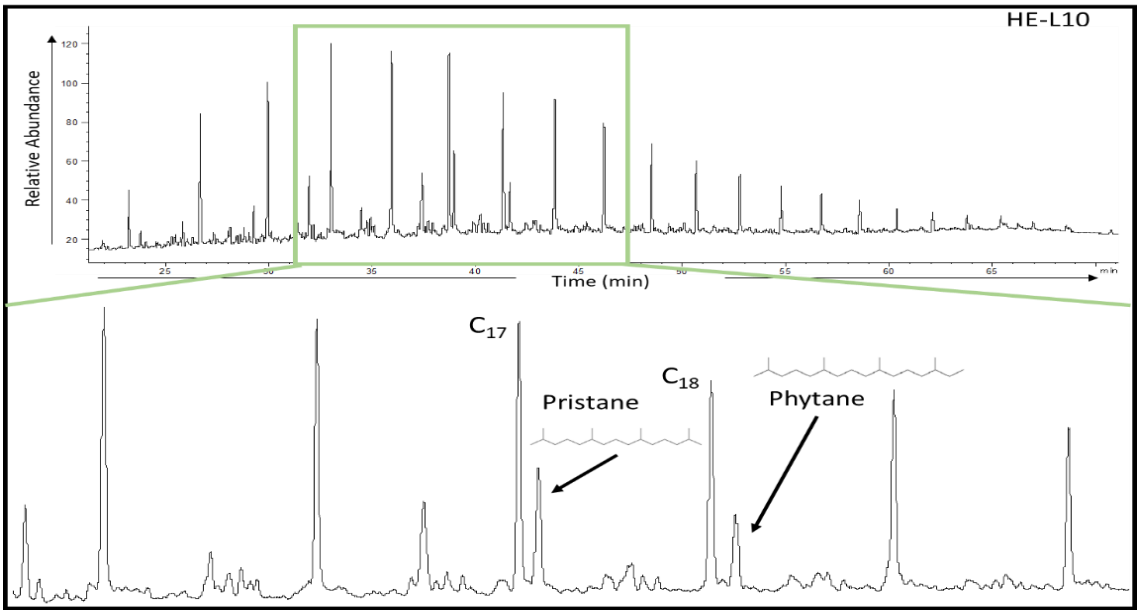

Figure 29. Saturate GC chromatogram of HE-L10 identifying n-C_{17}, n-C_{18}, pristane, and phytane (**APPX. II**).

Sample	Pr/C_{17}	Ph/C_{18}	Pr/Ph
HE-A1	0.44	0.41	1.33
HE-A2	0.68	0.75	1.27
HE-C1	0.52	0.49	1.23
HE-C2	0.64	0.52	1.60
HE-C3	0.51	0.42	1.19
HE-C4	0.52	0.44	1.35
HE-C5	0.52	0.44	1.43
HE-F1	0.55	0.43	1.47
HE-F2	0.62	0.44	1.23
HE-H1	0.32	0.37	1.51
HE-L1	0.65	0.47	1.43
HE-L2	0.53	0.43	1.50
HE-L3	0.48	0.43	1.41
HE-L4	0.51	0.46	1.38
HE-L5	0.58	0.52	1.42
HE-L6	0.47	0.46	1.51
HE-L7	1.49	1.17	1.12
HE-L8	1.65	1.34	1.18
HE-L9	0.52	0.46	1.50
HE-L10	0.52	0.44	1.48
HE-L11	0.37	0.42	1.39
HE-L12	0.50	0.44	1.54
HE-L13	0.13	0.16	1.02
HE-L14	0.48	0.54	1.18
HE-L15	0.50	0.37	1.30
HE-M1	0.48	0.40	1.37
HE-M2	0.46	0.44	1.36
HE-M3	0.60	0.44	1.15
HE-M4	0.67	0.58	1.19
HE-M5	0.53	0.46	1.51
HE-M6	0.50	0.43	1.37
HE-S1	0.37	0.45	1.21
HEC-C1	1.16	0.68	2.14
HEC-C2	1.19	1.01	1.66
HEC-L1	0.73	0.83	1.31
HEC-L2	0.42	0.56	1.50
HEC-L3	0.49	0.53	2.63
WF-B1	0.34	0.40	1.17
WF-B2	0.40	0.39	0.39
WF-B3	0.47	0.38	0.72
WF-B4	0.50	0.43	0.73
WF-H1	0.39	0.42	1.16
WF-H2	0.54	0.50	0.89
WF-H3	0.59	0.53	0.35
WF-P1	0.40	0.41	1.32

Table 5. Values of n-C_{17}, n-C_{18}, pristane, and phytane ratios determined from saturate GC chromatograms used for inferring the depositional environment (**APPX. I**).

The ratios of pristane/n-C_{17} and phytane/n-C_{18} are illustrated in **Fig. 30**, and they show that most of the samples, the Woodford oils and the oils from the Hugoton Embayment, have mixed marine organic matter source and the redox conditions during deposition were that of a transitional to reducing environment. The trend here, highlighted with a red circle in **Fig. 30**, shows the depositional environment changing from a transitional to reducing environment is likely due to the reduction of phytols to phytane in reducing/anoxic environments, particularly in the anaerobic stages of organic matter decay (Powell and McKirdy, 1973). This trend correlates with what is known about the depositional environment of the Woodford Shale during the Devonian/Mississippian (Romero and Philp, 2012). However, there are two Lansing-Kansas City oils from the Hugoton Embayment that fall outside of the main grouping of oils, seen in the blue circle in **Fig. 30**, which appear to have been affected by biodegradation, possibly from groundwater movement through the formation (Evans, 2011).

Regular steranes **(Fig. 31**; **Table 6**) reflect the organic matter input which is mainly derived from eukaryotes (higher plants or algae) and occasionally prokaryotes (bacteria) and are extremely useful as a correlation parameter (Peters et al., 2004b). The most common visualization of regular steranes is through the use of a ternary diagram. In the ternary diagram, the C_{27} sterane (cholestane, **APPX. II**) is indicative of an open marine environment with phytoplankton as the main organic matter input (Huang and Meinschen, 1979; Waples and Machihara, 1990), the C_{28} sterane (ergostane, **APPX. II**) indicates algae from a lacustrine environment (Huang and Meinschen, 1979; Kirson and Glotter, 1981; van Koeverden et al., 2010), and the C_{29} sterane (stigmastane, **APPX. II**) could be indicative of either terrestrial higher plant input (Huang and Meinschen, 1979) or cyanobacteria, marine blue-green algae (Fowler and Douglas, 1984; Brocks et al., 2017; Summons and Erwin, 2018). In looking at the C_{29} sterane, it would not have a higher plant input

as higher plants began to evolve in the Devonian but were not widespread until the Mississippian (Volkman, 1986; Dahl et al., 2010) and therefore the C_{29} steranes, in this case, should not be present in high quantities unless they were derived from an algal source (Volkman, 1986; Waples and Machihara, 1990).

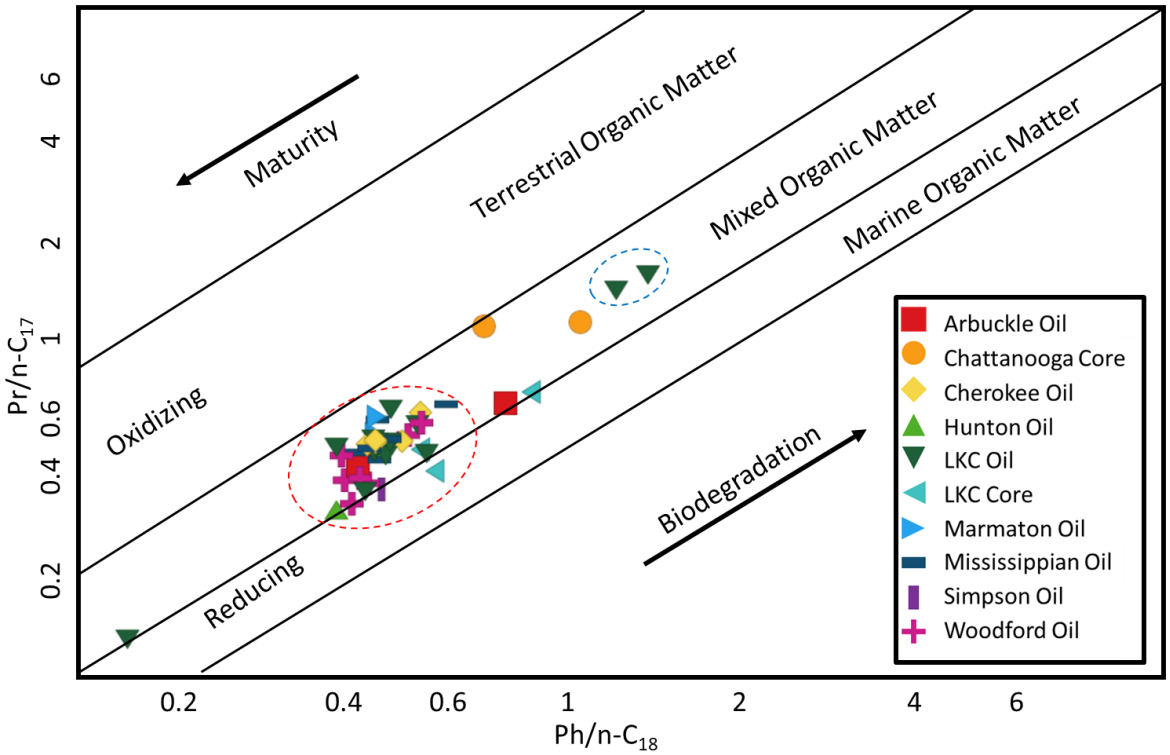

Figure 30. Redox conditions of most of the oils in the Hugoton Embayment group well with the conventional Woodford oils (red outline) and plot in the mixed organic matter and show a mixed to reducing environment. The extracts from core samples in this study are also plotted here and show a mixed organic matter input (modified from Shanmugam, 1985; **APPX. I**).

The ternary diagram of these oil and extract samples is seen in **Fig. 32** (value in **Table 7**), there is an elevated abundance of C_{29} steranes (with an average of 48.2%) – indicative of marine blue-green algae input as the main organic matter (Volkman, 1986). The low values of the C_{28} sterane, averaging 22.2%, indicate low or no terrigenous or lacustrine organic matter and the relatively high concentration of C_{27} steranes, 29.5%, indicates a planktonic organic matter from an

open marine environment. This ternary diagram shows that the organic matter is composed mainly of C_{29} steranes indicating marine algae and it does not have many characteristics of an open marine environment. This strongly correlates with what was seen in **Fig. 30**, where the organic matter is mixed to marine and was deposited in a mixed to slightly reducing environment.

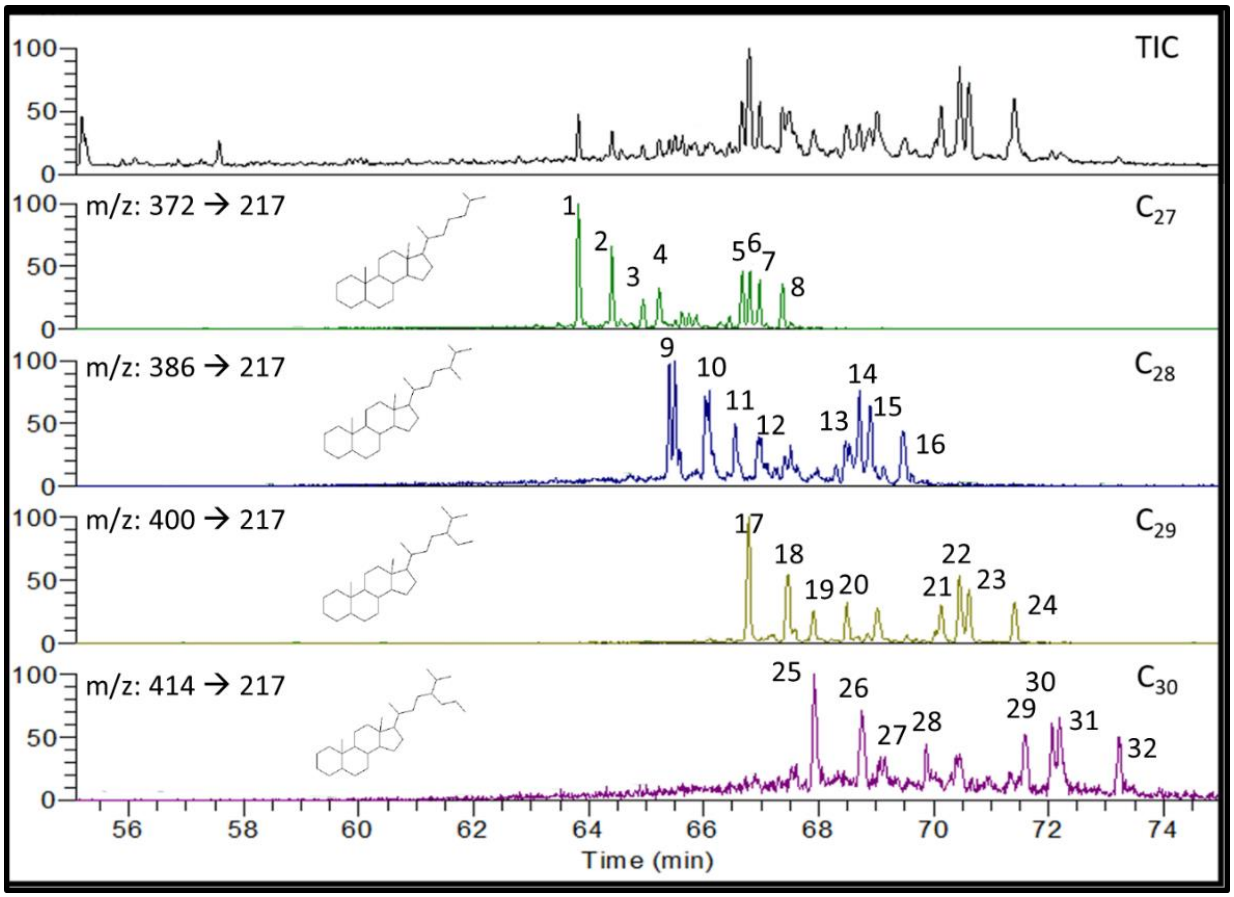

Figure 31. Regular sterane distribution of HE-L5. The top panel, the total ion chromatogram (TIC), shows the entire distribution of regular steranes. The descending panels show the C_{27}, C_{28}, C_{29}, and C_{30} steranes (**APPX. II**) from parent-daughter relationships on the GCMS-MS.

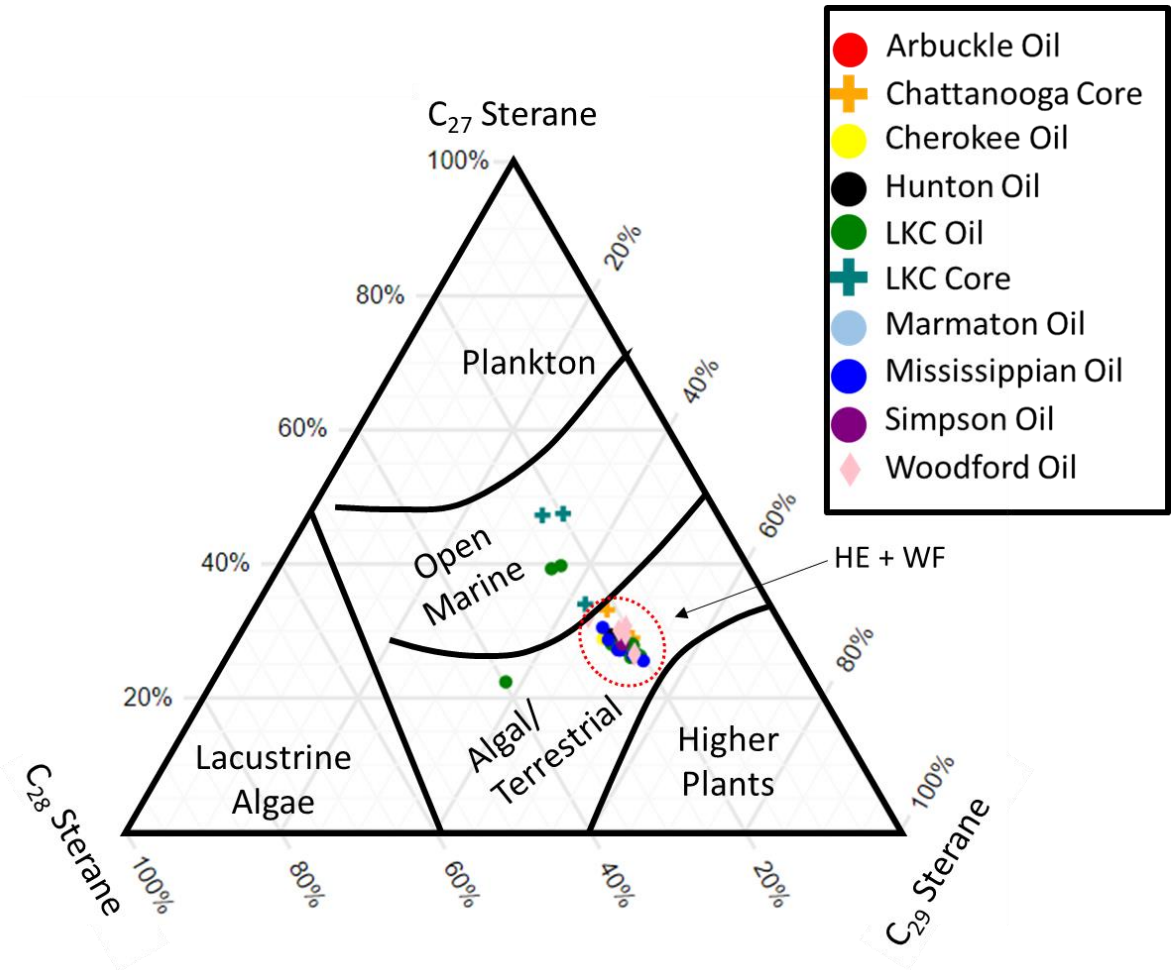

Figure 32. Ternary plot showing Woodford and Hugoton Embayment oils and rock extracts enriched in C_{29} steranes which indicates that the organic matter input is a marine algae; (HE) Hugoton Embayment oil; (WF) Woodford Oil (Volkman, 1986; Wang, 2016; plot modified from Moldowan et al., 1985).

Peak Number	Peak Identification
1	13β,17α-Diacholestane 20S
2	13β,17α-Diacholestane 20R
3	13α,17β-Diacholestane 20S
4	13α,17β-Diacholestane 20R
5	5α,14α,17α-Cholestane 20S
6	5α,14β,17β-Cholestane 20R
7	5α,14β,17β-Cholestane 20S
8	5α,14α,17α-Cholestane 20R
9	13β,17α-Diaergostane 20S
10	13β,17α-Diaergostane 20R
11	13α,17β-Diaergostan 20S
12	13α,17β-Diaergostane 20R
13	5α,14α,17α-Ergostane 20S
14	5α,14β,17β-Ergostane 20R
15	5α,14β,17β-Ergostane 20S
16	5α,14α,17α-Ergostane 20R
17	13β,17α-Diastigmastane 20S
18	13β,17α-Diastigmastane 20R
19	13α,17β-Diastigmastane 20S
20	13α,17β-Diastigmastane 20R
21	5α,14α,17α-Stigmastane 20S
22	5α,14β,17β-Stigmastane 20R
23	5α,14β,17β-Stigmastane 20S
24	5α,14α,17α-Stigmastane 20R
25	C30 13β,17α-Diasterane 20S
26	C30 13β,17α-Diasterane 20R
27	C30 13α,17β-Diasterane 20S
28	C30 13α,17β-Diasterane 20R
29	C30 5α,14α,17α-24-n-Propylcholestane 20S
30	C_{30} 5α,14β,17β-24-n-Propylcholestane 20R
31	C_{30} 5α,14β,17β-24-n-Propylcholestane 20S
32	C_{30} 5α,14α,17α-24-n-Propylcholestane 20R

Table 6. Peak identification of steranes found above in **Fig. 31**.

Sample	%C27	%C28	%C29
HE-A1	27.36	21.81	50.84
HE-A2	26.82	21.47	51.70
HE-C1	29.12	22.52	48.35
HE-C2	29.42	21.83	48.75
HE-C3	27.51	23.03	49.46
HE-C4	28.44	21.54	50.02
HE-C5	28.85	23.91	47.24
HE-F1	27.69	22.26	50.06
HE-F2	28.02	22.66	49.32
HE-H1	29.45	22.64	47.92
HE-L1	28.01	23.26	48.73
HE-L2	26.29	20.41	53.31
HE-L3	27.68	20.89	51.43
HE-L4	27.85	20.54	51.61
HE-L5	26.46	20.79	52.76
HE-L6	27.37	20.83	51.80
HE-L7	39.28	25.37	35.34
HE-L8	39.73	23.93	36.33
HE-L9	27.16	21.88	50.96
HE-L10	28.08	20.58	51.34
HE-L11	27.13	21.68	51.19
HE-L12	26.49	20.94	52.57
HE-L13	26.04	21.76	52.20
HE-L14	27.24	21.06	51.70
HE-L15	22.39	39.72	37.89
HE-M1	27.12	22.63	50.25
HE-M2	25.54	20.39	54.07
HE-M3	27.19	22.86	49.95
HE-M4	30.50	23.16	46.34
HE-M5	26.35	21.29	52.36
HE-M6	28.67	23.33	48.00
HE-S1	28.01	21.86	50.14
HEC-C1	28.96	20.13	50.91
HEC-C2	33.15	21.28	45.57
HEC-L1	47.27	22.55	30.18
HEC-L2	47.50	19.76	32.73
HEC-L3	34.00	23.66	42.34
WF-B1	29.41	20.76	49.84
WF-B2	26.73	20.91	52.35
WF-B3	32.00	24.26	43.74
WF-B4	26.37	21.16	52.47
WF-H1	30.11	21.25	48.64
WF-H2	30.71	20.04	49.25
WF-H3	30.20	20.56	49.25
WF-P1	30.00	21.32	48.67

Table 7. Values of the C_{27}, C_{28}, and C_{29} steranes for the oil and rock extract samples in this study potted in **Fig. 32**.

Steranes that have been used as organic matter source indicators may also be used for oil/oil and oil/source rock correlations. As the abundance of the C_{29} sterane increases due to the abundance of an algal source (Volkman, 1986) and the C_{27} sterane decreases due to the lower planktonic input, the ratio of $C_{27}/C_{27}+C_{29}$ steranes decreases as is expected (**APPX. I**). The Pr/Ph ratio indicates anoxic depositional environments at low values (<1.5) due to the high values of phytane in anoxic environments, oxic environments at higher values (>1.5) due to the elevated levels of pristane found in oxidizing and generally terrigenous depositional environments (Waseda and Nishita, 1998; Farahat and El-Gendy, 2008; Hossain et al., 2009). It was mentioned in Hossain et al. (2009) that a high Pr/Ph ratio (>4) is present biodegradation may have occurred due to early diagenesis of organic matter or it may be a signature of higher plant input, such as deposition in an inland peat swamp environment (Shanmugam, 1985; Ahmed et al., 1991; Farahat and El-Gendy, 2008; Hossain et al., 2009). When the $C_{27}/C_{27}+C_{29}$ sterane ratio is combined with the Pr/Ph ratio, the overall organic matter source input and depositional environment may be indicated.

The plot of the $C_{27}/C_{27}+C_{29}$ sterane ratio and Pr/Ph, seen in **Fig. 33**, shows that these oils and rock extracts were deposited in an anoxic environment with terrestrial or algal organic matter (Huang and Meinschen, 1979; Volkman, 1986; Hossain et al., 2009). However, it is well known that the conventional Woodford oils (WF) have a marine algal source (Romero and Philp, 2012; Wang, 2016) – not a terrestrial source, and the Hugoton Embayment oils (HE) closely aligns with the Woodford oils as both groups of oils plot in the low Pr/Ph and low $C_{27}/(C_{27}+C_{29})$ range. With regards to the core samples plotted here, the Lansing-Kansas City cores do not follow any trend and the Chattanooga cores, an extension of the Woodford Shale into Kansas, show a more oxic depositional environment as it becomes more oxidized toward the north Anadarko Basin (Newell

and Hatch, 2000). This parameter is seen to be a correlative tool as well (Hossain et al., 2009; Villalba, 2016), where the core samples from the Lansing-Kansas City do not plot near the Hugoton Embayment oils but the oils from the Hugoton Embayment and the Woodford oils group together individually as there may have been changes to the Hugoton Embayment oils during migration.

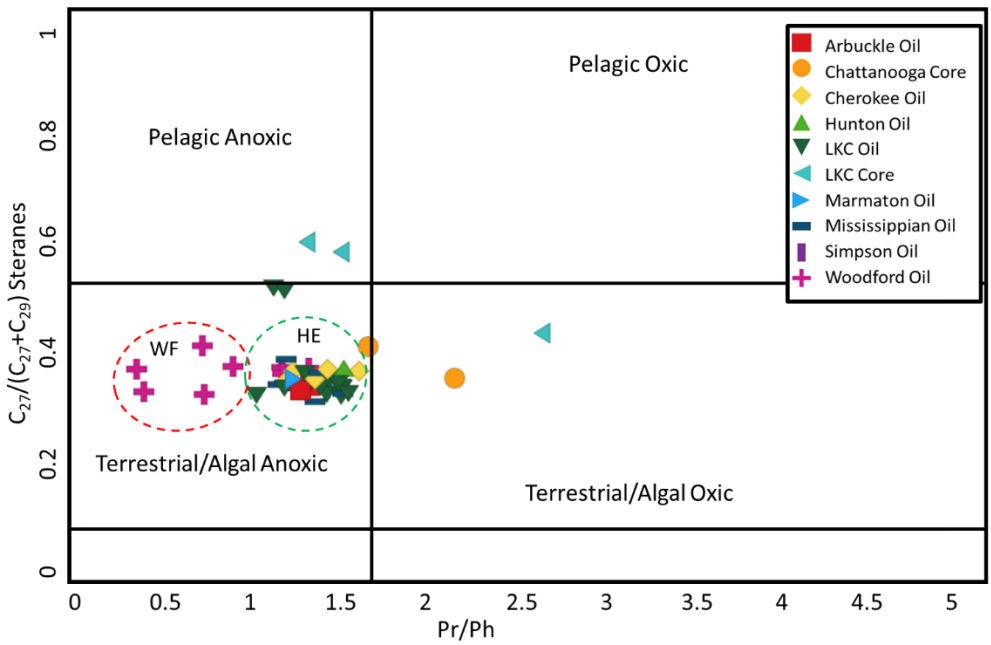

Figure 33. Plot of the $C_{27}/(C_{27}+C_{29})$ steranes vs. the Pr/Ph ratio that indicates an anoxic depositional environment and an algal rich organic matter input of the oils and rock extracts in this study where the Hugoton Embayment oils (HE) are have been separated from the conventional Woodford oils (WF) (plot modified from Hossain et al., 2009; **APPX. I**).

The sterane index ($C_{30}/[C_{27}+ C_{28}+ C_{29}+C_{30}]$ steranes; **APPX. I**) is valuable in identifying whether or not a crude oil is from an organic matter deposited in a marine setting as the C_{30} sterane has been linked to marine organic matter and marine environments (Moldowan et al., 1985). Extended hopanes (homohopanes) are also useful in correlating oils as they infer a bacterial source and redox conditions of the water column during deposition, by way of the homohopane index

(Rohmer, 1987). The higher the homohopane index (C_{35}/[C_{31}+C_{32}+C_{33}+C_{34}+C_{35}] hopanes; **APPX. I**), the more restricted the depositional environment is, and the reverse is also true – a lower homohopane index is a less restricted environment with a marine shale input (McKirdy et al., 1983; Peters et al., 2004b; Al-Khafaji et al., 2018).

The plot of the C_{35} homohopane index versus the C_{30} sterane index (**Fig. 34**) shows that conventional Woodford oils and Hugoton Embayment oils plot in a marine depositional environment with marine organic matter (McKirdy et al., 1983; Moldowan et al., 1985; Peters and Moldowan, 1991; Wang, 2016). This aligns well with conventional Woodford Shale oil samples which have marine organic matter (Romero and Philp, 2012). The two samples from the Lansing-Kansas City core seem to have been deposited in a more terrestrial depositional environment as they have a decreased value of C_{30} sterane (**APPX. II**) compared to the overall composition of the C_{30} sterane index which differentiates the Lansing-Kansas City core depositional environment from the Hugoton Embayment and conventional Woodford oils.

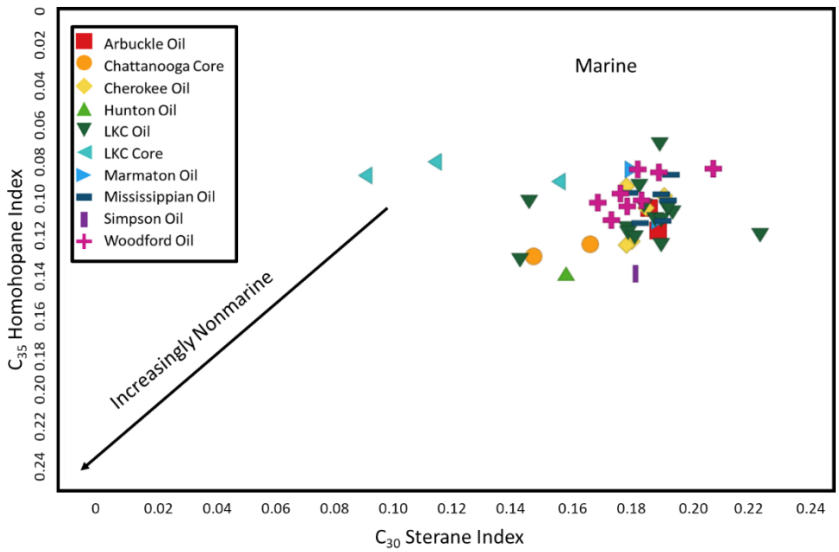

Figure 34. The plot of the homohopane index (C_{35}/[C_{31}+C_{32}+C_{33}+C_{34}+C_{35}] homohopanes) against the sterane index (C_{30}/ [C_{27}+ C_{28}+ C_{29}+C_{30}] steranes) shows that the source rock for these samples

was deposited in an open marine setting (modified from Moldowan et al., 1985; Wang, 2016; **APPX. I**).

Depositional Environment and Source Rock Lithology

The determination of source rock lithology uses the same saturate compounds and aromatic hydrocarbons that were mentioned in **Chapter 1**. The two most common polyaromatic hydrocarbons (PAH) used in determining source rock lithology are phenanthrene (PHEN, **APPX. II**) and dibenzothiophene (DBT, **APPX. II**) as seen in **Fig. 35** (peaks identified in **Table 8**). These aromatic compounds are useful in the identification of the depositional environment and the source rock lithology as they are abundant in the aromatic fraction of oils and rock extracts and are relatively resistant to weathering and biodegradation, evaporation, and water washing (Volkman, 1984; Hughes et al., 1995; Douglas et al., 1996; Li et al., 2013). The phenanthrenes are affected by source rock lithology, especially carbonates (Tissot and Welte, 1984; Wang, 2016), and DBT can be derived from early diagenesis using inorganic sulfur in the sediment or due to the presence of sulfur-reducing bacteria in euxinic environments (Hughes et al., 1995; Radke et al., 1997; Jones, 2017). The high resistance to biodegradation exhibited by phenanthrene and dibenzothiophene make the ratio of the two a useful tool for oil/oil (Douglas et al., 1996) and oil/source rock characterization.

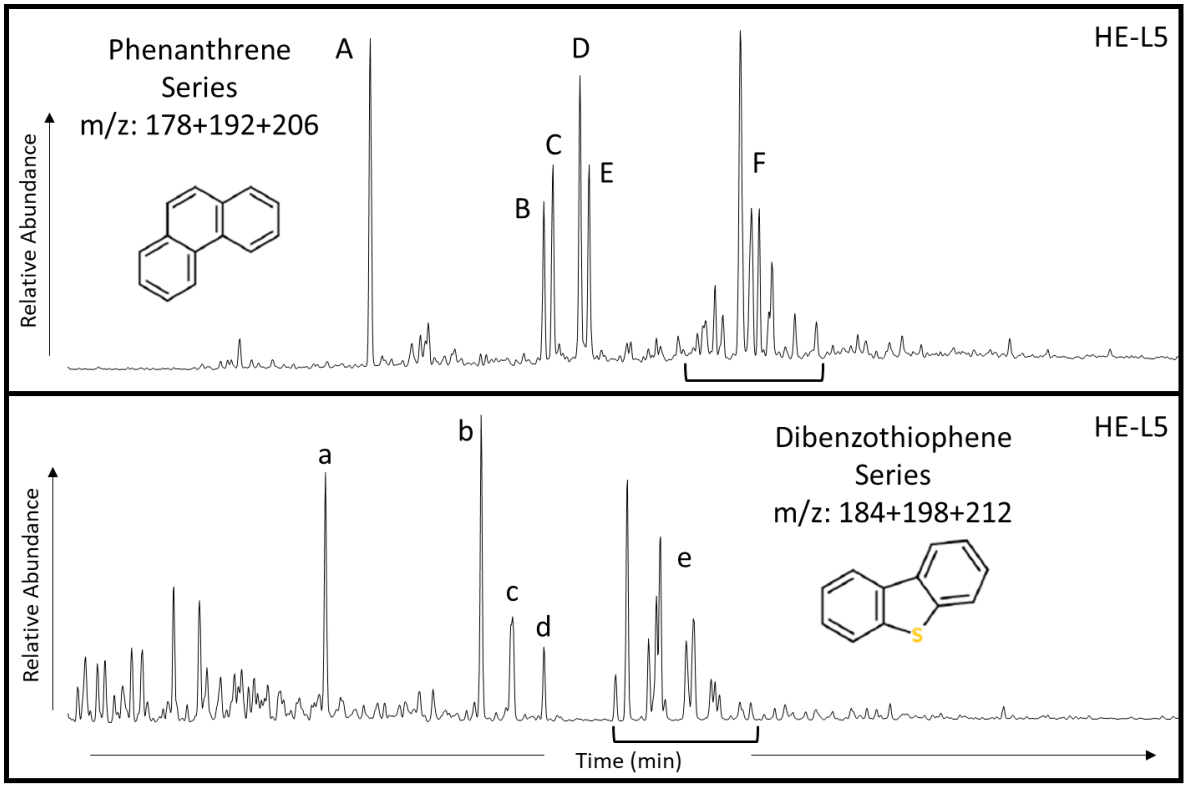

Figure 35. Sample HE-L5 showing the phenanthrene series compounds (**APPX. II**) on a mass chromatogram of the summed m/z 178+192+206 and the dibenzothiophene series compounds (**APPX. II**) on a summed mass chromatogram of m/z 184+198+212. See **Table 7** for peak identification.

Peak	Compound	m/z
A	Phenanthrene	178
B	3-Methylphenanthrene	192
C	2-Methylphenanthrene	192
D	9-Methylphenanthrene	192
E	1-Methylphenanthrene	192
F	Dimethylphenanthrenes	206
a	Dibenzothiophene	184
b	4-Methyldibenzothiophene	198
c	3+2-Methyldibenzothiophene	198
d	1-Methyldibenzothiophene	198
e	Dimethyldibenzothiophenes	212

Table 8. Peak identification for the phenanthrene (A-F) and dibenzothiophene (a-e) series chromatograms (**Fig. 35**).

In looking at some of the methylated dibenzothiophene (MDBT) compounds (identified in **Fig. 35** and **Table 8**), Wang and Fingas (1995) noticed that the use of the MDBT compounds could be used as an oil/source rock correlation tool as well as an indicator of weathered oils. This method of oil characterization is used because the MDBT compounds, along with the DBT compounds, are abundant in crude oils and well resolved on a GCMS (Wang and Fingas, 1995). These compounds also experience little effects from evaporative weathering, but they are susceptible to biodegradation (Williams et al., 1986; Wang and Fingas, 1995). In the plot proposed by Wang and Fingas (**Fig. 36**) the relationship of 1-MDBT/4-MDBT to 2+3-MDBT/4-MDBT, shows that most of the conventional Woodford oils, Hugoton Embayment oils, and Chattanooga (Woodford) core samples (circled) are related.

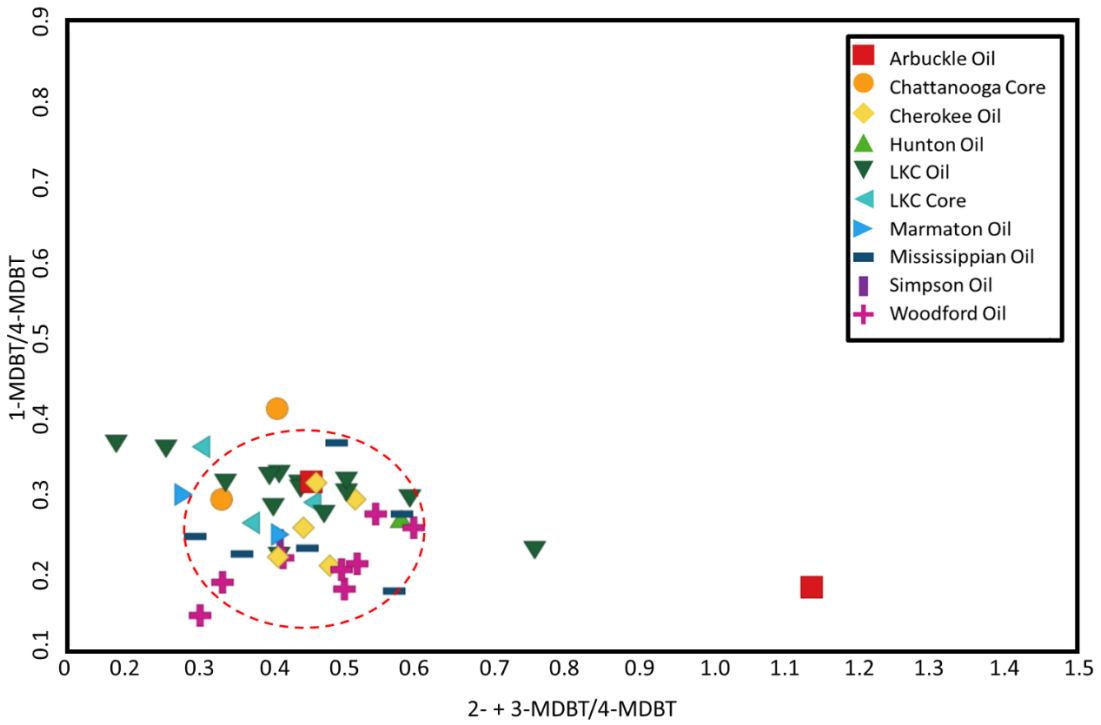

Figure 36. Analysis of conventional Woodford oils, Hugoton Embayment oils and rock extracts, and Chattanooga (Woodford) core use MDBT compounds for oil/source correlation. This plot shows that the circled oils and extracts are likely related (Wang and Fingas, 1995).

The ratios of dibenzothiophene/phenanthrene and pristane/phytane, when plotted against each other, permit depositional environment and source rock lithology to be determined for the related oils and extracts (Hughes et al., 1995; **APPX. I**). A low (<1) DBT/PHEN ratio is indicative of shale with little carbonate input (Masterson, 2001), and a low Pr/Ph value indicates an anoxic environment for marine sediments (Powell and McKirdy, 1973). The oils and rock extracts are plotted in **Fig. 37** and the samples from the Hugoton Embayment show a marine-lacustrine depositional environment with a shaly lithology while most of the conventional Woodford oil samples from Pauls Valley, OK, show a lacustrine depositional environment, with a variable lithology, according to Hughes et al., (1995). The lacustrine environment that Hughes et al. (1995) used in this plot is likely a reference to high water stratification that is typical in lacustrine environments but can also be found in environments that exhibit marine euxinia which was typical during the time of Woodford Shale deposition (Chen and Summons, 2001; Connock, 2015; Wang, 2016). The variation in the oil and source rock samples may infer an alteration of conventional Woodford oils, which have a Pr/Ph average of 0.84, to the Hugoton Embayment oils, which have an average Pr/Ph value of 1.35 potentially due to other oils in the Woodford that had a higher levels of oxidation during deposition (Shanmugam, 1985; Farahat and El-Gendy, 2008) or water washing from migration (Hughes et al., 1995). All the source rock samples plot in the marine/lacustrine shale area, as is expected, which indicates the ratios used are accurate in this system.

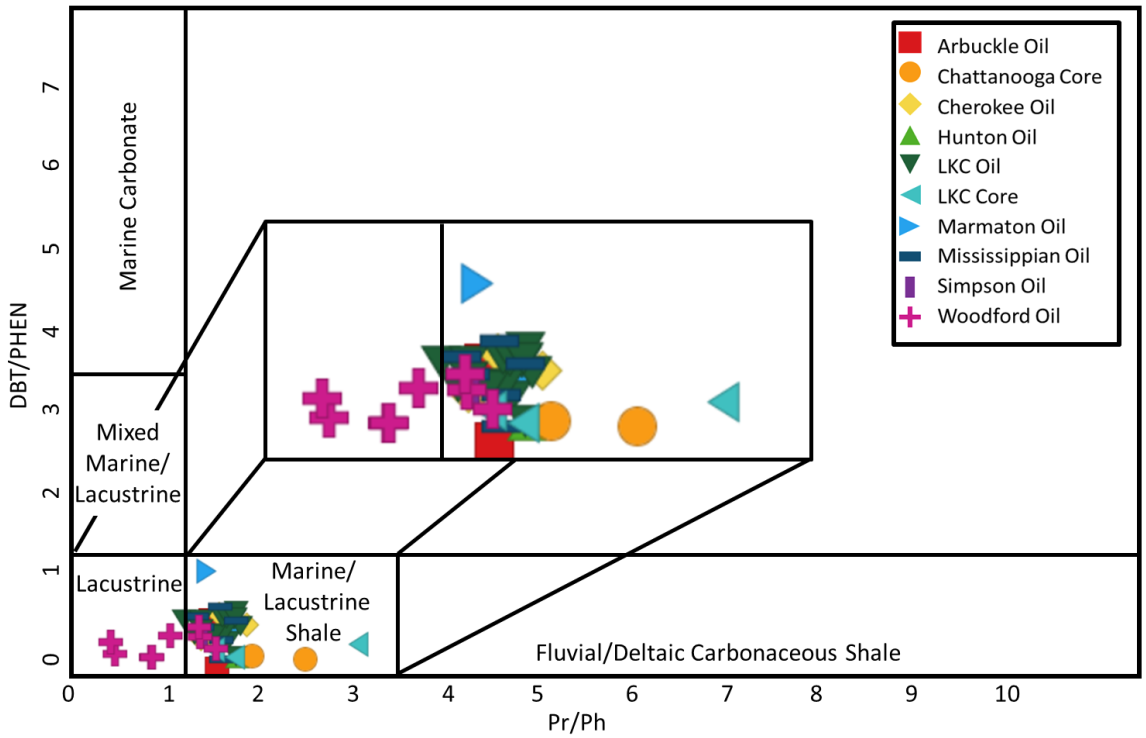

Figure 37. The samples show that the major lithology of the source rock is a mixed lacustrine/marine shale as seen by the low Pr/Ph and low DBT/PHEN ratios. The Chattanooga/Woodford Shale source rock samples also plot in the same area, inferring that this ratio is accurate (modified from Hughes et al., 1995; **APPX. I**).

Another group of compounds, tricyclic and tetracyclic terpanes (**APPX. II**) along with hopanes (**Fig. 37, APPX. II**), are generally abundant in oils and source rock extracts but tend to vary by facies and maturity (Waples and Machihara, 1990). The tricyclic terpanes (up to C_{29}) often increase relative to hopanes when exposed to biodegradation and thermal maturity (Seifert and Moldowan, 1980; Masterson, 2001). This makes the terpanes and hopanes less ideal compounds for determining lithology (Zumberge, 1987; Kim and Philp, 2001), however, using the core samples available, these compounds may indicate the primary source rock lithology the oils. The tricyclic terpanes are derived from either a marine source of bacterial origin or a primitive algal source such as *Tasmanites* (Zumberge, 1987; Volkman et al., 1989; Oung and Philp, 1994; Radke et al., 1997), so they can also be used for organic matter and depositional environment proxies.

The hopanes may also be used as are organic matter and depositional environment proxies, but they are highly ubiquitous and can be derived from either marine or terrestrial bacteria (Rohmer et al., 1984).

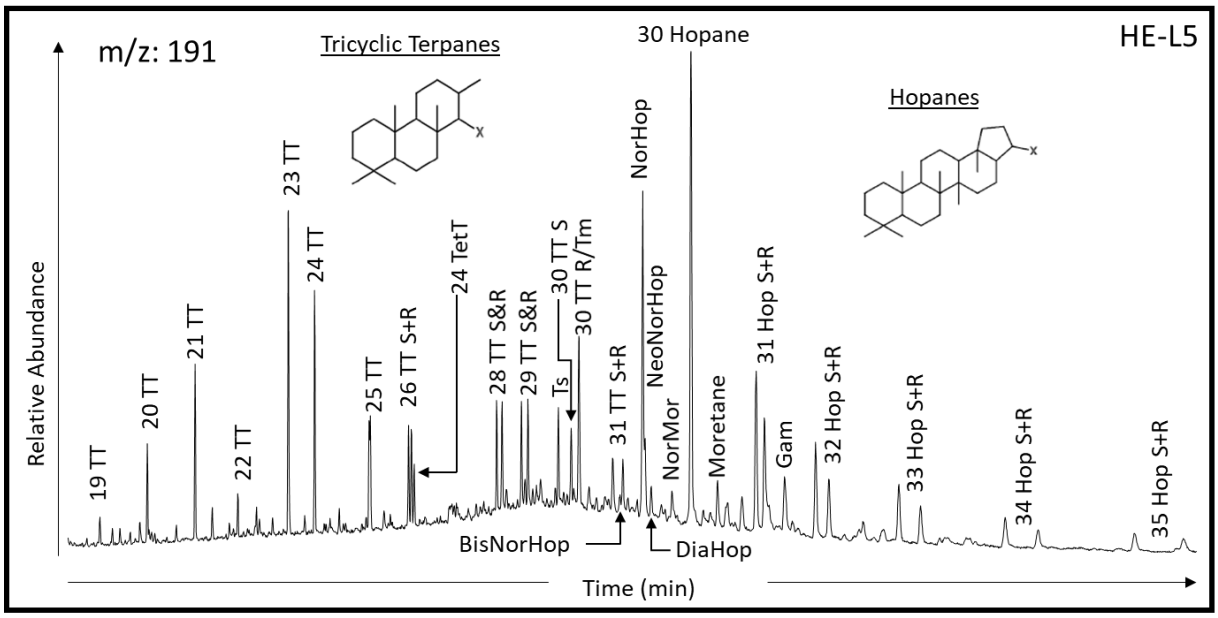

Figure 38. GCMS chromatogram of m/z 191 showing the terpanes and hopanes with the identified peaks in sample HE-L5 (**APPX. II**).

In **Fig. 37,** there is a discrepancy between the source rock lithology in the Woodford oils and the Hugoton Embayment oils and rock extracts. So, to better identify the source rock lithology, tricyclic terpanes and hopanes are used. The tricyclic terpanes and hopanes (**APPX. II**) can be useful indicators for source rock lithology, as well as the depositional environment (Zumberge, 1987). The tricyclic terpanes can be used to identify the source rock lithology by various tricyclic terpane ratios. A carbonate source rock is indicated by low ratios of C_{26}/C_{25} and C_{24}/C_{23} tricyclic terpanes and a high ratio of C_{22}/C_{23} tricyclic terpanes (Hays et al., 2007). A true lacustrine source rock is identified by a high C_{26}/C_{25} tricyclic terpane ratio and a marine shale source rock is identified by a high C_{24}/C_{23} tricyclic ratio (Waples and Machihara, 1990; Hays et al., 2007), The

ratio of $C_{31}R/C_{30}$ hopane can be used to indicate a marine or carbonate source rock at high values (Zumberge, 1987; Peters et al., 2004b).

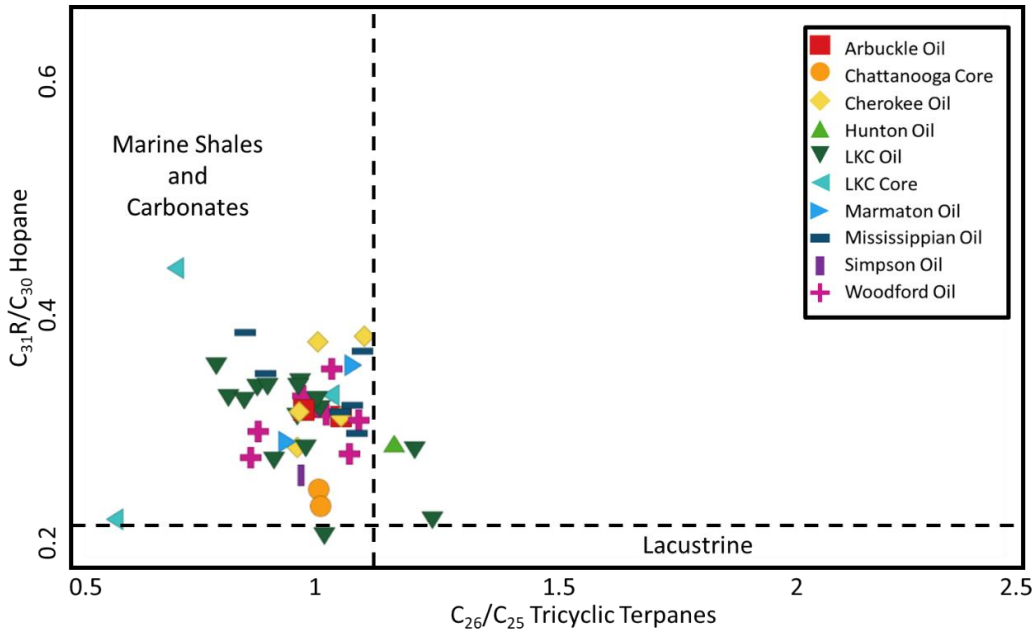

Figure 39. The source rock lithology of the oils from the Woodford Shale and the Hugoton Embayment show either a marine shale or carbonate lithology from the ratios of the $C_{31}R$ hopane/C_{30} hopane to the C_{26}/C_{25} tricyclic terpanes. The Chattanooga/Woodford source rock samples also plot in the same area, inferring that this ratio is accurate (modified from Hays et al., 2007; **APPX. I**).

The lithology of the source rock was determined using the C_{26}/C_{25} tricyclic terpane ratio against the $C_{31}R/C_{30}$ hopane ratio from the oils and rock extracts (**APPX. I**). The lithology was found to be either a marine shale or a carbonate, according to **Fig. 39**. The low values of the C_{26}/C_{25} tricyclic terpanes (ranging from 0.53 to 1.21) imply that the source rock for the Woodford oils and Hugoton Embayment oils were not deposited in a lacustrine environment, but rather in a highly stratified marine environment. To better identify the source rock lithology of the oil the ratios of C_{24}/C_{23} tricyclic terpanes and C_{22}/C_{21} tricyclic terpanes are plotted in **Fig. 40** (**APPX. I**) with the core samples to provide a reference point within in the plots. This plot indicates that most of the

oils in this study are marine shales, as shown by the low values of C_{22}/C_{21} tricyclic terpanes (ranging from 0.16-0.53) and the higher C_{24}/C_{23} tricyclic terpane values (ranging from 0.34-0.80).

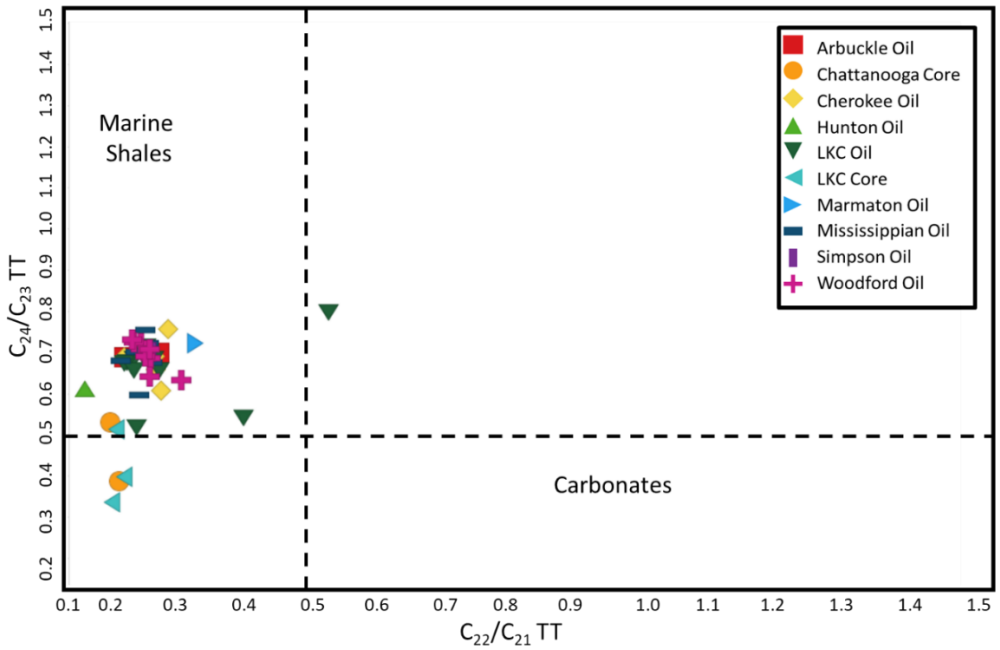

Figure 40. A plot of C_{24}/C_{23} tricyclic terpane verses C_{22}/C_{21} tricyclic terpane which indicated that the oils from the conventional Woodford Shale and the Hugoton Embayment are marine shales. The Chattanooga/Woodford source rock samples also plot in the marine shale area, as expected, inferring that this ratio is accurate (Zumberge, 1987; modified from Peters et al., 2004b; **APPX. I**).

Thermal Maturity

The thermal maturity of oil samples in this study was measured by using the methylphenanthrene index 1 (MPI-1) proposed by Radke and Welte in 1983. The MPI-1 equation:

$$\boldsymbol{MPI} \cdot \mathbf{1} = 1.5 \times \frac{(2 - methylphenanthrene + 3 - methylphenanthren)}{(phenanthrene + 1 - methylphenanthrene + 9 - methylphenanthrene)}$$

(**APPX. III**; Radke et al., 1982; Radke and Welte, 1983; Tissot and Welte, 1984). The MPI-1 is an important index that uses the increase in the ratios of 2- and 3-methylphenanthrene to 1- and 9-

methylphenanthrene to determine the thermal maturity of an oil (**Fig. 36, APPX. II**; Radke and Welte, 1983; Wang, 2016). This was done by calibrating the maturity of shales and coals from their measured vitrinite reflectance (%Ro) values to the MPI-1 calculation values from the extracted organic matter of those shales and coals (Radke and Welte, 1983; Cassani et al., 1987; Wang et al., 2016). The MPI-1 can be used to determine the maturity within a range of 0.65 to 1.35 %Ro, which is the predicted range of maturities for oil samples in this study (Jones and Philp, 1990) and the MPI-2 covers the range of 1.35 to 2.00 %Ro and was not used in this study (Radke and Welte, 1983; Tissot and Welte, 1984). The MPI-1 value is converted into a calculated maturity (MPI-1 %Rc) using the formula:

$$(\boldsymbol{MPI} \cdot \mathbf{1})\ \%\boldsymbol{Rc} = 0.60 \times MPI \cdot 1 + 0.40$$

(**APPX. III**; Radke et al., 1982; Radke and Welte, 1983). This calculated maturity value should be used with some caution as it may be affected by depositional systems, organic matter, or lithology (Radke et al., 1982; Tissot and Welte, 1984; Cassani et al., 1987).

The oil samples in this study show a MPI-1 %Rc (**Table 9**) that increases in maturity from the northwest (MPI-1 %Rc = 0.56) to the southeast (MPI-1 %Rc = 1.09) as is seen in **Fig. 41**. This is likely an indication of migrated oils because England (2007) suggested there are various mechanisms that can affect the lateral composition of hydrocarbon accumulations. One such mechanism is a change in lateral gradient as reservoirs fill from one (or two) source(s) where the oil nearest the source has a more mature geochemical signature. This lateral gradient can be seen in **Fig. 41** (England, 2007; Spencer, 2012) as most of the oils from Oklahoma have a higher calculated thermal maturity. Other mechanisms include variable biodegradation of oil in a reservoir as only certain areas experience biodegradation and the reservoir leakage or reservoir

seal failure that induces a lateral or vertical fractionation and movement of hydrocarbons (England, 2007). However, three samples in Kansas from the Arbuckle, Lansing-Kansas City, and Mississippian reservoirs exhibit a much higher thermal maturity than expected (>1 MPI-1 %Rc) and do not follow this trend which could be due to unknown conditions in the reservoir (England, 2007).

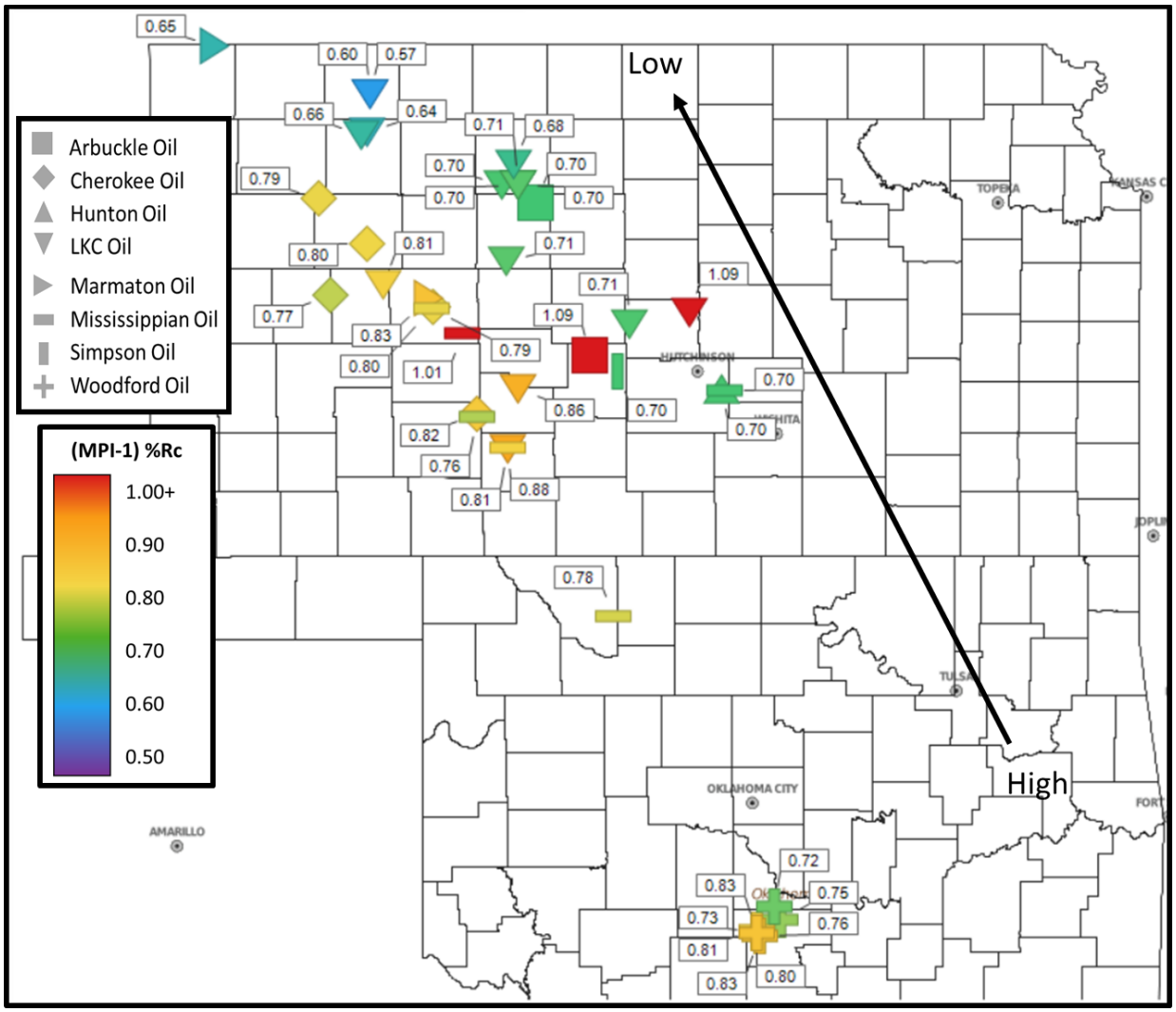

Figure 41. The %Rc from MPI-1 of oils and rock extracts are plotted on this map. The oils in the Hugoton Embayment show an overall decrease in thermal maturity from the SE to NW which could be the result of multi-stage migration that has not equilibrated (Radke and Welte, 1983; England, 2007).

Sample	MPI-1	(MPI-1) %Rc	C_{30}Mor/C_{30}Hop
HE-A1	1.16	1.09	0.09
HE-A2	0.50	0.70	0.11
HE-C1	0.70	0.82	0.09
HE-C2	0.62	0.77	0.20
HE-C3	0.66	0.80	0.14
HE-C4	0.66	0.79	0.09
HE-C5	0.66	0.80	0.11
HE-F1	0.42	0.65	0.11
HE-F2	0.72	0.83	0.12
HE-H1	0.50	0.70	0.13
HE-L1	0.68	0.81	0.11
HE-L10	0.40	0.64	0.09
HE-L11	0.51	0.71	0.14
HE-L12	0.29	0.57	0.12
HE-L13	0.33	0.60	0.11
HE-L14	0.51	0.70	0.10
HE-L15	0.52	0.71	0.10
HE-L2	1.16	1.09	0.09
HE-L3	0.50	0.70	0.10
HE-L4	0.50	0.70	0.11
HE-L5	0.52	0.71	0.09
HE-L6	0.46	0.68	0.10
HE-L7	0.77	0.86	0.13
HE-L8	0.80	0.88	0.12
HE-L9	0.44	0.66	0.10
HE-M1	0.60	0.76	0.12
HE-M2	0.64	0.78	0.10
HE-M3	0.66	0.79	0.11
HE-M4	0.68	0.81	0.13
HE-M5	0.50	0.70	0.10
HE-M6	1.02	1.01	0.10
HE-S1	0.50	0.70	0.12
WF-B1	0.58	0.75	0.09
WF-B2	0.55	0.73	0.11
WF-B3	0.68	0.81	0.10
WF-B4	0.66	0.80	0.10
WF-H1	0.60	0.76	0.10
WF-H2	0.72	0.83	0.09
WF-H3	0.72	0.83	0.09
WF-P1	0.54	0.72	0.13

Table 9. Maturity values of the oil samples in this study: MPI-1, MPI-1 %Rc, and C_{30} moretane/C_{30} hopane (**Fig. 44**).

Another proxy for thermal maturity of oils is the use of C_{30} moretane to C_{30} hopane ratio. This ratio is a maturity proxy because C_{30} moretane (**APPX. II**) has a stereochemistry that is less thermally stable than C_{30} hopane (**APPX. II**) so that the isomerization of C_{30} moretane occurs with increasing maturation (Mackenzie et al., 1980; Grantham, 1986; Peters et al., 2004b). The oil samples are plotted in **Fig. 42** to show the relationship of maturity (MPI-1 %Rc) vs. the C_{30} moretane/ C_{30} hopane ratio. The thermal maturity of conventional Woodford oils and Hugoton Embayment oil fall in the main oil window (Seifert and Moldowan, 1980; Robertson Research Inc., 1983; Tissot and Welte, 1984).

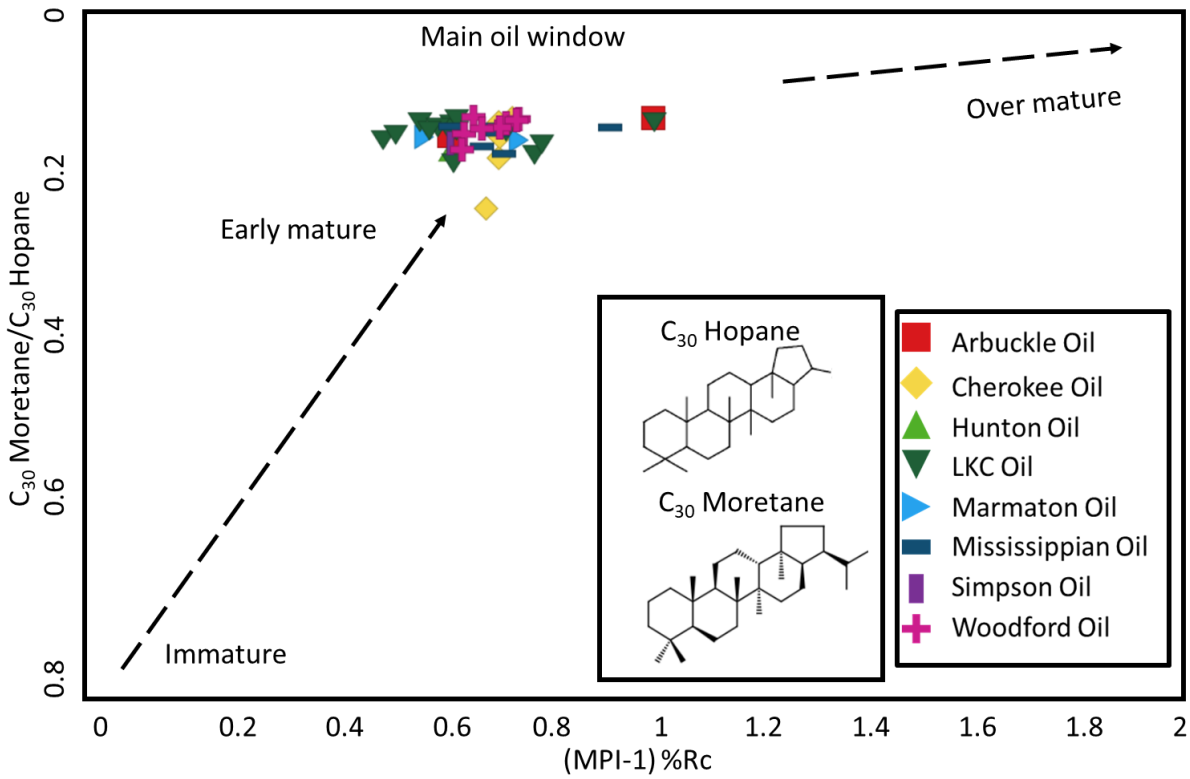

Figure 42. Conventional Woodford oils and Hugoton Embayment oils are all mature oils as they plot in the main oil window of the C_{30} moretane/C_{30} hopane (**APPX. II**) ratio vs. maturity (%Rc) from the MPI-1. This is due to the depletion of moretane relative to hopane as the oil samples become more mature (modified from van Graas, 1990; **APPX. I**).

Water Column Stratification

Stratification is defined as a division or arrangement into layers (Merriam-Webster, 2019). The depositional environment of the Woodford Shale was known to be a highly stratified water column exhibiting photic zone euxinia (PZE; Nowaczewski, 2011; Romero and Philp, 2012). PZE occurs when shallow anoxic waters extended into the photic zone of the water column (Connock, 2015; Connock et al., 2018). There are two types of circulation models (**Fig. 43**): an unstratified, well-mixed water column and a stratified, stagnate water column. The difference between these two types of circulation is that the unstratified water column is open to the ocean and has a deep chemocline, whereas a stratified water column is more restricted, has low circulation near the surface, and has a shallow chemocline in the photic zone. This stratified model enables sulfur-reducing bacteria to thrive on the free sulfur in the PZE of the static water column (Hays et al., 2007; Connock, 2015; Connock et al., 2018). The anaerobic organisms in the PZE help increase the preservation of organic matter by inhibiting oxygen from entering the organic rich sediments where heterotrophic organisms cannot destroy it (Connock, 2015).

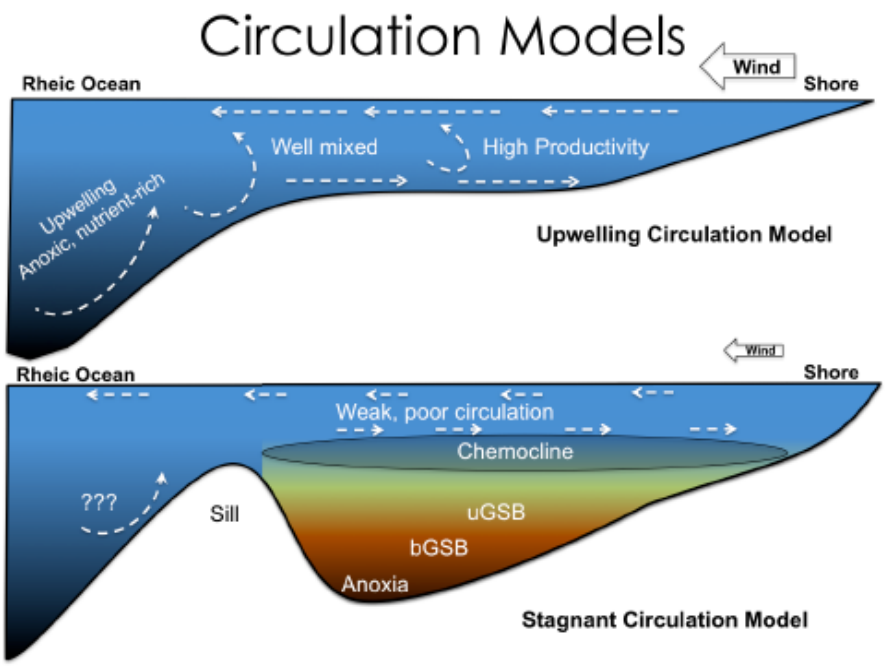

Figure 43. Top: unstratified water column, bottom: stratified water column showing photic zone euxinia (modified from Connock, 2015).

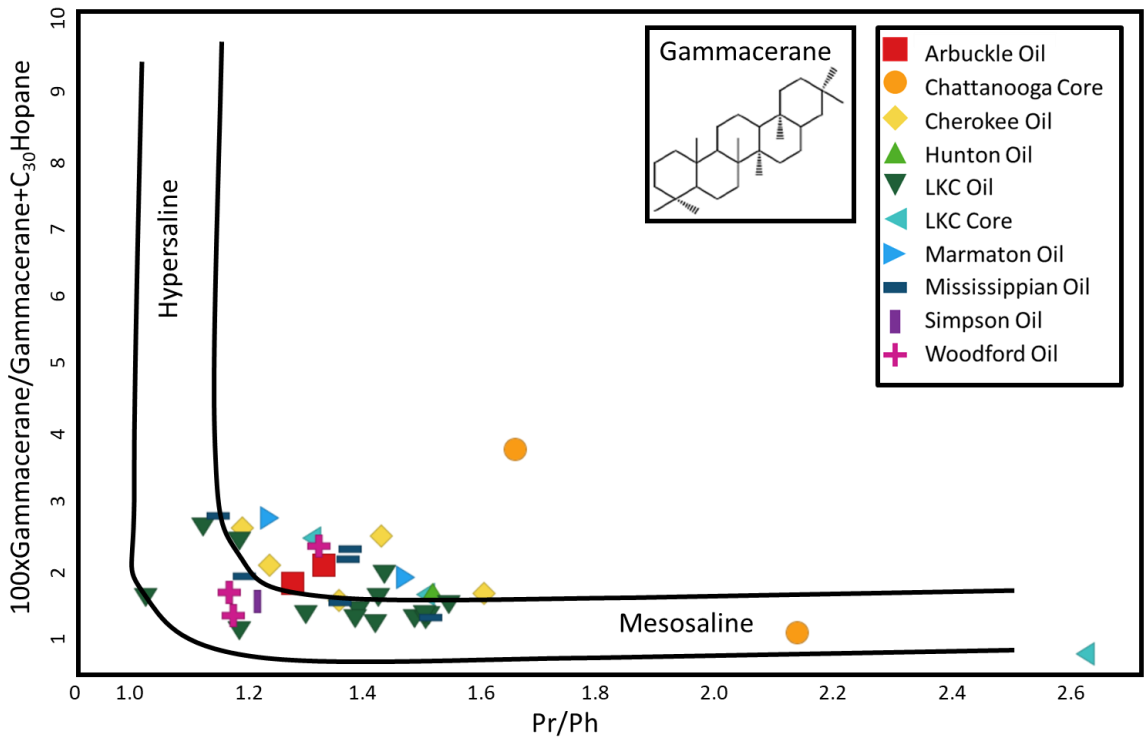

Figure 44. Gammacerane index verses pristane/phytane ratio indicates a low level of water stratification and a low salinity environment (Peng et al., 2004; **APPX. I**; **APPX. II**).

Water column stratification can be implied by high levels of gammacerane (Sinninghe-Damste et al., 1995; **APPX. II**) and the PZE can be inferred by the presence of carotenoids (Connock et al., 2018, **APPX. II**). The gammacerane index (100*gammacerane/gammacerane+C_{30} hopane) verses the pristane/phytane ratio is shown in **Fig. 44** and it infers a semi-stratified water column as the gammacerane index is not higher than 3.5% but the water has a low pristane/phytane value that indicates anoxia, as has been mentioned previously (**APPX. I**).

Carotenoids (**APPX. II**) are colored pigments that are C_{40} diaromatic biomarkers and are derived from tetraterpenes (Grice et al., 1996). Carotenoids are highly unsaturated and are rarely abundant in sediments due to the oxygenation of the hydrogen bonds that degrades the compound, but they can be preserved under anaerobic conditions as is commonly found in a stratified water column, like that of the Woodford Shale (Repeta and Gagosian, 1987; Connock, 2015). Carotenoids tend to fragment at the carbon-carbon bond where the tail-to-tail linkage of isoprenoids and this break yields aryl isoprenoids (Lu et al., 2015). Aryl isoprenoids (**APPX. II**) are more stable than carotenoids and are more commonly found in oils (Fernandes et al., 2018). They can be used to indicate the presence of an anoxic to euxinic environment as some of these aryl isoprenoids are likely derived from their carotenoid precursor, brown-colored green sulfur-reducing bacteria, *Chlorobiaceae* (Koopmans et al., 1996), or from the homologues series of 2-alkyl-1,3,4-trimethylbenzenes that have between a C_{10}-C_{30} isoprenoidal carbon chain (Summons and Powell, 1987; Requejo et al., 1992).

The carotenoids and aryl isoprenoids can be seen in either the saturate fraction or the aromatic fraction at either m/z 133 or 134 as they have one (aryl isoprenoids) or two (carotenoids)

methylated aromatic rings with a substituted isoprenoid side chain. To resolve this issue, the maltene fraction was analyzed by GCMS and a combined m/z 133+134 chromatogram (**Fig. 45**) illustrates the presence of aryl isoprenoids and carotenoids (paleorenieratane and isorenieratane). The presence of these carotenoids in Hugoton Embayment oil samples HE-L5 and HE-M2, Chattanooga (Woodford) rock extract HEC-C2, and Woodford oil sample WF-B1 indicate the Woodford Shale as the common source of petroleum in this system, as they all have a similar relative abundance of paleorenieratane and isorenieratane. This is strong evidence of oil migration from the Woodford into the reservoirs of the Hugoton Embayment. Furthermore, there is a lack of aryl isoprenoids and carotenoids in the Lansing-Kansas City core sample, HEC-L2, which shows that the Lansing-Kansas City core sample likely does not contribute any hydrocarbons to the surrounding formations.

The ratio of the carotenoids, paleorenieratane and isorenieratane (**Table 10**), was obtained by GCMS from the maltene fraction of thirty-five samples and the peak heights of m/z 133+134 were measured using MassHunter software (**APPX. IVC**). Even though many carotenoid peaks show relatively low abundances, they were still used in this study. This ratio does not seem to be affected by the thermal maturity of the oils or rock extracts (**Fig. 46**). It does change, however, with the redox conditions of the water column, as shown by the pristane/phytane ratio, as is expected (**Fig. 47**). This is strong evidence for a stratified to partly stratified water column during the deposition of this source rock. This, again, shows that the most likely source for oils in the Houghton Embayment is the Woodford Shale.

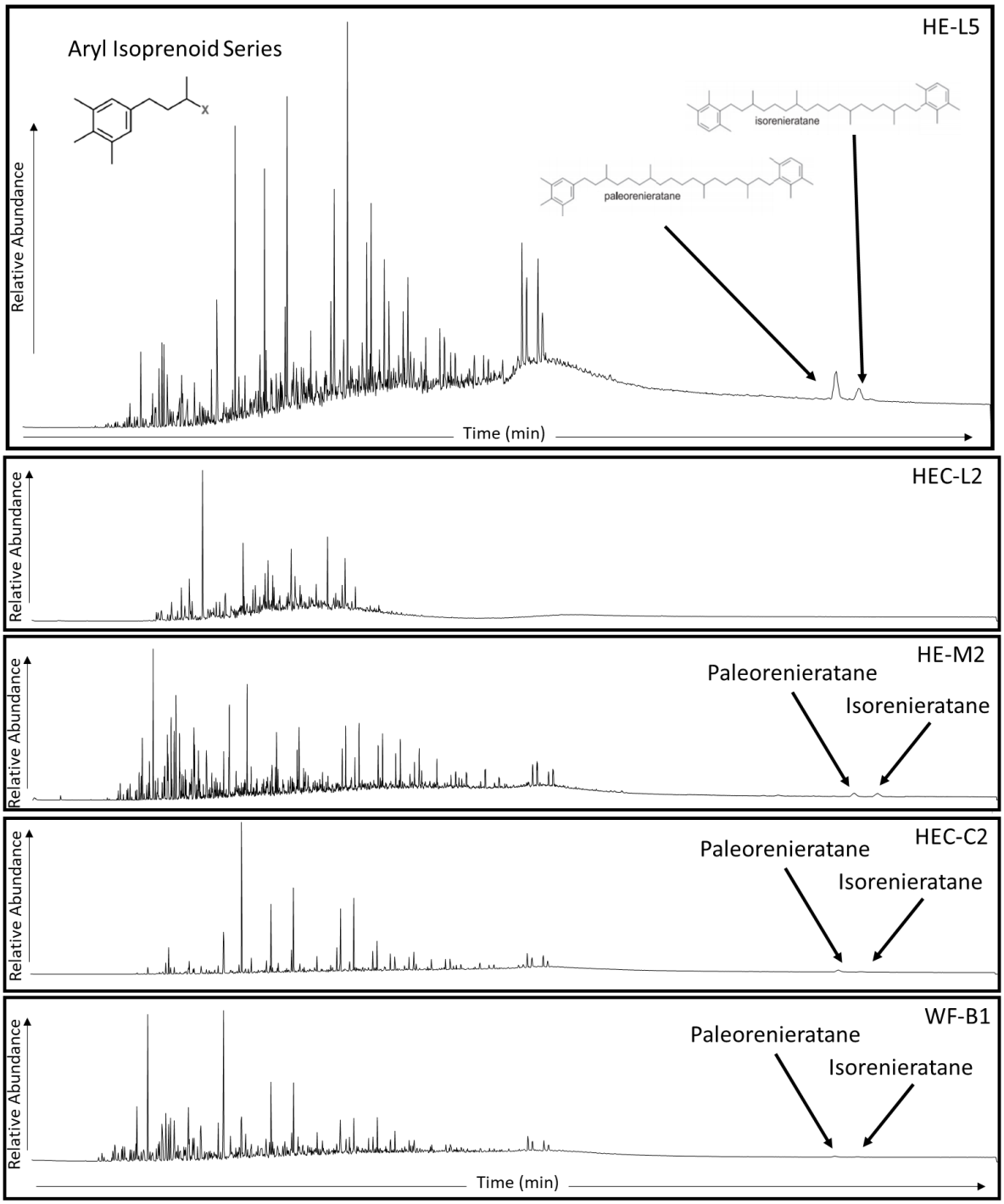

Figure 45. Chromatograms showing the aryl isoprenoids (**APPX. II**) and carotenoids (**APPX. II**) in the maltene fraction at m/z 133+134. The carotenoids, due to varying concentrations, are found near the baseline of most samples and may be seen as small peaks.

Sample	Paleorenieratane /Isorenieratane
HE-A1	2.08
HE-A2	2.43
HE-C1	1.43
HE-C2	2.16
HE-C3	2.69
HE-C4	2.41
HE-C5	2.45
HE-F1	2.64
HE-F2	2.18
HE-H1	4.31
HE-L1	2.81
HE-L10	1.79
HE-L11	2.17
HE-L12	2.10
HE-L13	1.50
HE-L14	1.93
HE-L15	1.93
HE-L2	1.66
HE-L3	2.02
HE-L4	2.05
HE-L5	2.14
HE-L6	2.08
HE-L7	0.04
HE-L8	0.15
HE-L9	1.94
HE-M1	1.76
HE-M2	0.93
HE-M3	3.32
HE-M4	1.33
HE-M5	2.55
HE-M6	3.60
HE-S1	2.82
HEC-C1	1.75
HEC-C2	3.79
HEC-L1	0.04
HEC-L2	1.22
HEC-L3	1.48
WF-B1	2.50
WF-H1	2.36
WF-P1	2.95

Table 10. Thirty-five maltene samples showing the ratio of paleorenieratane to isorenieratane (**Fig. 46** and **Fig. 47**).

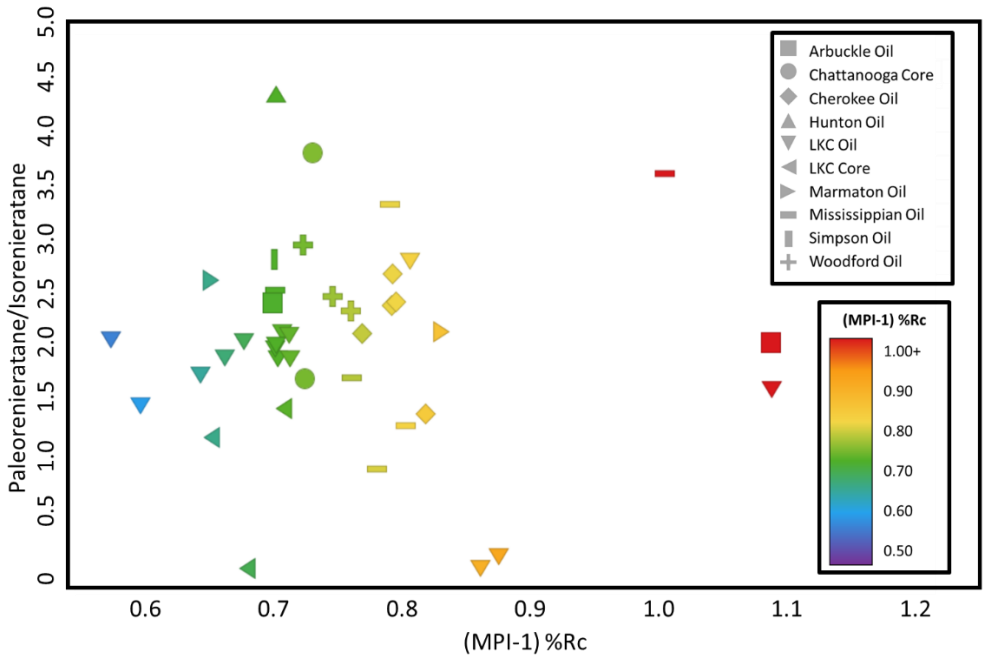

Figure 46. Plot of the ratio of paleoreineratane to isorenieratane vs. the MPI-1 based maturity value (%Rc) showing that the paleoreineratane/isorenieratane ratio in all oil and rock extract samples is not affected by maturity.

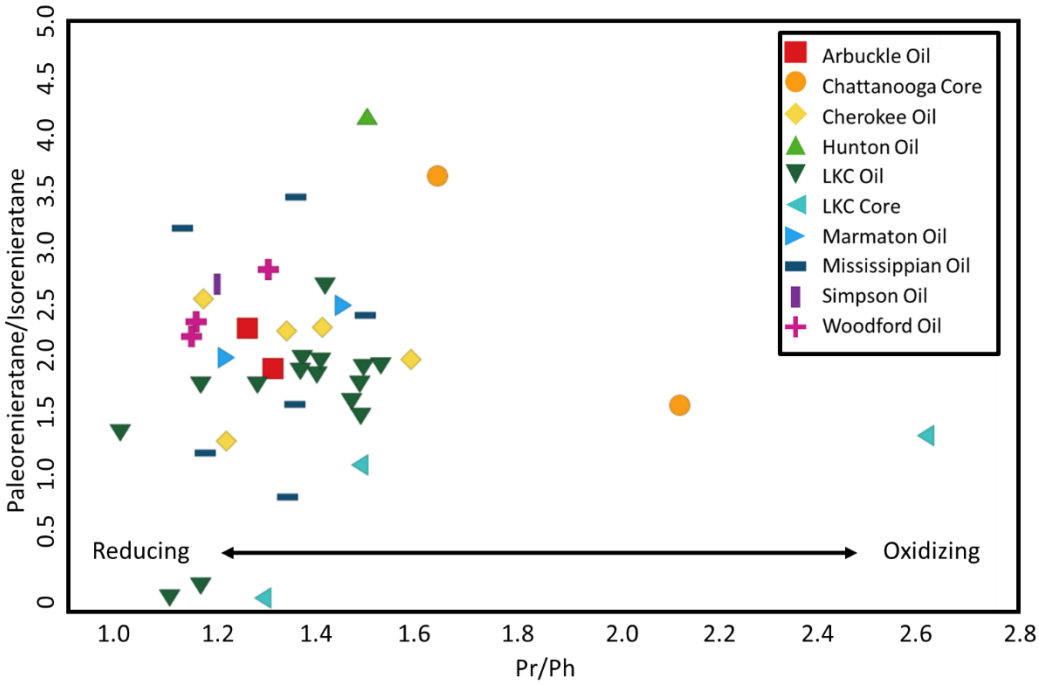

Figure 47. The paleoreineratane/isorenieratane ratio vs. pristane/phytane ratio shows the reducing nature of the anoxic depositional environment in which carotenoids are found (modified from Schwark and Frimmel, 2004).

Migration

In the Hugoton Embayment of the Greater Anadarko Basin, there are very few organic-rich sedimentary rocks that are viable for oil or gas production in an area where the reservoirs are so rich in hydrocarbons (Ball et al., 1991). This has led many scientists, including Burrus and Hatch (1989) and Ball et al. (1991) to assume long distance migration out from the deep, organic-rich Woodford Shale in the Anadarko Basin of southern Oklahoma into the shallower reservoirs of the Hugoton Embayment, and proposed pathways are seen in **Fig. 21**.

In this study, there is ample evidence supporting the migration of oils generated in the Woodford Shale in Southern Oklahoma into the reservoirs in Hugoton Embayment as the geochemical characteristics of these oils indicate similar depositional environments, organic matter input, lithology, and water stratification. However, there are occasionally distinct groupings, such as in **Fig. 33** and **Fig. 37**, where oils from the Hugoton Embayment are separated from the oils of the conventional Woodford oils by the Pr/Ph ratio. This indicates that there is something happening to the Hugoton Embayment oils as they migrate out of the Anadarko Basin. The migration is seen here is a secondary migration, because oil has already been expelled from the source rock (primary migration) and has moved along porous and/or permeable faults, fractures or carrier beds (Higley, 2014; Zumberge et al., 2016) and is caused by the movement of hydrocarbons into a reservoir (Zumberge et al., 2016).

There have been many different studies that tried to measure migration distance in the past, one by Burrus and Hatch in 1989, one in 1996 by Larter et al., and a recent study by Zhang et al. in 2013. Burrus and Hatch (1989) used the C_7 hydrocarbons (**APPX. II**) to correlate the ratio of toluene/(heptane+methylcyclohexane+toluene), found in whole-oil chromatograms, to migration

distance and were met with some success. Larter et al. (1996) used the ratio of benzocarbazoles (BC) to determine absolute migration distances that showed limited success. However, the BC ratio was found to be inaccurate as the carbazoles (**APPX. II**) retained maturity and facies information so that the measured migration distance was erroneous (Clegg et al., 1998; Bakr and Wilkes, 2002; Zhang et al., 2013). Later, Zhang et al. (2013) used a new method to better quantify long distance migration distances using heavy polar compounds to potentially eliminate the potential contamination of organofacies, maturity, lithology, and biodegradation. This new method suggests a secondary migration fractionation index which would use low abundance, large polar compounds such as methyl- and dimethylcarbazoles, the relative lateral migration distances could be calculated with the use of a reference point (Zhang et al., 2013).

Using the BC ratio proposed by Larter et al. (1996), the benzocarbazoles (**APPX. II**), nitrogen-bearing, triaromatic compounds, were measured to try to determine a migration distance. The BC ratio:

$$\boldsymbol{BC\ Ratio} = \frac{benzo[a]carbazole}{benzo[a]carbazole + benzo[c]carbazole}$$

uses the benzocarbazole compounds (**APPX. III**; **Fig. 48**) that are found in the low polarity compound (LPC) fraction that has been separated from the NSO (Larter et al., 1996; Clegg et al., 1998).

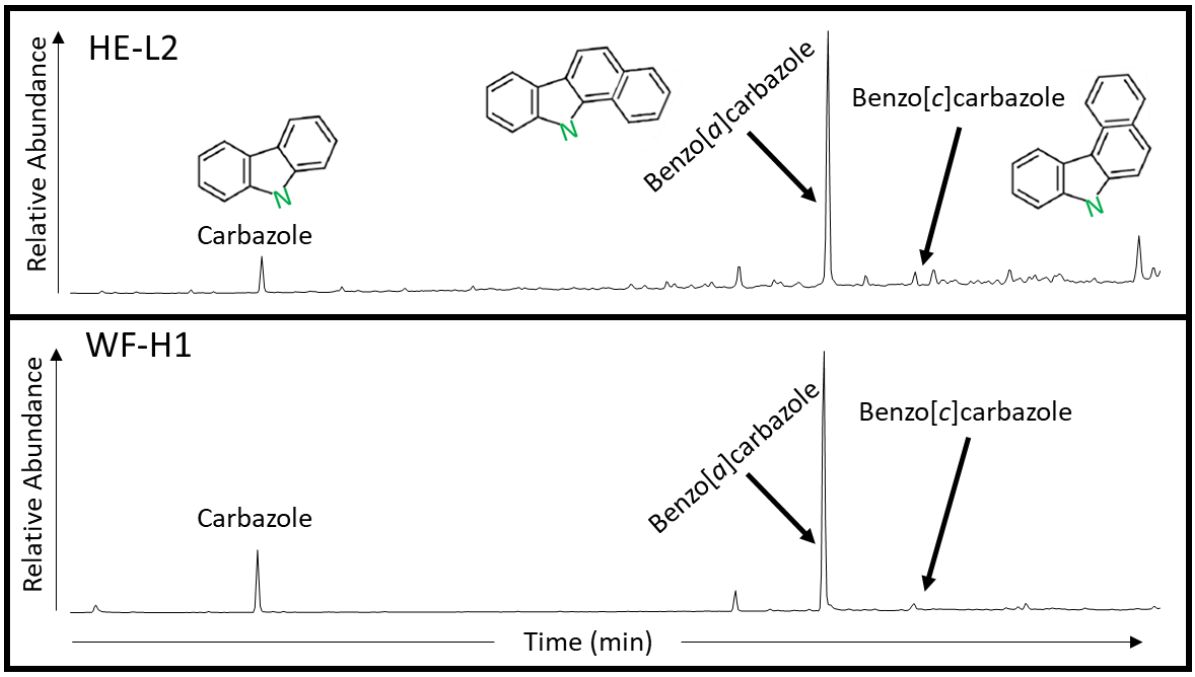

Figure 48. Mass chromatogram of the LPC fraction, from the NSOs, showing carbazole (m/z 167; **APPX. II**) and the benzocarbazoles (m/z 217; **APPX. II**) over the time range of 30-50 minutes in samples HE-L2 and WF-H1 (**APPX. IVF**).

Ideally, oils that have migrated further should have a lower BC ratio due to the preferential loss and possible sorption onto clays during migration of the linear benzo[a]carbazole as compared to the benzo[c]carbazole (Larter et al., 1996; Peters et al., 2004b) but this is not observed in the samples. Eleven oil samples from the Hugoton Embayment, three oil samples from conventional Woodford reservoirs, and one rock extract sample from the Lansing-Kansas City were analyzed for benzocarbazole compounds (**Table 11**). The Hugoton Embayment oils have a BC ratio ranging from 0.99 to 0.96, which show no migration to very slight migration (**Fig. 49**). All three locally sourced, conventional Woodford oils from Pauls Valley have a BC ratio of 0.99. Surprisingly, the Lansing-Kansas City rock extract has the lowest BC ratio of all the samples, 0.87, implying that this ratio does not work for this basin as it shows the highest amount of migration in a source rock.

Also, the oils from the Hugoton Embayment may have been affected by maturity (Clegg et al., 1998).

Sample	BC Ratio
HE-L1	0.99
HE-L2	0.97
HE-L3	0.99
HE-L6	0.99
HE-L7	0.99
HE-L8	0.96
HE-L9	0.99
HE-L11	0.99
HE-L13	0.99
HE-L14	0.99
HE-L15	0.99
HEC-L1	0.87
WF-B1	0.99
WF-H1	0.99
WF-P1	0.99

Table 11. BC ratio values for the conventional Woodford oils (WF), Hugoton Embayment oils (HE), and Lansing-Kansas City rock extract (HEC-L) evaluated, also shown below in **Fig. 49**.

The small difference of 0.12 in the BC ratio is not well understood in this case. It could be that the Woodford oil samples have already been affected by secondary migration as they are not source rocks from the Woodford Shale itself, only oils from the near reservoirs, and there is not a good benchmark to compare a non-migrated Woodford oil with to be able to determine migration distance.

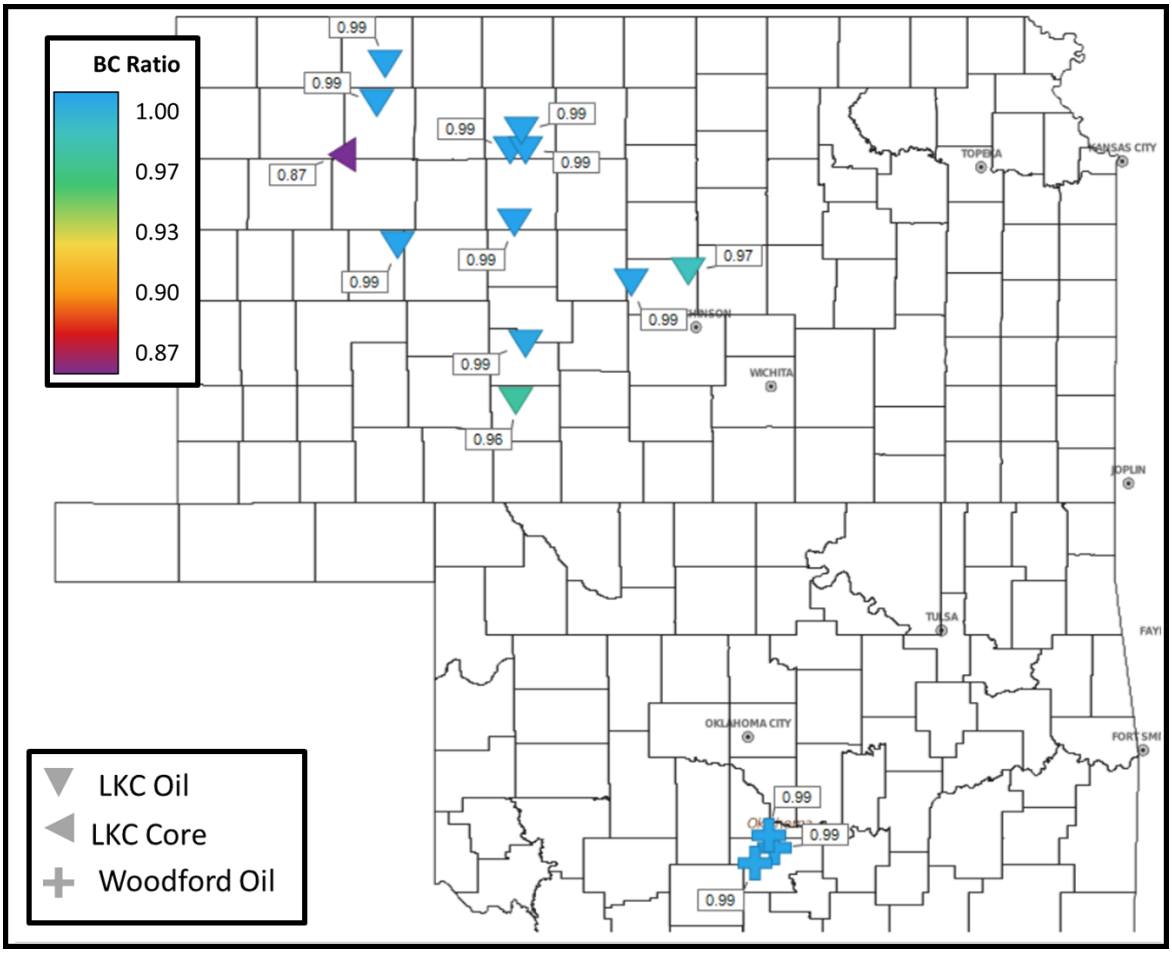

Figure 49. The BC ratio (**APPX. I**) shows no variation in the Woodford oils (crosses), some variation in the Hugoton Embayment oils from the Lansing-Kansas City (inverted triangles), and an unusually low sample in the Lansing-Kansas City cores (left triangles). This demonstrates that Larter's BC ratio (1996) does not apply to these oils that were analyzed.

Previous work by Fang et al. (2016) has attempted to demonstrate the use of methyldibenzothiophenes (MDBT), dimethyldibenzothiophenes (DMDBT), and benzo[b]naphthothiophene (BNT, **APPX. II, Fig. 50**) to determine relative oil migration pathways. These benzothiophenes and benzo[b]naphthothiophenes were used in this study because they have a slightly higher electronegativity than hydrocarbons due to the sulfur atom bonding with hydrogen. When these molecules migrate, a dipole interaction occurs between the thiophene compounds and carrier beds which causes preferential adsorption of thiophene compounds onto

clays of the carrier bed (Fang et al., 2016). The use of these sulfur-bearing compounds has been found to work well in determining the oil migration direction of oils that are derived from the same source. The lithology, organic matter input, and maturity have little to no effect on these compounds, leaving the oil migration pathway as the only variable (Fang et al., 2016).

In the study by Fang et al. (2016), it was found that the ratios: 4-/1-MDBT, 4,6/(1,4+1,6)-DMDBT, (2,6+3,6)/(1,4+1,6)-DMDBT, and 2,1/(2,1+1,2)-BNT were efficient in determining the migration pathway of geochemically related migrated oils (**Table 12**; **APPX. I**). Fang et al. (2016) used regular steranes and triaromatic steranes to show that all the samples in the study were genetically related. After proving their genetic relationship, the proposed ratios successfully showed migration pathways and filling points over 30 miles in the Tarim Basin. These studies show that a change from a higher ratio to a lower ratio indicates the oil migration pathway(s).

In **Fig. 51,** the ratio of 4-/1-MDBT shows an overall oil migration pathway that moves from south to north, out of Oklahoma from the local Woodford Shale source rock and into the Hugoton Embayment in Kansas. The 4,6/(1,4+1,6)-DMDBT ratio (**Fig. 52)** also shows a northward oil migration pathway. However, the ratio of (2,6+3,6)/(1,4+1,6)-DMDBT (**Fig. 53**) shows the opposite migration pathway – oil samples show a migration pathway that trends from north to south, out of the Hugoton Embayment in Kansas and into Oklahoma. The (2,6+3,6)/(1,4+1,6)-DMDBT ratio does not reflect the known migration pathway and does not work in this petroleum system.

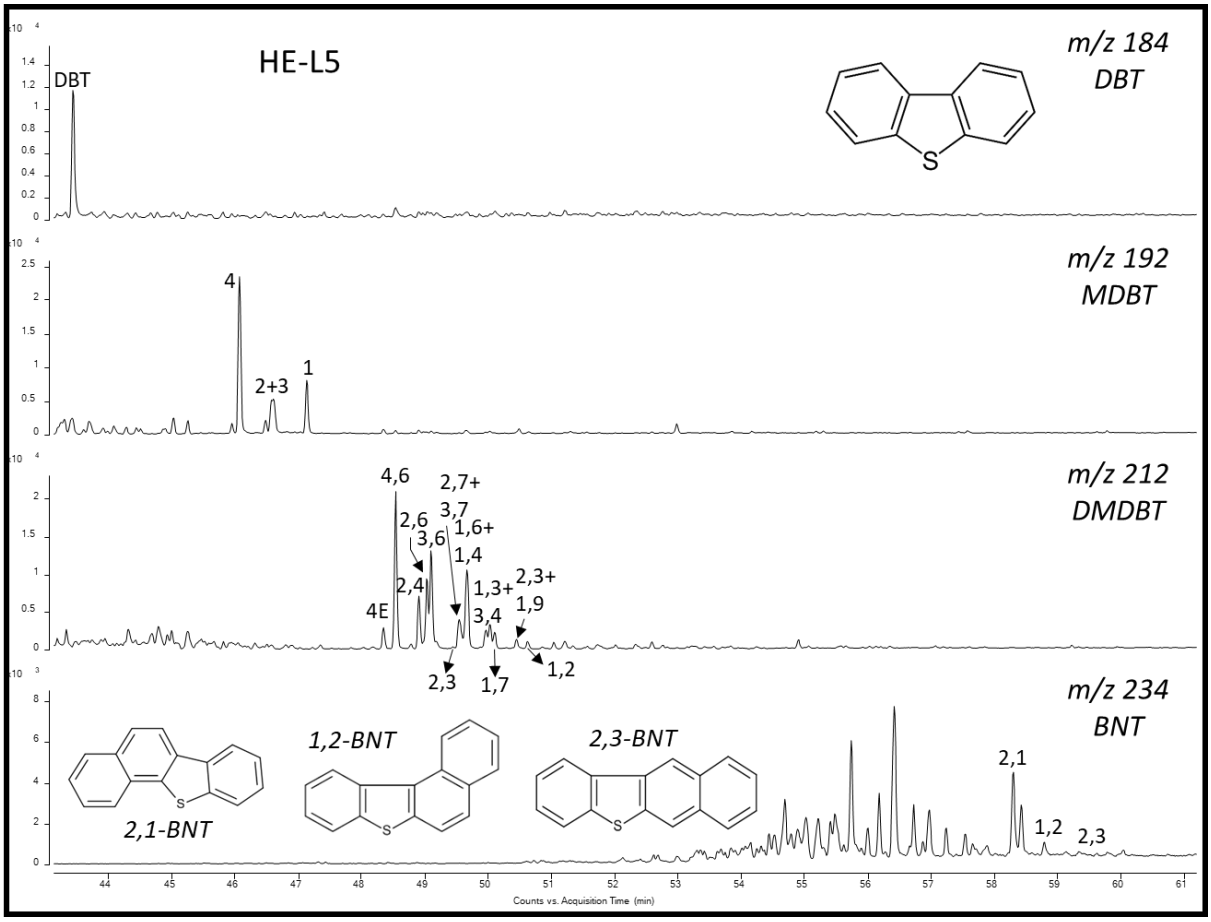

Figure 50. Chromatogram of sample HE-L5 showing the identification of the thiophene compounds. DBT: Dibenzothiophene; MDBT: Methyldibenzothiophene; DMDBT: Dimethyldibenzothiophene, BNT: Benzo[b]naphthothiophene.

The final ratio, 2,1/(2,1+1,2)-BNT (**Fig. 54**), shows an oil migration orientation from the south to the north and the oil seems to split into two directions: to the northwest toward the Hugoton Embayment and to the northeast into the Sedgwick and Salina Basins. The principle behind the use of benzo[b]naphthothiophene is similar to the benzocarbazole ratio used in the work of Larter et al. (1996) where the rod-shaped 2,1-BNT (**Fig. 50**; **APPX. II**) is adsorbed onto the clays during migration relative to the curved 1,2-BNT (**Fig. 50**; **APPX. II**; Fang et al., 2016). This ratio confirms the oil migration orientation that is seen in **Fig. 51** and **Fig. 52**, as well as what is

known about the petroleum system in the area. However, while the overall migration orientation is shown, more data points need to be added to fill void spaces so that the migration orientation can be better determined, and a filling point – the area where migration begins – can be identified (Fang et al., 2016).

Sample	4/1-MDBT	4,6/(1,4+1,6)-DMDBT	(2,6+3,6)/(1,4+1,6)-DMDBT	2,1/(2,1+1,2)-BNT
HE-A1	5.49	0.82	0.42	0.87
HE-A2	3.17	0.97	0.56	0.79
HE-C1	4.76	1.02	0.47	0.89
HE-C2	3.40	1.07	0.66	0.86
HE-C3	4.53	0.99	0.56	0.88
HE-C4	3.88	0.98	0.59	0.83
HE-C5	3.17	1.23	0.72	0.81
HE-F1	3.34	1.10	0.67	0.88
HE-F2	4.01	1.01	0.52	0.88
HE-H1	3.71	0.87	0.74	0.87
HE-L1	4.50	0.91	0.57	0.87
HE-L10	3.06	1.07	0.69	0.88
HE-L11	3.63	0.98	0.64	0.88
HE-L12	2.75	1.20	0.80	0.84
HE-L13	2.79	1.20	0.80	0.84
HE-L14	3.52	0.99	0.65	0.87
HE-L15	3.10	1.09	0.76	0.85
HE-L2	4.36	0.75	0.44	0.83
HE-L3	3.19	0.97	0.66	0.79
HE-L4	3.30	1.12	0.77	0.80
HE-L5	3.25	1.07	0.69	0.87
HE-L6	3.15	0.95	0.56	0.89
HE-L7	3.38	0.83	0.71	0.91
HE-L8	1.96	0.87	0.72	0.88
HE-L9	3.17	1.02	0.67	0.86
HE-M1	4.45	1.06	0.49	0.53
HE-M2	3.64	0.85	0.48	0.80
HE-M3	4.04	1.14	0.57	0.56
HE-M4	4.32	1.10	0.64	0.70
HE-M5	2.73	0.92	0.75	0.86
HE-M6	5.61	0.88	0.44	0.88
HE-S1	4.13	1.07	0.62	0.89
WF-B1	4.54	0.98	0.56	0.73
WF-B2	4.71	0.66	0.31	0.92
WF-B3	4.89	0.83	0.41	0.92
WF-B4	3.63	0.71	0.47	0.87
WF-H1	5.30	1.17	0.62	0.86
WF-H2	3.88	0.95	0.63	0.91
WF-H3	5.57	1.08	0.59	0.85
WF-P1	6.82	1.25	0.58	0.86

Table 12. Values used to infer the migration filling pathways. MDBT = Methyldibenzothiophene, DMDBT = Dimethyldibenzothiophene, BNT = Benzo[b]naphthothiophene.

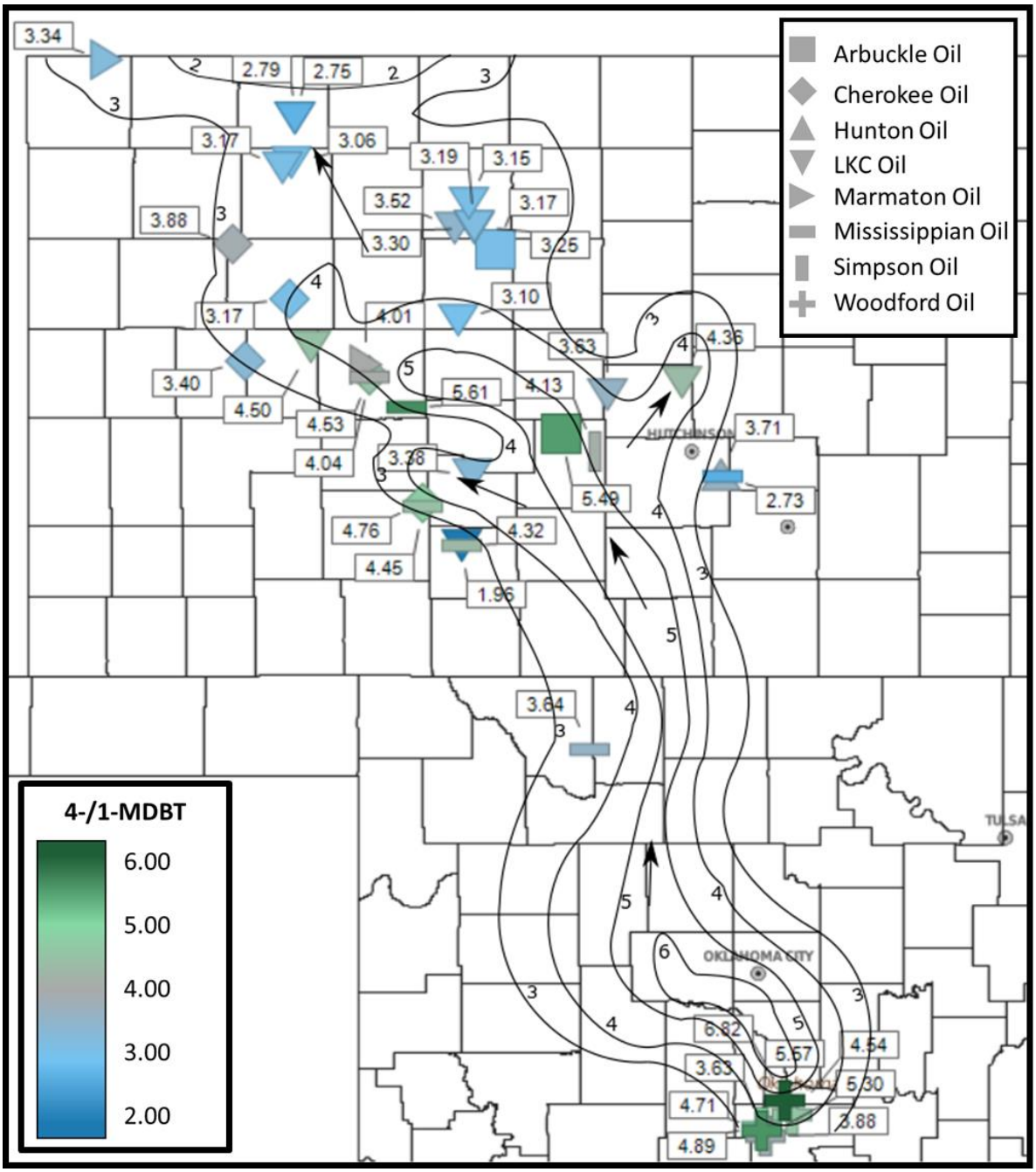

Figure 51. Contour map showing the distribution of the 4-/1-MDBT ratio (**APPX. I**) identifying filling trends of oils out of the Woodford source and into the reservoirs of the Hugoton Embayment.

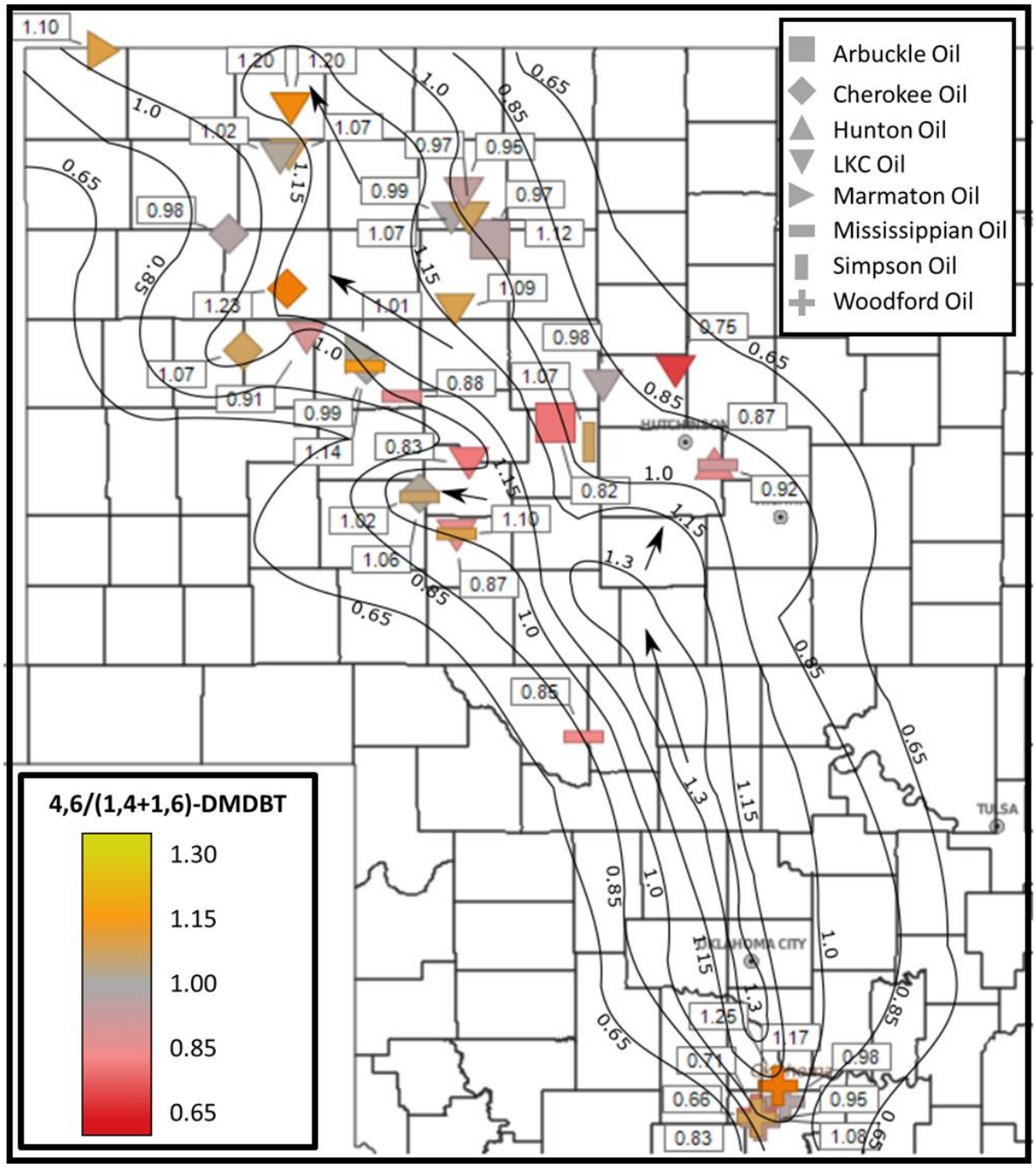

Figure 52. Contour map showing the distribution of the 4,6/(1,4+1,6)-DMDBT ratio (**APPX. I**) identifying filling trends of oils out of the Woodford source and into the reservoirs of the Hugoton Embayment.

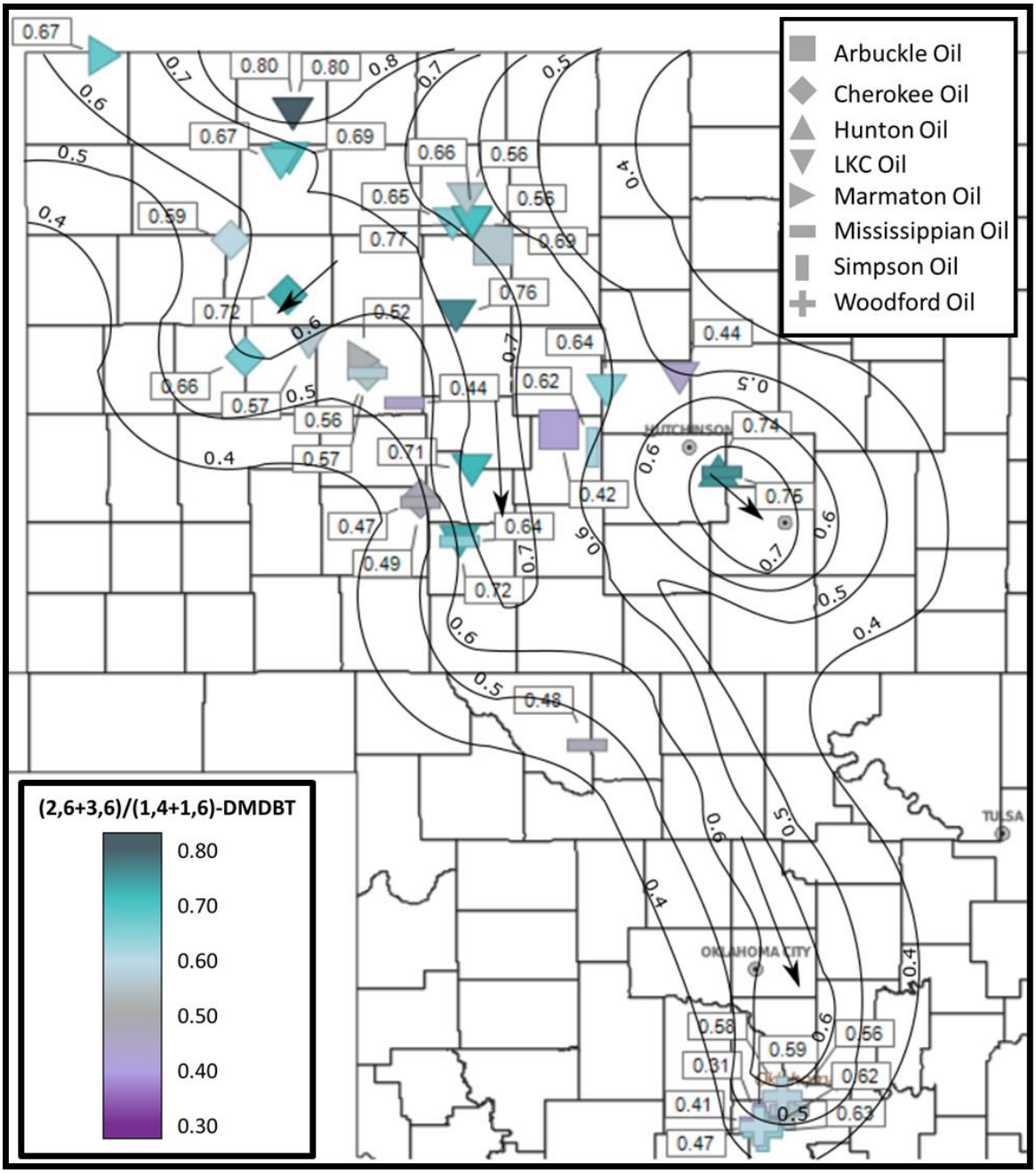

Figure 53. Contour map showing the distribution of the (2,3+3,6)/(1,4+1,6)-DMDBT ratio (**APPX. I**) identifying filling trends of oils into the Woodford source from the reservoirs of the Hugoton Embayment.

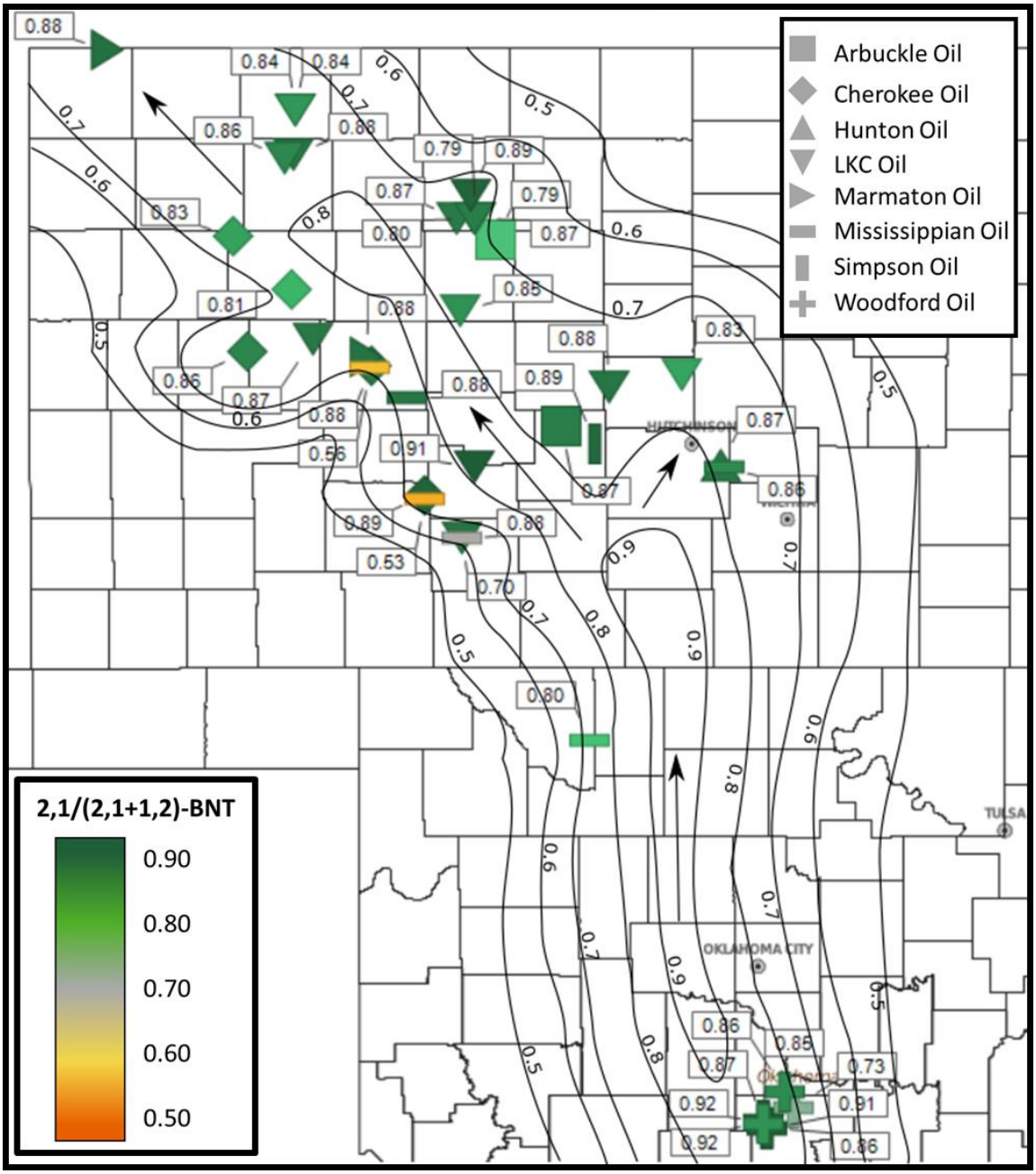

Figure 54. Contour map showing the distribution of the 2,1/(2,1+1,2)-BNT ratio identifying (**APPX. I**) filling trends of oils out of the Woodford source and into the reservoirs of the Hugoton Embayment.

4.4. Source Rock Evaluation

Five core samples collected for Rock-Eval analysis were, analyzed by GeoMark Research Lab in Houston. The samples consisted of two Chattanooga (Woodford) core samples from Kansas and three core samples from Lansing-Kansas City formation shales. The Rock-Eval data (**Table 13**) shows the data and measurements that were measured and calculated. These various measurements were oxygen index (OI), hydrogen index (HI) and production index (PI) measurements from the S1, S1, S3, T_{max}, and LECO TOC are useful in analyzing core samples (Peters, 1986; Jones, 2017).

Sample	Depth (ft)	Formation	Carbonate (wt. %)	Leco TOC (wt. %)	T_{max} (˚C)
HEC-C1	2491	Chattanooga Shale	7.6	4.3	445.0
HEC-C2	2531	Chattanooga Shale	4.1	3.1	440.0
HEC-L3	3784	LKC	13.7	0.6	439.0
HEC-L1	4194	LKC	20.2	15.9	425.0
HEC-L2	4226	LKC	7.8	2.5	435.0

S1 (mgHC/g)	S2 (mgHC/g)	S3 ($mgCO_2$/g)	(T_{max}) %Rc	HI	OI	S2/S3	S1/TOC	PI
1.1	19.3	0.3	0.9	449.1	6.0	74.3	26.3	0.1
1.0	13.2	0.3	0.8	426.5	8.4	50.8	31.6	0.1
0.1	0.4	0.6	0.7	61.5	99.1	0.6	13.7	0.2
3.5	81.3	0.9	0.5	511.1	5.6	91.3	21.9	0.0
0.4	1.5	0.5	0.7	61.0	18.1	3.4	14.5	0.2

Table 13. Rock-Eval data of the two core samples from the Chattanooga (Woodford) Shale and the three Lansing-Kansas City shales in Kansas (Formulas found in **APPX. III**).

The overall composition of the analyzed core samples shows high values of carbonate in the two of the Lansing-Kansas City core samples (13.7 and 20.2 wt. %) while the remaining samples have an average carbonate content of 5.9 wt %. The Chattanooga (Woodford) core samples have an average TOC of 3.7 wt.%, and the Lansing-Kansas City core samples have a TOC range of 15.9 wt% to 0.6 wt.%. The T_{max} ranges from 425ºC to 445 ºC which yields an average

T_{max} calculated maturity value of 0.70 T_{max} %Rc that has been calculated from the T_{max} temperatures using the formula:

$$(\boldsymbol{T_{max}})\ \%\boldsymbol{Rc} = 0.0180 \times T_{max} - 7.16$$

(**APPX. III**; Jarvie, 1991; Wust et al., 2013). The measurements of HI, OI, and S2/S3 were used to determine the kerogen type, while PI and S1/TOC are useful in identifying how much produced petroleum is in each sample (**APPX. III**; Tissot and Welte, 1984; Peters, 1986; El Sharawy and Gaafar, 2012).

Thermal Maturity

The thermal maturity calculated from Rock-Eval data is done by relating the T_{max}, the maximum temperature the S2 peak reaches, to the measured vitrinite reflectance to determine a T_{max} %Rc (Peters, 1986). The thermal maturity for the Lansing-Kansas City core extracts averages 0.60 T_{max} %Rc, which puts these rock extracts in the early oil window (**Fig. 55**) such that they could have, potentially, contributed to a small amount of the oil accumulations of the Hugoton Embayment. The Chattanooga (Woodford) core samples show that the rock extracts both have a T_{max} %Rc value of 0.73. This value puts the Chattanooga (Woodford) core samples from the Hugoton Embayment in the peak oil generation window, as can be seen in **Fig. 55** (Robertson Research Inc., 1983), which was expected.

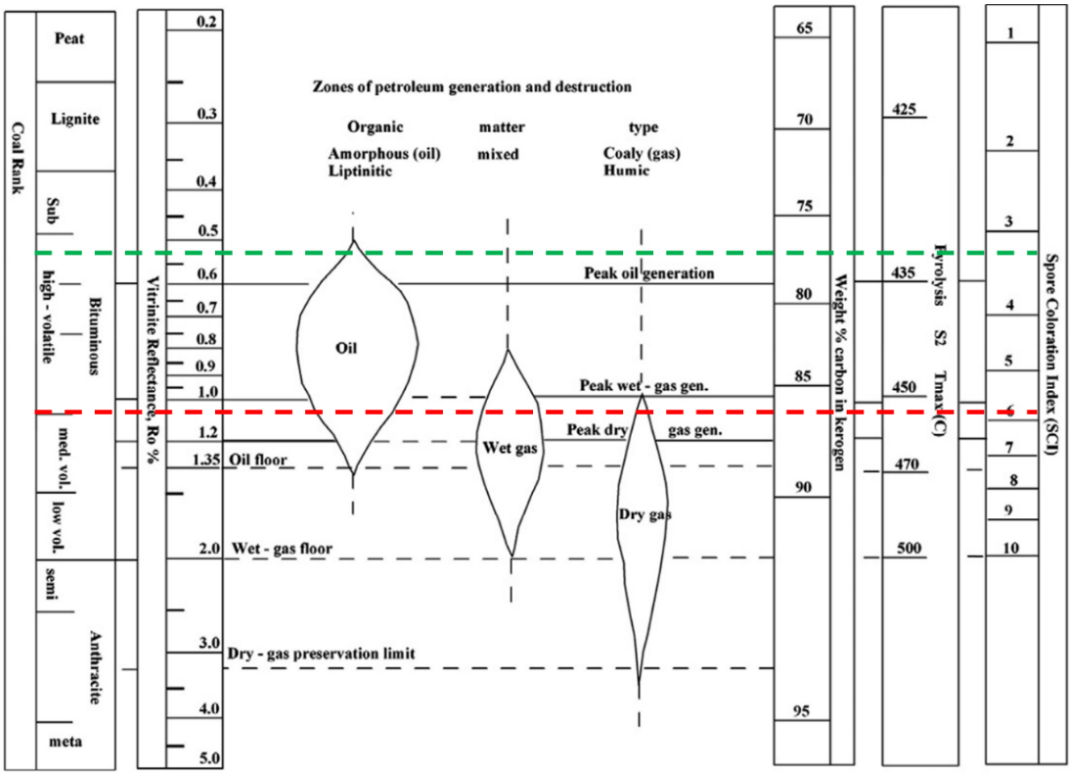

Figure 55. Zones of petroleum generation showing the top and bottom of the %Ro range (0.57-1.09 %Ro) from the samples in this study. All samples plot in the oil zone (plot modified from Robertson Research Inc., 1983).

Organofacies

Organofacies can be determined from the Rock-Eval data by predicting kerogen type which infers hydrocarbon type, organic material, and depositional environment as seen in **Table 14**. A pseudo van Krevelen diagram (**Fig. 56**) plots the HI against the OI, which is used to infer the kerogen type (Hackley et al., 2017). This figure shows that the two Chattanooga (Woodford) cores (HEC-C1 and HEC-C2) and the Lansing-Kansas City core (HEC-L2) all plot as oil prone type II marine kerogens which is what is expected for the Woodford Shale (Romero and Philp, 2012). The other samples, HEC-L1 and HEC-L3 plot in the kerogen type III-IV range and are likely immature rock of an unknown source than from the coastal plains environment.

Kerogen Type	Hydrocarbon	Organic Material	Depositional Environment
Type I	Oil Prone	Freshwater Algae/Bacteria	Lacustrine
Type II	Oil Prone	Marine Algae/Bacteria	Marine (Clastic or Carbonate)
Type III	Oil/gas Prone	Higher Plant Cuticle, Bacteria	Wet Coastal Plains
Type III-IV	Gas Prone	Lignin	Coastal Plains
Type IV	Inert	-	-

Table 14. Kerogen types with their corresponding depositional environments and biomass composition (modified from Pepper and Corvi, 1995).

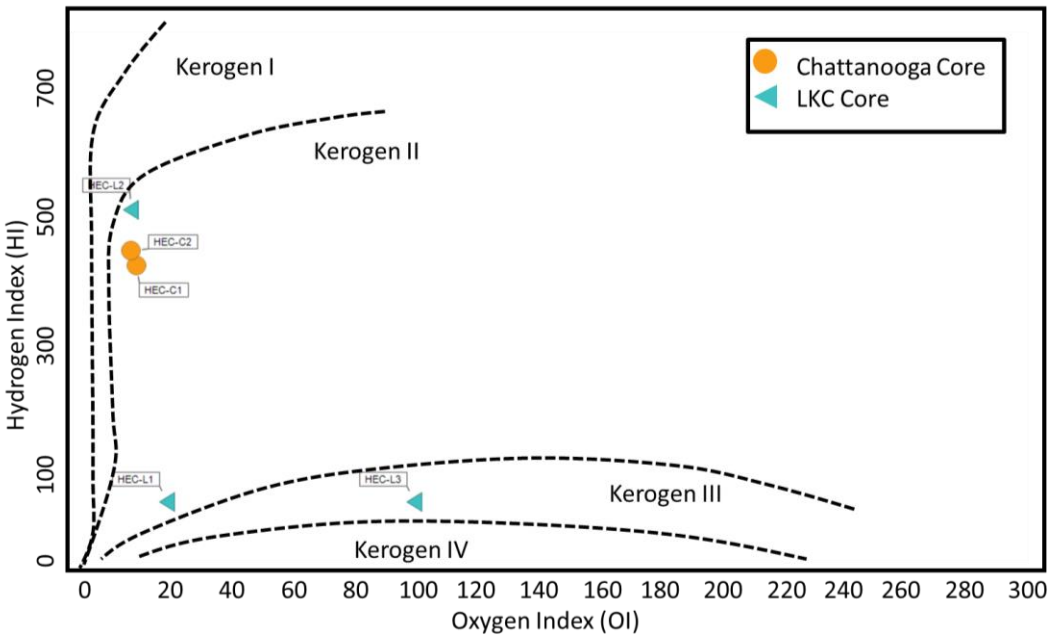

Figure 56. Pseudo van Krevelen diagram, using the HI against the OI, showing that Chattanooga core samples plot in the same kerogen type II range and the Lansing-Kansas City cores plot in both the type II and type III range (plot modified from Baudin et al., 1990).

Production Potential

The production potential of these core samples comes from the ratio of the S2 peak and the TOC% of the raw Rock-Eval data and is useful in evaluating the quantity of recoverable hydrocarbons from a reservoir (Al-Areeq, 2018). In **Fig. 57** the Chattanooga core samples are shown to have a very good potential to produce hydrocarbons, while the Lansing-Kansas City cores are drastically variable. Sample HEC-L2 shows an excellent potential for hydrocarbons

while HEC-L1 and HEC-L3 show a hydrocarbon potential that decreases from good/poor to poor. This could indicate that there is some potential production that could come out of the Lansing-Kansas City, but it is not likely as these shales are quite thin and there is high variability within the Lansing-Kansas City formation. This high variation has been seen in the Lansing-Kansas City formation since the 1920s, when the reservoirs began being produced, because there are no consistently productive reservoirs (Merriam, 1963).

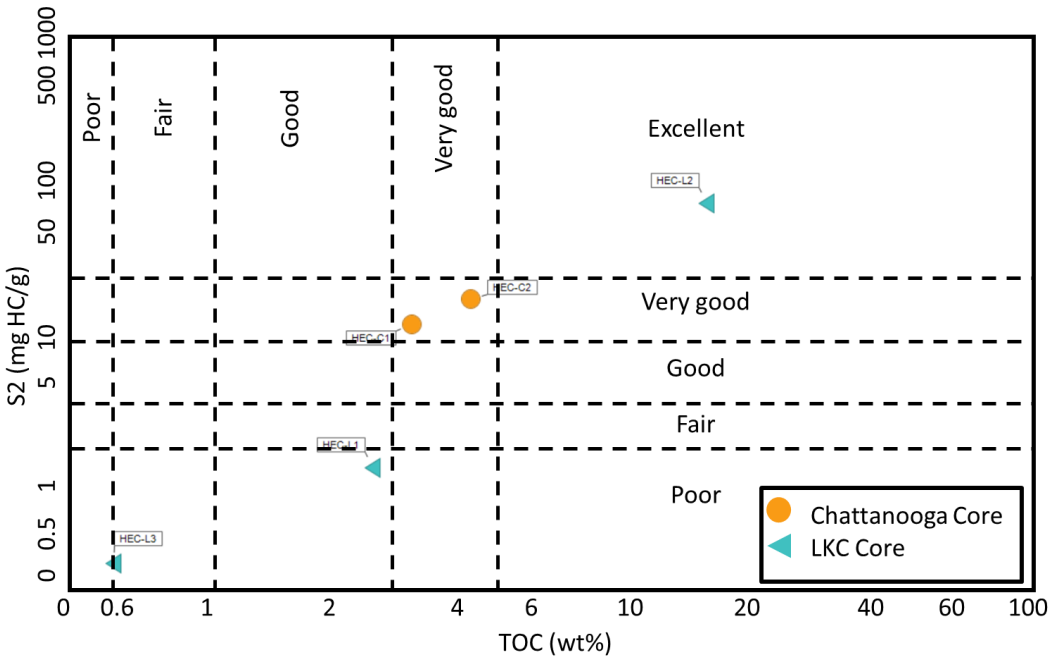

Figure 57. Hydrocarbon potential of the evaluated core samples. This plot of S2 peak and the TOC% show how the Chattanooga cores are considered very good source rocks while the Lansing-Kansas City core samples are more variable (plot modified from Peters et al., 2004b; Wang, 2016).

4.5. Isotope Analysis

Isotopes are a useful tool for oil/oil or oil/source rock correlation (Sofer, 1984). Three representative oil samples in this study have $\delta^{13}C$ saturate values ranging from -30.50 to -30.67 and $\delta^{13}C$ aromatic values that range from -29.38 to -29.98 (**Fig. 58**), similar to the oils analyzed

by Burrus and Hatch (1989). This relationship provides strong evidence that the oils on the Hugoton Embayment originated and migrated from the Woodford Shale.

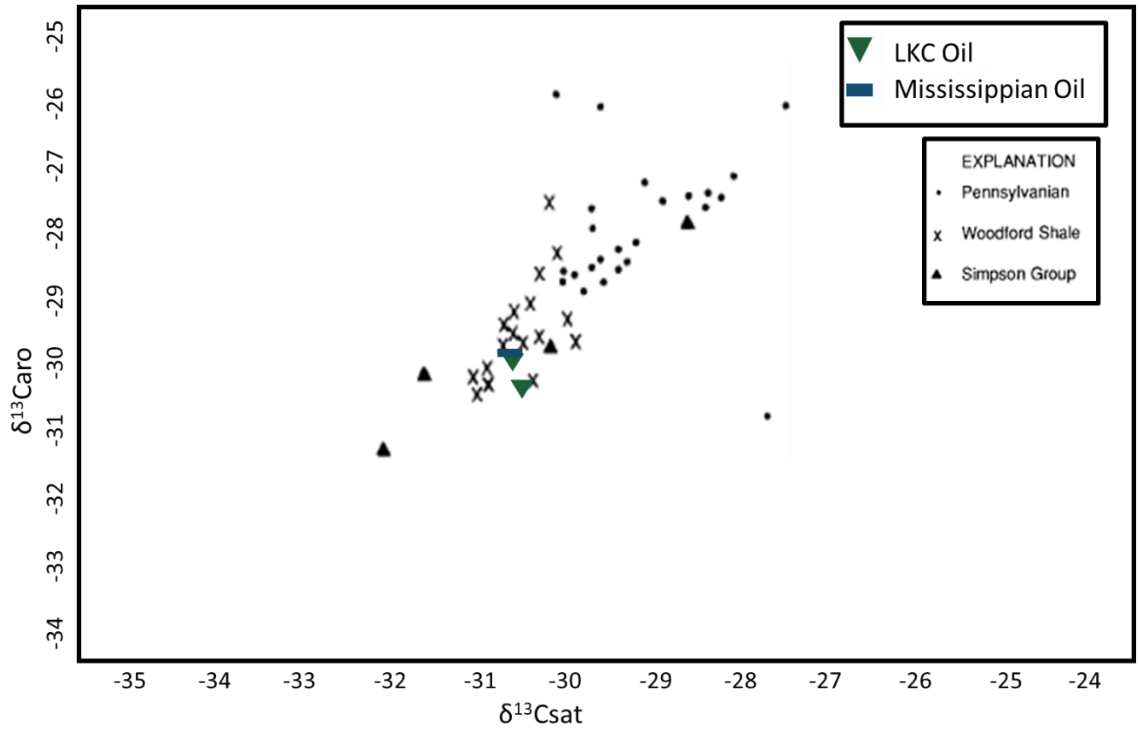

Figure 58. Isotope values for three of the samples, HE-L6, HE-L10, and HE-M2, display a light isotope composition which is characteristic of the Woodford oils. The Woodford Shale samples from the Burrus and Hatch study "X" show this same light isotope signature (Burrus and Hatch 1989; plot modified from Sofer, 1984).

CHAPTER 5: CONCLUSIONS

5.1. Source and Nature of Kansas Oils

The use of organic geochemistry to look at the oil/oil and oil/source correlation between conventional Woodford oils and those in this study found in Kansas shows striking similarities between the two types of oils. Biomarkers such as carotenoids, tricyclic terpanes, pristane, phytane, steranes, and many more, along with the use of other compounds like the phenanthrenes, dibenzothiophenes, and benzocarbazoles, were used to analyze the origin of the Hugoton Embayment oils. Through oil/source rock correlations, it has been determined that the oils found in the Hugoton Embayment of the Greater Anadarko Basin were sourced from the conventional Woodford oils. The analyses indicate a semi-stratified marine depositional environment and a marine shale lithology with a strong algal organic matter input and an average thermal maturity of 0.68 %Rc (MPI-1).

To visualize the overall characterization of the Woodford oils and Chattanooga source rocks, and the Hugoton Embayment oils and source rocks, twenty parameters (**APPX. I**) were compiled together and run through hierarchal clustering analysis to show the relationships between these samples. This is done by machine learning where data, compiled together, sorts the data points based on similarities (Kaufman and Rousseeuw, 1990; Zhang, 2016) This analysis shows a slight separation between the Hugoton Embayment oils and the conventional Woodford oils with a variance of 1.43 (**Fig. 59**). The oils on the Hugoton Embayment cluster very tightly and overlap with the conventional Woodford oils with a very minimal difference. However, the core samples from the Lansing-Kansas City do not cluster with either the conventional Woodford oils or the Hugoton Embayment oils, which was expected, as they are not of the same oil family. Rock-Eval

data also confirms that the Lansing-Kansas City core did not contribute major reserves to the surrounding reservoirs.

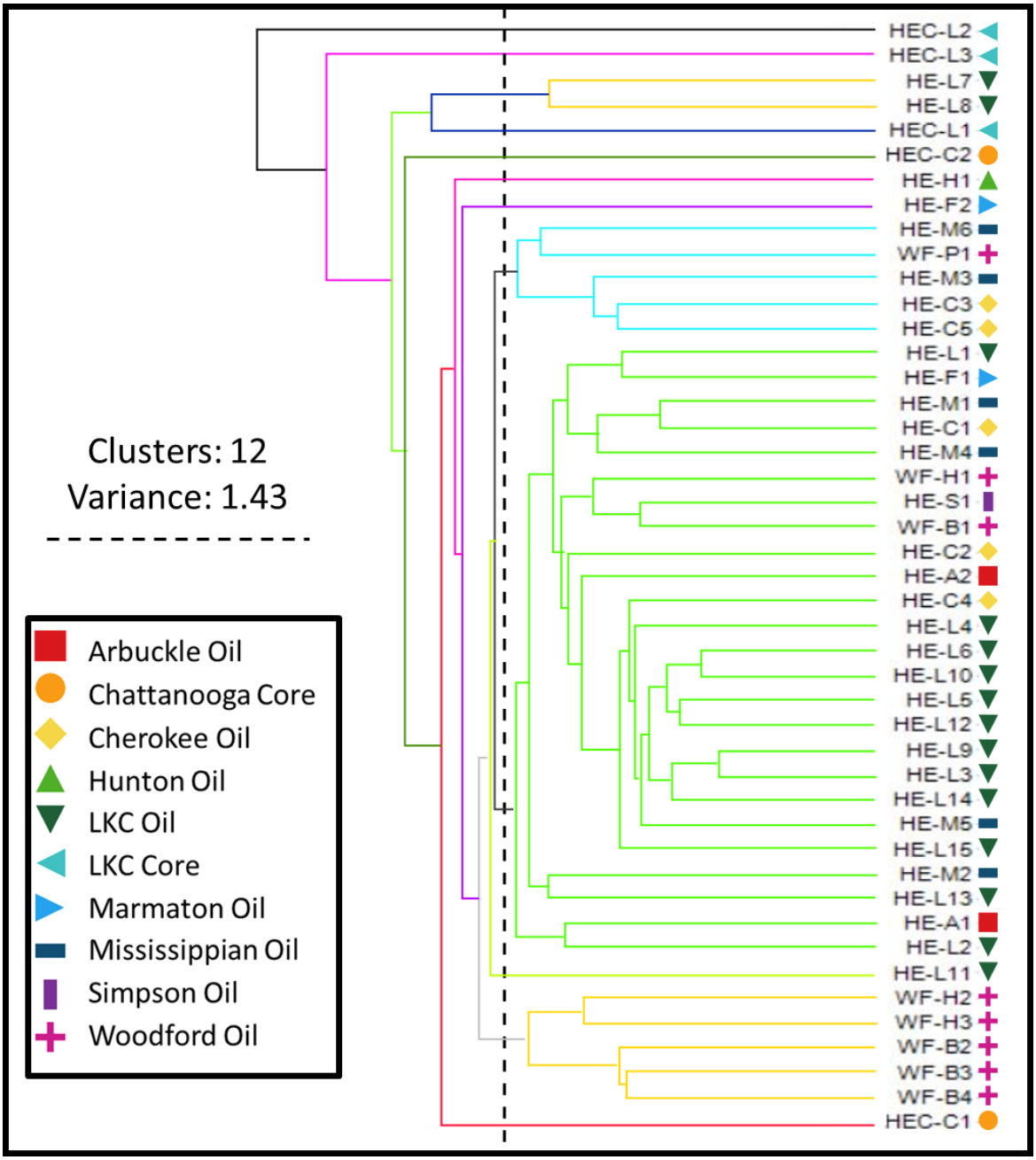

Figure 59. Hierarchal cluster analysis of all oil and rock extract samples using the following variables: MPI-1 %Rc, DBT/PHEN, 4/1MDBT, paleorenieratane/isorenieratane, Pr/C_{17}, Ph/C_{18}, Pr/Ph, C_{27}/C_{29} sterane, hopane index, $H_{31}R/H_{30}$, C_{26}/C_{25} tricyclic terpanes, C_{24}/C_{23} tricyclic terpanes, C_{22}/C_{21} tricyclic terpanes, C_{26} tricyclic terpane/C_{24} tetracyclic terpane, C_{29}/C_{30} hopanes, C_{19}/C_{23} tricyclic terpanes, C_{23}/C_{28} tricyclic terpanes, gammacerane/C_{30} hopane, C_{23} tricyclic terpane/C_{30} hopane, and the homohopane index (**APPX. I**).

5.2. Migration of Kansas Oils

The oils found on the Hugoton Embayment have many of the characteristics of conventional Woodford oils, yielding positive evidence that these oils have migrated long distances, up to 350 miles, out of Southern Oklahoma and into Kansas and the Greater Anadarko Basin. Previous work on similar oils also indicated that this was the case, but this current study used a multitude of biomarkers, whole oil analysis, and Rock-Eval to illustrate the similarities better. Some of the lines of evidence include a similar distribution of carotenoids – a characteristic of conventional Woodford oils – in Hugoton Embayment oils, a decrease in thermal maturity as oils move north into Kansas, and the maps of migration pathways that were determined by the sulfur-bearing compounds. Also, in the organic rich shales of the Lansing-Kansas City formation, GCMS data shows a lack of carotenoids – and many other differences – that confirms that the oils found in the Hugoton Embayment reservoirs are not sourced locally.

5.3. Future Work

1. Analyze the individual reservoirs, on a small scale, to better understand the variability of the production from the reservoirs.

2. Evaluate individual reservoir changes over longer distance to show a gradual change in characteristics that could be tied into migration and maybe migration distance.

3. Evaluate the benzocarbazole and benzonaphthothiophene ratios as migration indicators over a larger area to better understand the effects of migration on this ratio.

4. Undertake a more detailed core analysis of the Lansing-Kansas City formation to better determine the variability of the organic rich shales.

REFERENCES

Ahmed, M., Khan, S. I. and Sattar, M. A. (1991). Geochemical characterization of oils and condensates in the Bengal Foredeep, Bangladesh. *Journal of Southeast Asian Earth Sciences* **5**, 391-399.

Al-Khafaji, A. J., Hakimi, M. H. and Najaf, A. A. (2018). Organic geochemistry characterization of crude oils from Mishrif reservoir rocks in the southern Mesopotamian Basin, South Iraq: Implication for source input and paleoenvironmental conditions. *Egyptian Journal of Petroleum* **27**(1), 117-130.

Al-Areeq, N. M. (2018). Petroleum source rocks characterization and hydrocarbon generation. In: *Recent insights in Petroleum Science and Engineering*. (N. M. Al-Areeq, ed.), 1-30.

Althoff, C. D. (2012). Characterization of depositional megacycles in the Woodford through of Central Oklahoma. University of Oklahoma M. S. Thesis, 107pp.

Baars, D.L. and Watney, W.L. (1991). Paleotectonic control of reservoir facies. In: *Sedimentary Modelling: Computer Simulations and Methods for Improved Parameter Definition*. (F. K. Franseen, W. L.Watney, C.G. Sr. Kendal, Eds.). *Kansas Geological Survey Bulletin* **233**, 253-262.

Bakr, M. M. Y. and Wilkes, H. (2002). The influence of facies and depositional environment on the occurrence and distribution of carbazoles and benzocarbazoles in crude oil: A case study from the Gulf of Suez, Egypt. *Organic Geochemistry* **33**, 561-580.

Ball, M. M., Henry, M. E. and Frezon, S. E. (1991). Petroleum geology of the Anadarko Basin region, Province (115), Kansas, Oklahoma, Texas. *U. S. Geological Survey* **88**-450W, 1-38.

Baudin, R., Herbin, J. P., Bassoullet, J. P., Dercourt, J. Lachkar, G., Manivit, H. and Renard, M. (1990). Distribution of organic matter during the Toarcian in the Mediterranean Tethys and Middle East. In: *Deposition of organic facies* (A. Y. Huc, Ed.). Tulsa,OK: AAPG, 73-91.

Beebe, W. (1956). Geology of Northwestern Anadarko Basin [Abstract]. *American Association of Petroleum Geology Bulletin* **40**(2), 430.

Bragg, J. B., Prince, R. C. Harner, E. J. and Atlas, R. M. (1994). Effectiveness of bioremediation for the Exxon Valdez oil spill. *Nature* **368**, 413-418.

Brocks, J. J., Jarrett, A. J. M., Sirantoine, E., Hallmann, C., Hoshino, Y., and Liyanage, T. (2017). The rise of algae in Cryogenian oceans and the emergence of animals. *Nature* **548**, 578-581.

Burns, W., McKervey,, M. A., Mitchell, T. R. B., and Rooney, J. J. (1978). A new approach to the construction of diamondoid hydrocarbons. Synthesis of anti-Tetramantane. *Journal of the American Chemical Society* **100**(3), 906-911.

Burruss, R. C. and Hatch, J. R. (1989). Geochemistry of oils and hydrocarbon source rocks, Greater Anadarko Basin: Evidence for multiple sources of oil and long-distance oil migration. *Oklahoma Geological Survey* **90**, 53-64.

Canipa-Morales, N. K., Galan-Vidal, C. A., Guzman Vega, M. A. and Jarvie, D. M. (2003). Effect of evaporation on C_7 light hydrocarbon parameters. *Organic Geochemistry* **34**(6), 813-826.

Cardott, B. J. (2012). Thermal maturity of Woodford Shale gas and oil plays, Oklahoma, USA. *International Journal of Coal Geology* **103**, 109-119.

Cardott, B. J. (2013). Woodford Shale: From hydrocarbon source rock to reservoir. *American Association of Petroleum Geologists Search and Discovery* **50817**.

Cardott, B. J. (2017). Oklahoma Shale Resource Plays. *Oklahoma Geology Notes*, 21-30.

Cassani, F., Gallango, O., Talukdar, S., Vallejos, C. and Ehrmann, U. (1987). Methylphenanthrene maturity index of marine source rock extracts and crude oils from the Maracaibo Basin. In: *Advances in Organic Geochemistry* (A. G. Douglas and J. R. Maxwell, eds.). **13**(1-3), 73-80.

Chen, J. and Summons, R. (2001). Complex patterns of steroidal biomarkers in Tertiary lacustrine sediments of the Biyang Basin, China. *Organic Geochemistry* **32**, 115-126.

Clegg, H., Wilkes, H., Oldenburg, T., SantaMaria-Orozco, D., and Horsefields, B. (1998). Influence of maturity on carbazole and benzocarbazole distributions in crude oils and source rocks from the Sonda de Campeche, Gulf of Mexico. *Organic Geochemistry* **29**(1-3), 183-194.

Connock, G. T. (2015). Paleoenvironmental interpretation of the Woodford Shale, Wyche Farm Shale Pit, Pontotoc County, Arkoma Basin, Oklahoma with primary focus on water column structure. University of Oklahoma M.S. Thesis, 235pp.

Connock, G. T., Nguyen, T. X. and Philp, R. P. (2018). The development and extent of photic-zone euxinia concomitant with Woodford Shale deposition. *American Association of Petroleum Geologists Bulletin* **102**(6), 959-986.

Dahl, T. W., Hammarlund, E. U., Anbar, A. D., Bond, D. P. G., Gill, B. C., Gordon, G. W., Knoll, A. H., Nielsen, A. T., Schovsbo, N. H. and Canfield, D. E. (2010). Devonian rise in atmospheric oxygen correlated to the radiations of terrestrial plants and large predatory fish. *Proceedings of the National Academy of Science of the United States* **107**(42), 17911-17915.

Dahl, J., Moldowan, J. M., Peters, K., Claypool, G. Rooney, M., Michael, G., Mellos, M. and Kohnen, M. (1999). Diamondoid hydrocarbons as indicators of oil cracking. *Nature* **399**, 54-56.

Dembicki, H. (2017). *Practical Petroleum Geochemistry for Exploration and Production*. Elsevier, 342pp.

Dolton, G. L. and Fin, T. M. (1989). Petroleum geology of the Nemaha Uplift, Central Mid-Continent. *U. S. Geological Survey* **88**(450D), 1-39.

Douglas, A. G., Bence, A. E., McMillen, S. J., Prince, R. C. and Butler, E. L. (1996). Environmental stability of selected petroleum hydrocarbon source and weathering ratios. *Environmental Science & Technology* **30**, 2332-2339.

El Sharawy, M. S. and Gaafar, G. R. (2012). Application of well log analysis for source rock evaluation in the Duwi Formation, Southern Gulf of Suez, Egypt. *Journal of Applied Geophysics* **80**, 129-143.

El-Sabagh, S. M., El-Naggar, A. Y., El Nady, M. M., Badr, I. H., Rashad, A. M., Ebiad, M. A. and Abdullah, E. S. (2015). Bulk geochemical characterization of crude oils from Gulf of Suez, Egypt. *International Journal of Current Research* **7**(9), 20574-20380.

El-Sabagh, S. M., El-Naggar, A. Y., El Nady, M. M., Ebiad, M. A., Rashad, A. M. and Abdullah, E. S. (2018). Distribution of triterpanes and steranes biomarkers as indication of organic matters input and depositional environments of crude oils of oilfields in Gulf of Suez, Egypt. *Egyptian Journal of Petroleum* **27**(4), 969-977.

Ekwunife, I. C. (2017). Assessing mudrock characteristics, high-resolution chemostratigraphy, and sequence stratigraphy of the Woodford Shale in the McAlister Cemetery Quarry, Ardmore Basin, Oklahoma. University of Oklahoma M.S. Thesis, 153pp.

England, W. A. (2007). Reservoir geochemistry – A reservoir engineering perspective. *Journal of Petroleum Science and Engineering* **58**, 344-354.

Evans, C. S. (2011). Geothermal energy and heat pump potential in Kansas. *Kansas Geological Survey* **31**, 1-6.

Fahl, K and Stein, R. (1999). Biomarkers as organic-carbon-source and environmental indicators in the Late Quaternary Artic Ocean: Problems and Perspectives. *Marine Chemistry* **63**(3-4), 293-309.

Fang, R., Wang, T. G., Li, M., Xiao, Z., Zhang, B., Huang, S., Shi, S., Wang, D. and Deng, W. (2016). Dibenzothiophenes and benzo[b]naphthothiophenes: Molecular markers for tracing oil filling pathways in the carbonate reservoir of the Tarim Basin, NW China. *Organic Geochemistry* **91**, 68-80.

Farahat, L. A. and El-Gendy, N. S. (2008). Biodegradation of the Baleym mix crude oil in soil microcosm by some locally isolated Egyptian bacterial strains, soil and sediment contamination. *International Journal* **17**(2), 150-162.

Fernandes, A. S., Casagrande do Nascimento, T., Jacob-Lopes, E., de Rosso, V. V. and Zepka, L. Q. (2018). Carotenoids – A brief overview on its structure, biosynthesis, synthesis, and applications. In: *Progress in Carotenoid Research*. (L. Q. Zepka, ed.). IntechOpen, 659pp.

Fowler, M. G. and Douglas, A. G. (1984). Distribution and structure of hydrocarbons in four organic rich Ordovician rocks. *Organic Geochemistry* **6**, 105-114.

Futrell, J. H. (2000). Development of tandem mass spectrometry: One perspective. *International Journal of Mass Spectrometry* **200**, 495-508.

Gallardo, J. D. and Blackwell, D. D. (1999). Thermal structure of the Anadarko Basin. *American Association of Petroleum Geologists Bulletin* **83**(2), 333-361.

GeoMark Research (2013). Detailed analysis of source rock, gas, and oil samples from the Woodford and Chattanooga Formation in Oklahoma and Kansas. https://geomarkresearch.com/studies/mid-continent-woodford-petroleum-system-study/

Gerhard, L. C. (2004). A new look at an old petroleum province. *Current Research in Earth and Science Bulletin* **250**(1), 1-27.

Grantham, P. J. (1986). Sterane isomerization and moretane/hopane ratios in crude oils derived from Tertiary source rocks. *Organic Geochemistry* **9**(6), 293-304.

Grayson, M. A. (2016). A history of gas chromatography mass spectrometry (GC/MS). In: *The Encyclopedia of Mass Spectrometry*. (M. A. Gross, and R. M. Caprioli, eds.). Elsevier, 152-158.

Grice, K. Schaeffer, P. Schwark, L. and Maxwell, J. R. (1996). Moleculecular indicators of paleoenvironmental conditions in an immature Permian shale (Kupferschiefer, Lower Rhine Basin, north-west Germany) from free sulfide-bound lipids. *Organic Geochemistry* **25**, 131-147.

Hackley, P. C., Walters, C. C., Kelemen, S. R., Mastalerz, M. and Lowers, H. A. (2017). Organic petrology and micro-spectroscopy of Tasmanites microfossils: Applications to kerogen transformations in the early oil window. *Organic Geochemistry* **114**, 23-44.

Hakimi, M. H. and Al-Sufi, S. A. (2018). Organic geochemistry investigations of crude oils from Bayoot oilfield in the Masila Basin, east Yemen and their implications for origin of organic matter and source-related type. *Egyptian Journal of Petroleum* **27**, 37-54.

Hays, L. E., Beatty, T., Henderson, C. M., Love, G. D., and Summons, R. E. (2007). Evidence for photic zone euxinia through the end-Permian mass extinction in the Panthalassic Ocean (Peace River Basin, Western Canada). *Palaeoworld* **16**, 39-50.

Hester, T., Sahl, H. and J. Schnoker (1988). Cross sections based on gamma-ray density, and resistivity log showing the stratigraphic unites of the Woodford Shale in Anadarko basin, Oklahoma: United States Geological Survey, Miscellaneous Field Studies Map 2054, 2 sheets.

Higley, D. H. (2014). Assessment of undiscovered oil and gas resources of the Anadarko Basin Province of Oklahoma, Kansas, Texas, and Colorado. In: *Petroleum Systems and Assessment of Undiscovered Oil and Gas in the Anadarko Basin Province, Colorado, Kansas, Oklahoma, and Texas—USGS Province 58* (D. H. Higley, ed.). Chapter: 4. U.S. Geological Survey, 1-31.

Ho, T. Y., Rogers, M. A., Drushel, H. V., and Koons, C. B. (1974). Evolution of sulfur compounds in crude oils. *American Association of Petroleum Geologists Bulletin* **58**(11), 2338-2348.

Hossain, Z. M., Sampei, Y. and Roser, B. P. (2009). Characterization of organic matter and depositional environment of Tertiary mudstones from the Sylhet Basin, Bangladesh. *Organic Geochemistry* **40**, 743–754.

Huang, W. Y. and Meinschein, W. G. (1979). Sterols as ecological indicators. *Geochimica et Cosmochimica Acta* **43**, 739-745.

Hughes, W. B. (1984). Use of thiophenic organosulfur compounds in characterizing crude oils derived from carbonate versus siliciclastic sources. In: *Petroleum Geochemistry and Source Rock Potential of Carbonate Rocks* (J. G. Palacas, ed.). AAPG, Tulsa, OK, 181-196.

Hughes, W. B., Holba, A. G., and Dzou, L. I. P. (1995). The ratios of dibenzothiophene to phenanthrene and pristane to phytane as indicator of depositional environment and lithology of petroleum source rocks. *Geochimica et Cosmochimica Acta* **59**(17), 3581-3598.

Hunt, J. M. (1996). *Petroleum Geochemistry and Geology*. New York, W. H. Freeman and Company, 743pp.

Jalees, M. I., Bianchi, T. S, Sassen, R., and Tahira, F. (2011). Diamondoids and biomarkers: as a tool to better define the effects of thermal cracking and microbial oxidation on oils/condensates from reservoirs of the Upper Indus Basin, Pakistan. *Carbonates Evaporites* **26**, 155-165.

Jarvie, D. M. (1991). Factors affection Rock-Eval derived kinetic parameters. *Chemical Geology* **93**, 79-99.

Johnson, K. S. (1989). Geologic evolution of the Anadarko Basin. *Oklahoma Geological Survey Bulletin* **90**, 3-12.

Jones, P. J. and Philp, R. P. (1990). Oils and source rocks from Pauls Valley, Anadarko Basin, Oklahoma, U.S.A. *Applied Geochemistry* **5**, 429-448.

Jones, L. C. (2017). An integrated analysis of sequence stratigraphy, petroleum geochemistry, and Devonian Mass Extinction events in the Woodford Shale, Southern Oklahoma. University of Oklahoma M.S. Thesis, 198pp.

Kansas Geological Survey (2009). Oil and gas fields of Kansas. *Kansas Geological Survey*, https://maps.kgs.ku.edu/oilgas/.

Kashirtsev, V. A., Parfenova, T. M., Golovko, A. K., Nikitenko, B. L., Zueva, I. N. and Chalaya, O. N. (2018). Phenanthrene biomarkers in the organic matter of Precambrian and Phanerozoic deposits and in the oils of the Siberian Platform. *Russian Geology and Geophysics* **59**, 1380-1388.

Kaufman, L. and Rousseeuw, P. J. (1990*). Finding Groups in Data – An Introduction to Cluster Analysis*. Hoboken:John Wiley & Sons, 349pp.

Kim, D. and Philp, R. P. (2001). Extended tricyclic terpanes in Mississippian rocks from the Anadarko Basin, Oklahoma. *Oklahoma Geological Survey Bulletin* **105**, 109-127.

Kirson, I. and Glotter, E. (1981). Recent developments in naturally occurring ergostane-type steroids. A review. *Journal of Natural Products* **44**(6), 633-647.

Koopmans, M. P., Schouten, S., Kohnen, M. E. L. and Sinninghe-Damste, S. (1996). Restricted utility of aryl isoprenoids as indicators for photic zone anoxia. *Geochimica et Cosmochimica Acta* **60**(23), 4873-4876.

Kornacki, A. S. and Dahl, J. E. (2016). Evidence of some oil accumulations in the Woodford Formation and the Meramec Formation received an additional charge of very dry thermal gas. *American Association of Petroleum Geologists Search and Discovery* **41879**.

Kvale, E. and Bynum, J. (2014). Regional upwelling during Late Devonian Woodford deposition in Oklahoma and its influences on hydrocarbon production and well completion. *American Association of Petroleum Geologists Search and Discovery* **80410**.

Larter, D. W., Lee, M. L. and Bartle, K. D. (1981). Chemical class separation and characterization of organic compounds in synthetic fuels. *Analytical Chemistry* **53**(11), 1612-1620.

Larter, S. R., Bowler, B. F. J., Li, M., Chen, M., Brincat, D., Bennett, B., Noke, K., Donohoe, P., Simmons, D., Kohnen, M., Allan, J., Telnaes, N., and Horstand, I. (1996). Molecular indicators of secondary oil migration distances. *Nature* **383**, 593-597.

Lewan, M. D. (1983). Effects of thermal maturation on stable organic carbon isotopes as determined by hydrous pyrolysis of Woodford Shale. *Geochimica et Cosmochimica Acta* **47**, 1471-1479.

Li, M., Larter, S. R., and Soddart, D. (1992). Liquid chromatography separation schemes for pyrrole and pyridine nitrogen aromatic heterocycle fractions from crude oils suitable for rapid characterization of geochemical samples. *Analytical Chemistry* **64**, 1337-1344.

Li, M., Wang, T., Zhong, N., Zhang, W., Sadik, A. and Li, H. (2013). Ternary diagram of fluorenes, dibenzothiophenes and dibenzofurans: Indicating depositional environment of crude oil source rocks. *Energy Exploration & Exploitation* **31**, 569-588.

Liborius, A. and Sneddon, A. (2017). Organic-inorganic distribution of the Woodford Shale in Kingfisher County, STACK play, Northern Oklahoma. *American Association of Petroleum Geologists Search and Discovery* **51444**.

Liu, M. (2015). The utilization of carbazole and benzocarbazole as possible indicators of relative migration distances for Woodford oils in the Anadarko Basin. University of Oklahoma M.S. Thesis, 120pp.

Lu, H., Shen, C., Zhang, Z., Liu, M., Sheng, G., Peng, P., and Hsu, C. S. (2015). 2,3,6-/2,3,4-Aryl isoprenoids in Paleocene crude oils from Chinese Jianghan Basin: Constrained by water column stratification. *Energy Fuels* **29**, 4690-4700.

Mackenzie, A., Patience, R. L. and Maxwell, J. R. (1980). Molecular parameters of maturation in the Toarcian shales, Paris Basin, France - I. Changes in the configurations of acyclic isoprenoid alkanes, steranes and triterpanes. *Geochimica et Cosmochimica Acta* **44**, 1709-1721.

Mango, F. D. (1997). The light hydrocarbons in petroleum: A critical review. *Organic Geochemistry* **26** (7/8), 417-440.

Masterson, W. D. (2001). Petroleum filling history of central Alaskan North Slope fields. University of Texas - Dallas, Ph. D. Dissertation, 222pp.

McKirdy, D. M., Aldridge, A. M. and Ypma, P. J. M. (1983). A geochemical comparison of some crude oils from Pre-Ordovician carbonate rocks. In: *Advances in Organic Geochemistry 1981* (M. Bjoroy, C. Albrecht, C. Cornford, et al. eds.). John Wiley & Sons:New York, NY, 99-107.

McWilliam, I. G and Dewar, R. A. (1958). Flame ionization detector for gas chromatography. *Nature* **181**(4611), 760pp.

Merriam, D. F. (1963). The geologic history of Kansas. *Kansas Geological Survey Bulletin* **162**, http://www.kgs.ku.edu/Publications/Bulletins/162/index.html.

Merriam-Webster (2019). Stratify. Received 6 November 2019 from https://www.merriam-webster.com/dictionary/stratifying.

Mitchell, J. (2012). The Anadarko Basin: Oil and gas exploration - past, present and future. *Oklahoma Geological Survey*, 61pp.

Moldowan, J. M., Seifert, W. K., and Gallegos, E. J. (1985). Relationship between petroleum composition and depositional environment of petroleum source rocks. *American Association of Petroleum Geologists Bulletin* **69**, 1255-1268.

Moustafa, Y. M and Morsi, R. E. (2012). Biomarkers. In: *Chromatography and Its Applications*. (S. Dhanarasu, ed.). InTech, 165-186.

Mpanje, L. (2016). Geology of the Lansing-Kansas City Group in the O'Connor Field, Stafford County, Kansas. *Kansas Geological Survey Bulletin* **51**(2), 11-18.

Newell, K. D. and Hatch, J. R. (1999). Petroleum geology and geochemistry of a production trend along the McPherson anticline, in central Kansas, with implications for long- and short-distance oil migration. In: *Transactions of the American Association of Petroleum Geologists Midcontinent Section Meeting* (D. F. Merriam, ed.). Kansas Geological Society Open-file Report 99-28, 22-28.

Newell, K. D., Hatch, J. R. (2000). A petroleum system for the Salina Basin in Kansas based on organic geochemistry and geologic analog. *Natural Resources Research 9*(3), 169-200.

Newell, K. D., Watney, W. L., Cheng, S. W. L. and Brownrigg, R. L. (1987). Stratigraphic and spatial distribution of oil and gas production in Kansas. Kansas Geological Survey: Subsurface Geology **9**, 1-86.

Northcutt, R. A. and Campbell, J. A. (1996). Geologic provinces of Oklahoma. In: *Transactions of the 1995 American Association of Petroleum Geologists Mid-Continent Section Meeting*. (D. L Swindler, and C. P. Williams, Eds.). Tulsa Geological Society, 128-134 .

Nowaczewski, V. (2011). Biomarker and paleontological investigations of the Late Devonian Extinctions, Woodford Shale, Southern Oklahoma. University of Kansas M.S. Thesis, 96pp.

Oung, J. N. and Philp, R. P. (1994). Geochemical characterizes of oils from Taiwan. *Journal of Southeast Asian Earth Sciences* **9**(3), 193-206

Pearson, C. A, (2016). Geochemical characterization of the Upper Mississippian Goddard Formation, Springer Group, in the Anadarko Basin of Oklahoma. University of Oklahoma M.S. Thesis, 169pp.

Pedentchouk, N. and Turich, C. (2017). Carbon and hydrogen isotopic compositions of *n*-alkanes as a tool in petroleum exploration. In: *From Source to Seep: Geochemical Applications in Hydrocarbon Systems*. (M. Lawson, M. J. Formolo, and J. M. Eiler, eds.). Geological Society, London, Special Publications, 468pp.

Peng, P. A.; Sheng, G. Y.; Jiang, J. G.; Fu, J. M.; Bao, J. P.; Yu, Z. Q. (2007). Hydrocarbon compositions of soluble organic matter and characteristics of biomarkers in source rocks in a hypersaline lacustrine basin. In: *Generation, Migration and Accumulation of Oils and Gases in Hypersaline Lacustrine Basin, China*. (J. G. Jiang, P. A. Peng, J. M. Fu, G. Y. Sheng, Eds.). Guangdong Science and Technology Press: Guangzhou, China, 357pp.

Pepper, A and Corvi, P. (1995). Simple kinetic models of petroleum formation. Part I: Oil and gas generation from kerogen. *Marine and Petroleum Geology* **12**, 291-319.

Perry, W. J. (1989). Tectonic evolution of the Anadarko Basin region, Oklahoma. *U. S. Geological Survey Bulletin* **1866-A**, 1-19.

Peters, K. E. (1986). Guidelines for evaluating Petroleum source rock using programmed pyrolysis. *American Association of Petroleum Geologists Bulletin* **70**, 318-329.

Peters, K.E. and Cassa, M.R. (1994). Applied source-rock geochemistry. *American Association of Petroleum Geologists Memoirs* **60**, 93-120.

Peters, K. E. and Fowler, M. G. (2002). Applications of petroleum geochemistry to exploration and reservoir management. *Organic Geochemistry* **33**, 5-36.

Peters, K. E. and Moldowan, J. M. (1991). Effects of source, thermal maturity, and biodegradation on the distribution and isomerization of homohopanes in petroleum. *Organic Geochemistry* **17**(1), 47-61pp.

Peters, K. E., Walters, C. C., and Moldowan, J. M. (2004a). *The Biomarker Guide, Volume 1: Biomarkers and Isotope in the Environment and Human History* (2nd ed.). Cambridge, UK: Cambridge University Press, 471pp.

Peters, K. E., Walters, C. C., and Moldowan, J. M. (2004b). *The Biomarker Guide, Volume 2: Biomarkers and Isotope in Petroleum Exploration and Earth History* (2nd ed.). Cambridge, UK: Cambridge University Press, 1155.

Philp, R. P., Oung, J. and Lewis, C. A. (1988). Biomarker determinations in crude oils using a triple-stage quadrupole mass spectrometer. *Journal of Chromatography* **446**, 3-16.

Philp, R. P. (2007). The emergence of stable isotopes in environmental and forensic geochemistry studies: A review. *Environmental Chemistry Letters* **5**, 57-66.

Powell, T. G. and McKirdy, D. M. (1973). Relationship between ration of pristine to phytane, crude oil composition and geological environment in Australia. *Bureau of Mineral Resources, Geology and Geophysics: Canberra*, 38-40.

Price, L. (1980). Shelf and shallow basin oil as related to hot-deep origin of petroleum. *Journal of Petroleum Geology* **3**(1), 91-116.

Pu, F., Philp, R P., Zhenxi, L. and Guangguo, Y. (1990). Geochemical characteristics of aromatic hydrocarbons of crude oils and source rocks from different sedimentary environments. *Advances in Organic Geochemistry* **16**(1-3), 427-435.

Radke, M. and Welte, D. H. (1983). The methylphenanthrene index (MPI): A maturity parameter based on aromatic hydrocarbons. In: *Advances in Organic Geochemistry* (M. Bjoroy et al., Eds.). Wiley: Chichester, 504-512.

Radke, M., Welte, D. H., and Willsch, H. (1982). Geochemical study on a well in the Western Canada Basin: Relation of the aromatic distribution pattern to maturity of organic matter. *Geochimica et Cosmochimica Acta* **46**, 1-10.

Radke, M., Horsefield, B., Littke, R. and Rullkotter, J. (1997). Maturation and Petroleum Generation. In: *Petroleum and Basin Evolution* (D. H. Welte, B. Horsefield, and D. R. Baker, eds.). Springer: Berlin, Germany, 168-229.

Repeta, D. J. and Gagosian, R. B. (1987). Carotenoid diagenesis in recent marine sediments - I. The Peru continental shelf (15S, 75W). *Geochimica et Cosmochimica Acta* **51**, 1001-1009.

Requejo, A. G., Allan, J., Creaney, S., Gray, N. R. and Cole, K. S. (1992). Aryl isoprenoids and diaromatic carotenoids in Paleozoic source rocks and oils from the Western Canada and Williston Basins. *Organic Geochemistry* **9**(1-3), 245-264.

Robertson Research (US) Inc. (1983). Geochemical analysis of north Aleutian Shelf, Coast no. 1 well, Alaska, Report no. 825/135. 318.

Rohmer, M., Bouvier-Nave, P. and Ourisson, G. (1984). Distribution of hopanoid triterpenes in prokaryotes. *Journal of General Microbiology* **130**, 1137-1150.

Rohmer, M (1987). The hopanoids, prokaryotic triterpenoids and sterol surrogates. In: *Surface Structures of Microorganisms and Their Interactions with the Mammalian Host* (E. Schriner et al., Eds.). VCH Publishing: Weinlein, Germany, 227-242.

Romero, A. M. and Philp, R. P. (2012). Organic geochemistry of the Woodford Shale, southeastern Oklahoma: How variable can shales be? *American Association of Petroleum Geologists Bulletin* **96**(3), 493-517.

Schwark, L. and Frimmel, A. (2004). Chemostratigraphy of the Posidonia Black Shale, southwest Germany: II. Assessment of extent and persistence of photic zone anoxia using aryl isoprenoids distributions. *Chemical Geology* **206**, 231-248.

Seifert, W. K. and Moldowan, J. M. (1980). The effect of thermal stress of source rock quality as measured by hopane stereochemistry. In: *Advances in Organic Geochemistry* (A. G. Douglas and J. R. Maxwell, eds.). Pergamon Press: Oxford, 229-237.

Shanmugam, G. (1985). Significance of coniferous rain forests and related organic matter in generating commercial quantities of oil, Gippsland Basin, Australia. *American Association of Petroleum Geologists Bulletin* **69**(8), 2141-1254.

Sinninghe-Damste, J. S., Kenig, F., Koopmans, M., P., Koster, J., Schouten, S., Hays, J. M. and de Leeuw, J. W. (1995). Evidence for gammacerane as an indicator of water column stratification. *Geochimica et Cosmochimica Acta* **59**(9), 1895-1900.

Slatt, R. M. (2019). Characterization of Unconventional Resource Shales (Mudstones). In: *The Necessity of Multiscale Scientific Integration* (T. Dewers, J. Heath and M. Sanchez, eds.). Shale: Subsurface Science Engineering: American Geophysical Union, 161-195.

Slatt, R. M. and Rodriguez, N. D (2012). Comparative sequence stratigraphy and organic geochemistry of gas shales: commonality or coincidence? *Journal of Natural Gas Science and Engineering* **8**, 68-84pp.

Slatt, R. M., Philp, R. P., Abousleiman, Y., Singh, P., Perez, R., Portas, R., Marfurt, K. J., Madrid-Arroyo, S., O'Brien, N, Eslinger, E. V. and Baruch, E. T. (2012). Pore-to-regional-scale integrated characterization workflow for unconventional gas shales. AAPG Memoir 97, 1-24pp.

Sofer, Z. (1984). Stable carbon isotope compositions of crude oils: Applications to source depositional environments and petroleum alteration. *American Association of Petroleum Geologists Bulletin* **68**(1), 31-49.

Spencer, A. M. (2012). *Generation, accumulation and production of Europe's hydrocarbons III: Special publication of the European Association of Petroleum Geoscientists* (Vol 3). (A. M. Spencer, Ed.). Berlin, Germany:Springer-Verlag, 375pp.

Summons, R. E. and Erwin, D. H. (2018). Chemical clues to the earliest animal fossils. *Science* **21**, 1198-1199.

Summons, R. E. and Powell, T. G. (1987). Identification of aryl isoprenoids in source rocks and crude oils: Biological markers for the green sulphur bacteria. *Geochimica et Cosmochimica Acta* **51**, 557-566.

Symcox, C. and Philp, R. P. (2019). Heterogeneity of STACK/SCOOP production in the Anadarko Basin, Oklahoma - Geochemistry of produced oils. *Unconventional Resources Technology Conference*. doi:10.15530/urtec-2019-513.

Thompson, K. F. M. (1987). Fractionated aromatic petroleum and the generation of gas-condensates. *Organic Geochemistry* **11**, 573-590.

Tissot B.P., Welte D.H. (1984). *Petroleum Formation and Occurrence*. Springer: Berlin, Heidelberg, 540pp.

van Grass, G. W. (1990). Biomarker maturity parameters for high maturities: Calibration of the working range up to the oil/condensate threshold. *Advances in Organic Geochemistry* **16**(4-6), 1025-1032.

van Koeverden, J. H., Karlsen, D. A., Schwark, L., Chpitsglouz, A., and Backer-Owe, K. (2010). Oil-prone Lower Carboniferous coals in the Norwegian Barents Sea: Implications for a Paleozoic petroleum system. *Journal of Petroleum Geology* **33**(2), 155-1822.

Villalba, D. M. (2016). Organic geochemistry of the Woodford Shale, Cherokee Platform, OK and its role in a complex petroleum system. University of Oklahoma M.S. Thesis, 126pp.

Volkman, J. K. (1984). Biodegradation of aromatic hydrocarbons in crude oils from Barrow Sub-basin of Western Australia. *Organic Geochemistry* **6**, 619-632.

Volkman, J. K. (1986). A review of sterol markers for marine and terrigenous organic matter. *Organic Geochemistry* **9**(2), 83-99.

Volkman, J. K., Banks, M. R., Denwer, K. and Aquino Neto, F. R. (1989). Biomarker composition and depositional setting of *Tasmanite* oil shale from northern Tasmania, Australia. Presented at the 14th International Meeting on Organic Geochemistry, Paris.

Wang, T. (2016). An organic geochemical study of the Woodford Shale and the Woodford-Mississippian tight oils from Central Oklahoma. University of Oklahoma Ph.D. Dissertation, 299pp.

Wang, Z. and Fingas, M. (1995). Use of methyldibenzothiophenes as markers for differentiation and source identification of crude and weathered oils. *Environmental Science and Technology* **29**, 2842-2849.

Wang, Z., Stout, S. A., and Fingas, M. (2007). Forensic fingerprinting of biomarkers for oil spill characterization and source identification. *Environmental Forensics* **7**, 105-146.

Wang, Z., Wang, Y., Wu, B., Wang, G., Sun, Z., Xu, L. and Wei, Z. (2016). Novel maturity parameters for mature to over-mature source rocks and oils based on the distribution of phenanthrene series compounds. *Heliyon*, **2**(3), 85.

Waples, D. W. and Machihara, T. (1990). Application of sterane and triterpane biomarkers in petroleum exploration. *Bulletin of Canadian Petroleum Geology* **38**(3), 357-380.

Wasea, A. and Nishita, H. (1998). Geochemical characteristics of terrigenous- and marine-sourced oils in Hokkaido, Japan. *Organic Geochemistry* **28**(1-2), 27-41

Watney, W. L. (1980). Swope Limestone (K-Zone) in central and southwestern Kansas, the role of core in understanding reservoir development and mechanisms responsible for cyclic sedimentation. *Kansas Geological Survey Subsurface Geology* **6**, 102-119.

Williams, J. A, Bjoroy, M., Solcater, D. L. and Winters, J. C. (1986). Biodegradation in South Texas Eocene oils - Effects on aromatics and biomarkers. *Organic Geochemistry* **10**, 451-461.

Wust, R. A. J., Nassichuk, B. R., Brezovski, R., Hackley, P. C. and Willment, N. (2013). Vitrinite reflectance versus pyrolysis T_{max} data: Assessing thermal maturity in shale plays with special reference to the Duvernay shale play of the Western Canadian Sedimentary Basin, Alberta, Canada. *Society of Petroleum Engineers Conference*. doi:10.2118/167031-MS.

Zeller, D. E., Jewett, J. M., Bayne, C. K., Goebel, E. D., O'Connor, H. G. and Swineford, A. (1968). The stratigraphic succession in Kansas. *Kansas Geological Survey Bulletin* **189**, 14-45.

Zhang, J. (2016). Comprehensive reservoir characterization of the Woodford Shale in parts of Garfield and Kingfisher Counties, Oklahoma. University of Oklahoma M.S. Thesis, 142pp.

Zhang, J. (2019). Multiscale natural fracture characterization workflow for unconventional shale, Woodford and Barnett Shales as examples. University of Oklahoma PhD Dissertation, 186pp.

Zhang, L., Li, M., Wang, Y., Yin, Q. and Zhang, W. (2013). A novel molecular index for secondary oil migration distance. *Scientific Reports* **3**(2487), 1-9.

Zimmerman, L. R. and Thurman, E. M. (1999). Method of analysis by the U.S. Geological Survey Organic Geochemistry Research Group - Determination of triazine and chloroacetanilide herbicides in water by solid-phase extraction and capillary-column gas chromatography/mass spectrometry with selected-ion monitoring. U. S. Geological Survey **98-634**, 1-21.

Zumberge, J. E., Curtis, J. B., Reed, J. D. and Sonnenfeld, M. D. (2016). Migration happens: Geochemical evidence for movement of hydrocarbons in unconventional petroleum systems. Unconventional Resources Technology Conference 2461914, 2-11.

Zumberge, J. A. (1987). Prediction of source rock characteristics based on terpane biomarkers in crude oils: A multivariate statistical approach. *Geochimica et Cosmochimica Acta* **51**, 1625-1637.

APPENDIX I: BIOMARKER RATIOS

DEPOSITIONAL ENVIRONMENT PROXIES

Ratio	*Reference*
Ph/n-C_{18}	Shanmugam, 1985
Pr/n-C_{17}	Shanmugam, 1985
Pr/Ph	Shanmugam, 1986
DBT/PHEN	Hughes et al., 1995

ORGANIC MATTER PROXIES

Ratio	*Formula*	*Reference*
$C_{27}/C_{27}+C_{29}$ Steranes	$C_{27}/[C_{27}+C_{28}+C_{29}]$ Steranes	Hossain et al., 2009
Sterane Index	$C_{30}/[C_{27}+C_{28}+C_{29}+C_{30}]$ Steranes	Moldowan et al., 1985
Homohopane Index	$C_{35}/[C_{31}+C_{32}+C_{33}+C_{34}+C_{35}]$ Hopanes	McKirdy et al., 1983

LITHOLOGY PROXIES

Ratio	*Reference*
C_{31}R Hopane/C_{30} Hopane	Hays et al., 2007
C_{26}/C_{25} Tricyclic Terpanes	Hays et al., 2007
C_{24}/C_{23} Tricyclic Terpanes	Zumberge, 1987
C_{22}/C_{21} Tricyclic Terpanes	Zumberge, 1987

THERMAL MATURITY PARAMETERS

Ratio	*Reference*
C_{30} Moretane/C_{30} Hopane	Tissot and Welte, 1984

WATER COLUMN STRATIFICATION PROXIES

Ratio	*Formula*	*Reference*
Gammacerane Index	100*Gammacerane/(*g*ammacerane+C_{30} hopane)	Sinninghe-Damste et al., 1995

MIGRATION INDICATORS

Ratio	*Formula*	*Reference*
Toluene Index	Toluene/(n-heptane +methylcyclohexane+toluene)	Burrus and Hatch, 1989
BC Ratio	Benzo[a]carbazole/(benzo[a]carbazole + benzo[c]carbazole)	Larter et al., 1996
Aromaticity	Toluene/n-heptane	Thompson, 1987
Paraffinicity	n-Heptane/methylcyclohexane	Thompson, 1987
4-/1-MDBT	4-Methyldibenzothiophene/ 1-methyldibenzothiophene	Fang et al., 2016
4,6/(1,4+1,6)-DMDBT	4,6-Dimethyldibenzothiophene/ (1,4+1,6)-dimethyldibenzothiophene	Fang et al., 2016
(2,6+3,6)/(1,4+1,6)-DMDBT	(2,6+3,6)-Dimethyldibenzothiophene/ (1,4+1,6)-dimethyldibenzothiophene	Fang et al., 2016
2,1/(2,1+1,2)-BNT	2,1-Benzonaphthothiophene/ (2,1+1,1)-benzonaphthothiophene	Fang et al., 2016

APPENDIX II: STRUCTURES

……Pristane

……. Phytane

……..n-Heptane

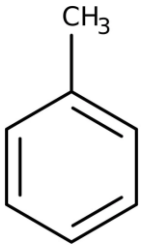

……..Toluene

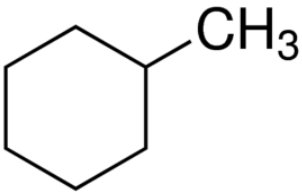

……Methylcyclohexane

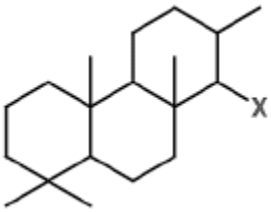

……Tricyclic terpane

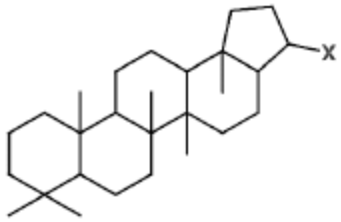

……..C_{30} Hopane

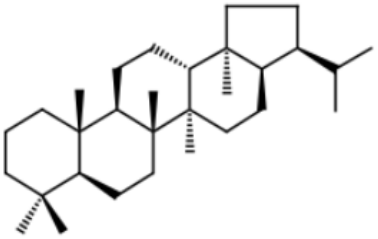

……..C_{30} Moretane

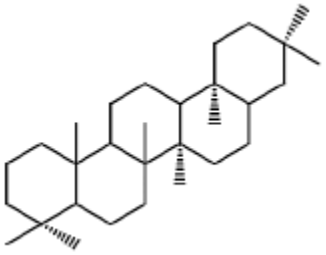

…….Gammacerane

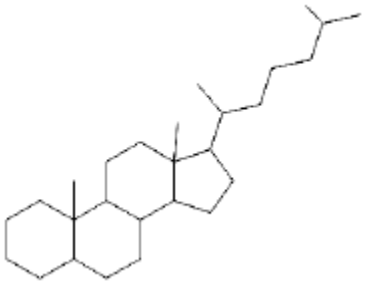

……Cholestane

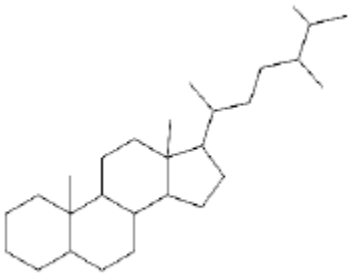

……..Ergostane

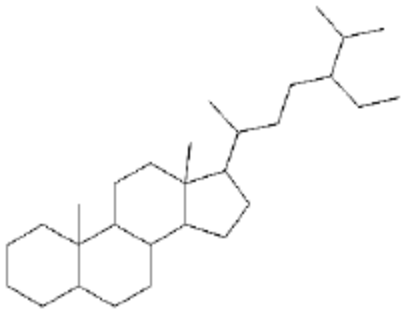

……..Stigmastane

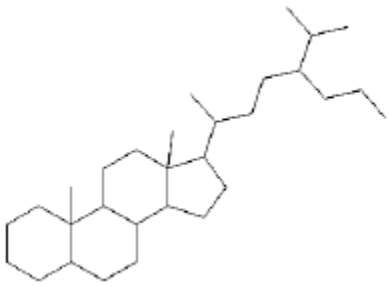

…….C_{30} Sterane

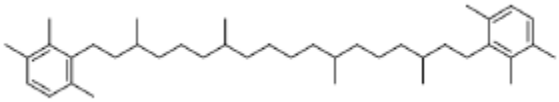

……..Isorenieratane

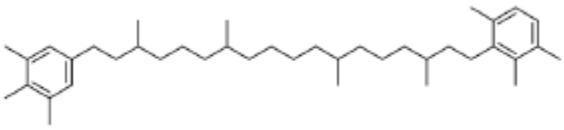

…….Paleorenieratane

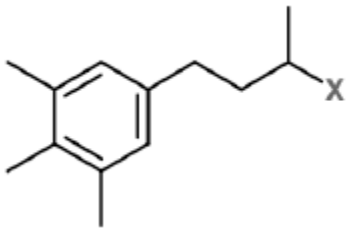

…….Aryl isoprenoid

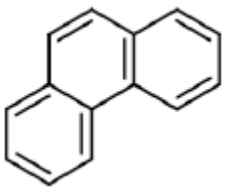

……..……. Phenanthrene

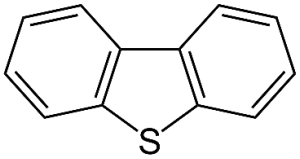

……Dibenzothiophene

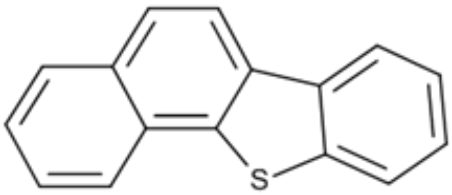

……Benzo[b]naphtho[2,1-d]thiophene

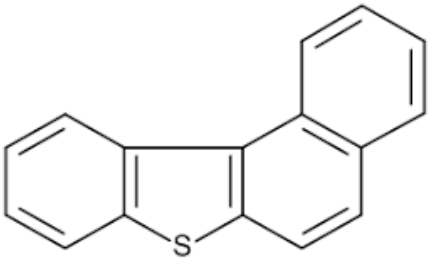

……..…Benzo[b]naphtho[1,2-d]thiophene

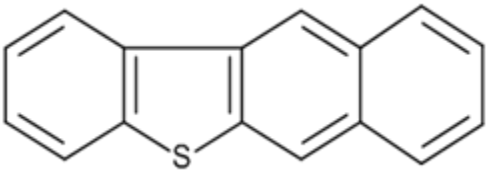

……...…Benzo[b]naphtho[2,3-d]thiophene

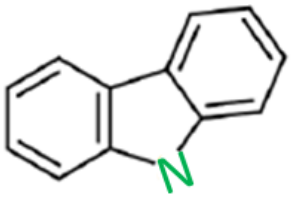

……...…….. Carbazole

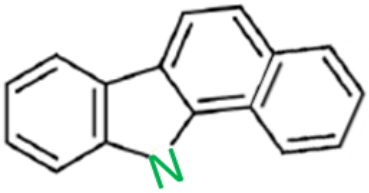

……...……...…. Benzo[a]carbazole

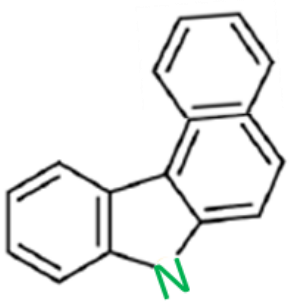

……Benzo[c]carbazole

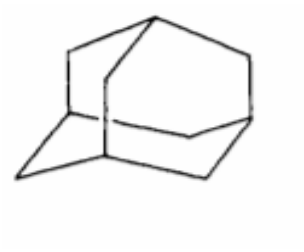

……Diamondoid (Adamantane)

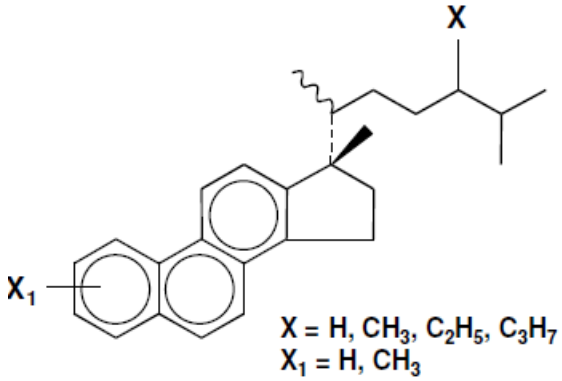

……. Triaromatic Steroid

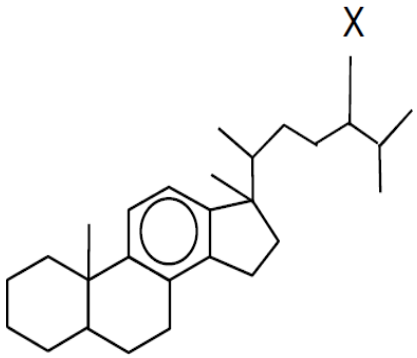

……Monoaromatic Steroid

APPENDIX III: FORMULAS

$$\boldsymbol{MPI\ 1} = 1.5 \times \frac{(2 - methylphenanthrene + 3 - \ methylphenanthrene)}{(phenanthrene + 1 - methylphenanthrene + 9 - methylphenanthrene)}$$

$$(\boldsymbol{MPI \cdot 1})\%\boldsymbol{Rc} \ = \ 0.60 * MPI\ 1 \ + \ 0.40$$

$$\boldsymbol{BC\ Ratio} \ = \frac{benzo[a]carbazole}{benzo[a]carbazole + benzo[c]carbazole}$$

$$\boldsymbol{HI} \ = \frac{S2 \times 100}{TOC}$$

$$\boldsymbol{OI} \ = \frac{S3 \times 100}{TOC}$$

$$\boldsymbol{PI} \ = \frac{S1}{S1 + S2}$$

$$(\boldsymbol{T_{max}})\ \ \%\boldsymbol{Rc} = 0.0180 \times T_{max} - 7.16$$

APPENDIX IV: CHROMATOGRAMS

A. Whole Oil GC Chromatograms

Chromatogram of C_7 hydrocarbons

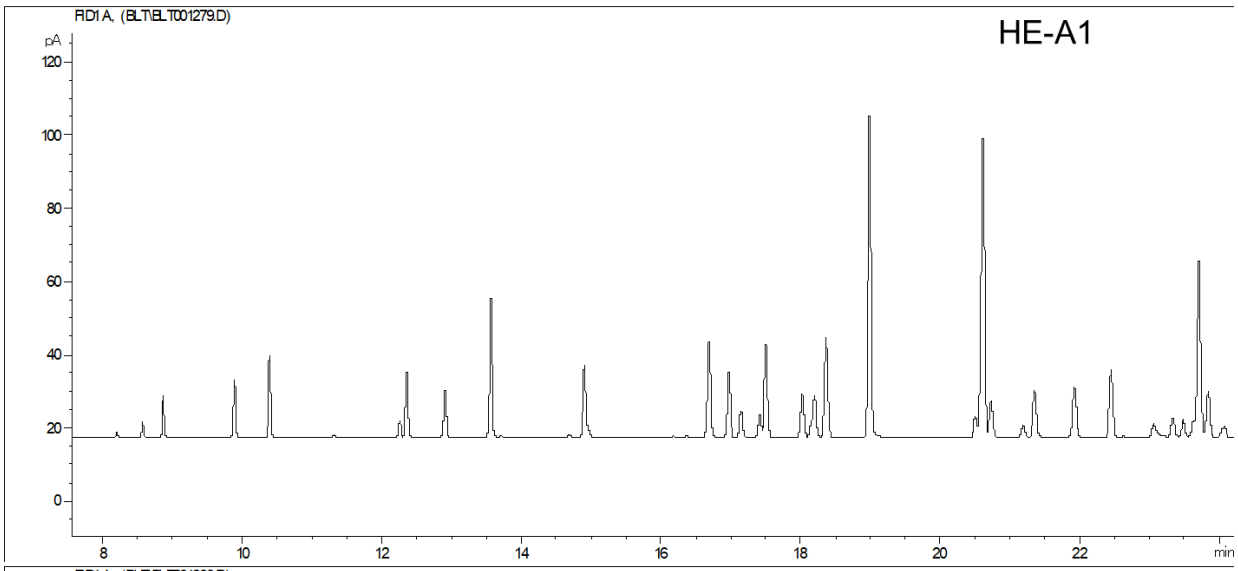

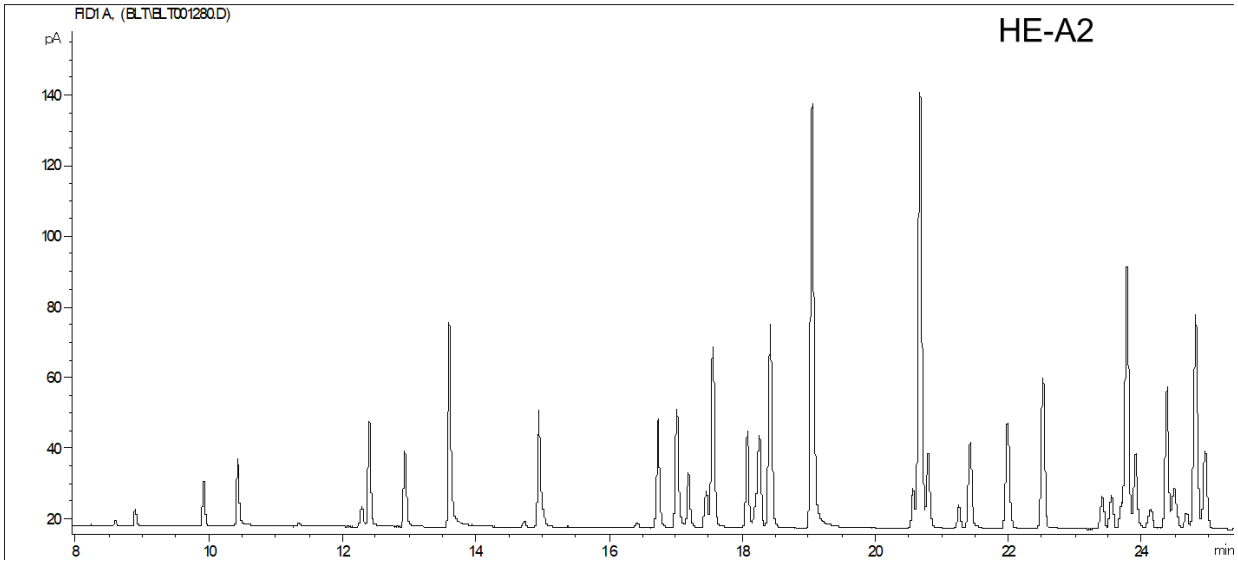

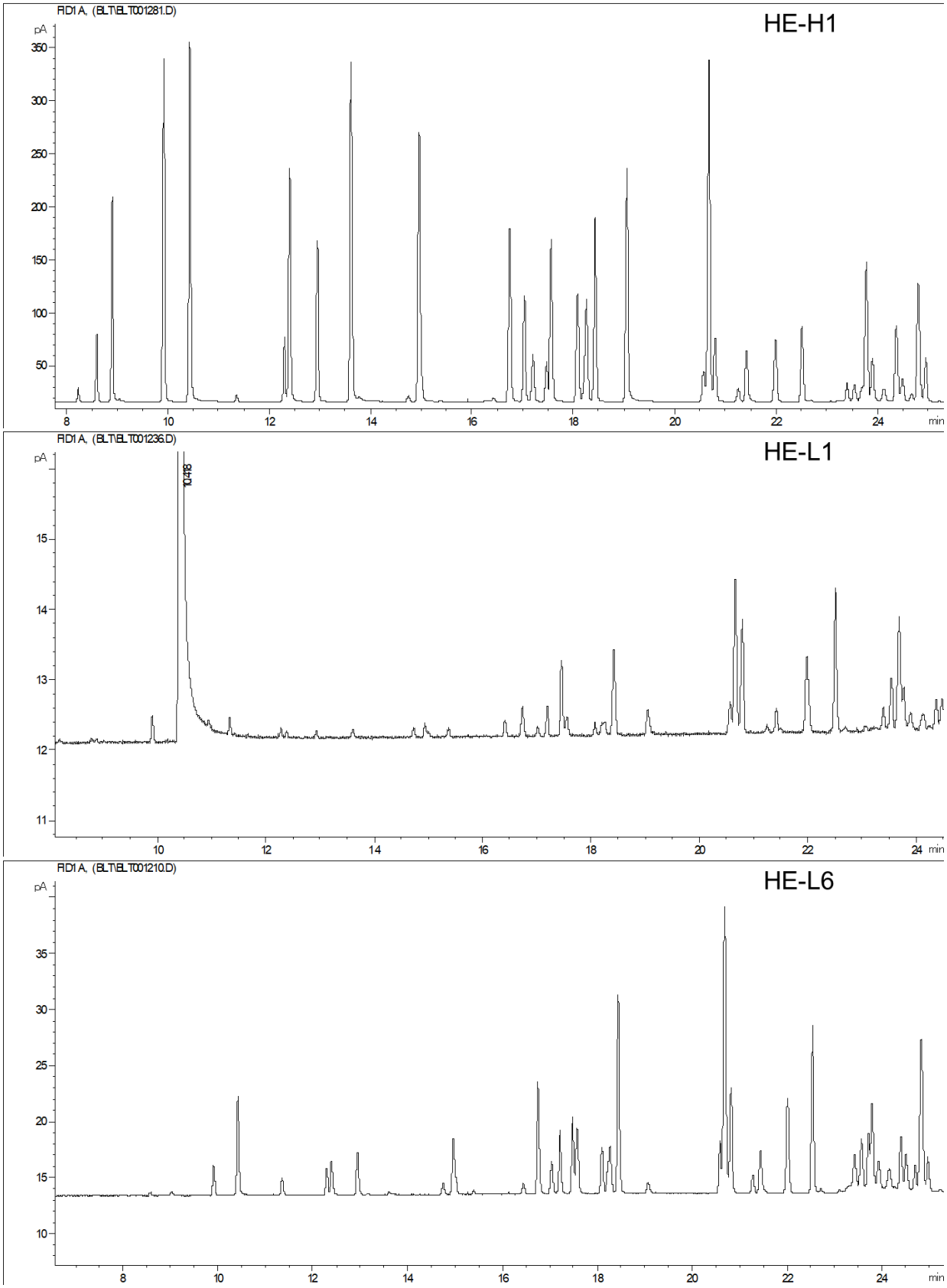
FID1 A, (BLT\BLT001281.D)
HE-H1
pA
min
FID1 A, (BLT\BLT001236.D)
HE-L1
10.418
pA
min
FID1 A, (BLT\BLT001210.D)
HE-L6
pA
min

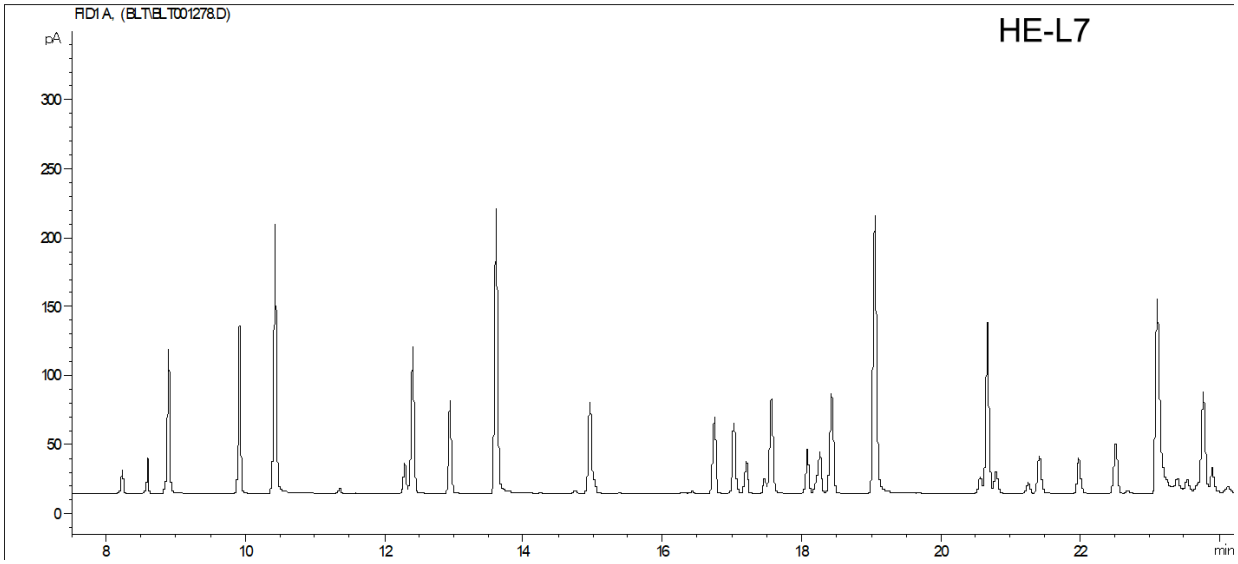
FID1 A, (BLT\BLT001278.D)
HE-L7
pA
300
250
200
150
100
50
0
8
10
12
14
16
18
20
22
min

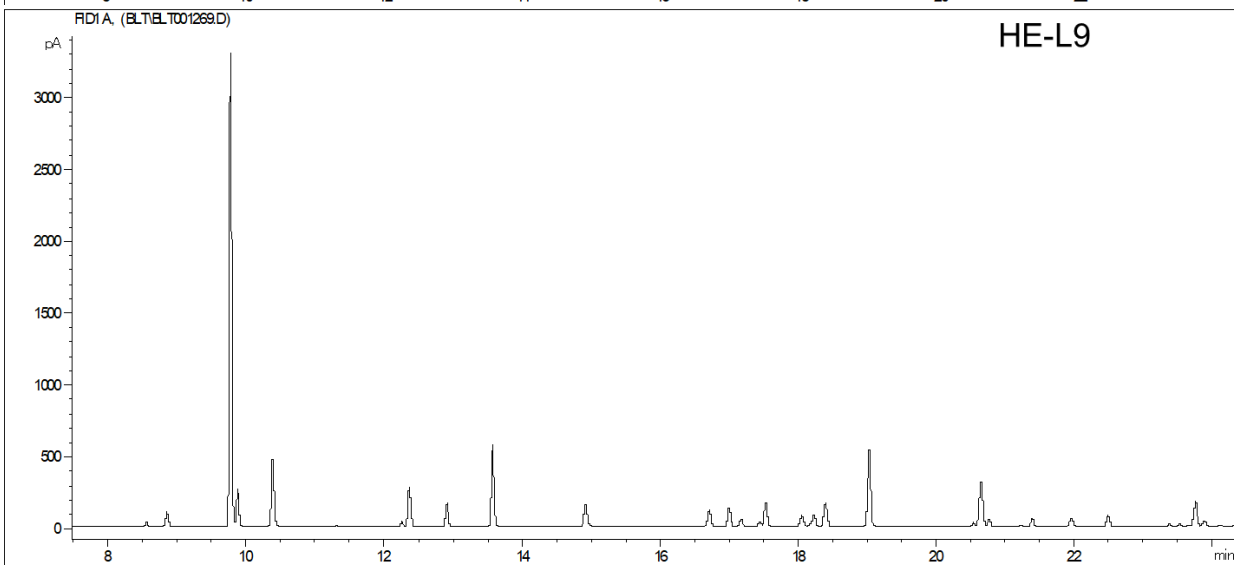
FID1 A, (BLT\BLT001269.D)
HE-L9
pA
3000
2500
2000
1500
1000
500
0
8
10
12
14
16
18
20
22
min

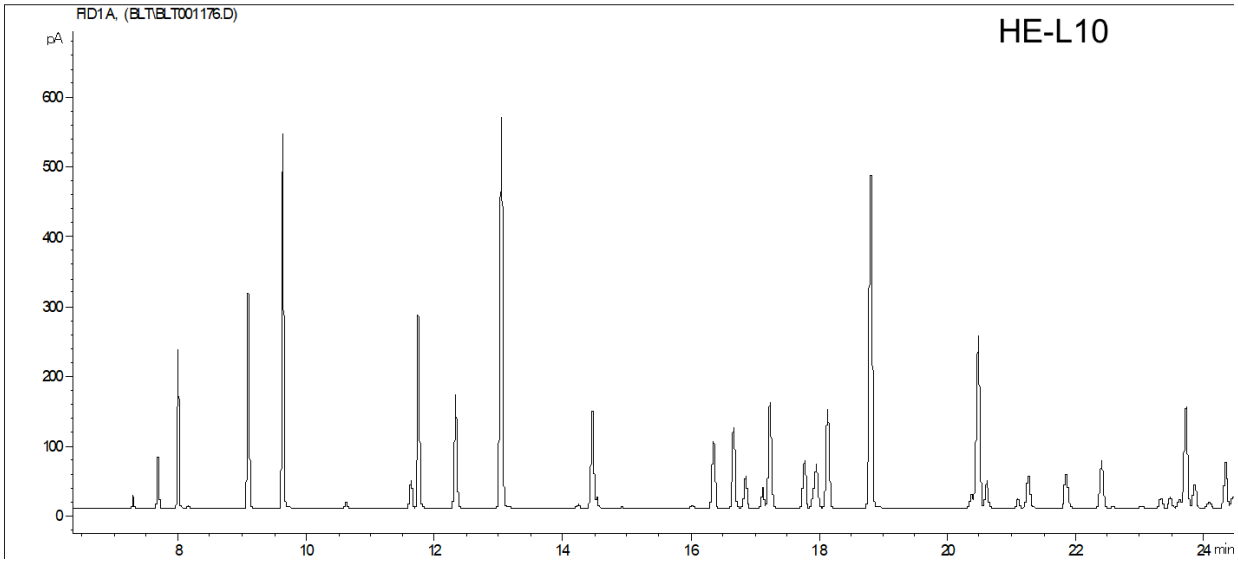
FID1 A, (BLT\BLT001176.D)
HE-L10
pA
600
500
400
300
200
100
0
8
10
12
14
16
18
20
22
24 min

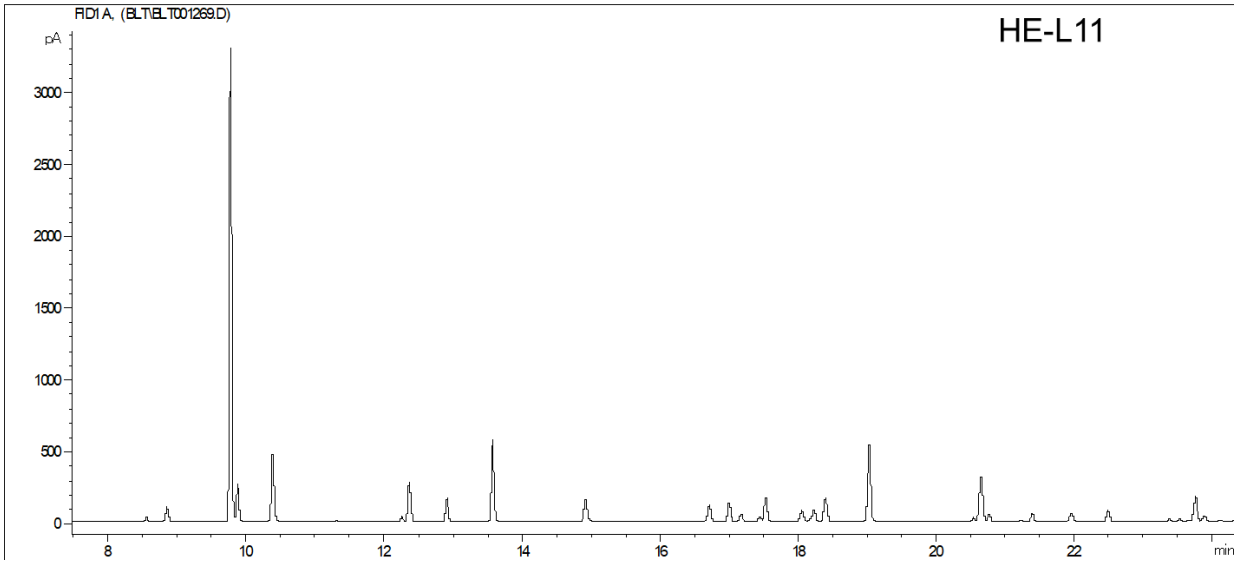
FID1 A, (BLT\BLT001269.D)
HE-L11
pA
3000
2500
2000
1500
1000
500
0
8
10
12
14
16
18
20
22
min

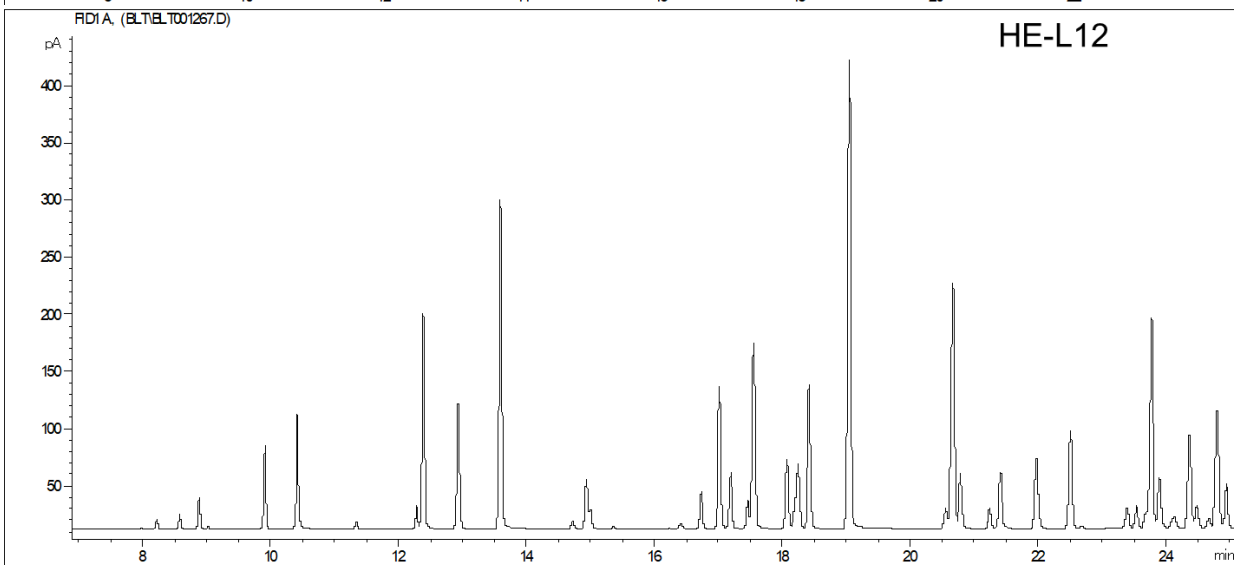
FID1 A, (BLT\BLT001267.D)
HE-L12
pA
400
350
300
250
200
150
100
50
8
10
12
14
16
18
20
22
24
min

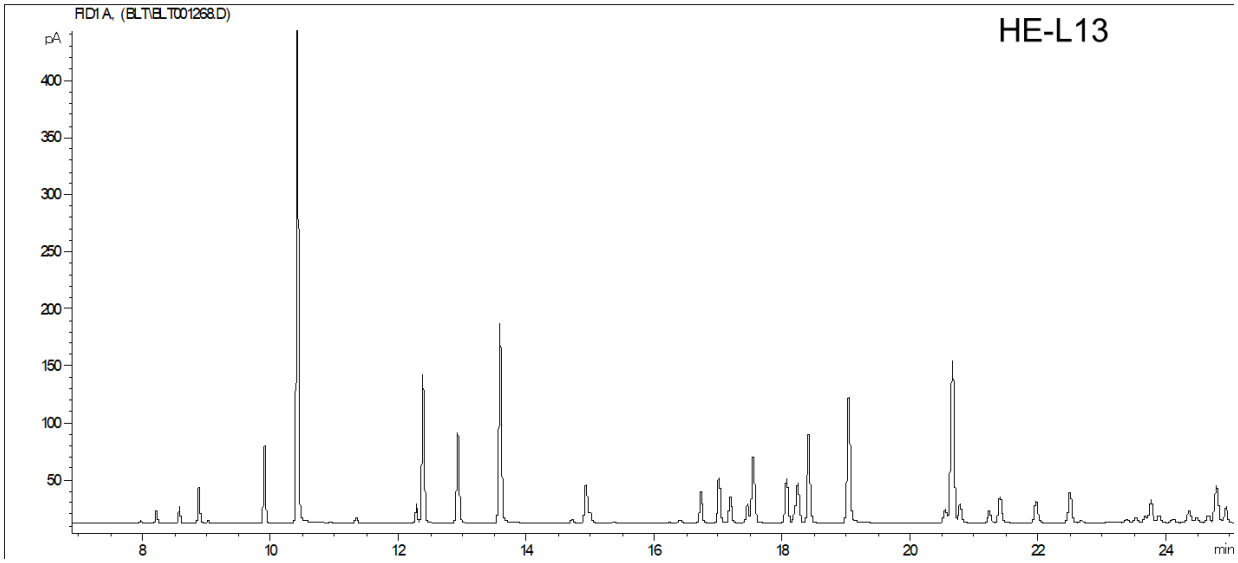
FID1 A, (BLT\BLT001268.D)
HE-L13
pA
400
350
300
250
200
150
100
50
8
10
12
14
16
18
20
22
24
min

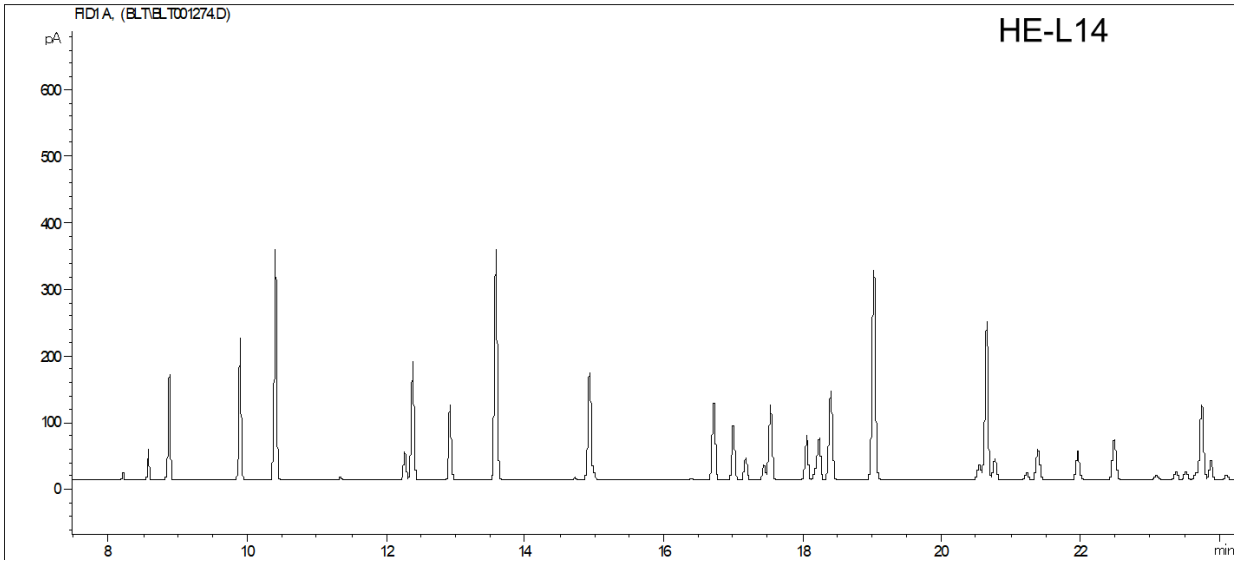
FID1 A, (BLT\BLT001274.D)
HE-L14
pA
600
500
400
300
200
100
0
8
10
12
14
16
18
20
22
min

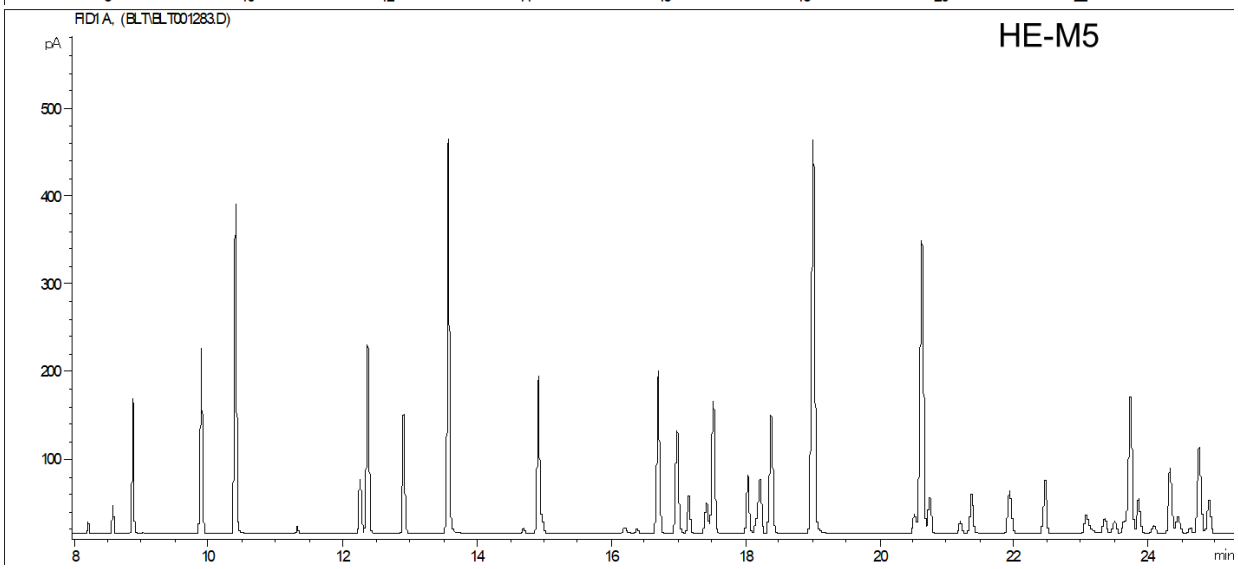
FID1 A, (BLT\BLT001283.D)
HE-M5
pA
500
400
300
200
100
8
10
12
14
16
18
20
22
24
min

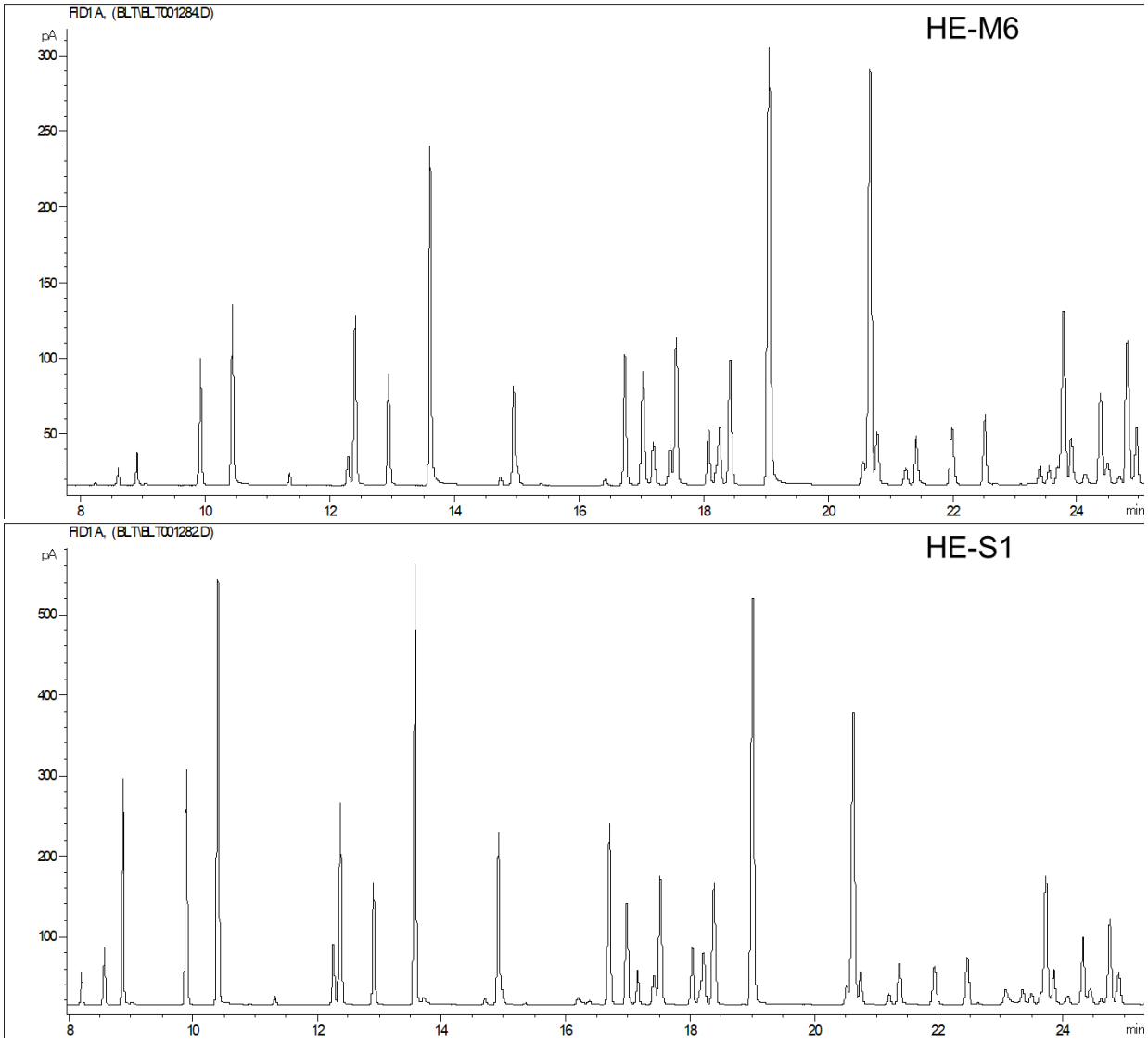
FID1 A, (BLT\BLT001284.D)
HE-M6
pA
300
250
200
150
100
50
8
10
12
14
16
18
20
22
24
min
FID1 A, (BLT\BLT001282.D)
HE-S1
pA
500
400
300
200
100
8
10
12
14
16
18
20
22
24
min

B. Saturate GC Chromatograms

Chromatogram of saturate compounds

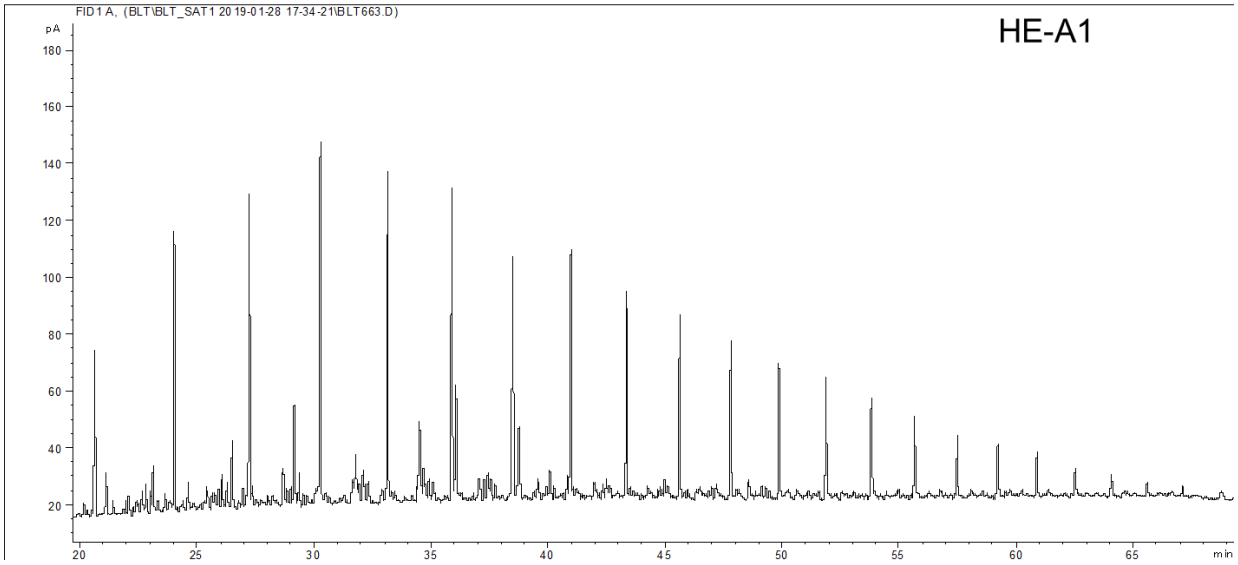

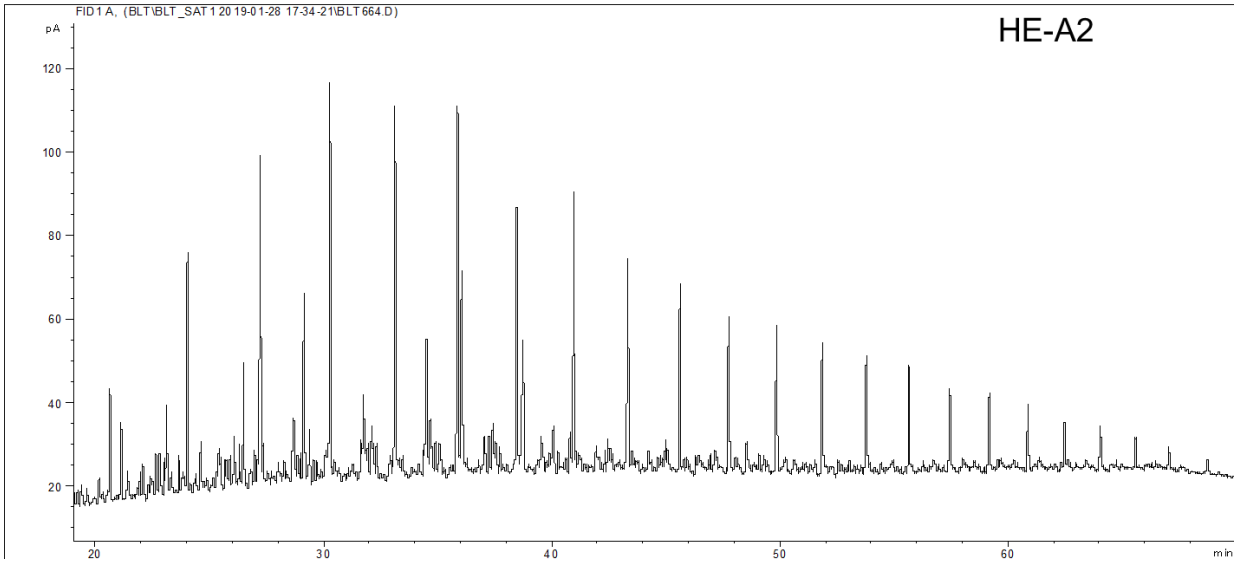

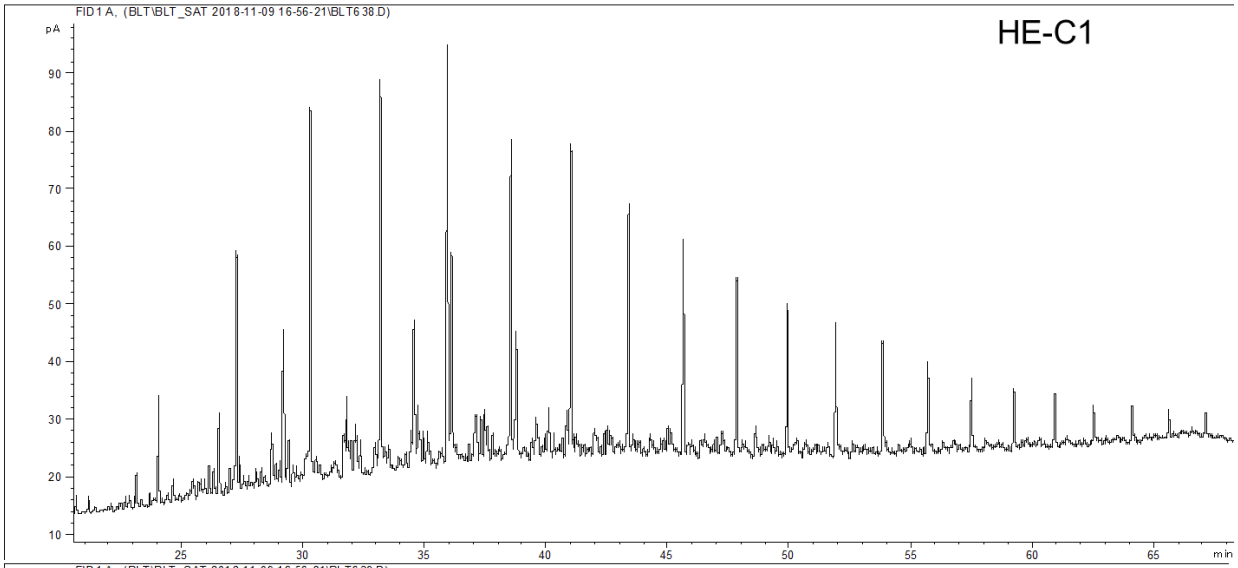
FID1 A, (BLT\BLT_SAT 2018-11-09 16-56-21\BLT6 38.D)
HE-C1
pA
min

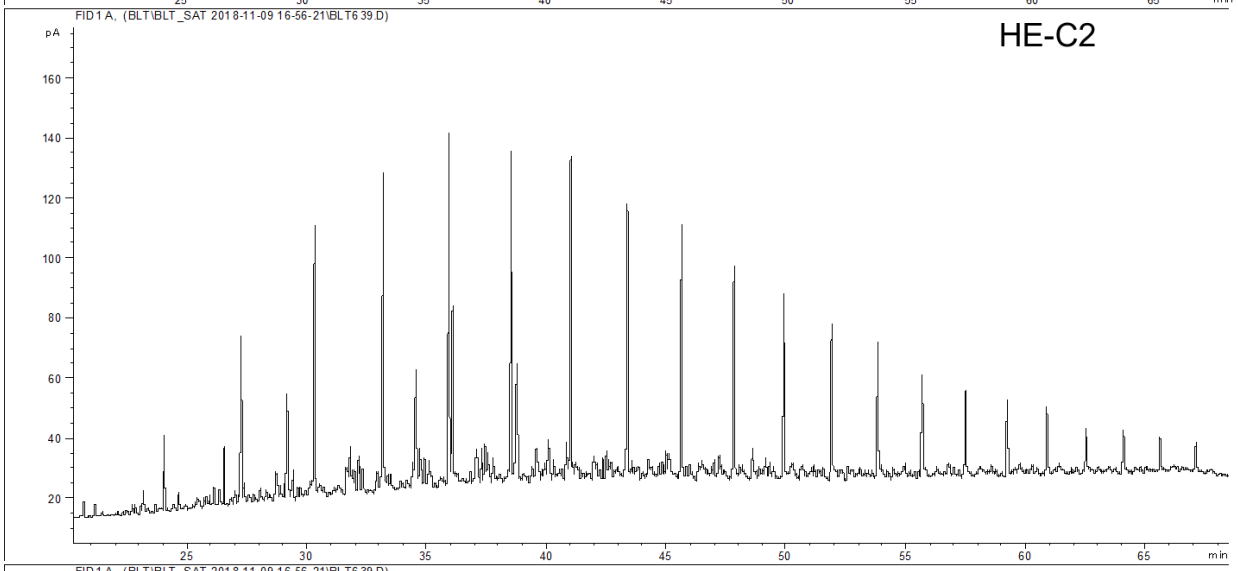
FID1 A, (BLT\BLT_SAT 2018-11-09 16-56-21\BLT6 39.D)
HE-C2
pA
min

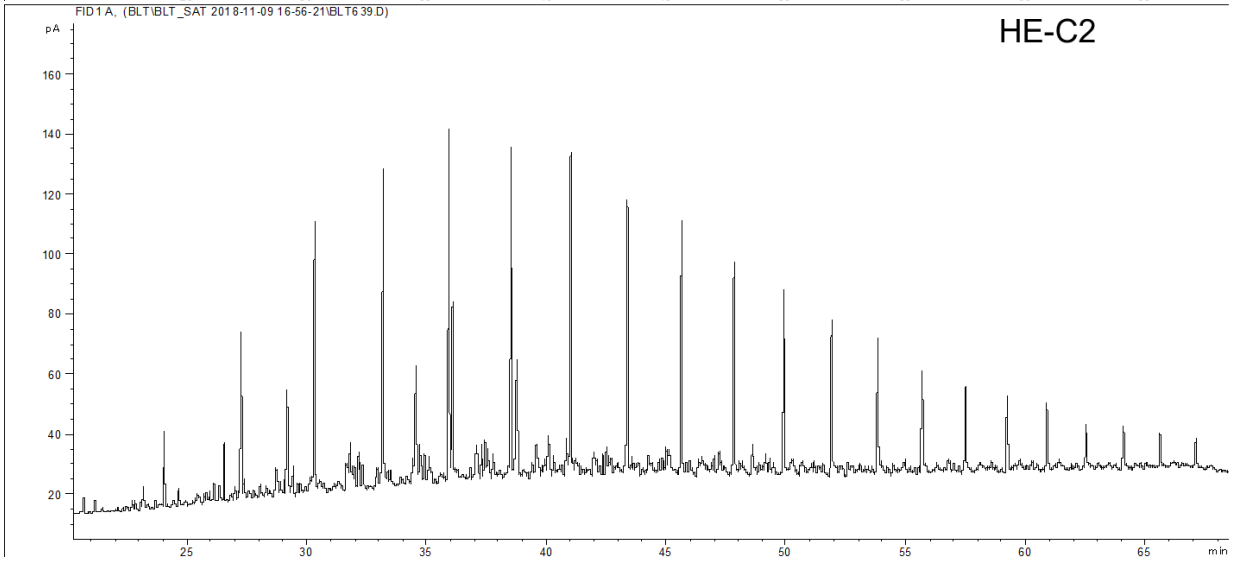
FID1 A, (BLT\BLT_SAT 2018-11-09 16-56-21\BLT6 39.D)
HE-C2
pA
min

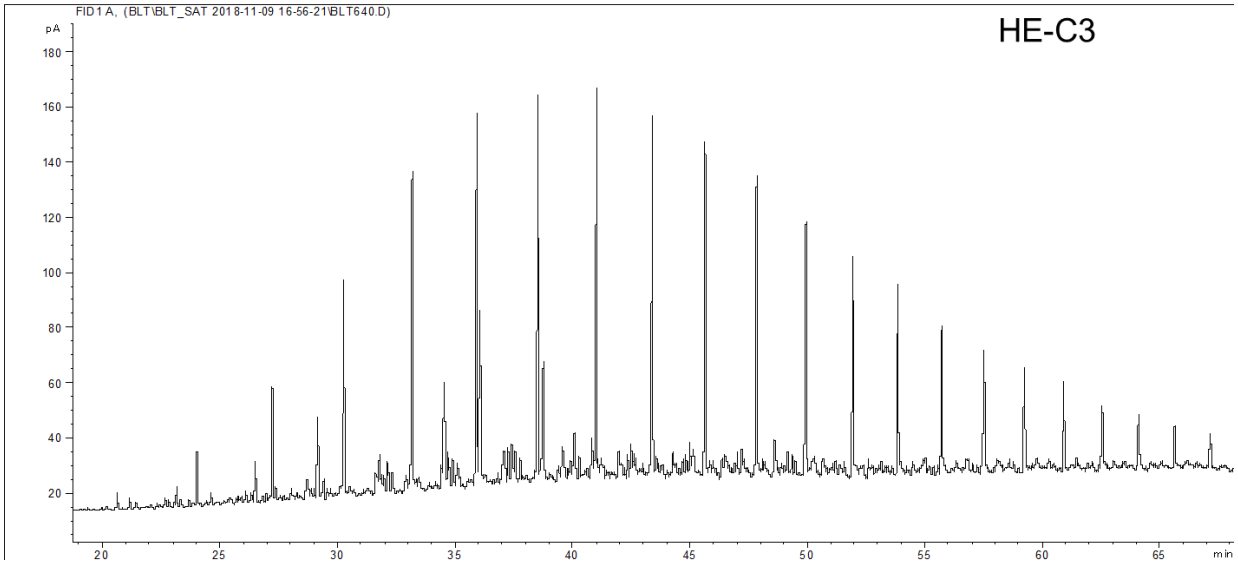
FID1 A, (BLT\BLT_SAT 2018-11-09 16-56-21\BLT640.D)
HE-C3
pA
min

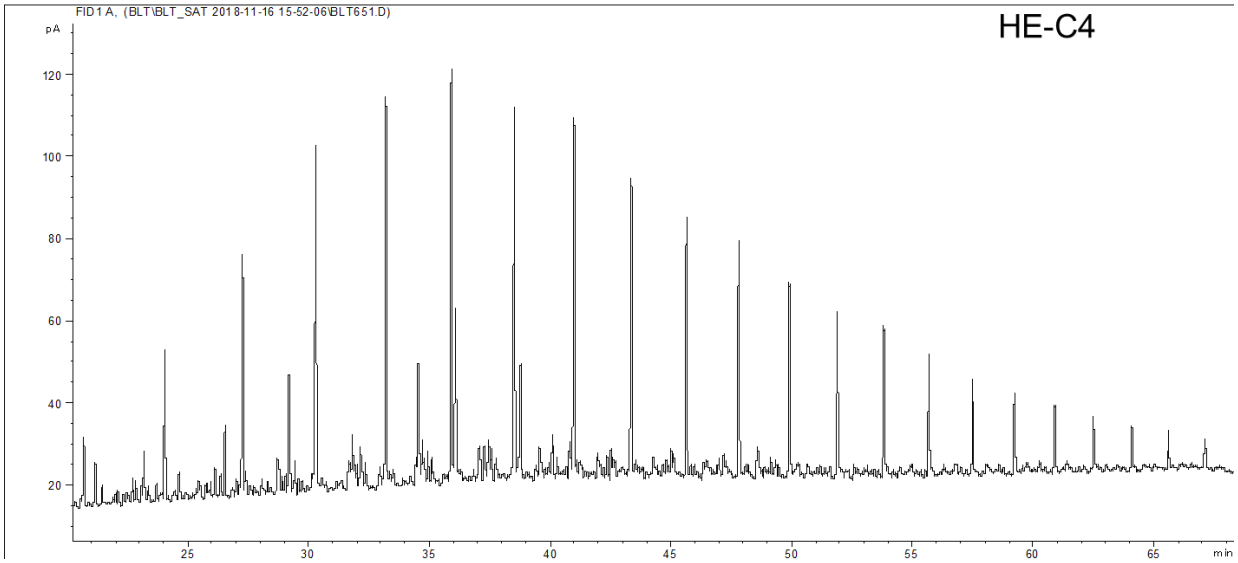
FID1 A, (BLT\BLT_SAT 2018-11-16 15-52-06\BLT651.D)
HE-C4
pA
min

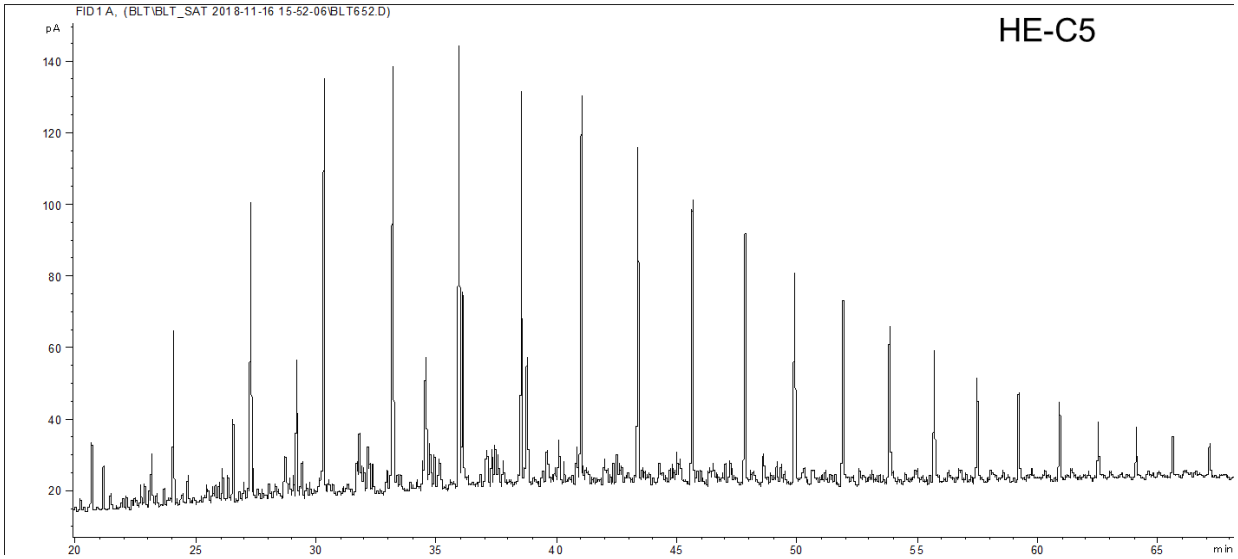
FID1 A, (BLT\BLT_SAT 2018-11-16 15-52-06\BLT652.D)
HE-C5
pA
min

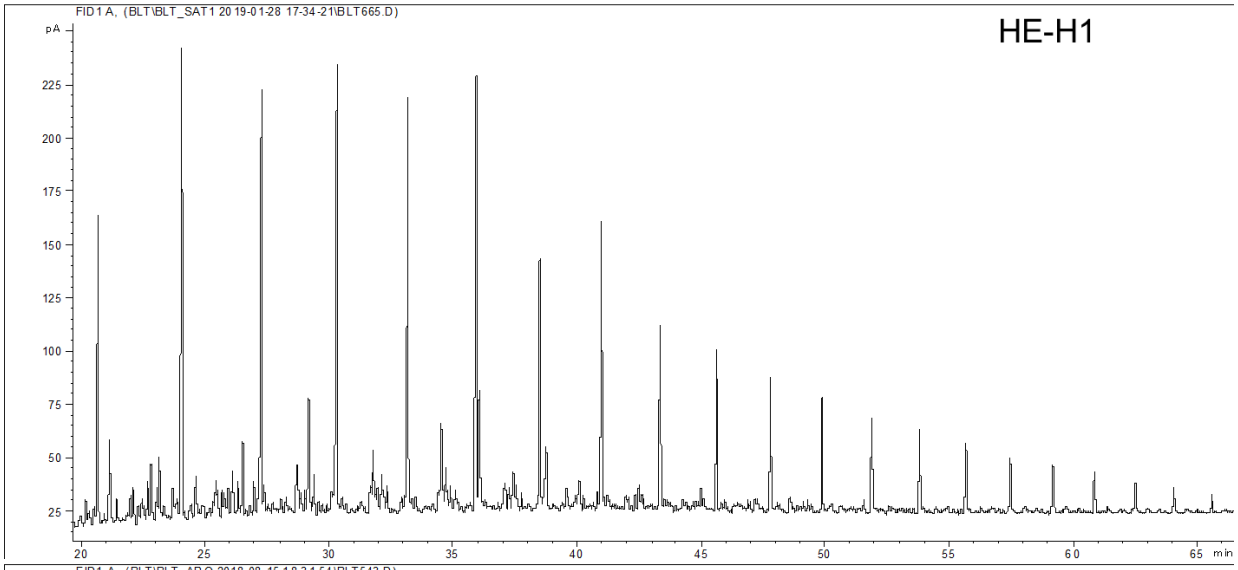
FID1 A, (BLT\BLT_SAT1 2019-01-28 17-34-21\BLT665.D)
HE-H1
pA
min

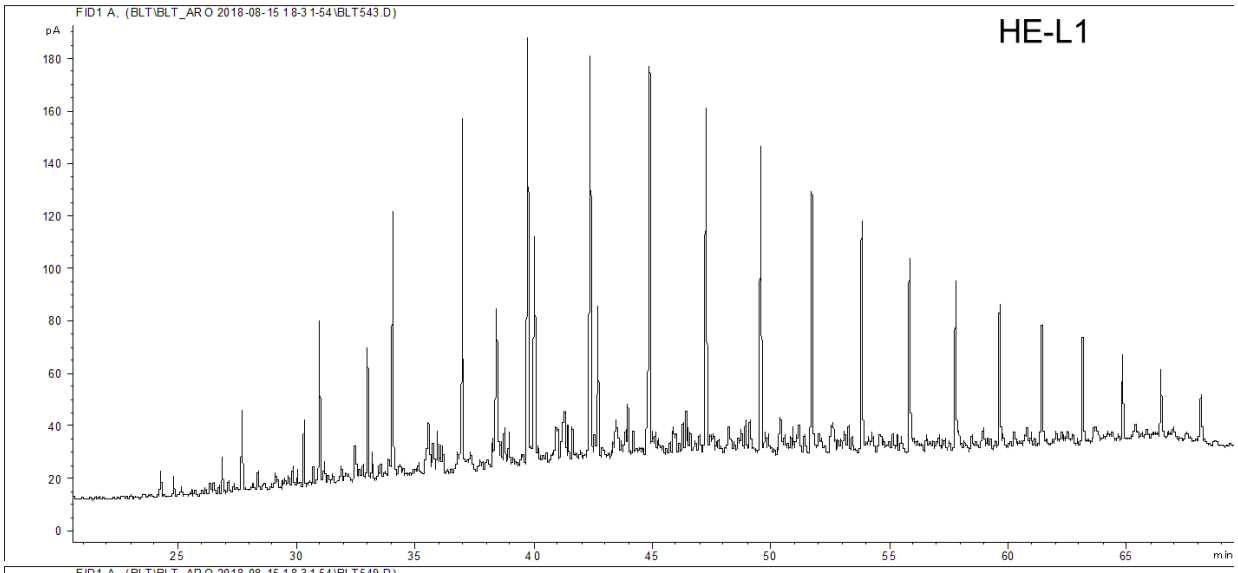
FID1 A, (BLT\BLT_ARO 2018-08-15 18-31-54\BLT543.D)
HE-L1
pA
min

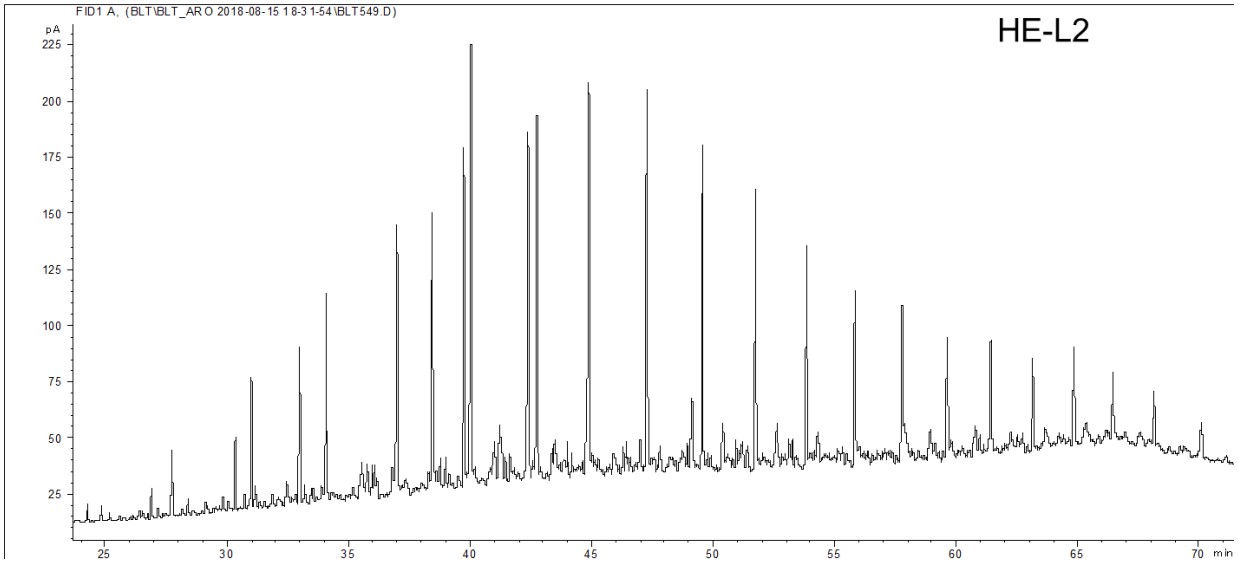
FID1 A, (BLT\BLT_ARO 2018-08-15 18-31-54\BLT549.D)
HE-L2
pA
min

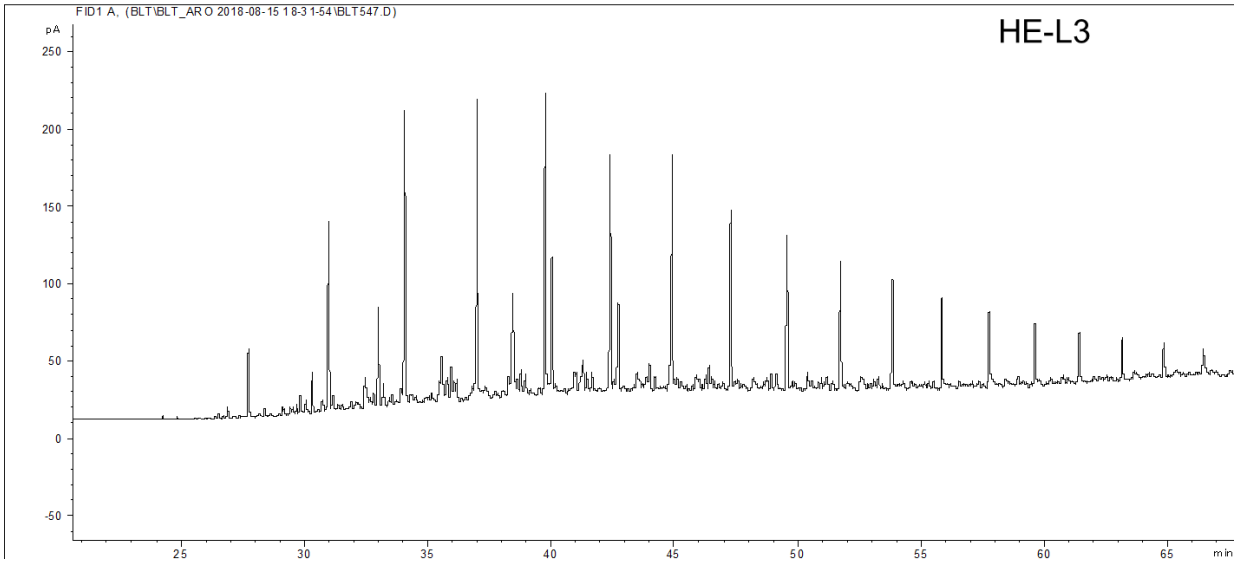
FID1 A, (BLT\BLT_ARO 2018-08-15 18-31-54\BLT547.D)
HE-L3
pA
min

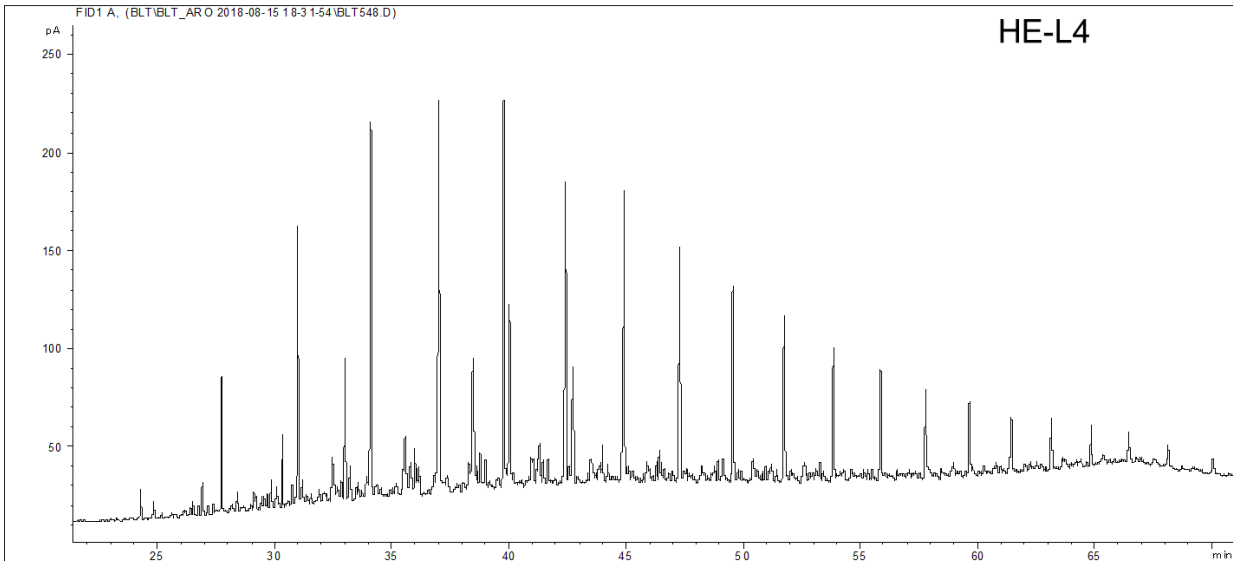
FID1 A, (BLT\BLT_ARO 2018-08-15 18-31-54\BLT548.D)
HE-L4
pA
min

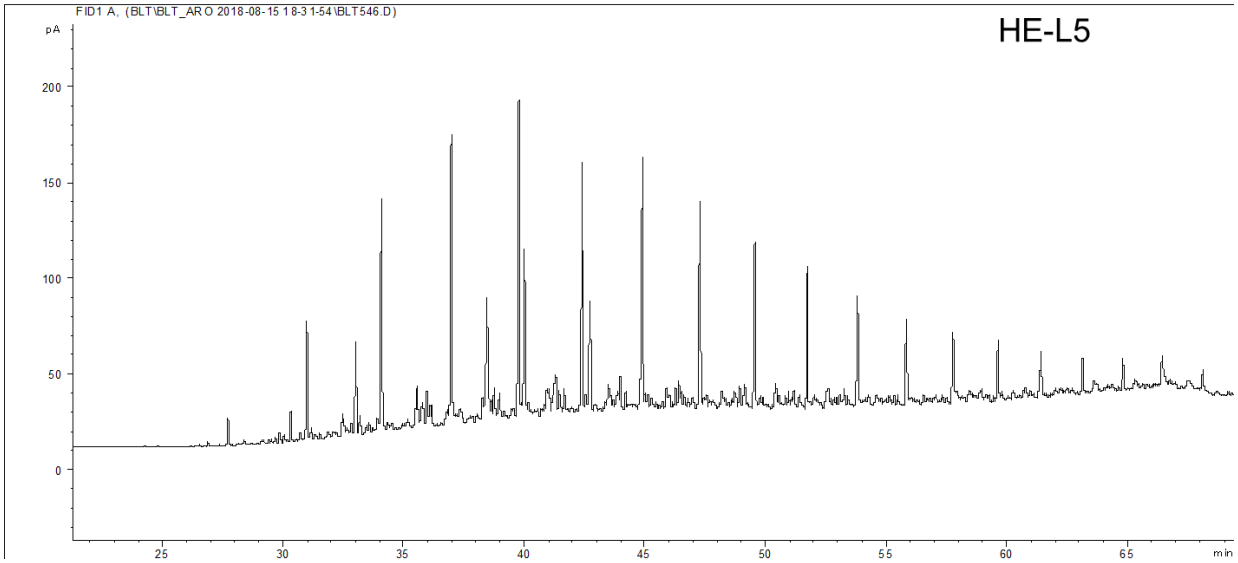
FID1 A, (BLT\BLT_ARO 2018-08-15 18-31-54\BLT546.D)
HE-L5
pA
min

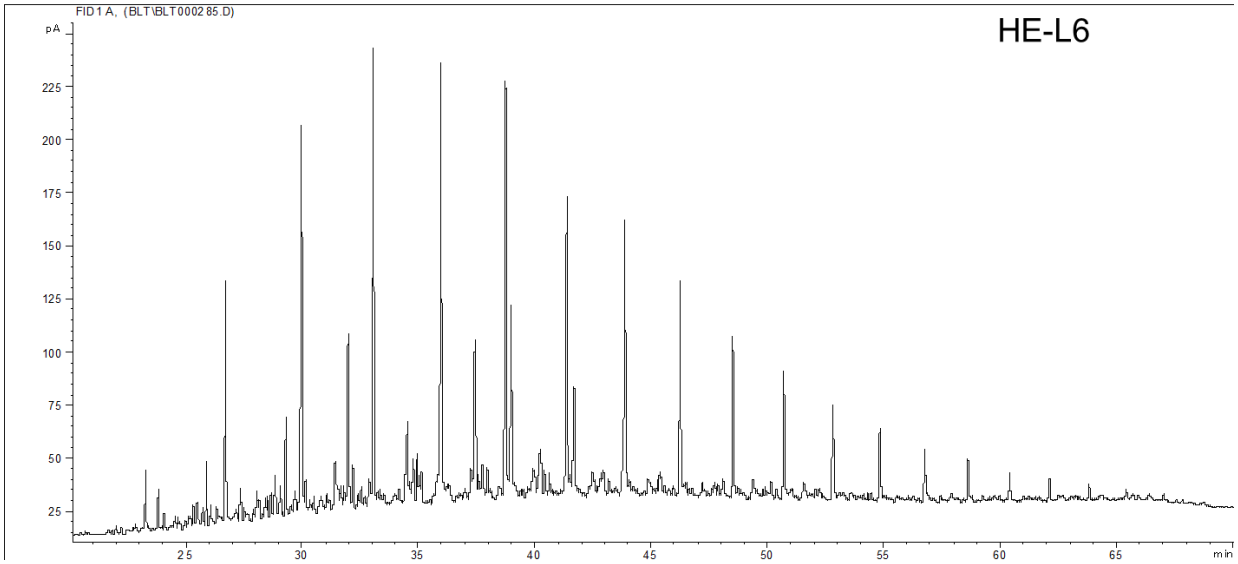
FID1 A, (BLT\BLT000285.D)
HE-L6
pA
min

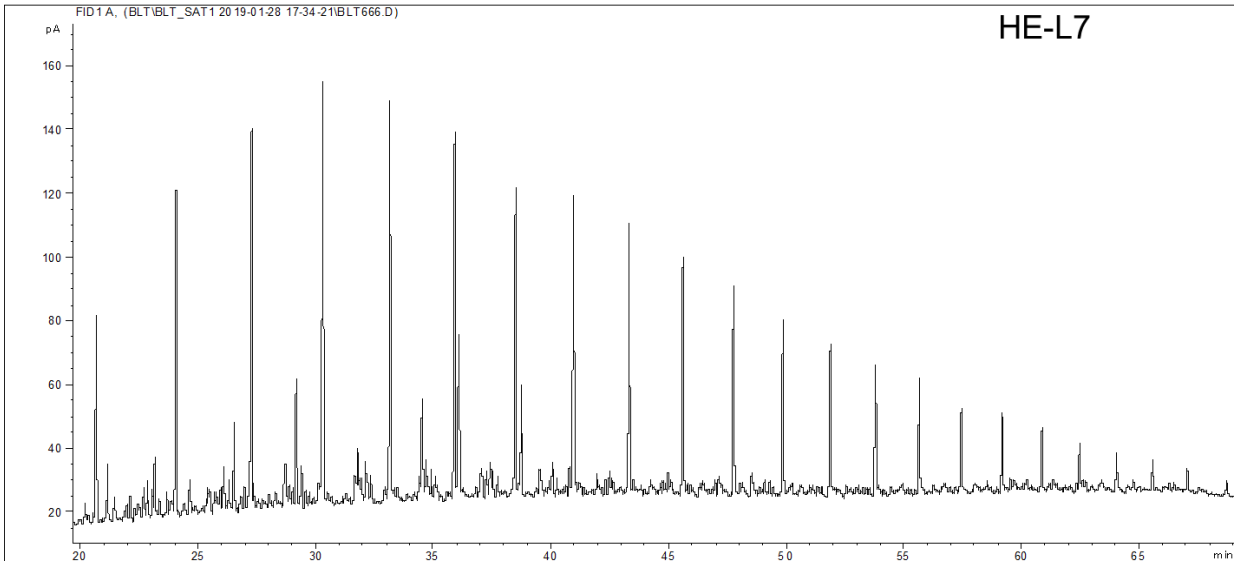
FID1 A, (BLT\BLT_SAT1 2019-01-28 17-34-21\BLT666.D)
HE-L7
pA
min

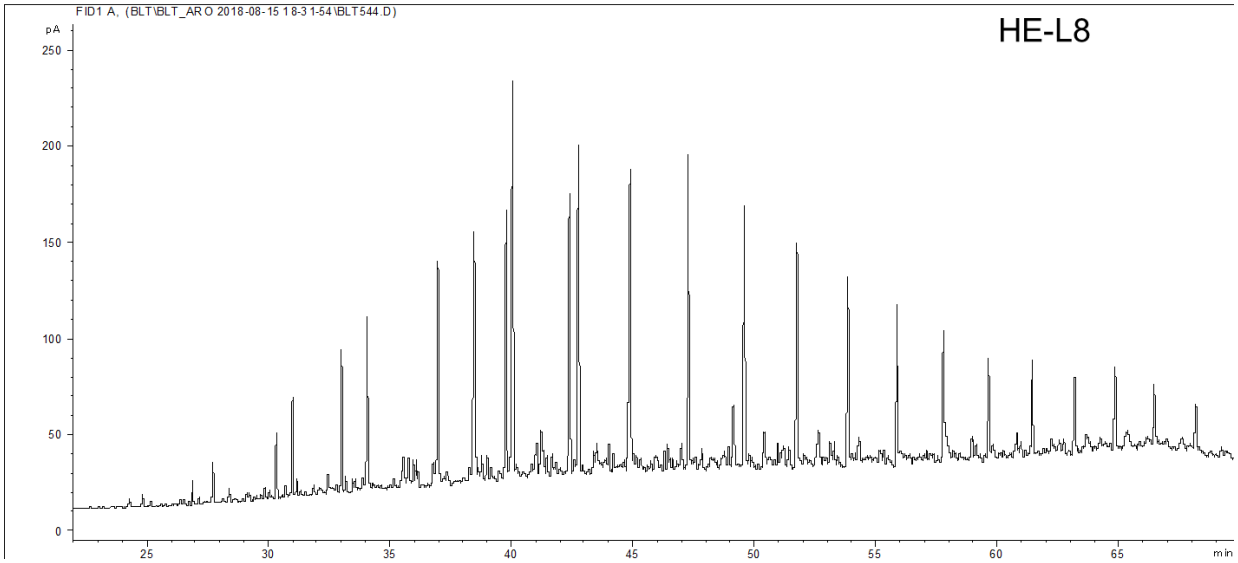
FID1 A, (BLT\BLT_ARO 2018-08-15 18-31-54\BLT544.D)
HE-L8
pA
min

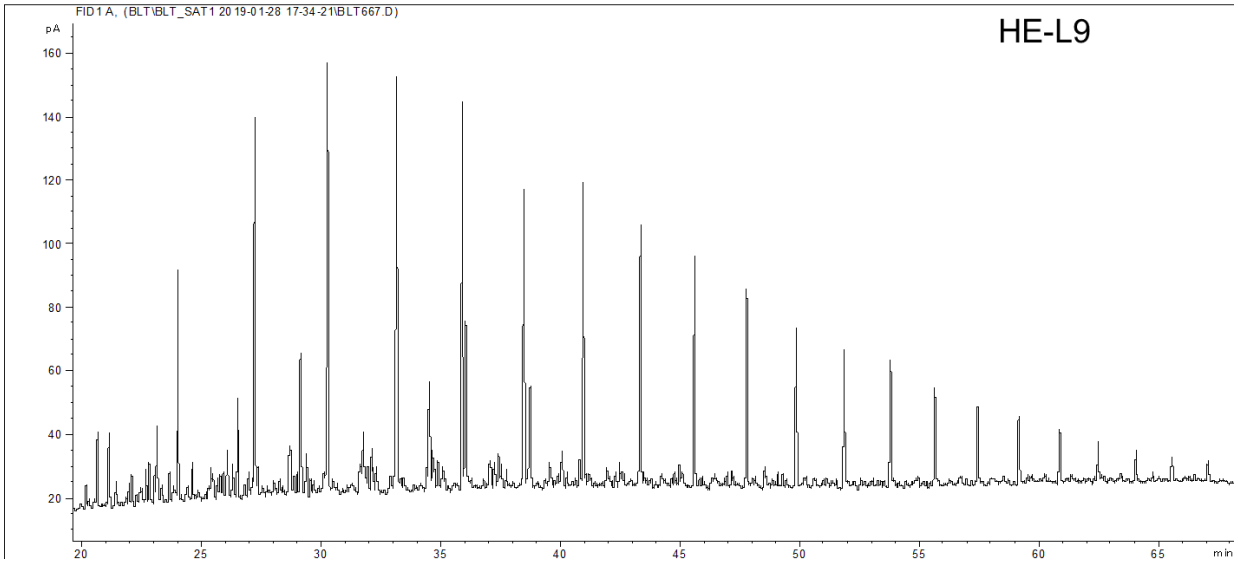
FID1 A, (BLT\BLT_SAT1 2019-01-28 17-34-21\BLT667.D)
HE-L9
pA
min

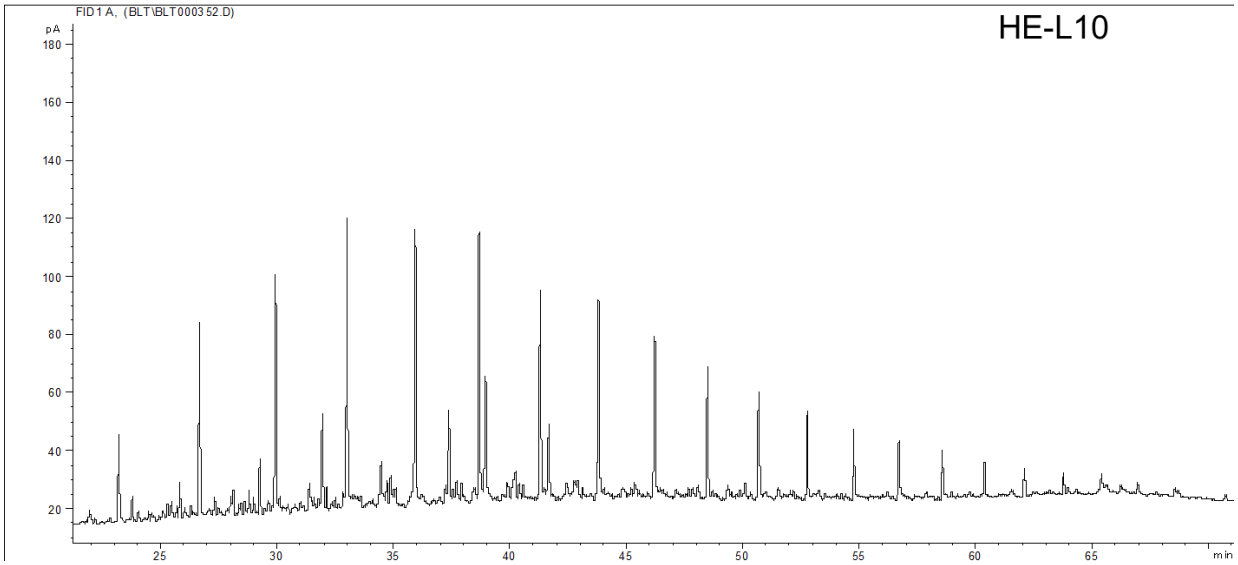
FID1 A, (BLT\BLT000352.D)
HE-L10
pA
min

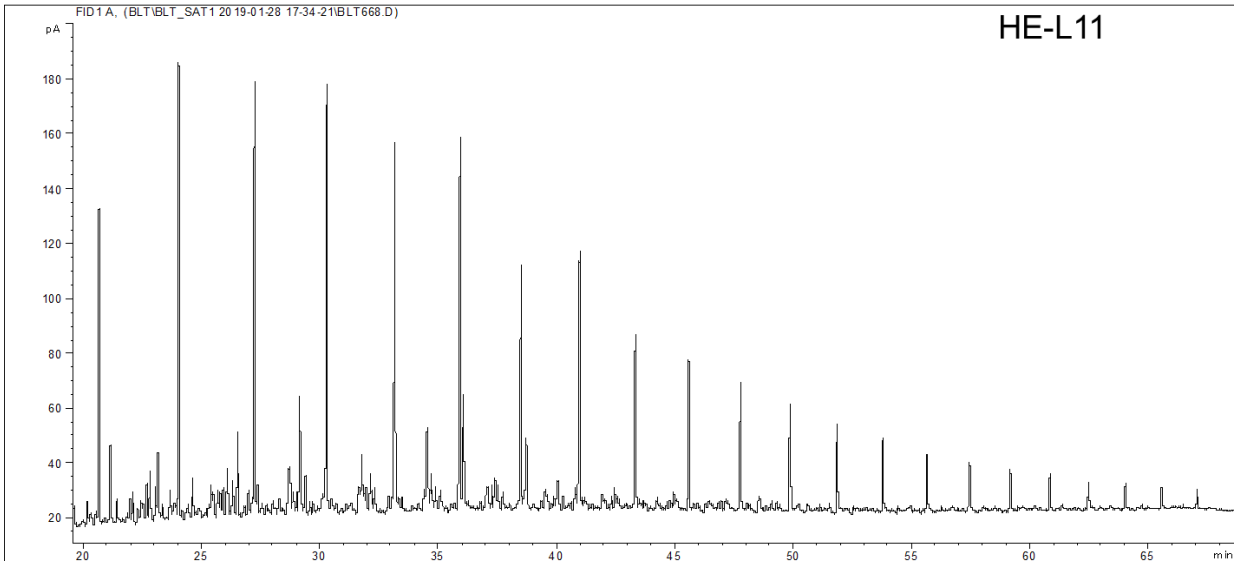
FID1 A, (BLT\BLT_SAT1 2019-01-28 17-34-21\BLT668.D)
HE-L11
pA
min

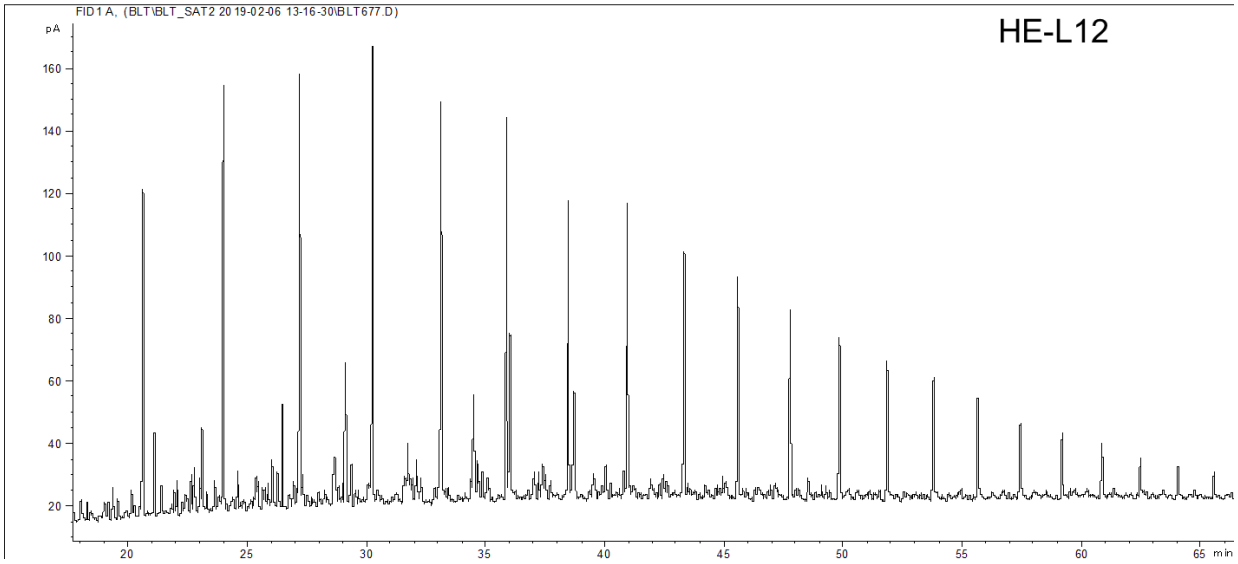
FID1 A, (BLT\BLT_SAT2 2019-02-06 13-16-30\BLT677.D)
HE-L12
pA
min

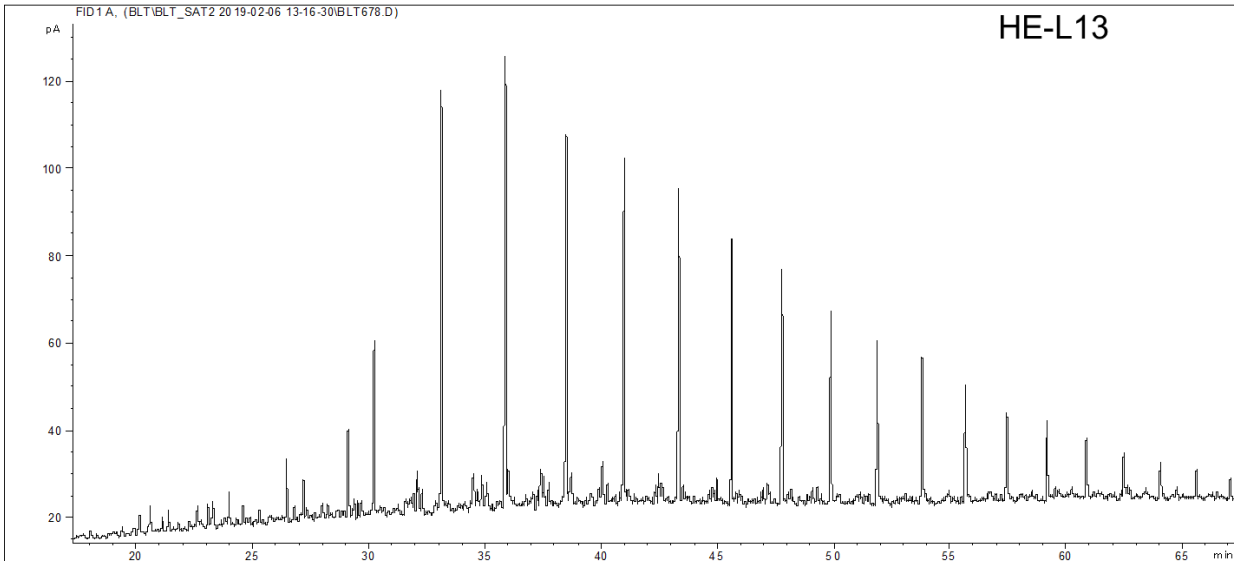
FID1 A, (BLT\BLT_SAT2 2019-02-06 13-16-30\BLT678.D)
HE-L13
pA
min

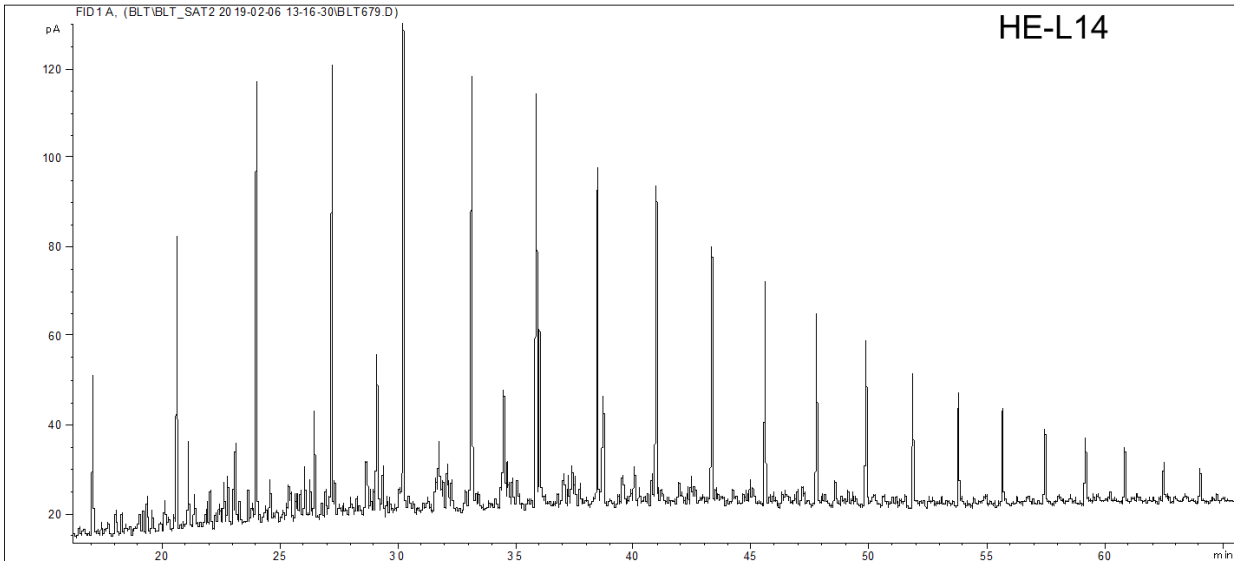
FID1 A, (BLT\BLT_SAT2 2019-02-06 13-16-30\BLT679.D)
HE-L14
pA
min

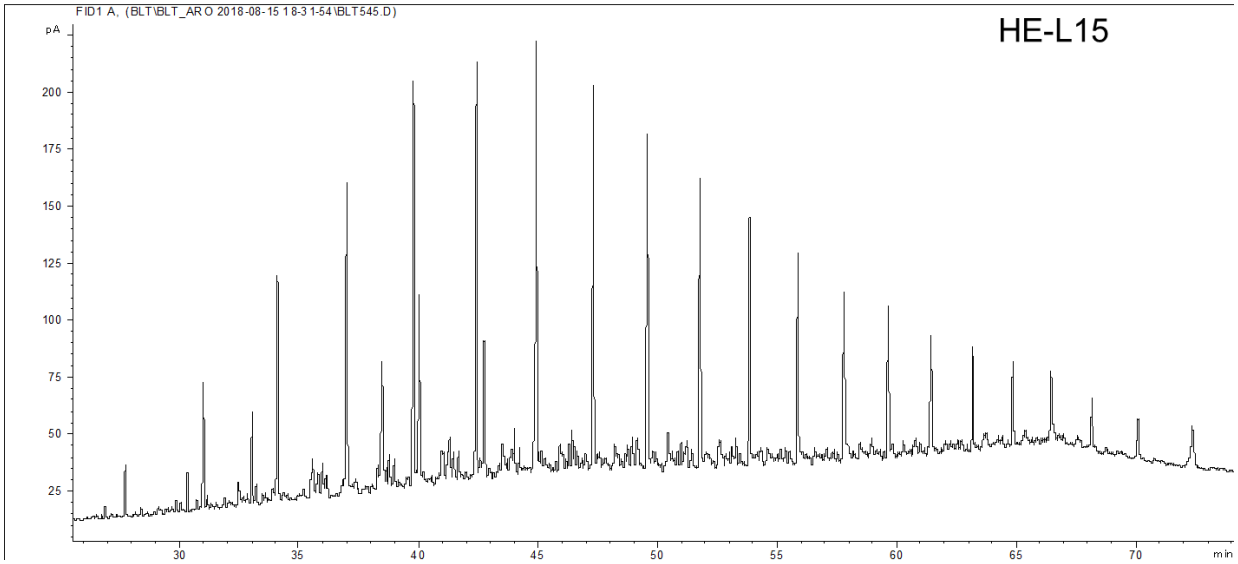
FID1 A, (BLT\BLT_ARO 2018-08-15 18-31-54\BLT545.D)
HE-L15
pA
min

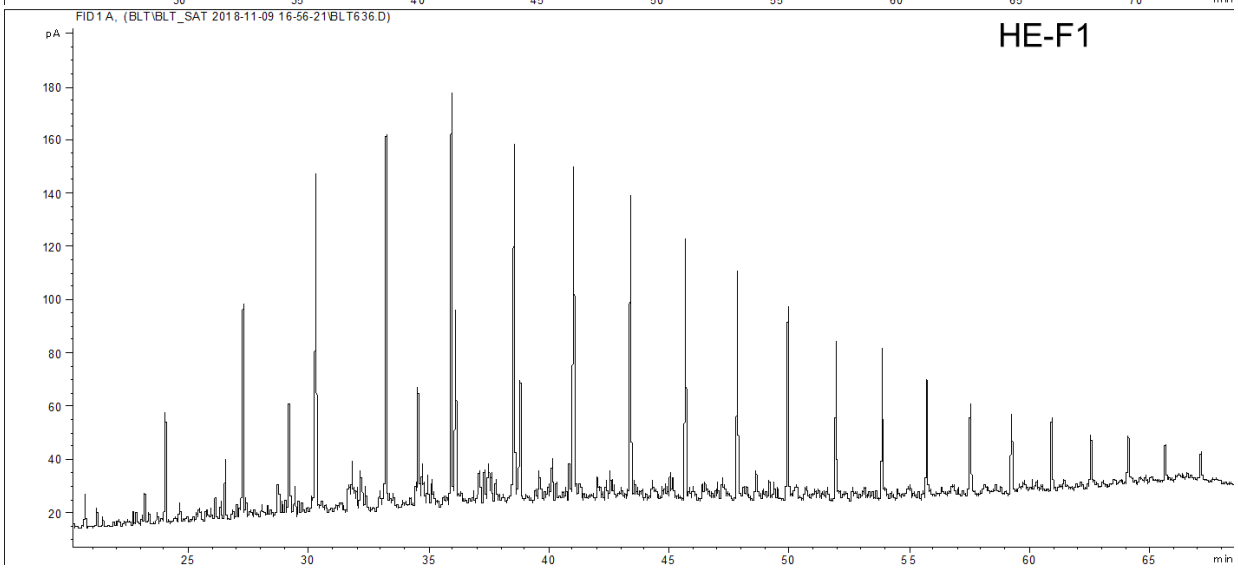
FID1 A, (BLT\BLT_SAT 2018-11-09 16-56-21\BLT636.D)
HE-F1
pA
min

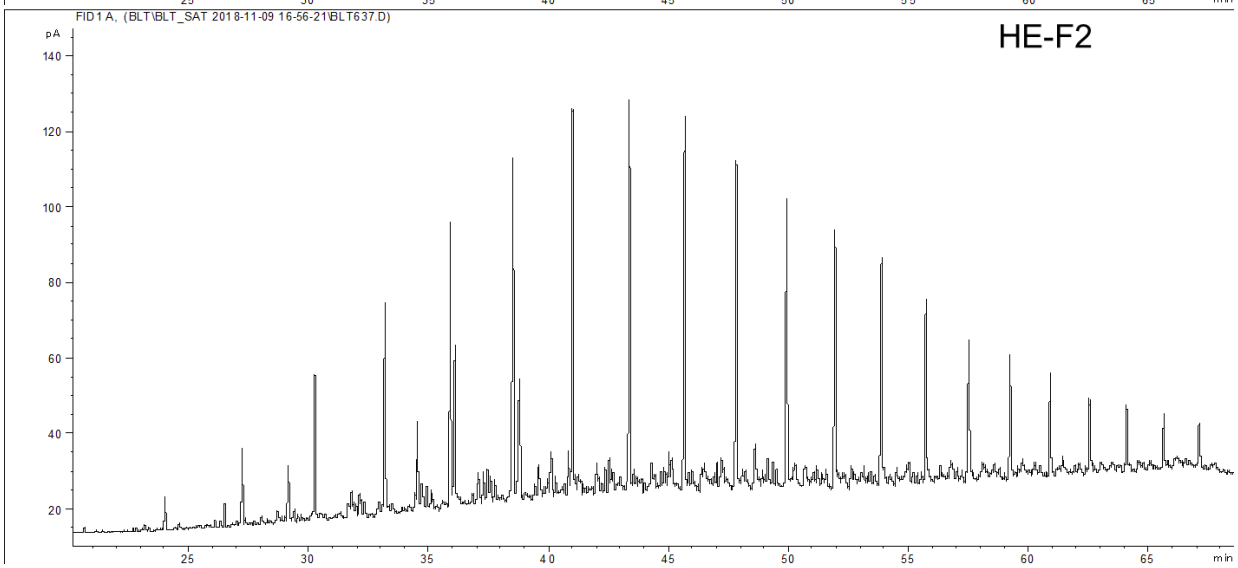
FID1 A, (BLT\BLT_SAT 2018-11-09 16-56-21\BLT637.D)
HE-F2
pA
min

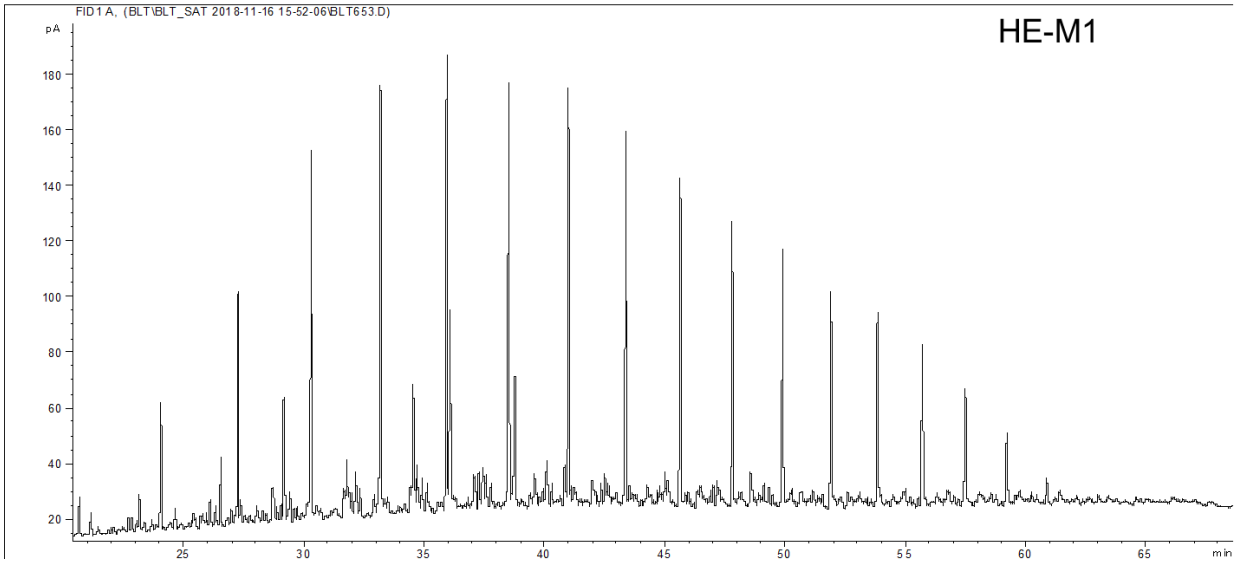
FID1 A, (BLT\BLT_SAT 2018-11-16 15-52-06\BLT653.D)
HE-M1
pA
min

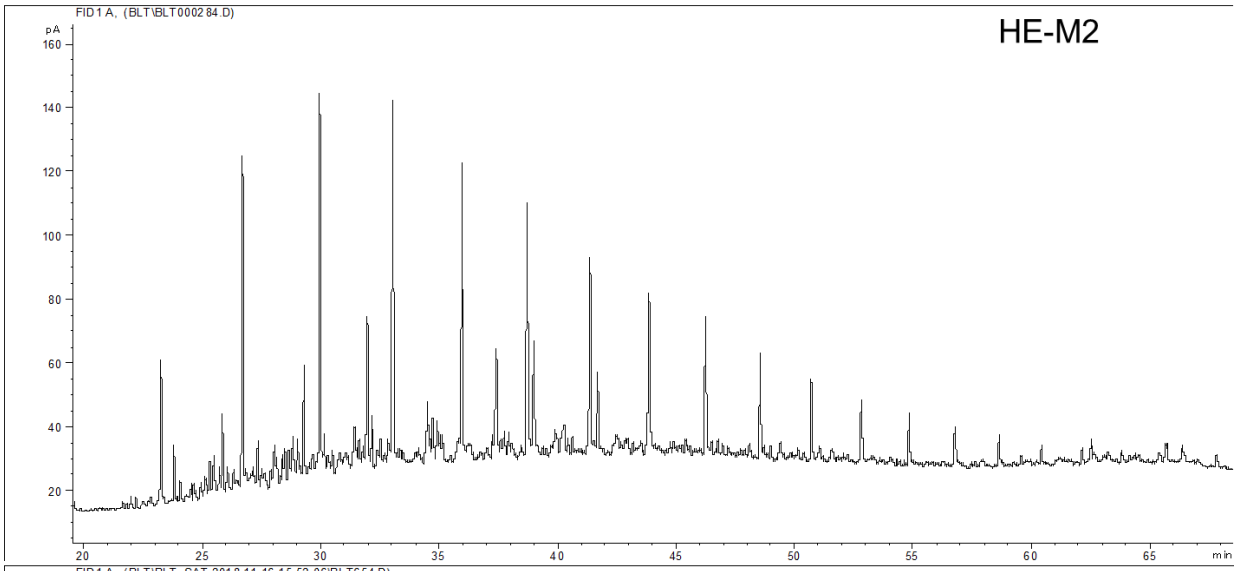
FID1 A, (BLT\BLT000284.D)
HE-M2
pA
min

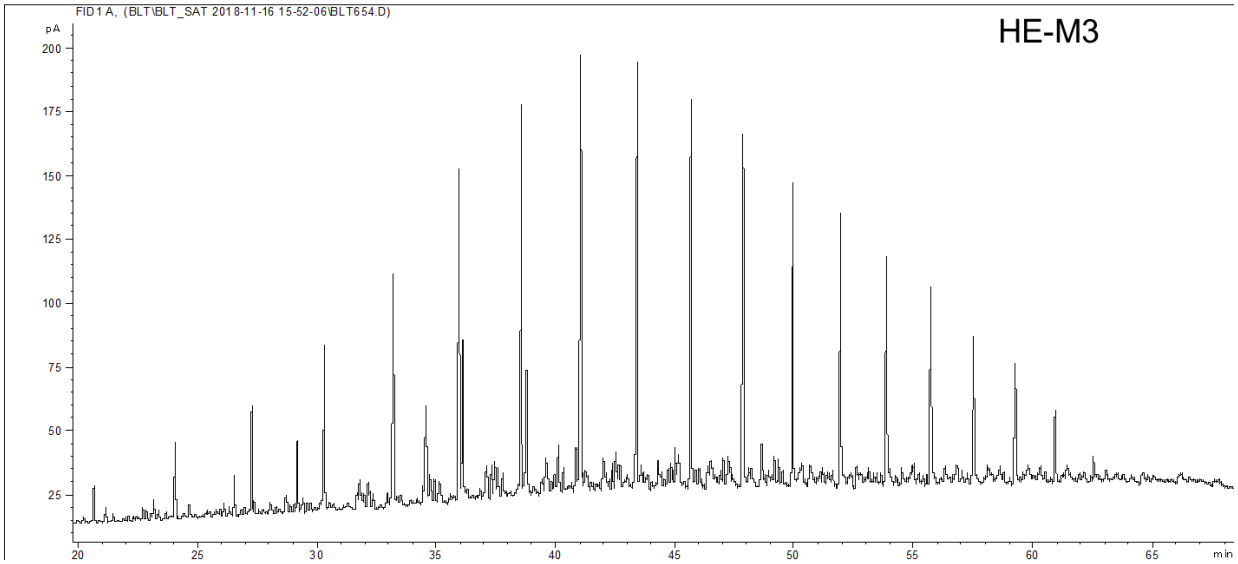
FID1 A, (BLT\BLT_SAT 2018-11-16 15-52-06\BLT654.D)
HE-M3
pA
min

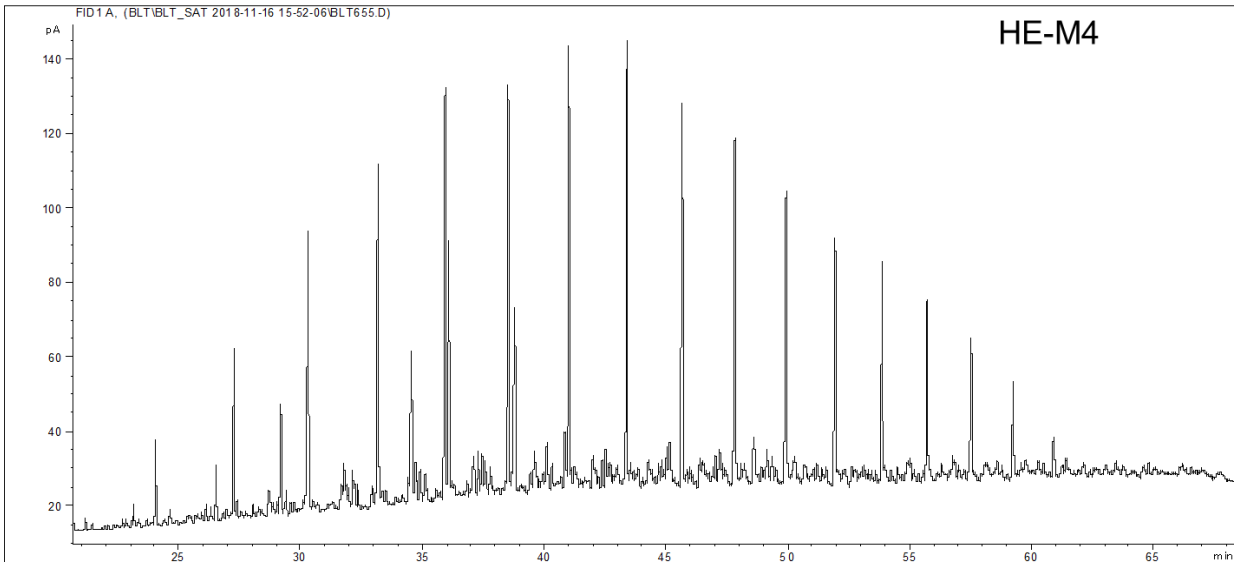
FID1 A, (BLT\BLT_SAT 2018-11-16 15-52-06\BLT655.D)
HE-M4
pA
min

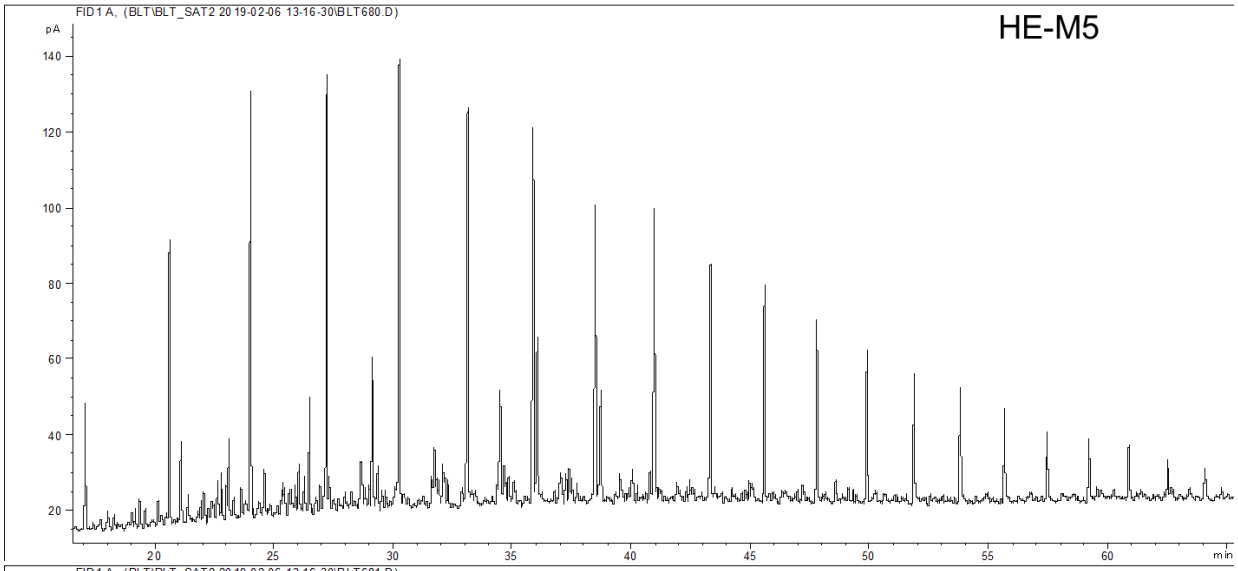
FID1 A, (BLT\BLT_SAT2 2019-02-06 13-16-30\BLT680.D)
HE-M5
pA
min

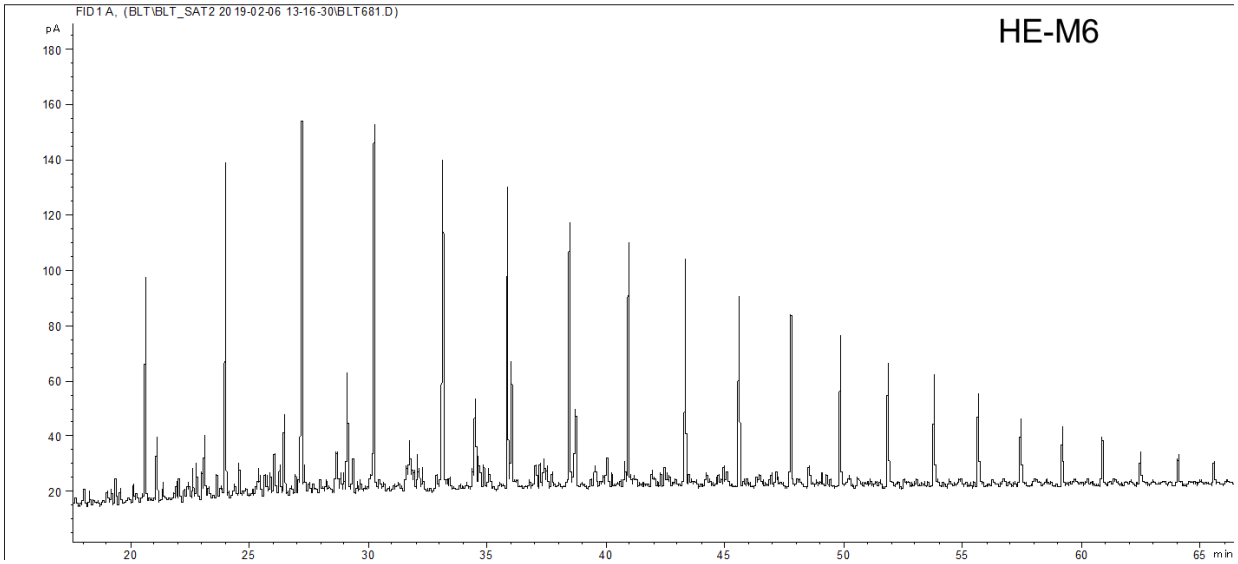
FID1 A, (BLT\BLT_SAT2 2019-02-06 13-16-30\BLT681.D)
HE-M6
pA
min

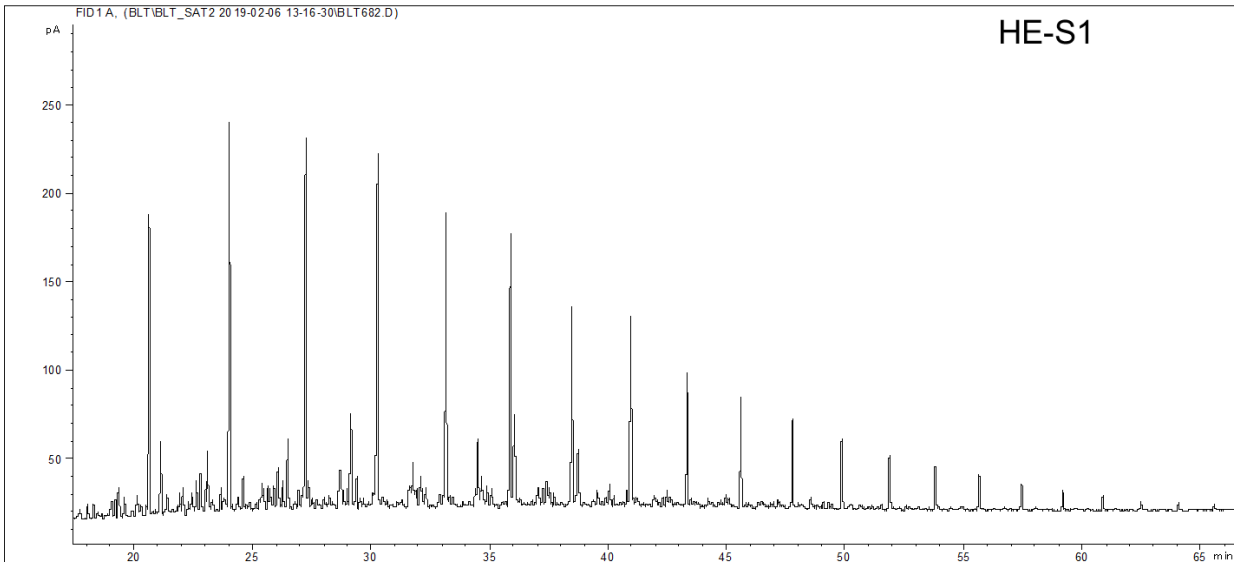
FID1 A, (BLT\BLT_SAT2 2019-02-06 13-16-30\BLT682.D)
HE-S1
pA
min

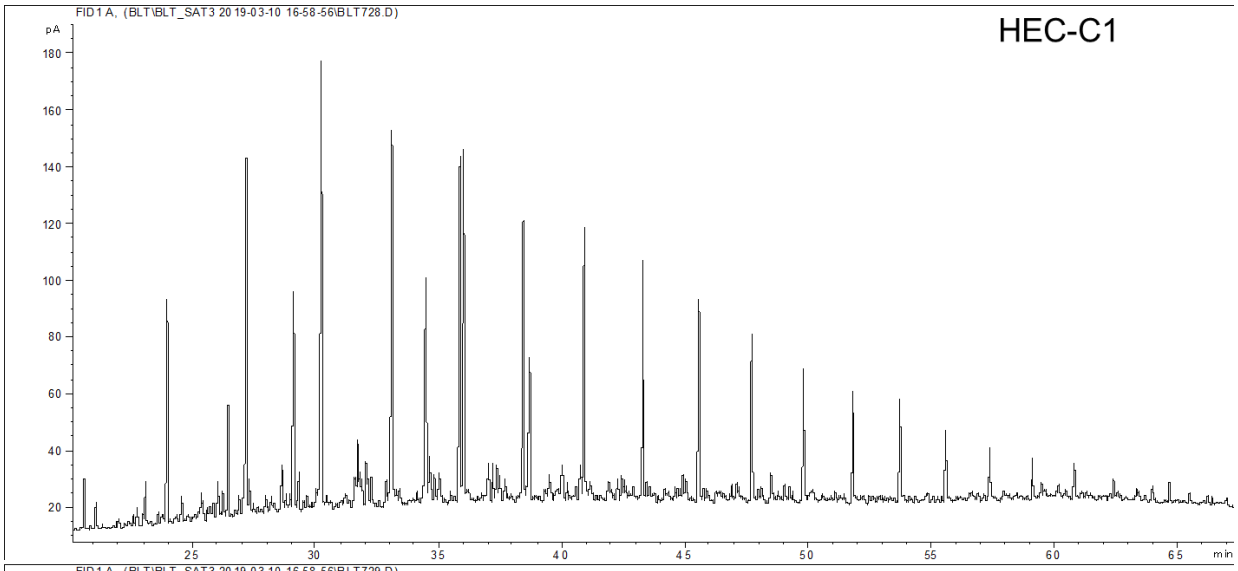
FID1 A, (BLT\BLT_SAT3 2019-03-10 16-58-56\BLT728.D)
HEC-C1
pA
min

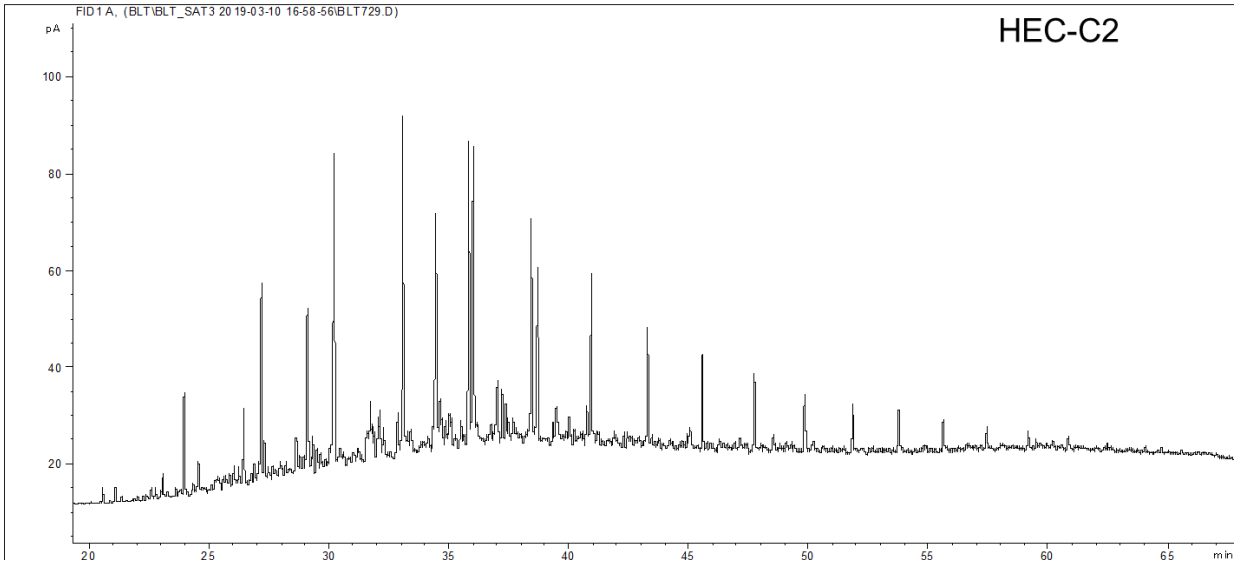
FID1 A, (BLT\BLT_SAT3 2019-03-10 16-58-56\BLT729.D)
HEC-C2
pA
min

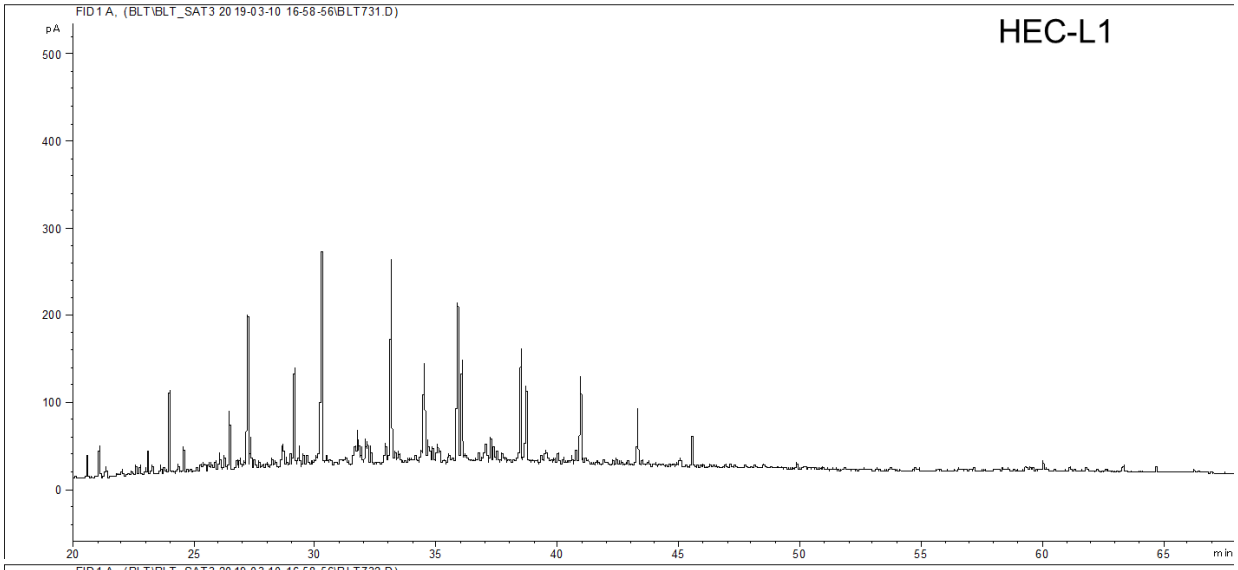
FID1 A, (BLT\BLT_SAT3 2019-03-10 16-58-56\BLT731.D)
HEC-L1
pA
500
400
300
200
100
0
20
25
30
35
40
45
50
55
60
65
min

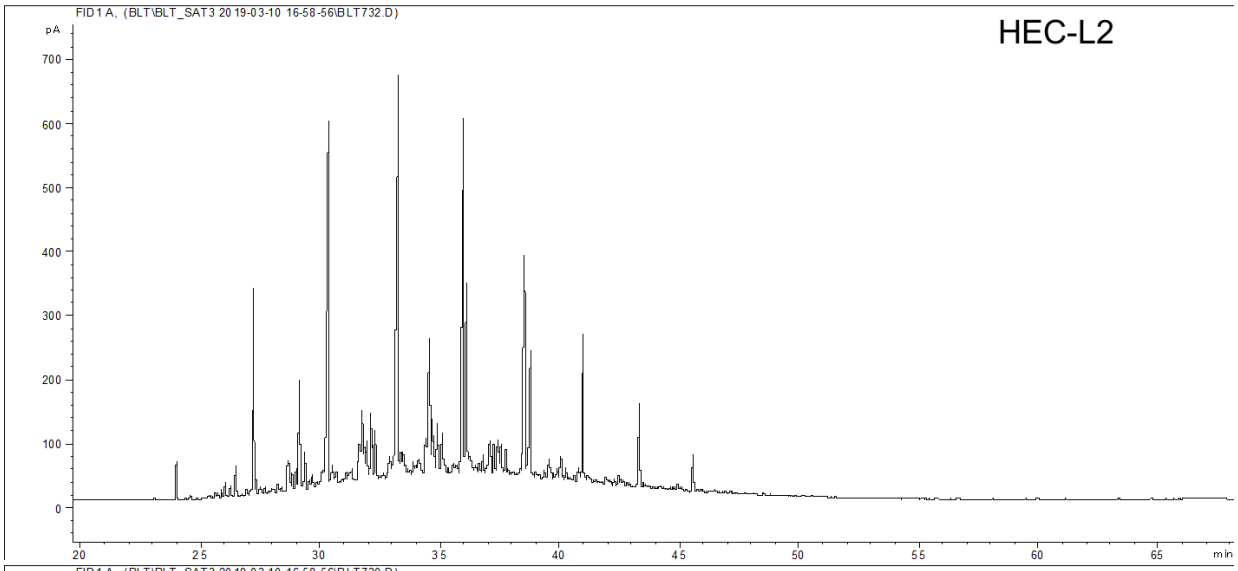
FID1 A, (BLT\BLT_SAT3 2019-03-10 16-58-56\BLT732.D)
HEC-L2
pA
700
600
500
400
300
200
100
0
20
25
30
35
40
45
50
55
60
65
min

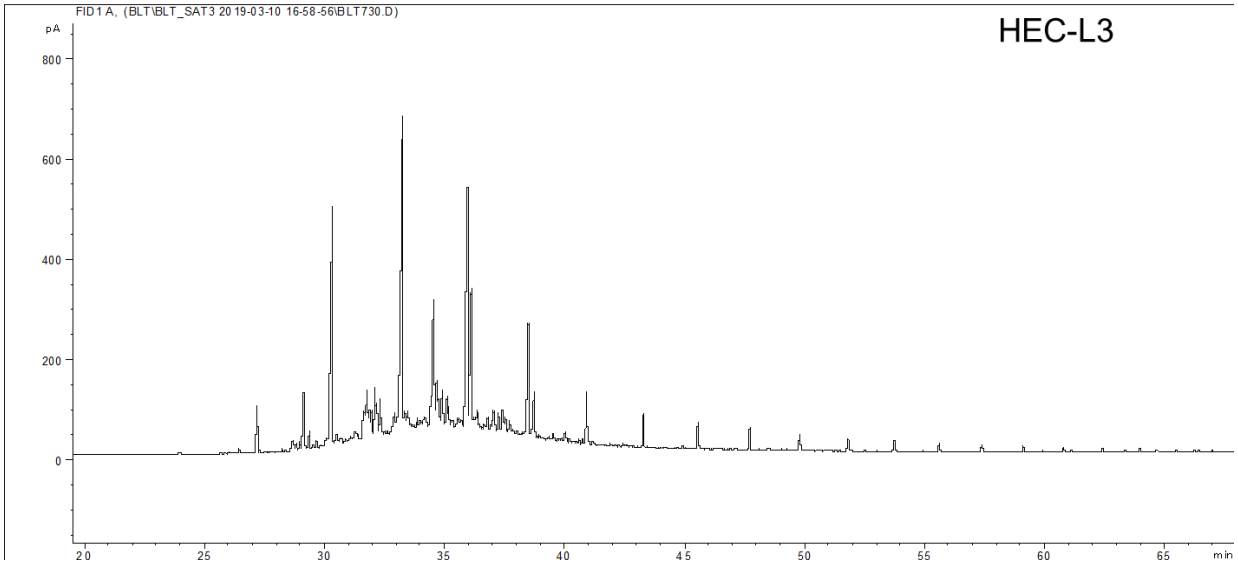
FID1 A, (BLT\BLT_SAT3 2019-03-10 16-58-56\BLT730.D)
HEC-L3
pA
800
600
400
200
0
20
25
30
35
40
45
50
55
60
65
min

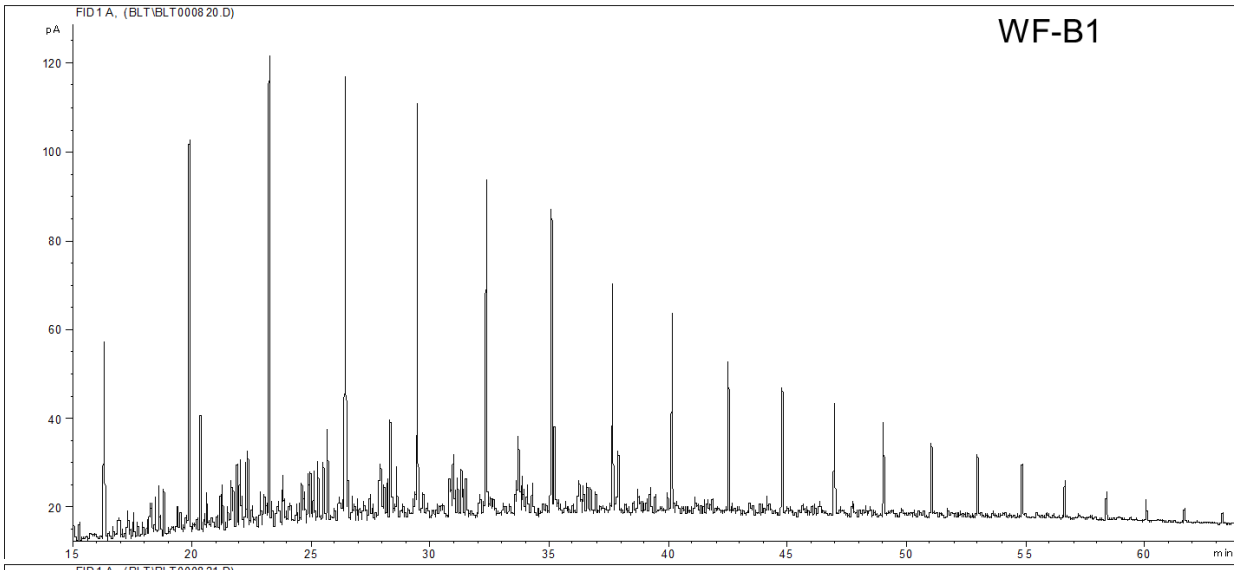
FID1 A, (BLT\BLT000820.D)
WF-B1
pA
120
100
80
60
40
20
15
20
25
30
35
40
45
50
55
60
min

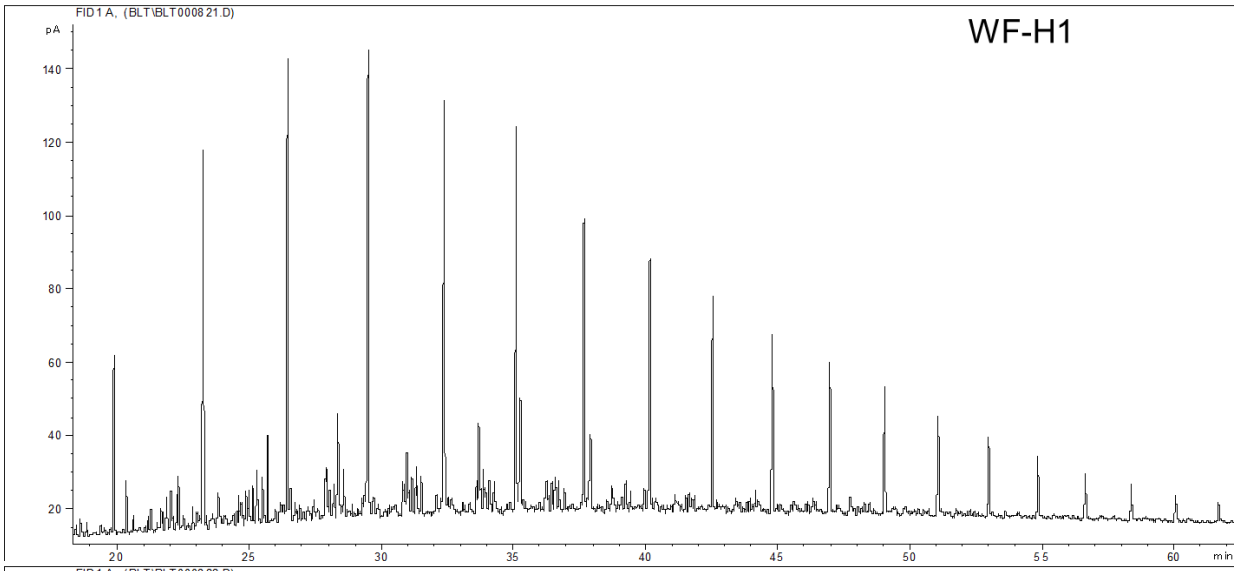
FID1 A, (BLT\BLT000821.D)
WF-H1
pA
140
120
100
80
60
40
20
20
25
30
35
40
45
50
55
60
min

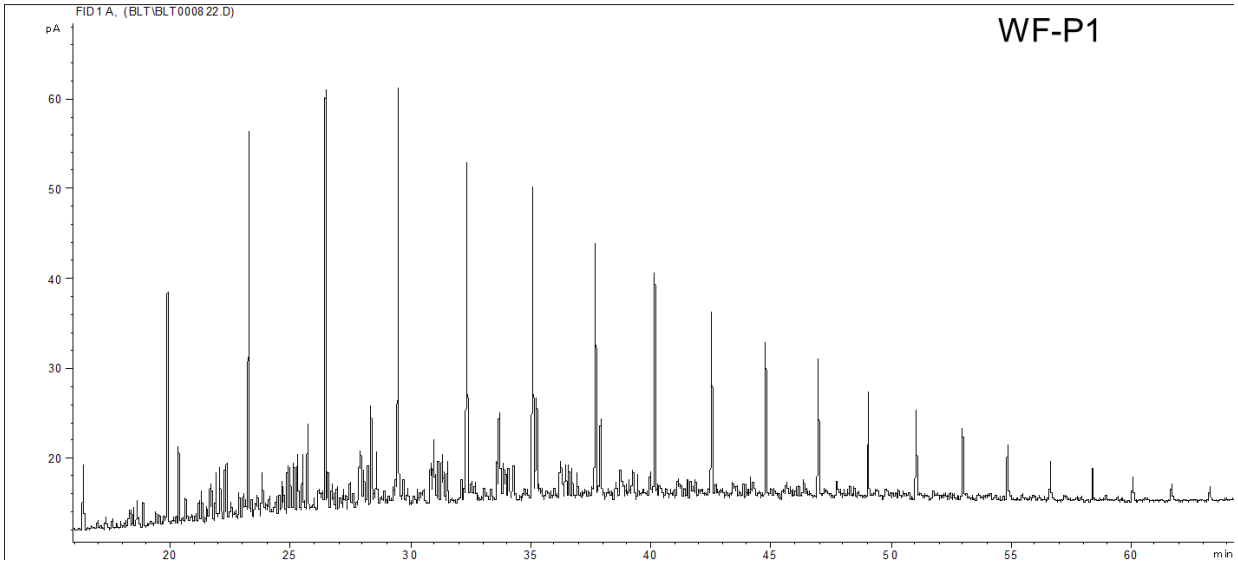
FID1 A, (BLT\BLT000822.D)
WF-P1
pA
60
50
40
30
20
20
25
30
35
40
45
50
55
60
min

C. Maltene GCMS Chromatograms

Chromatogram of aryl isoprenoids and carotenoids (m/z 133+134)

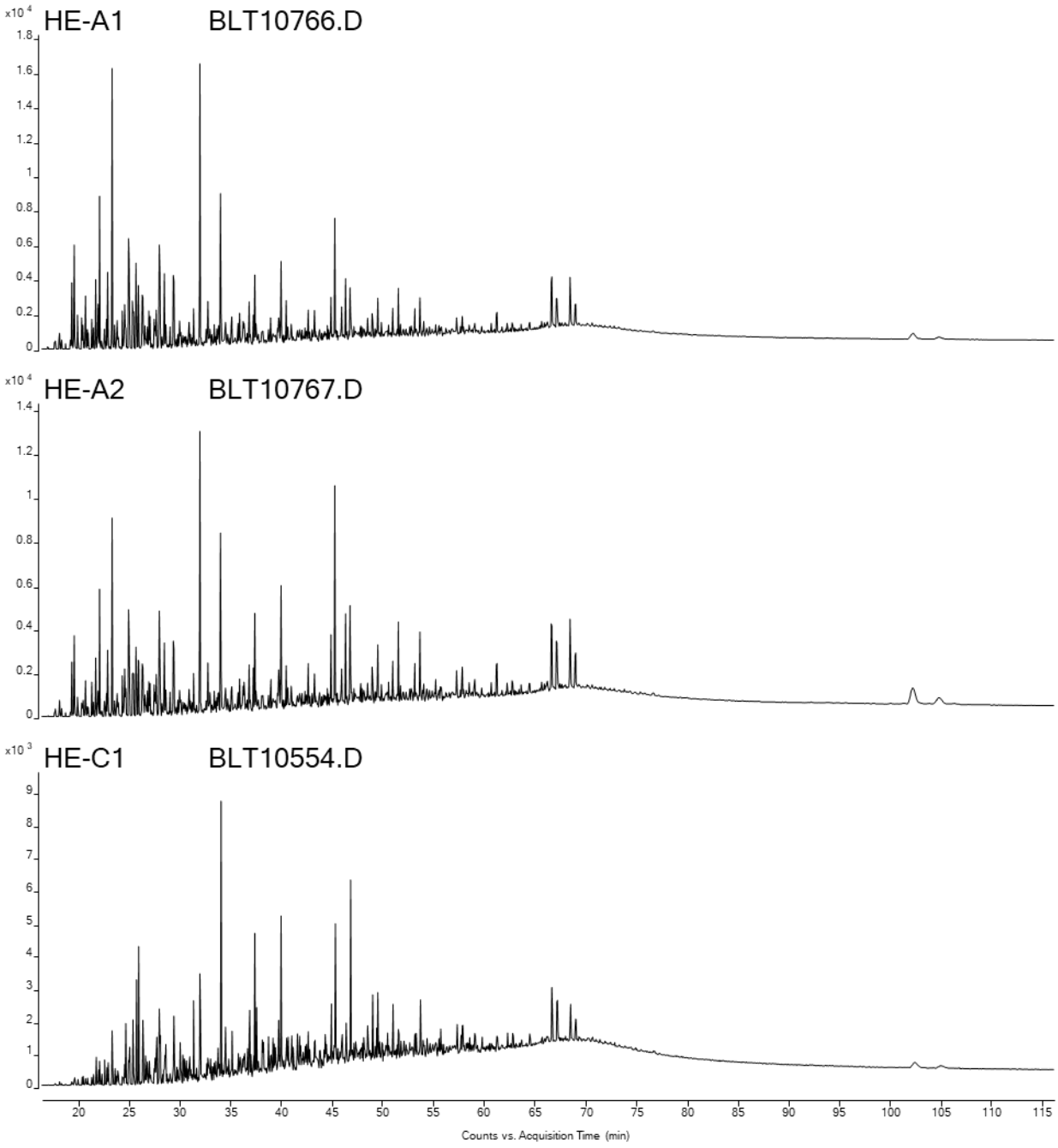

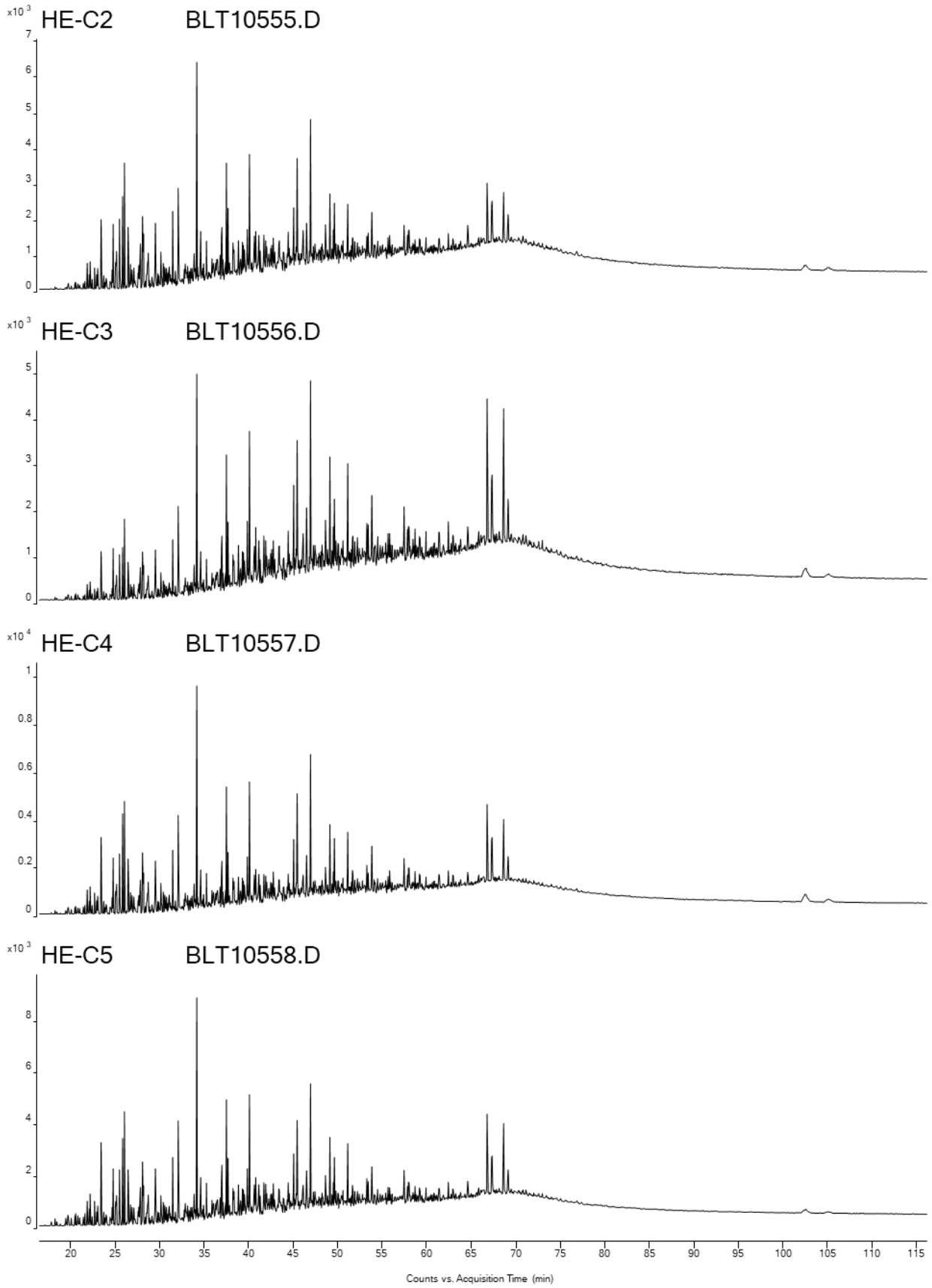
x10 3
HE-C2
BLT10555.D
x10 3
HE-C3
BLT10556.D
x10 4
HE-C4
BLT10557.D
x10 3
HE-C5
BLT10558.D
Counts vs. Acquisition Time (min)

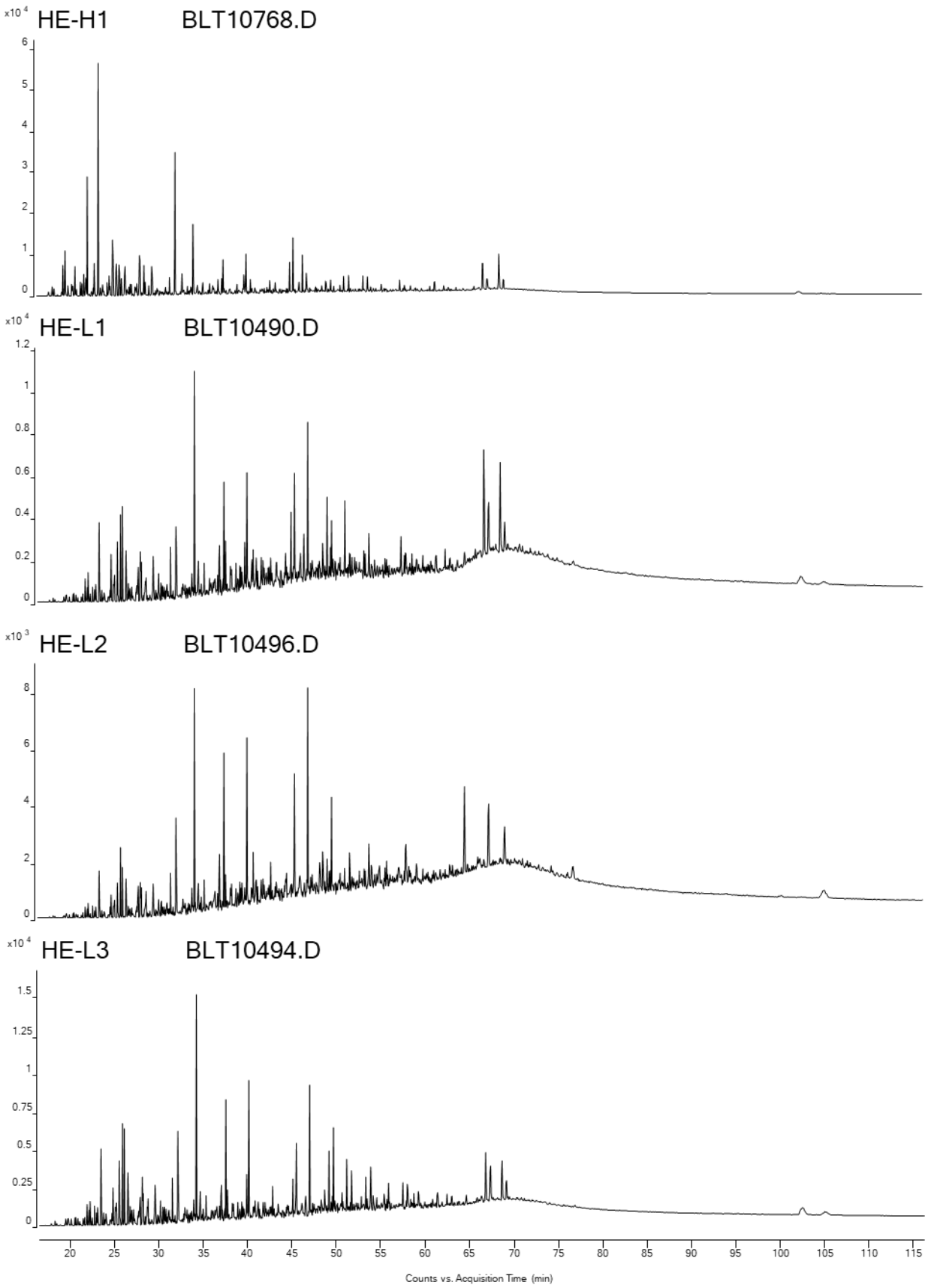
x10 4
HE-H1
BLT10768.D
x10 4
HE-L1
BLT10490.D
x10 3
HE-L2
BLT10496.D
x10 4
HE-L3
BLT10494.D
Counts vs. Acquisition Time (min)

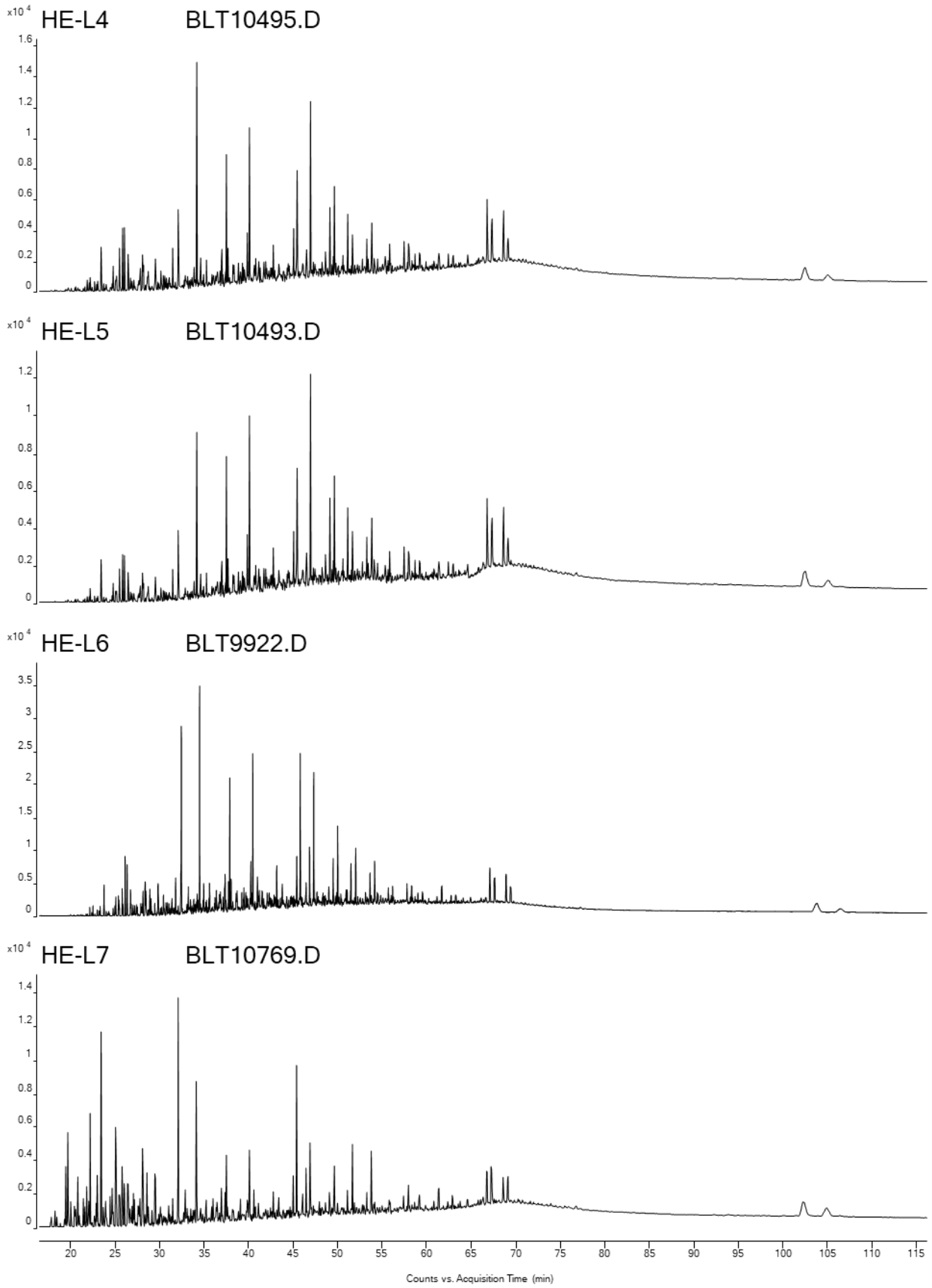
x10 4
HE-L4
BLT10495.D
x10 4
HE-L5
BLT10493.D
x10 4
HE-L6
BLT9922.D
x10 4
HE-L7
BLT10769.D
Counts vs. Acquisition Time (min)

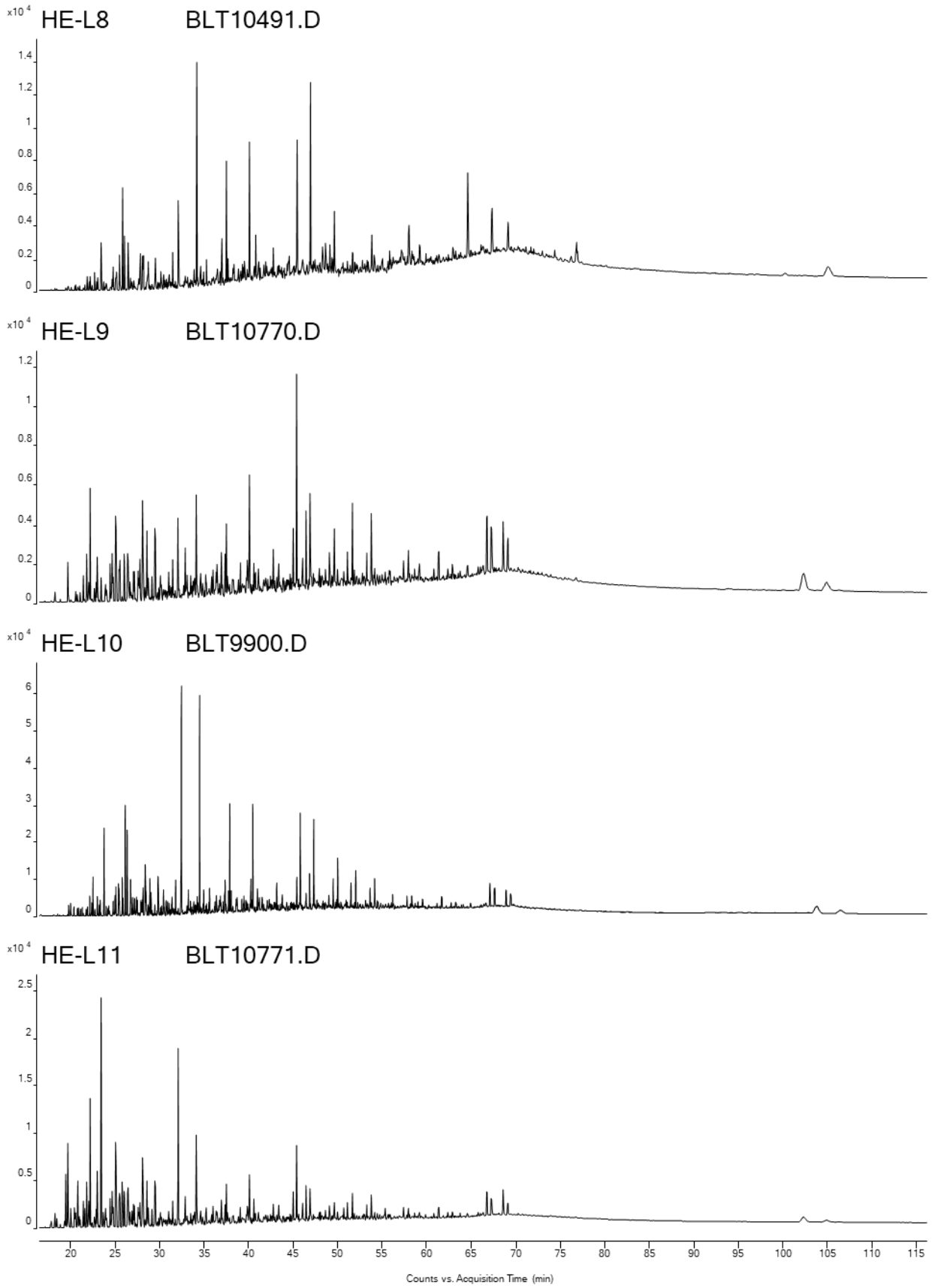
x10 4
HE-L8
BLT10491.D
x10 4
HE-L9
BLT10770.D
x10 4
HE-L10
BLT9900.D
x10 4
HE-L11
BLT10771.D
Counts vs. Acquisition Time (min)

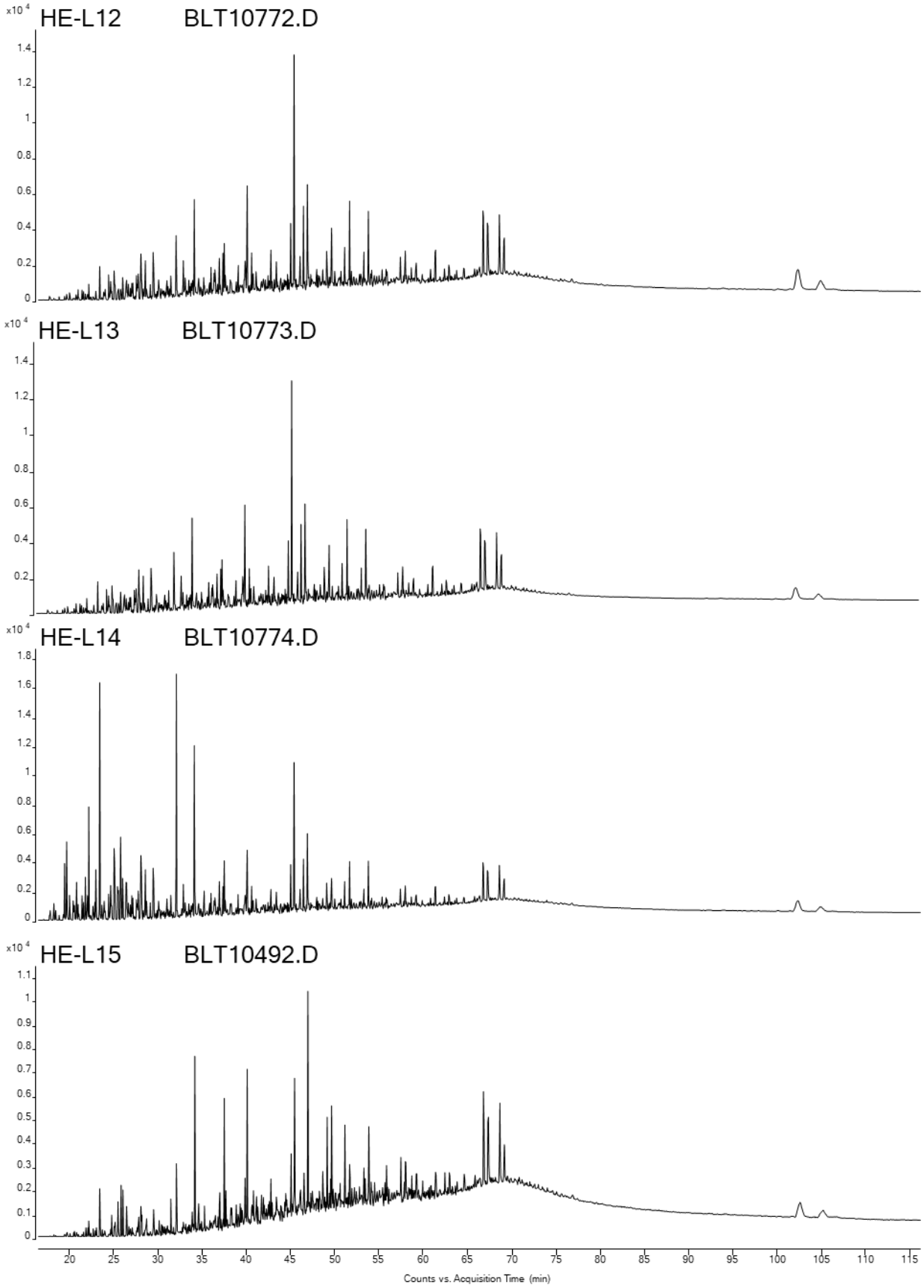
HE-L12 BLT10772.D
HE-L13 BLT10773.D
HE-L14 BLT10774.D
HE-L15 BLT10492.D
x10 4
Counts vs. Acquisition Time (min)

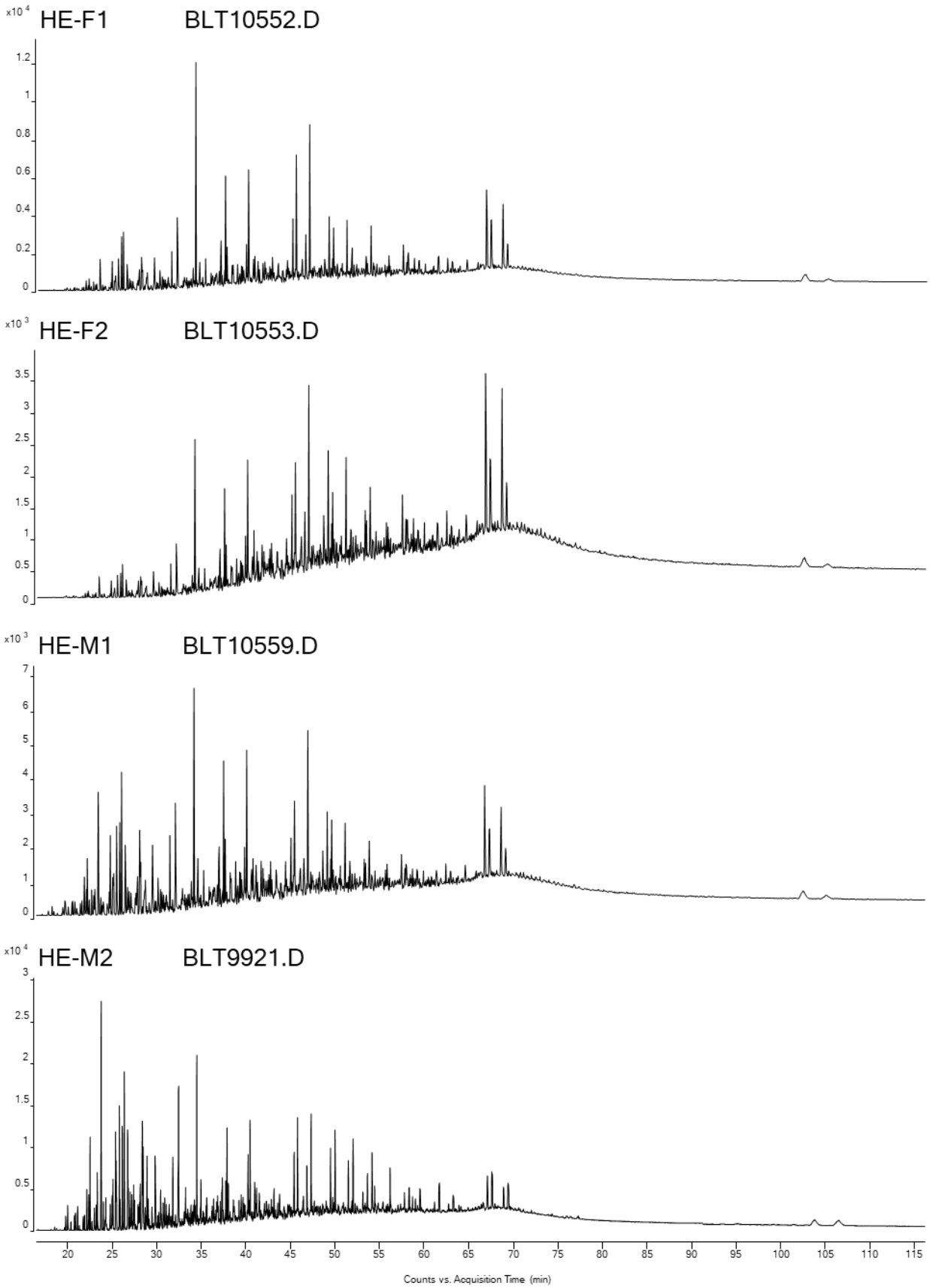
x10 4
HE-F1
BLT10552.D
x10 3
HE-F2
BLT10553.D
x10 3
HE-M1
BLT10559.D
x10 4
HE-M2
BLT9921.D
Counts vs. Acquisition Time (min)

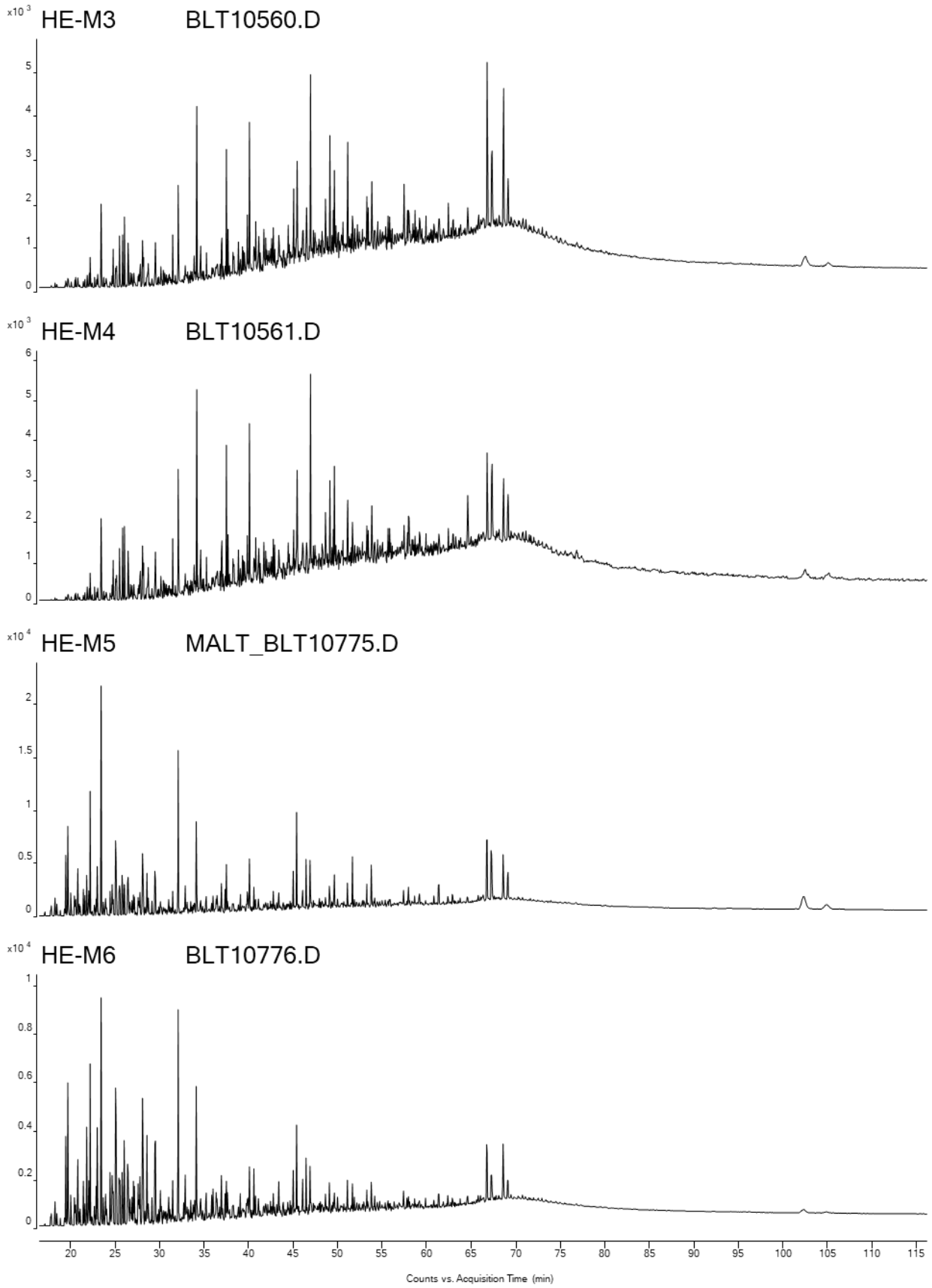
x10 3
HE-M3
BLT10560.D
x10 3
HE-M4
BLT10561.D
x10 4
HE-M5
MALT_BLT10775.D
x10 4
HE-M6
BLT10776.D
Counts vs. Acquisition Time (min)

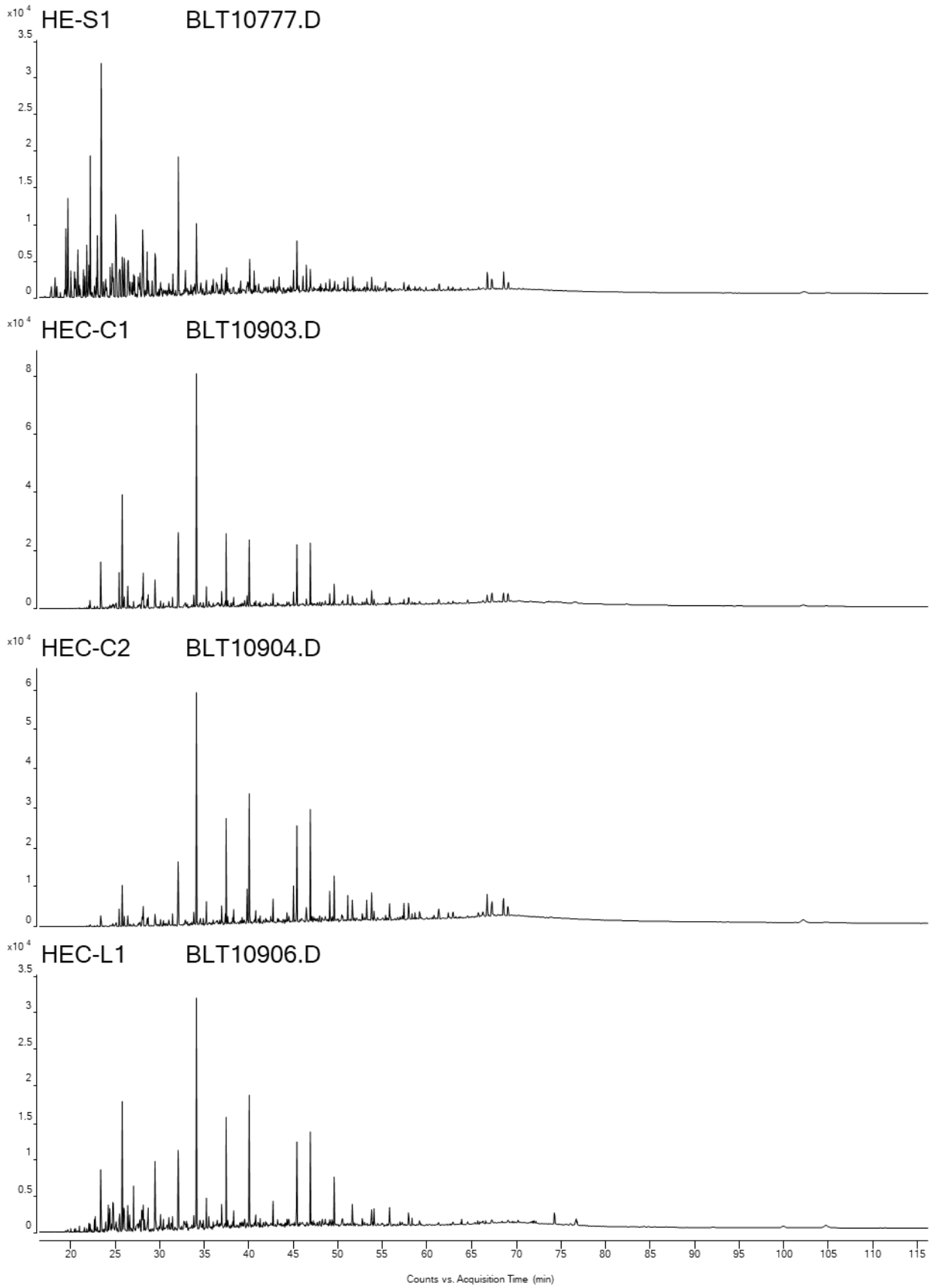
x10 4
HE-S1
BLT10777.D
x10 4
HEC-C1
BLT10903.D
x10 4
HEC-C2
BLT10904.D
x10 4
HEC-L1
BLT10906.D
Counts vs. Acquisition Time (min)

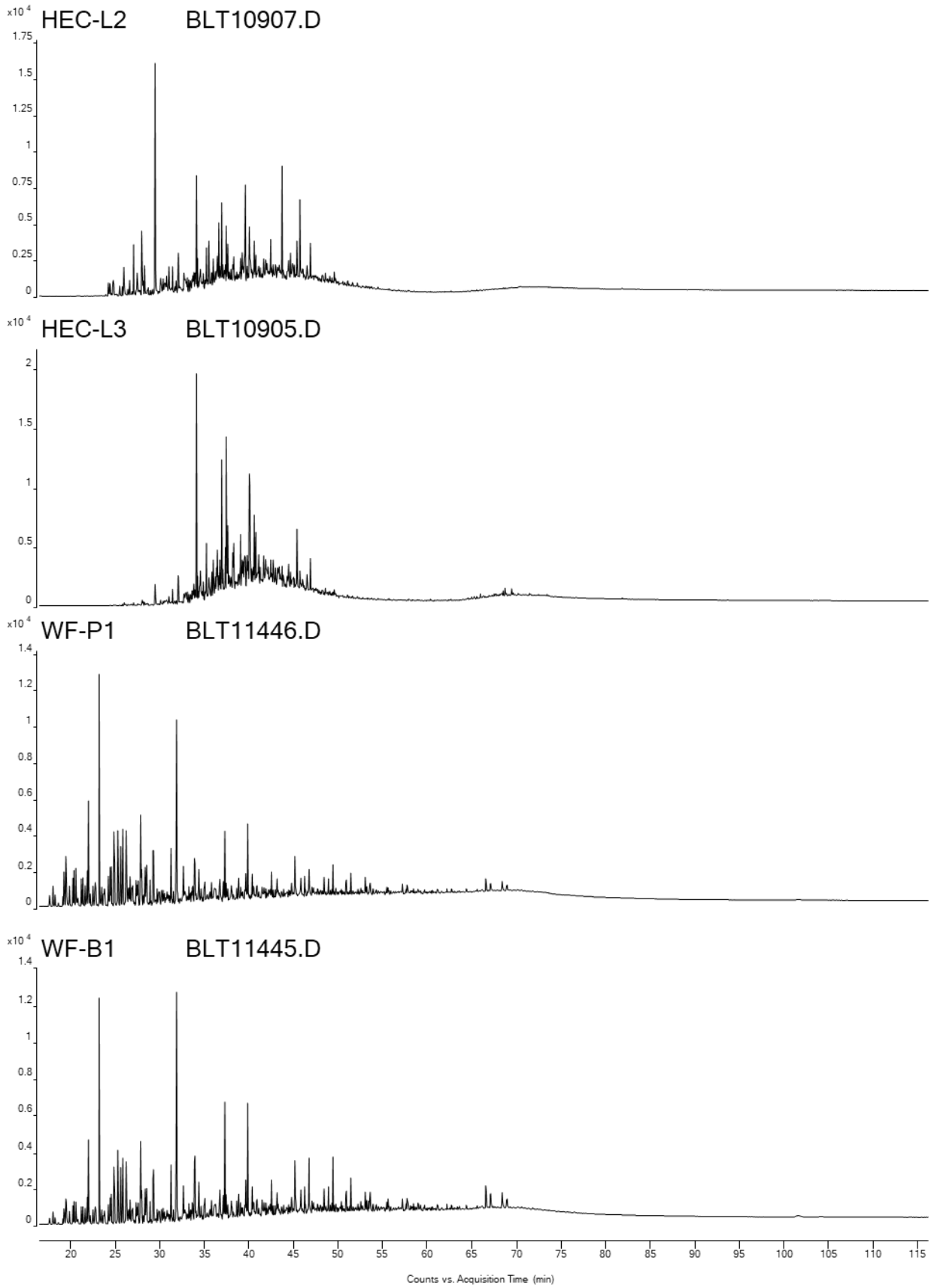
x10 4
HEC-L2
BLT10907.D
x10 4
HEC-L3
BLT10905.D
x10 4
WF-P1
BLT11446.D
x10 4
WF-B1
BLT11445.D
Counts vs. Acquisition Time (min)

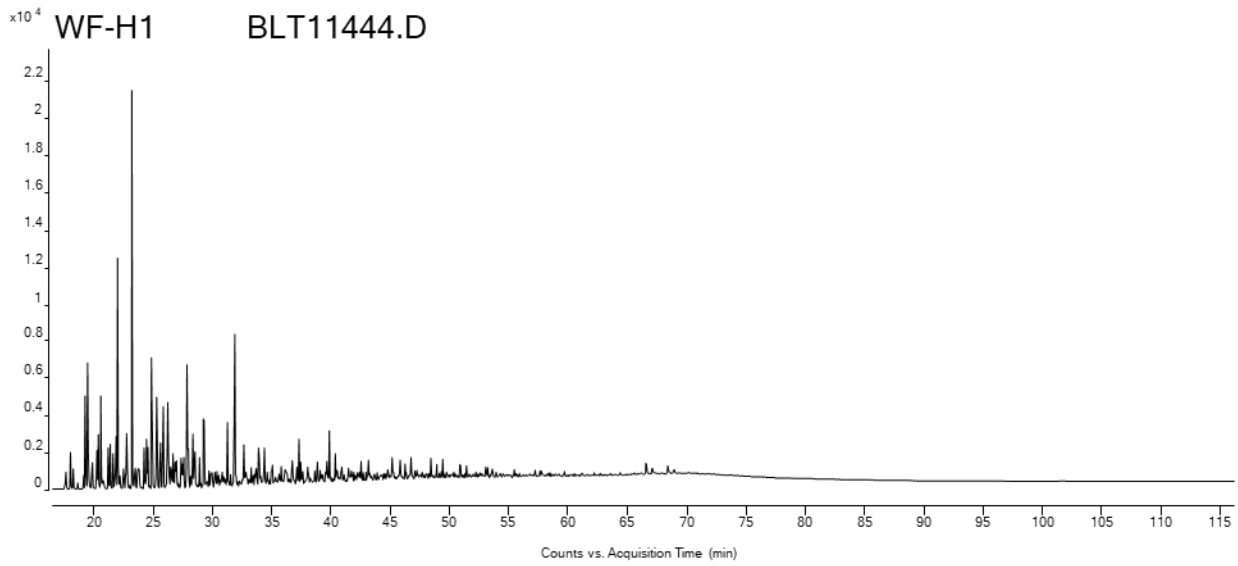
x10 4
WF-H1
BLT11444.D
2.2
2
1.8
1.6
1.4
1.2
1
0.8
0.6
0.4
0.2
0
20
25
30
35
40
45
50
55
60
65
70
75
80
85
90
95
100
105
110
115
Counts vs. Acquisition Time (min)

D. Saturate GCMS Chromatograms

Chromatograms of terpanes (m/z 191) and steranes (m/z 217)

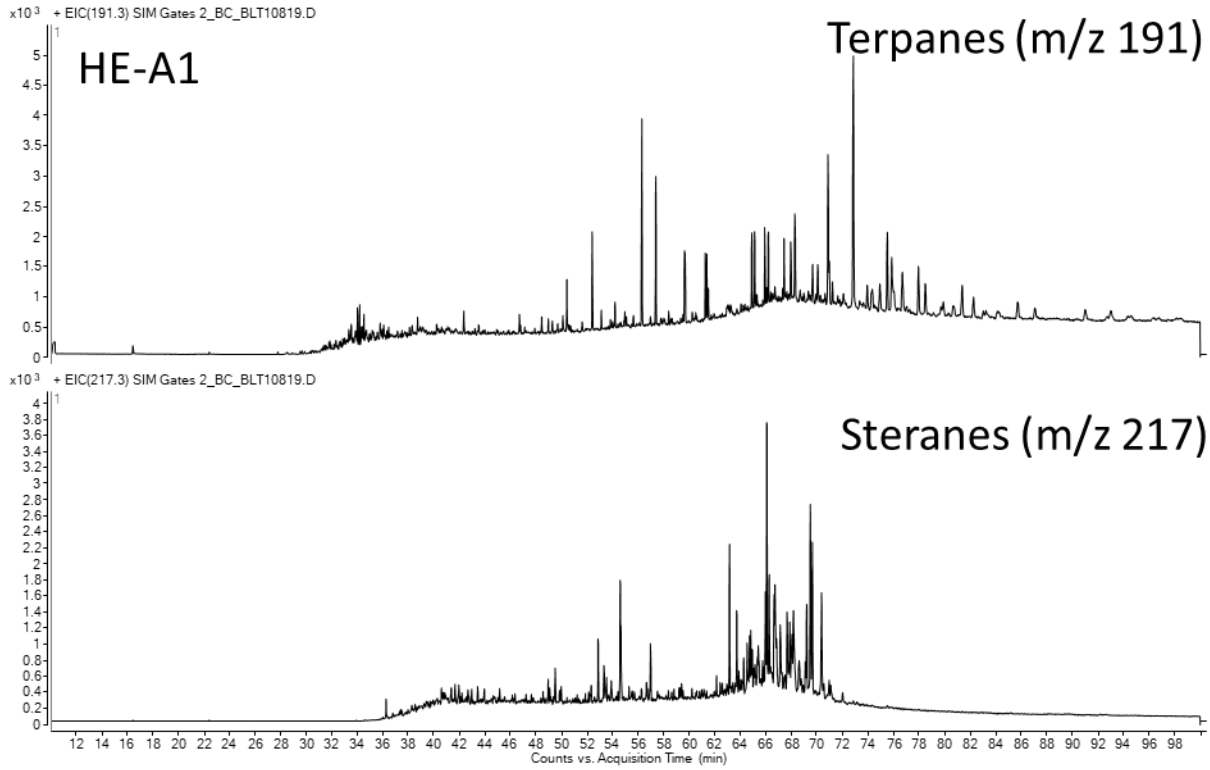

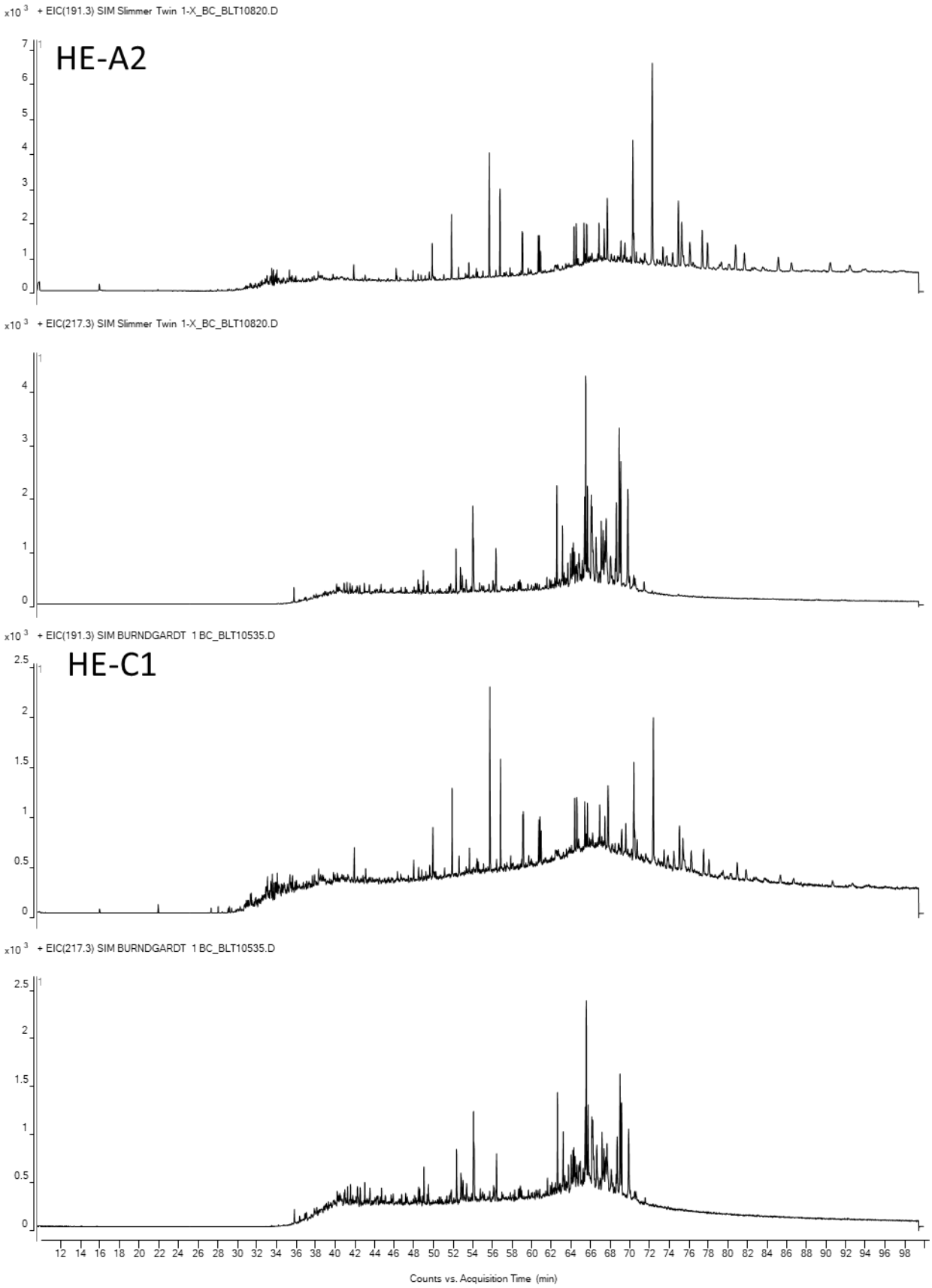
x10 3 + EIC(191.3) SIM Slimmer Twin 1-X_BC_BLT10820.D
HE-A2
x10 3 + EIC(217.3) SIM Slimmer Twin 1-X_BC_BLT10820.D
x10 3 + EIC(191.3) SIM BURNDGARDT 1 BC_BLT10535.D
HE-C1
x10 3 + EIC(217.3) SIM BURNDGARDT 1 BC_BLT10535.D
Counts vs. Acquisition Time (min)

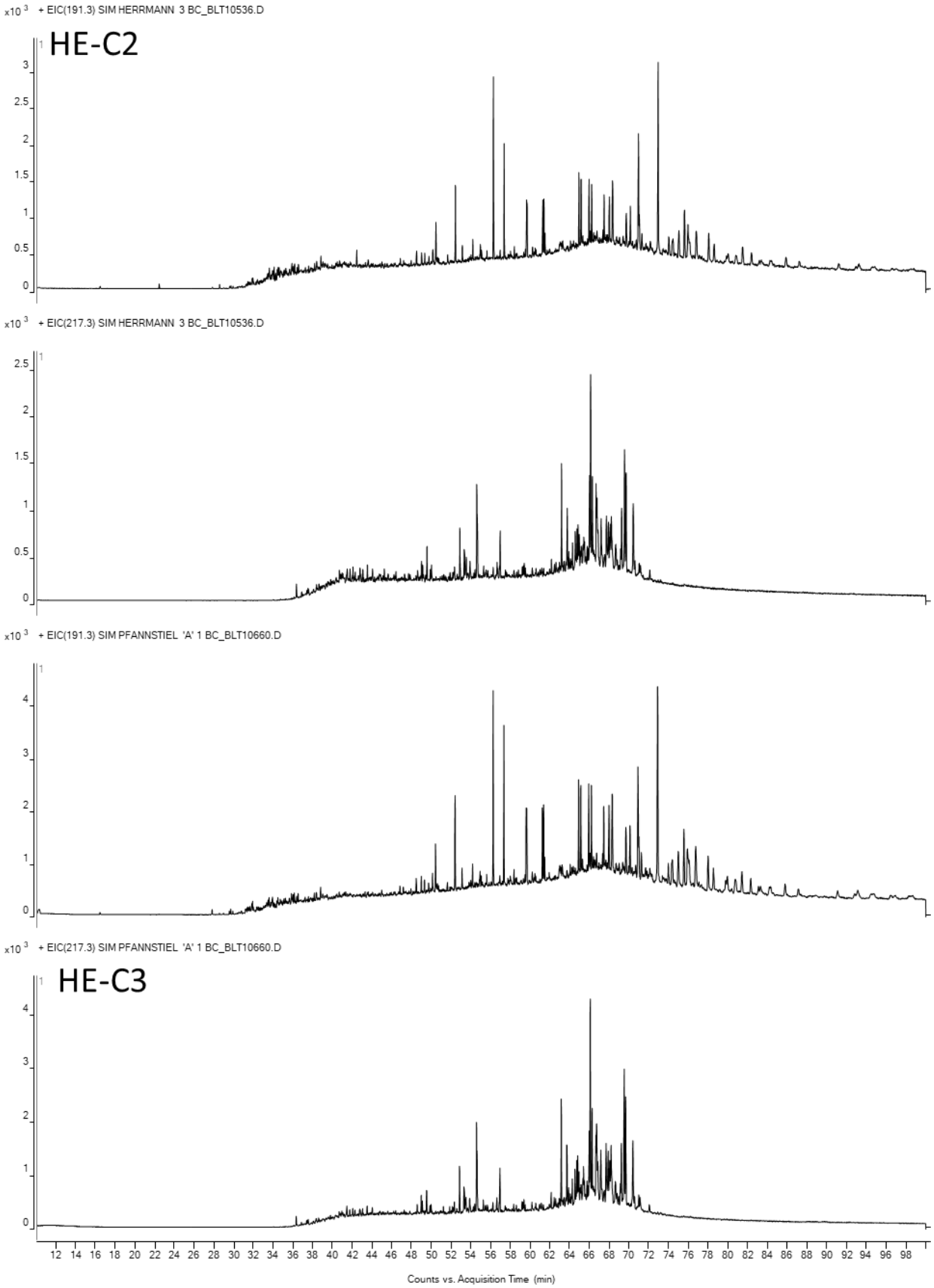
x10 3 + EIC(191.3) SIM HERRMANN 3 BC_BLT10536.D
HE-C2
x10 3 + EIC(217.3) SIM HERRMANN 3 BC_BLT10536.D
x10 3 + EIC(191.3) SIM PFANNSTIEL 'A' 1 BC_BLT10660.D
x10 3 + EIC(217.3) SIM PFANNSTIEL 'A' 1 BC_BLT10660.D
HE-C3
Counts vs. Acquisition Time (min)

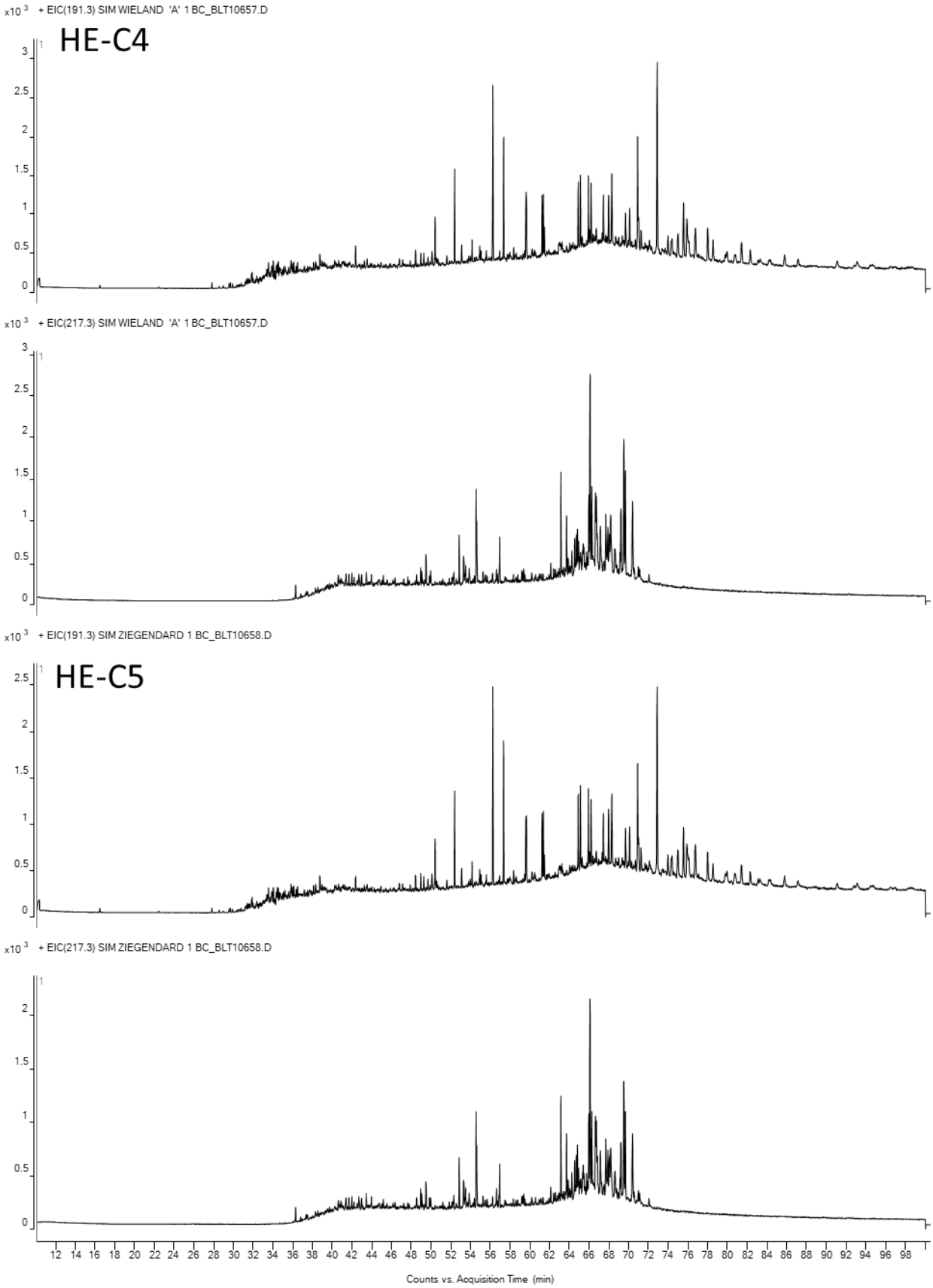
x10 3 + EIC(191.3) SIM WIELAND 'A' 1 BC_BLT10657.D
HE-C4
x10 3 + EIC(217.3) SIM WIELAND 'A' 1 BC_BLT10657.D
x10 3 + EIC(191.3) SIM ZIEGENDARD 1 BC_BLT10658.D
HE-C5
x10 3 + EIC(217.3) SIM ZIEGENDARD 1 BC_BLT10658.D
Counts vs. Acquisition Time (min)

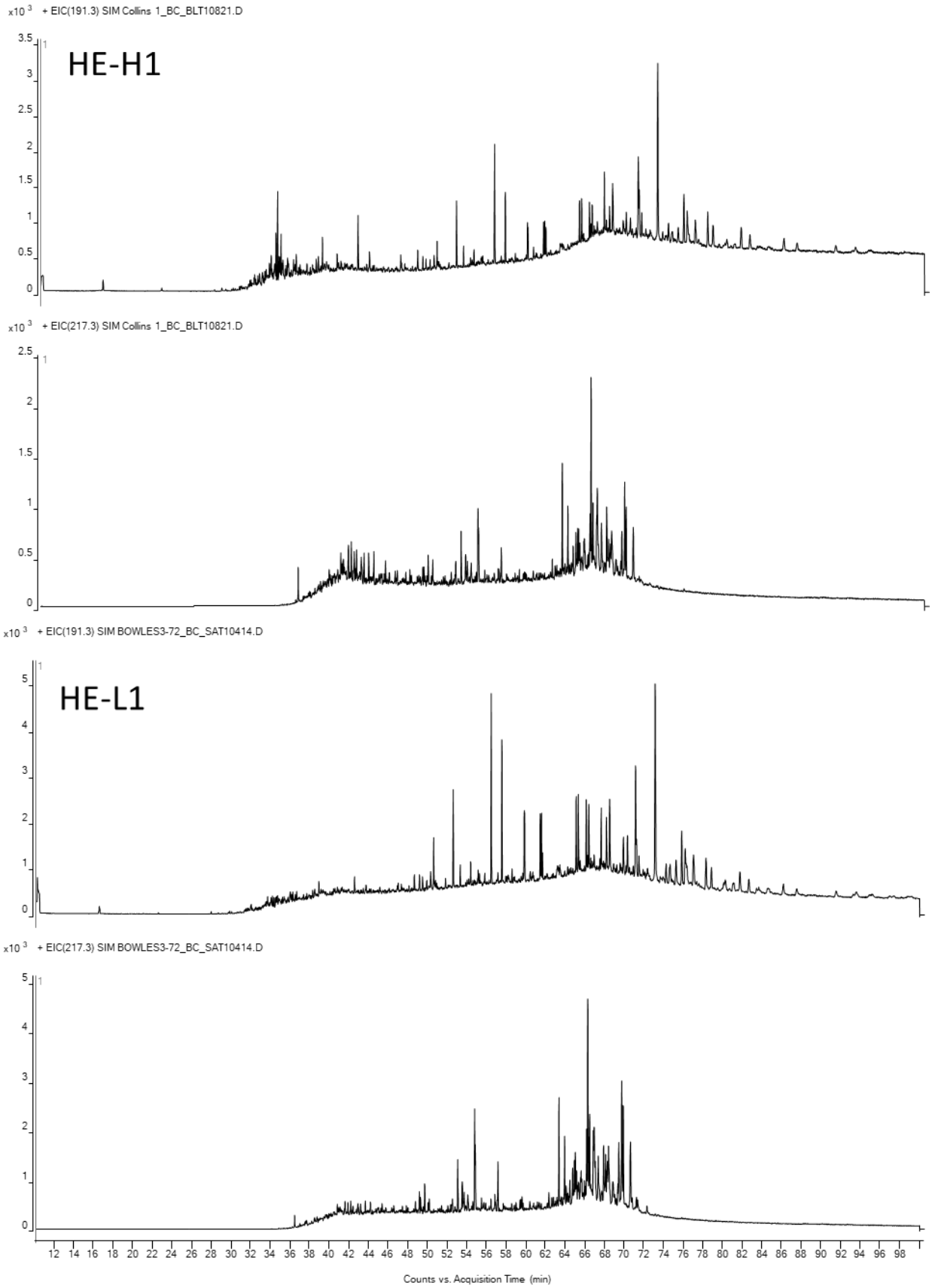
x10 3 + EIC(191.3) SIM Collins 1_BC_BLT10821.D
HE-H1
x10 3 + EIC(217.3) SIM Collins 1_BC_BLT10821.D
x10 3 + EIC(191.3) SIM BOWLES3-72_BC_SAT10414.D
HE-L1
x10 3 + EIC(217.3) SIM BOWLES3-72_BC_SAT10414.D
Counts vs. Acquisition Time (min)

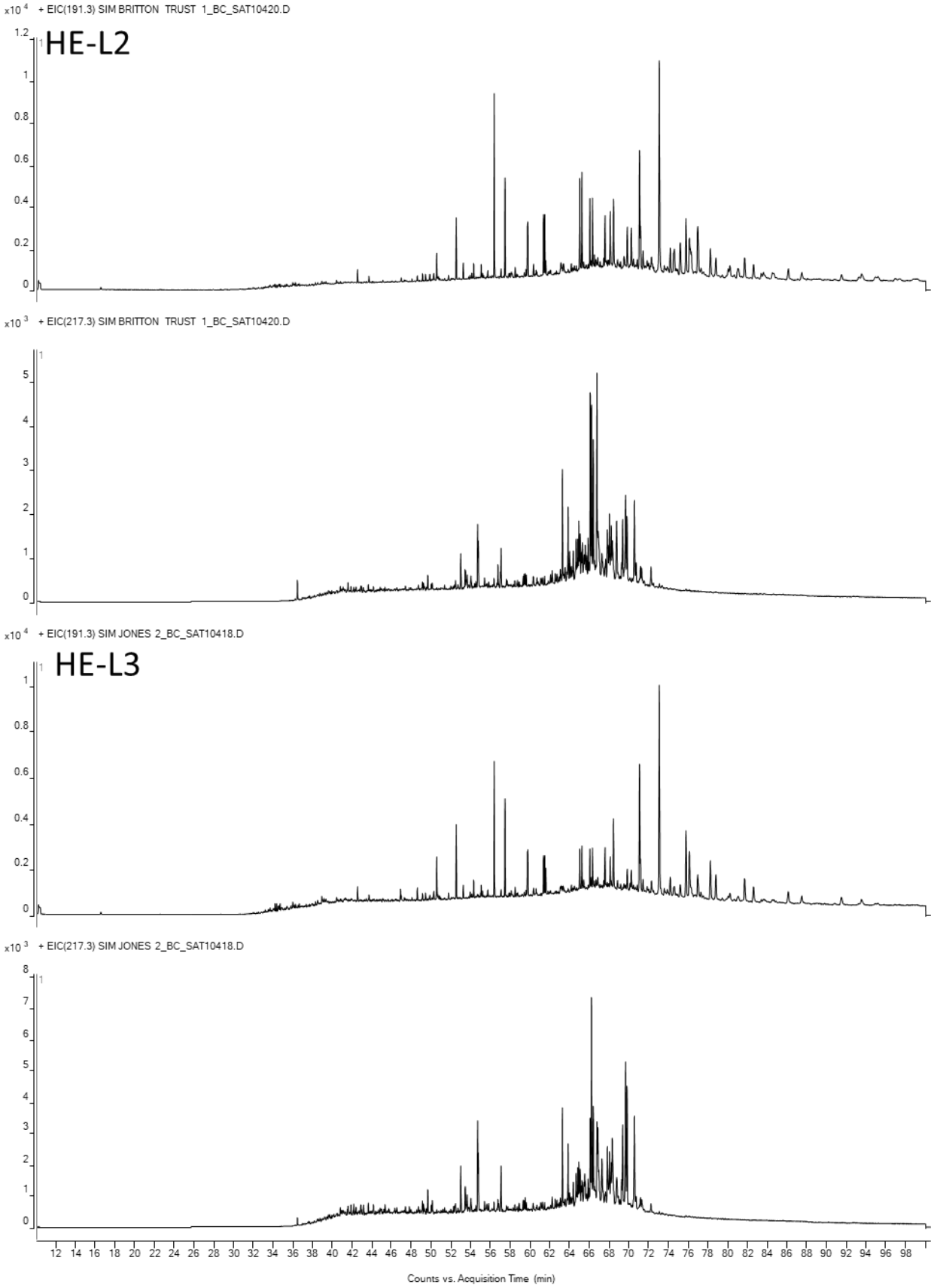
x10 4 + EIC(191.3) SIM BRITTON TRUST 1_BC_SAT10420.D
HE-L2
x10 3 + EIC(217.3) SIM BRITTON TRUST 1_BC_SAT10420.D
x10 4 + EIC(191.3) SIM JONES 2_BC_SAT10418.D
HE-L3
x10 3 + EIC(217.3) SIM JONES 2_BC_SAT10418.D
Counts vs. Acquisition Time (min)

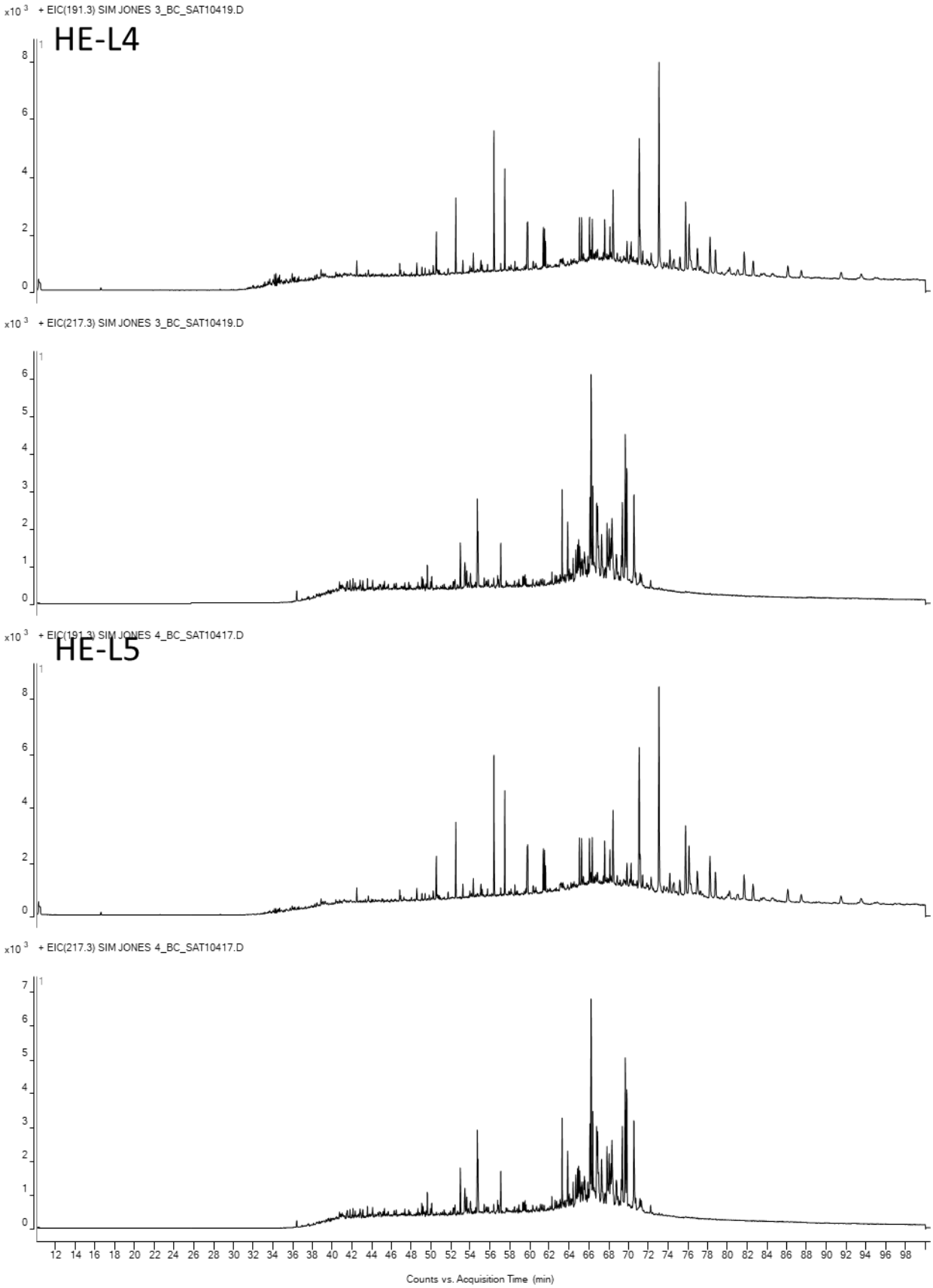
x10 3 + EIC(191.3) SIM JONES 3_BC_SAT10419.D
HE-L4
x10 3 + EIC(217.3) SIM JONES 3_BC_SAT10419.D
x10 3 + EIC(191.3) SIM JONES 4_BC_SAT10417.D
HE-L5
x10 3 + EIC(217.3) SIM JONES 4_BC_SAT10417.D
Counts vs. Acquisition Time (min)

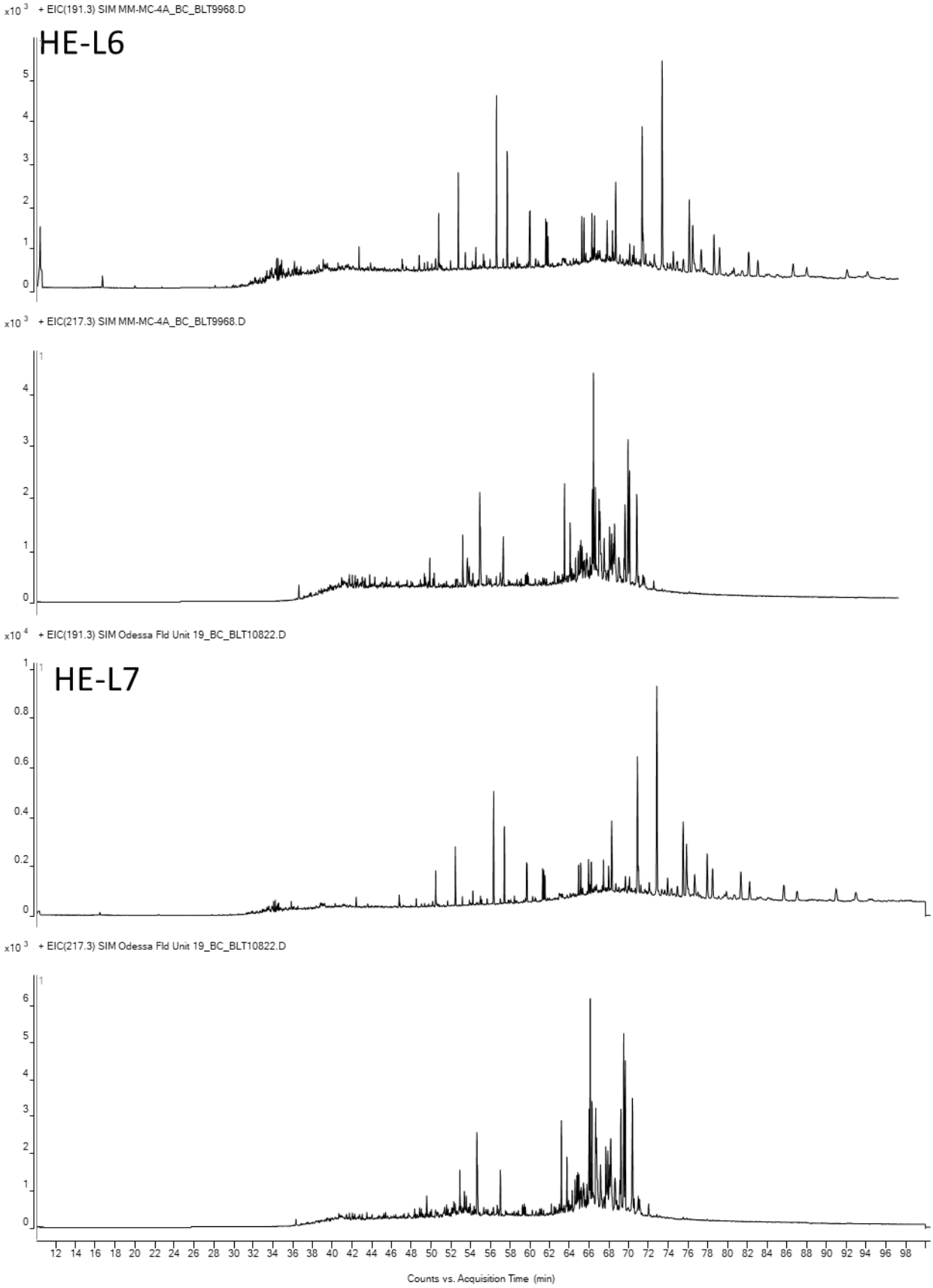
x10 3 + EIC(191.3) SIM MM-MC-4A_BC_BLT9968.D
HE-L6
x10 3 + EIC(217.3) SIM MM-MC-4A_BC_BLT9968.D
x10 4 + EIC(191.3) SIM Odessa Fld Unit 19_BC_BLT10822.D
HE-L7
x10 3 + EIC(217.3) SIM Odessa Fld Unit 19_BC_BLT10822.D
Counts vs. Acquisition Time (min)

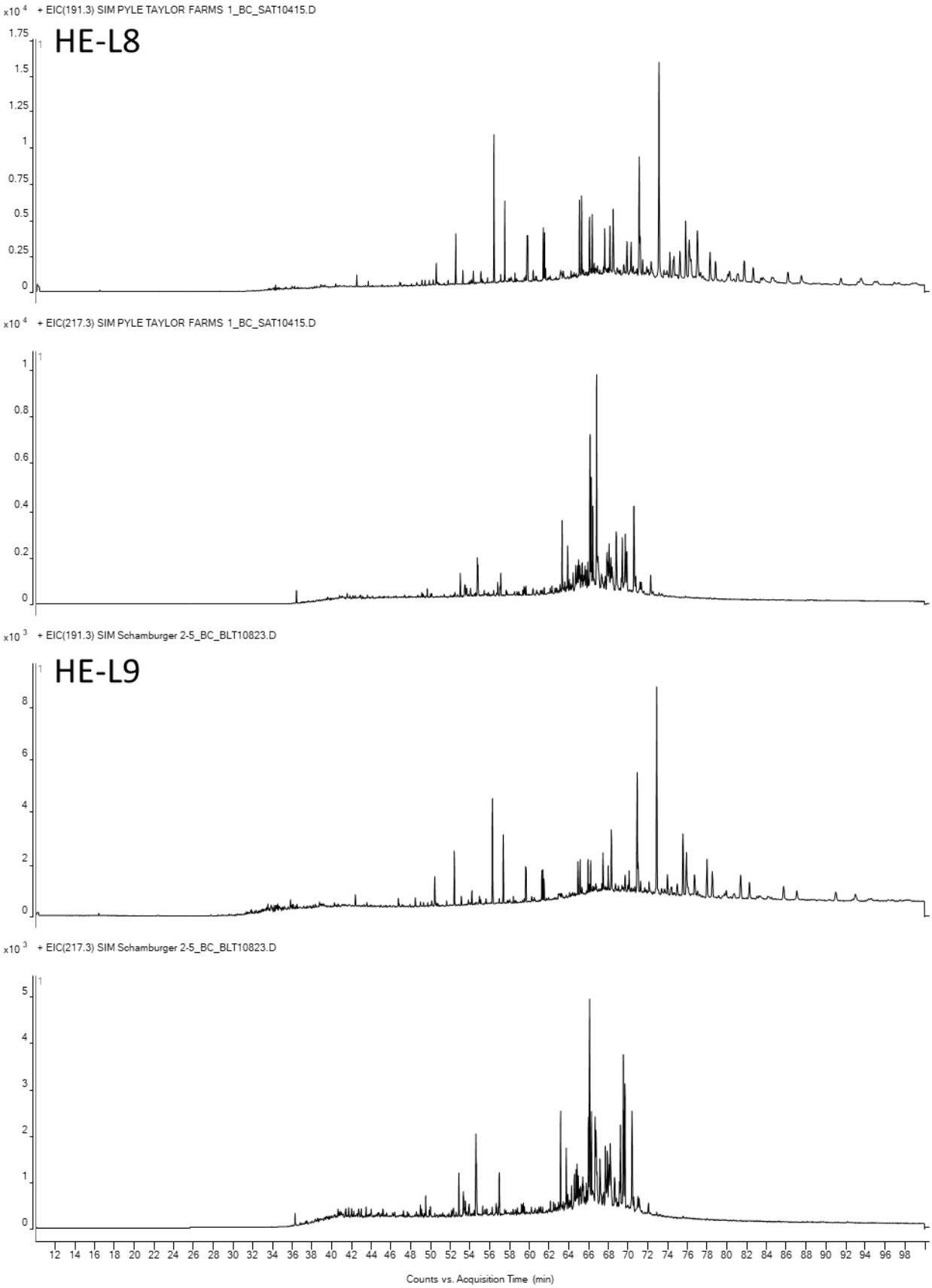
x10 4 + EIC(191.3) SIM PYLE TAYLOR FARMS 1_BC_SAT10415.D
HE-L8
x10 4 + EIC(217.3) SIM PYLE TAYLOR FARMS 1_BC_SAT10415.D
x10 3 + EIC(191.3) SIM Schamburger 2-5_BC_BLT10823.D
HE-L9
x10 3 + EIC(217.3) SIM Schamburger 2-5_BC_BLT10823.D
Counts vs. Acquisition Time (min)

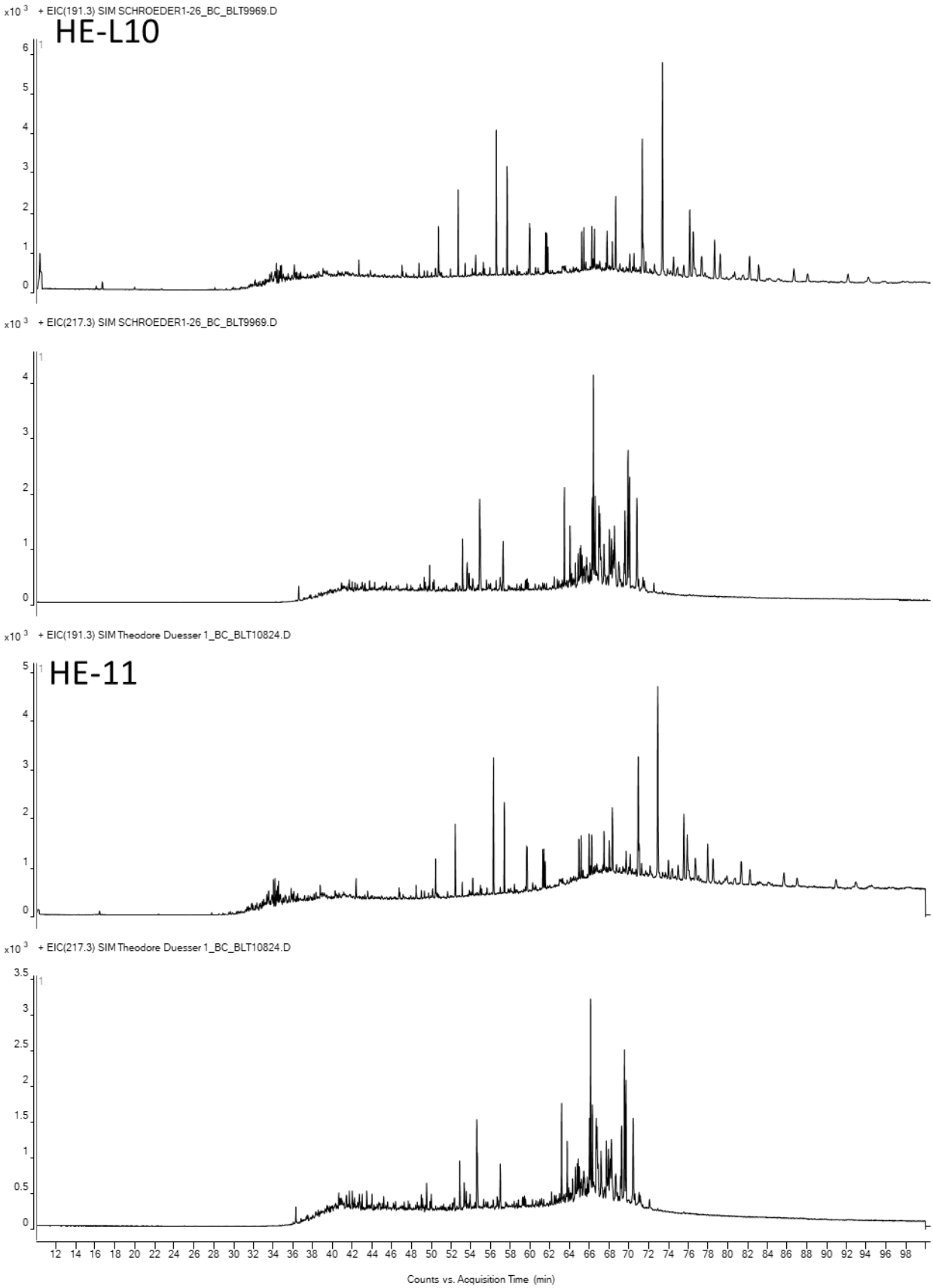
x10 3 + EIC(191.3) SIM SCHROEDER1-26_BC_BLT9969.D
HE-L10
x10 3 + EIC(217.3) SIM SCHROEDER1-26_BC_BLT9969.D
x10 3 + EIC(191.3) SIM Theodore Duesser 1_BC_BLT10824.D
HE-11
x10 3 + EIC(217.3) SIM Theodore Duesser 1_BC_BLT10824.D
Counts vs. Acquisition Time (min)

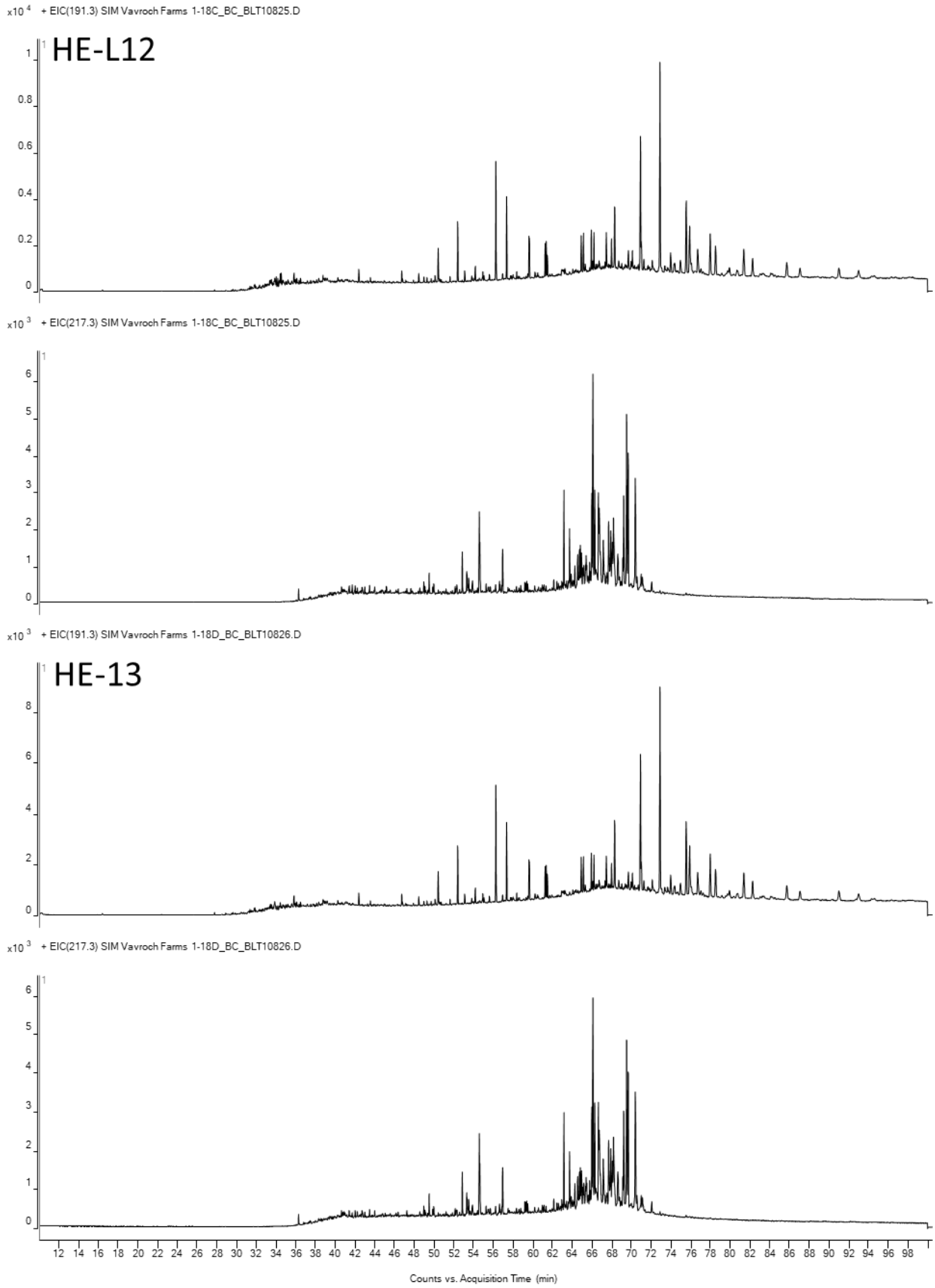
x10 4 + EIC(191.3) SIM Vavroch Farms 1-18C_BC_BLT10825.D
HE-L12
x10 3 + EIC(217.3) SIM Vavroch Farms 1-18C_BC_BLT10825.D
x10 3 + EIC(191.3) SIM Vavroch Farms 1-18D_BC_BLT10826.D
HE-13
x10 3 + EIC(217.3) SIM Vavroch Farms 1-18D_BC_BLT10826.D
Counts vs. Acquisition Time (min)

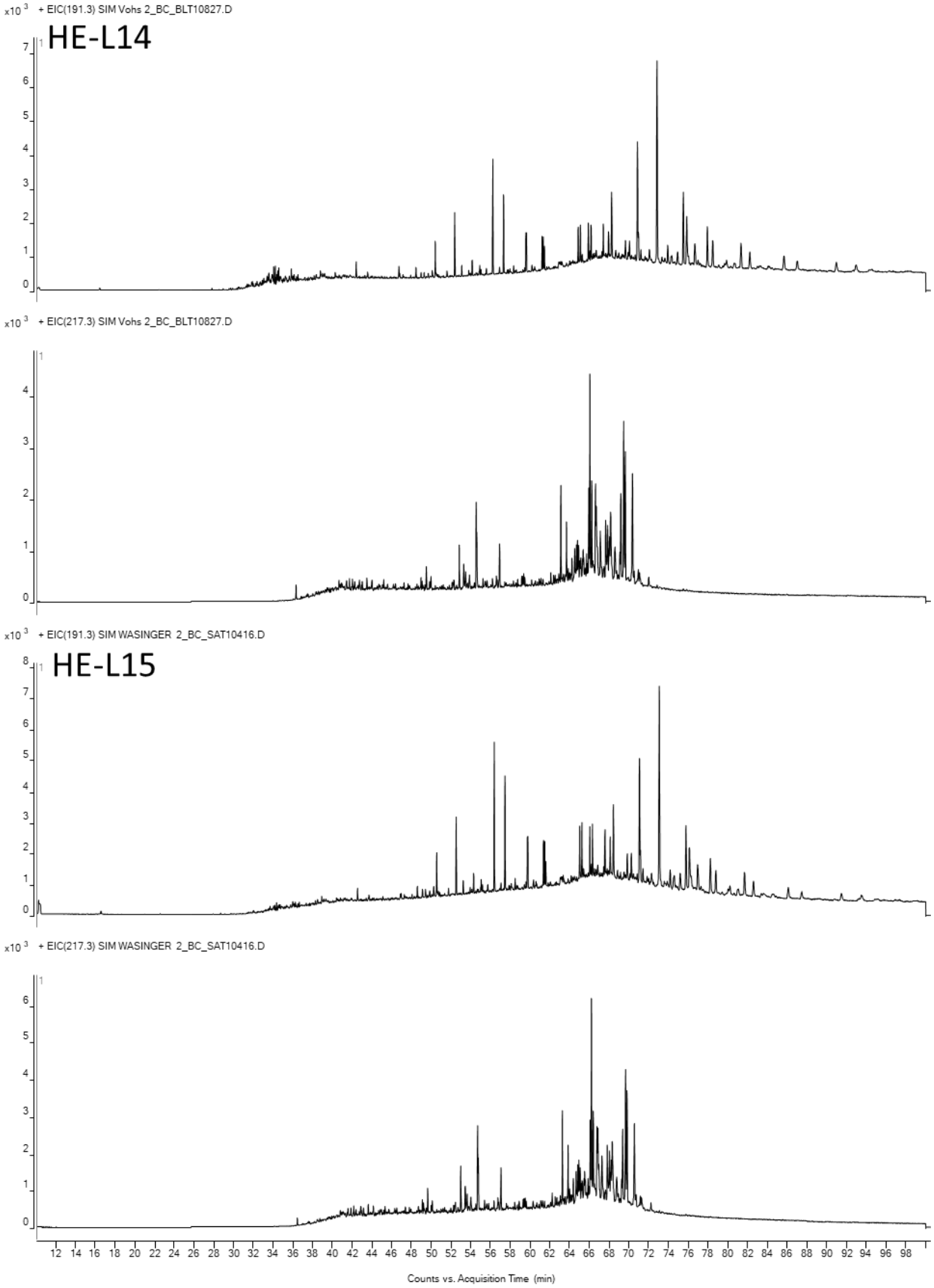
x10 3 + EIC(191.3) SIM Vohs 2_BC_BLT10827.D
HE-L14
x10 3 + EIC(217.3) SIM Vohs 2_BC_BLT10827.D
x10 3 + EIC(191.3) SIM WASINGER 2_BC_SAT10416.D
HE-L15
x10 3 + EIC(217.3) SIM WASINGER 2_BC_SAT10416.D
Counts vs. Acquisition Time (min)

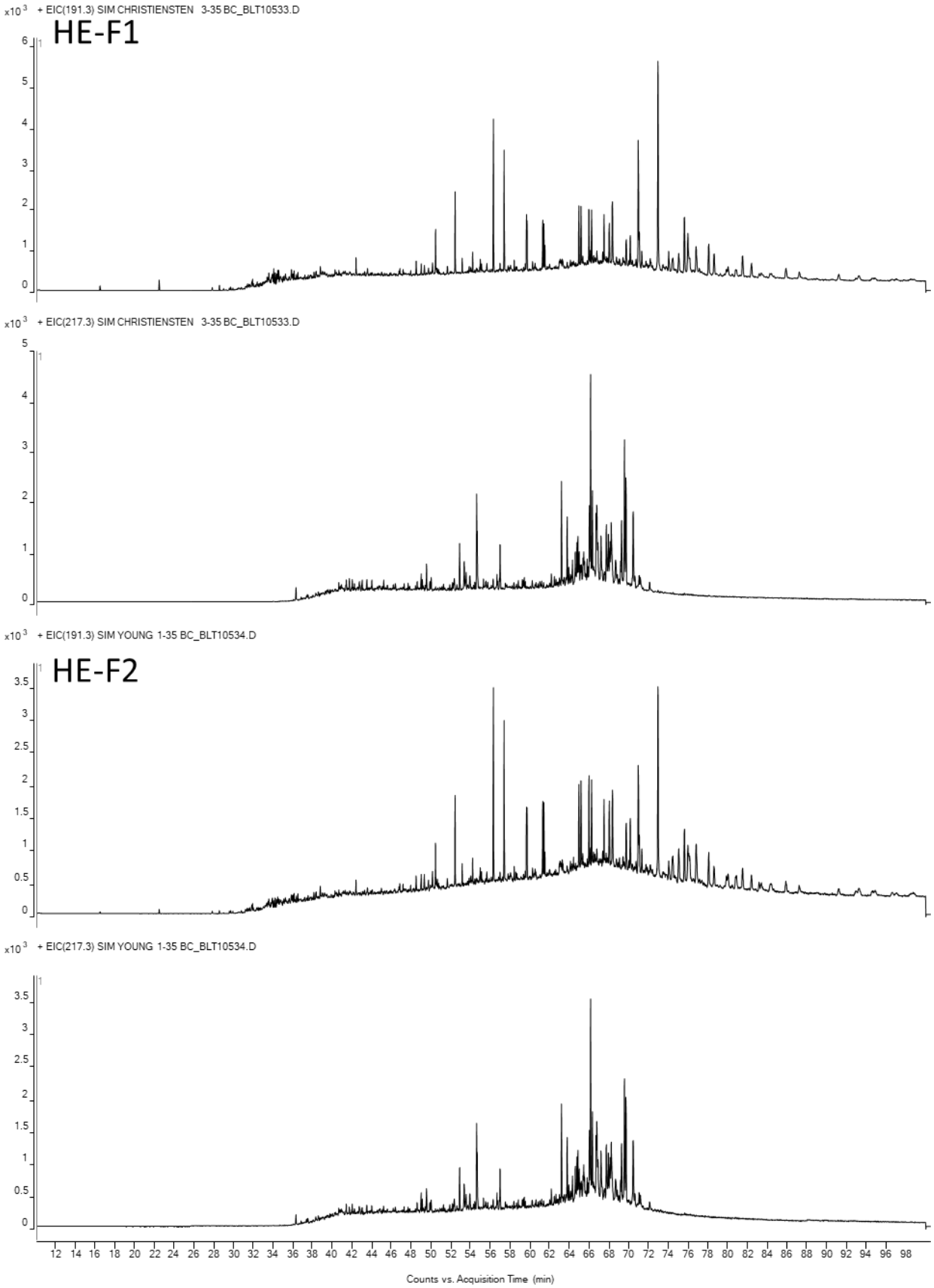
x10^3 + EIC(191.3) SIM CHRISTIENSTEN 3-35 BC_BLT10533.D
HE-F1
x10^3 + EIC(217.3) SIM CHRISTIENSTEN 3-35 BC_BLT10533.D
x10^3 + EIC(191.3) SIM YOUNG 1-35 BC_BLT10534.D
HE-F2
x10^3 + EIC(217.3) SIM YOUNG 1-35 BC_BLT10534.D
Counts vs. Acquisition Time (min)

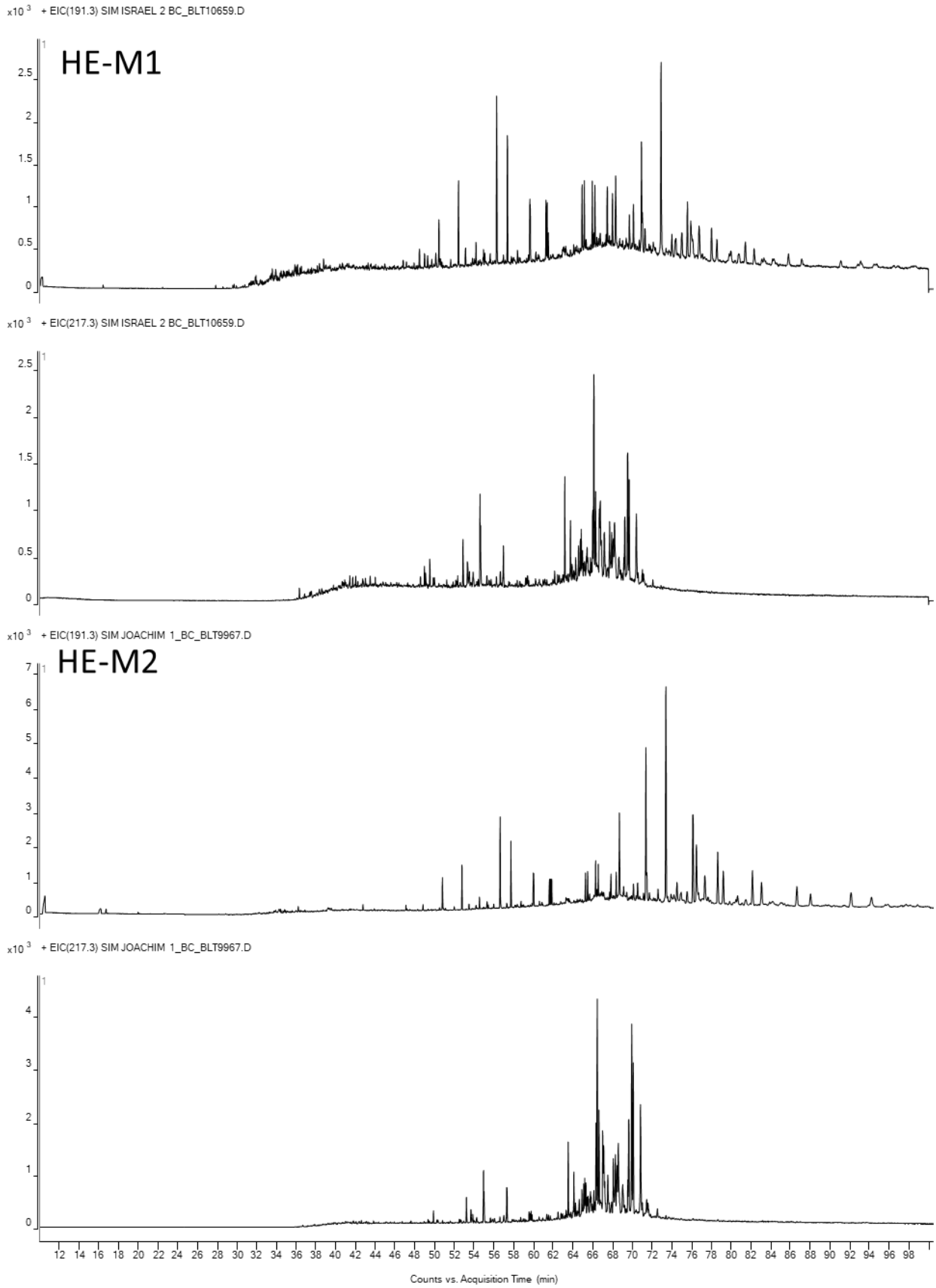
x10 3 + EIC(191.3) SIM ISRAEL 2 BC_BLT10659.D
HE-M1
x10 3 + EIC(217.3) SIM ISRAEL 2 BC_BLT10659.D
x10 3 + EIC(191.3) SIM JOACHIM 1_BC_BLT9967.D
HE-M2
x10 3 + EIC(217.3) SIM JOACHIM 1_BC_BLT9967.D
Counts vs. Acquisition Time (min)

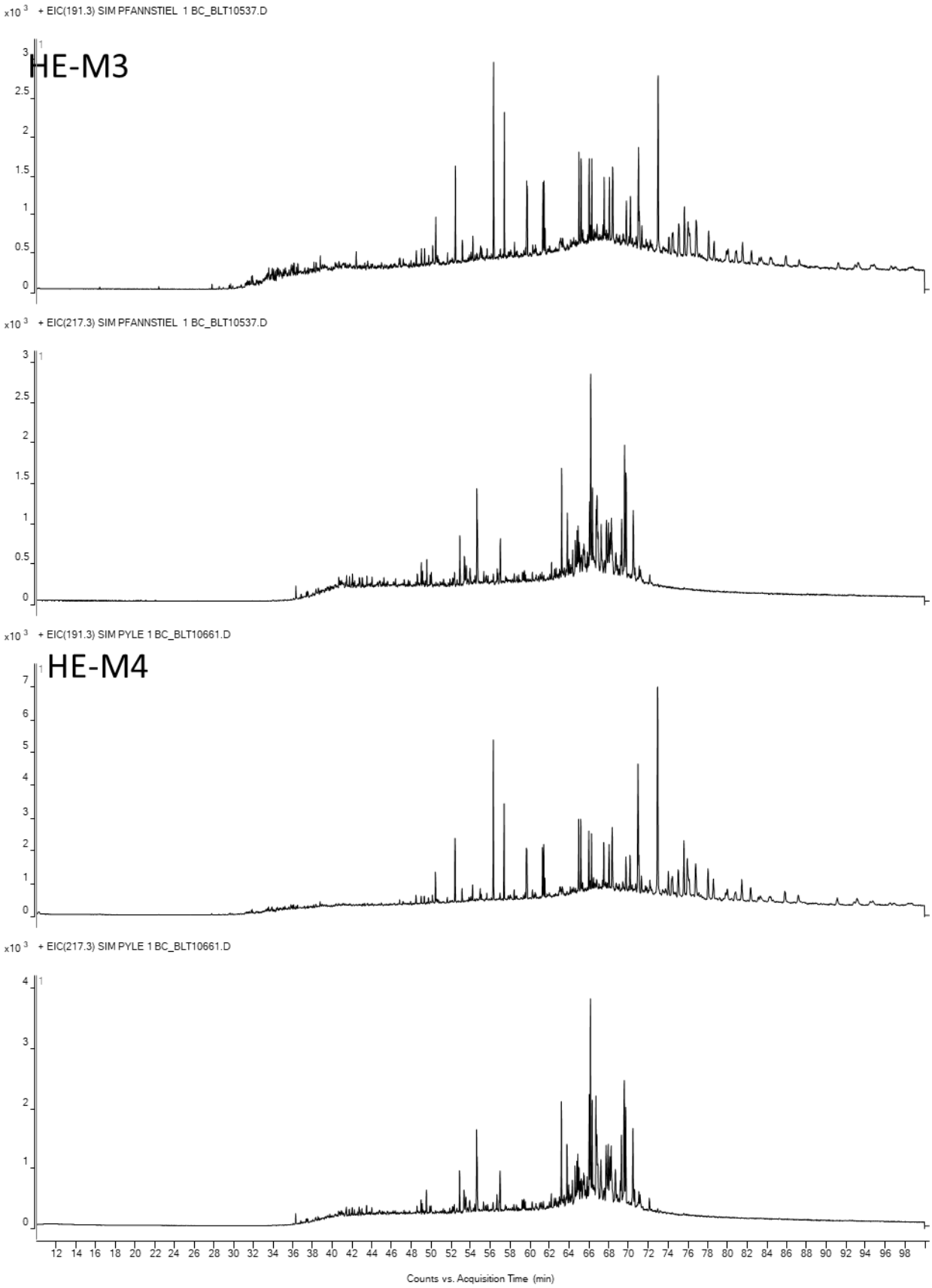
x10 3 + EIC(191.3) SIM PFANNSTIEL 1 BC_BLT10537.D
HE-M3
x10 3 + EIC(217.3) SIM PFANNSTIEL 1 BC_BLT10537.D
x10 3 + EIC(191.3) SIM PYLE 1 BC_BLT10661.D
HE-M4
x10 3 + EIC(217.3) SIM PYLE 1 BC_BLT10661.D
Counts vs. Acquisition Time (min)

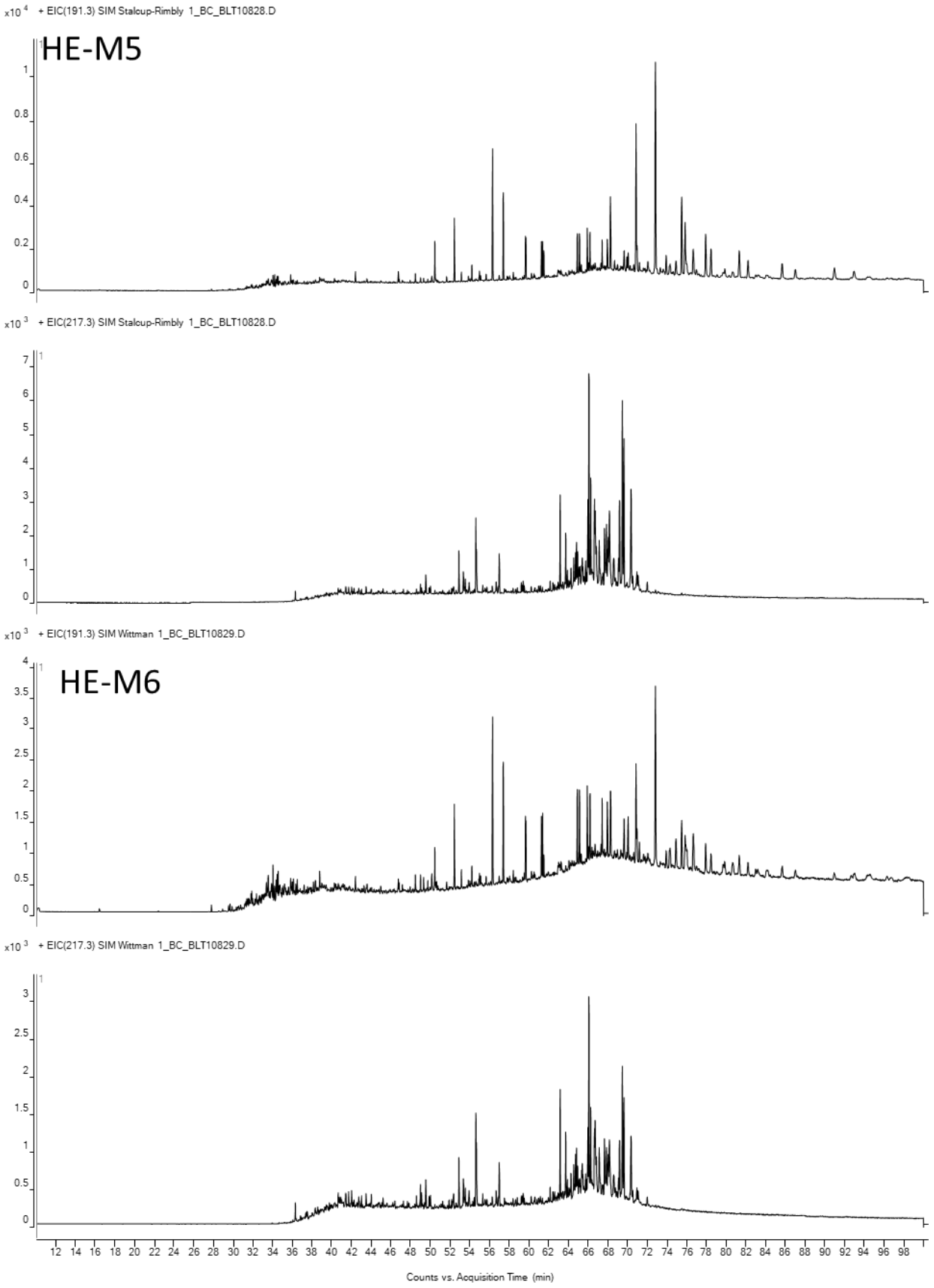
x10 4 + EIC(191.3) SIM Stalcup-Rimbly 1_BC_BLT10828.D
HE-M5
x10 3 + EIC(217.3) SIM Stalcup-Rimbly 1_BC_BLT10828.D
x10 3 + EIC(191.3) SIM Wittman 1_BC_BLT10829.D
HE-M6
x10 3 + EIC(217.3) SIM Wittman 1_BC_BLT10829.D
Counts vs. Acquisition Time (min)

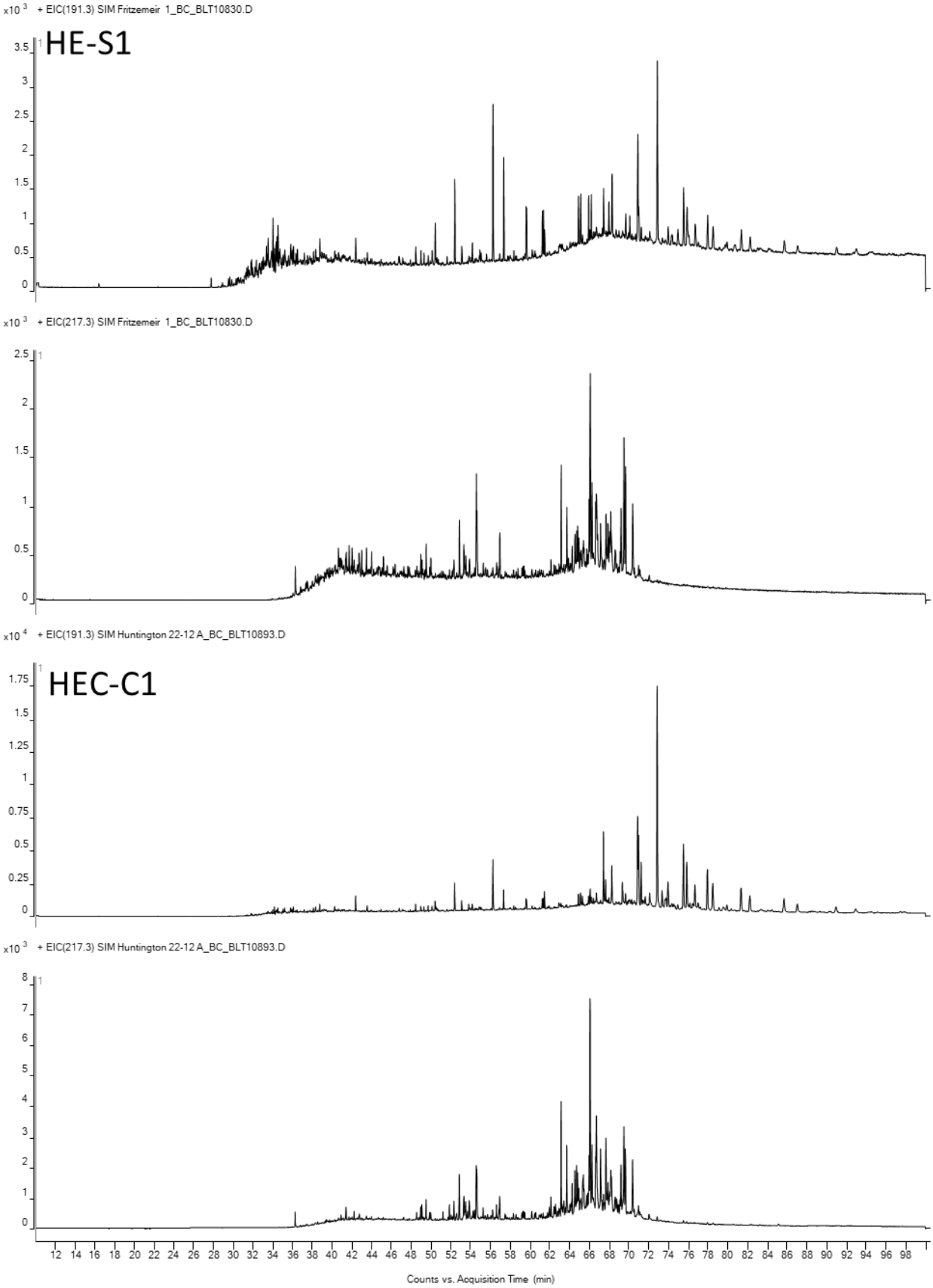
x10 3 + EIC(191.3) SIM Fritzemeir 1_BC_BLT10830.D
HE-S1
x10 3 + EIC(217.3) SIM Fritzemeir 1_BC_BLT10830.D
x10 4 + EIC(191.3) SIM Huntington 22-12 A_BC_BLT10893.D
HEC-C1
x10 3 + EIC(217.3) SIM Huntington 22-12 A_BC_BLT10893.D
Counts vs. Acquisition Time (min)

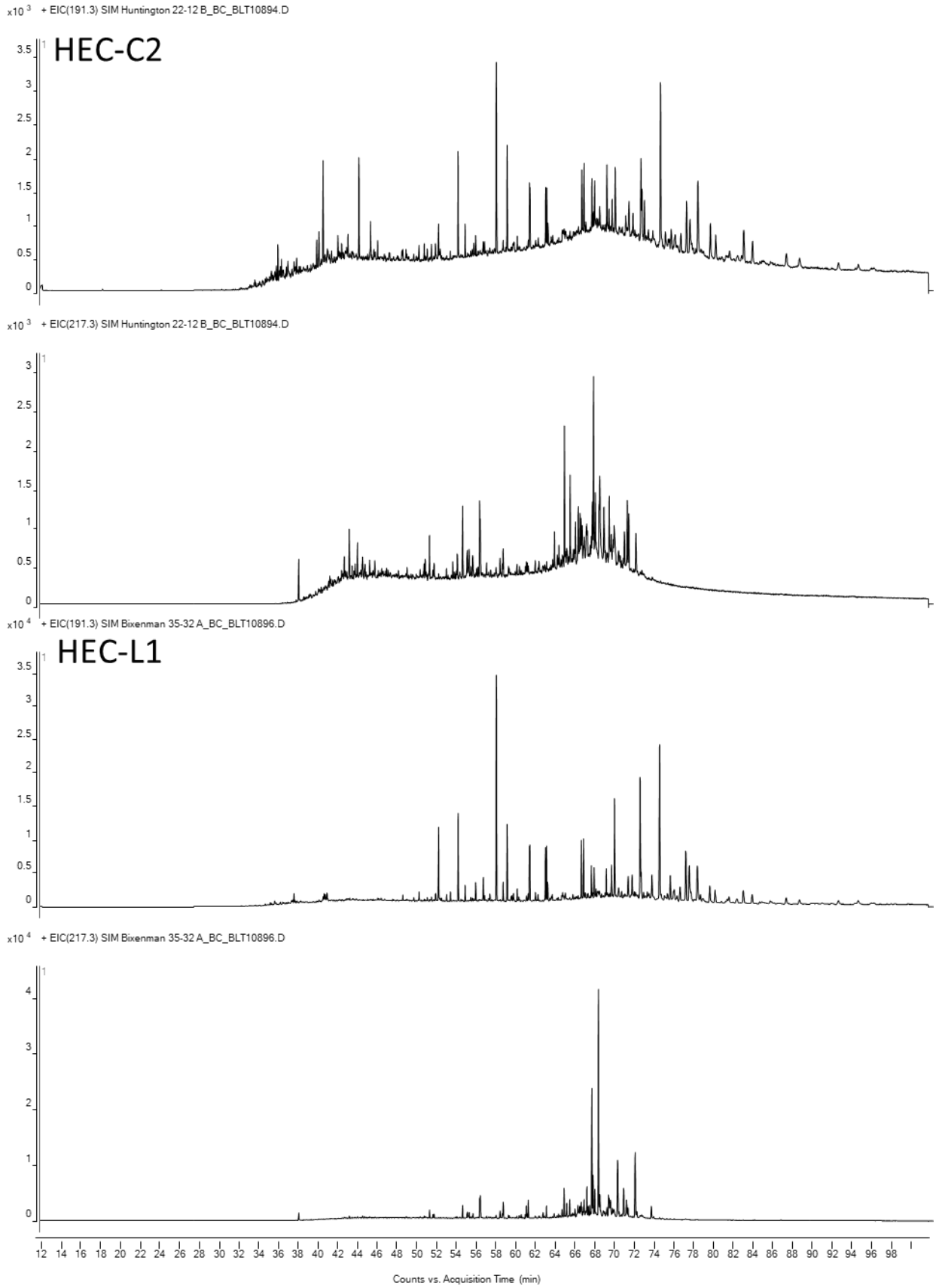
x10 3 + EIC(191.3) SIM Huntington 22-12 B_BC_BLT10894.D
HEC-C2
x10 3 + EIC(217.3) SIM Huntington 22-12 B_BC_BLT10894.D
x10 4 + EIC(191.3) SIM Bixenman 35-32 A_BC_BLT10896.D
HEC-L1
x10 4 + EIC(217.3) SIM Bixenman 35-32 A_BC_BLT10896.D
Counts vs. Acquisition Time (min)

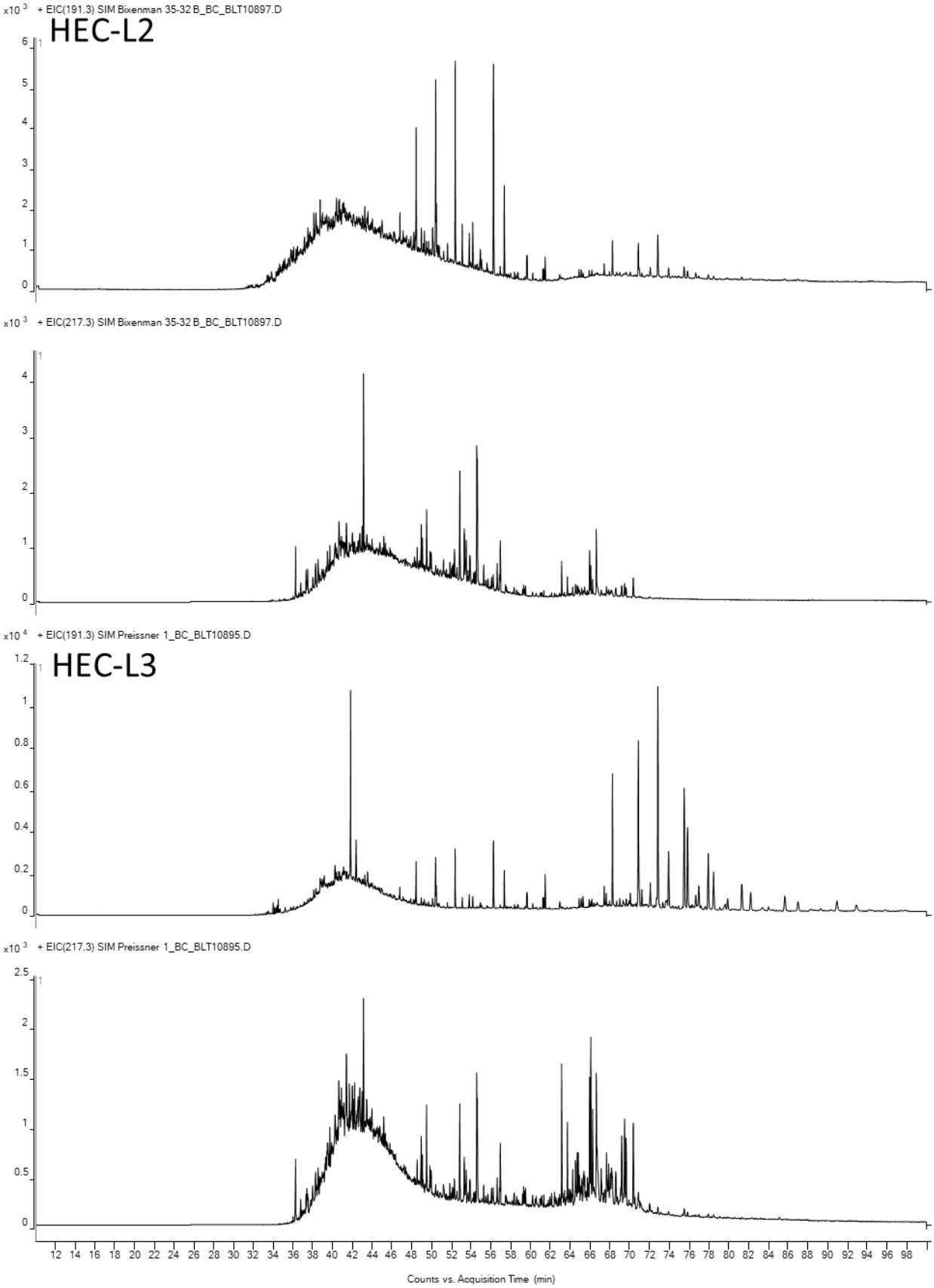
x10 3 + EIC(191.3) SIM Bixenman 35-32 B_BC_BLT10897.D
HEC-L2
x10 3 + EIC(217.3) SIM Bixenman 35-32 B_BC_BLT10897.D
x10 4 + EIC(191.3) SIM Preissner 1_BC_BLT10895.D
HEC-L3
x10 3 + EIC(217.3) SIM Preissner 1_BC_BLT10895.D
Counts vs. Acquisition Time (min)

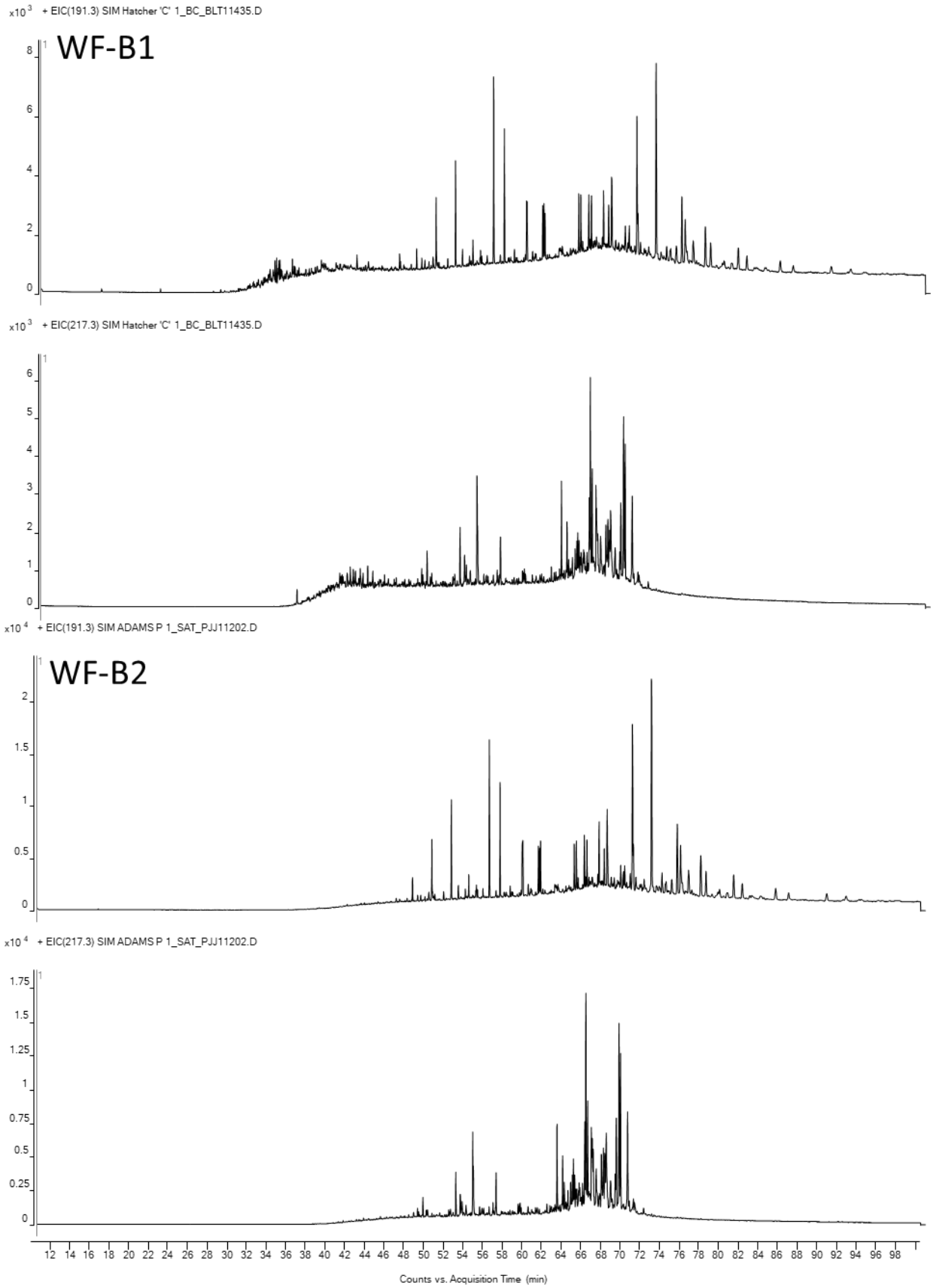
x10 3 + EIC(191.3) SIM Hatcher 'C' 1_BC_BLT11435.D
WF-B1
x10 3 + EIC(217.3) SIM Hatcher 'C' 1_BC_BLT11435.D
x10 4 + EIC(191.3) SIM ADAMS P 1_SAT_PJJ11202.D
WF-B2
x10 4 + EIC(217.3) SIM ADAMS P 1_SAT_PJJ11202.D
Counts vs. Acquisition Time (min)

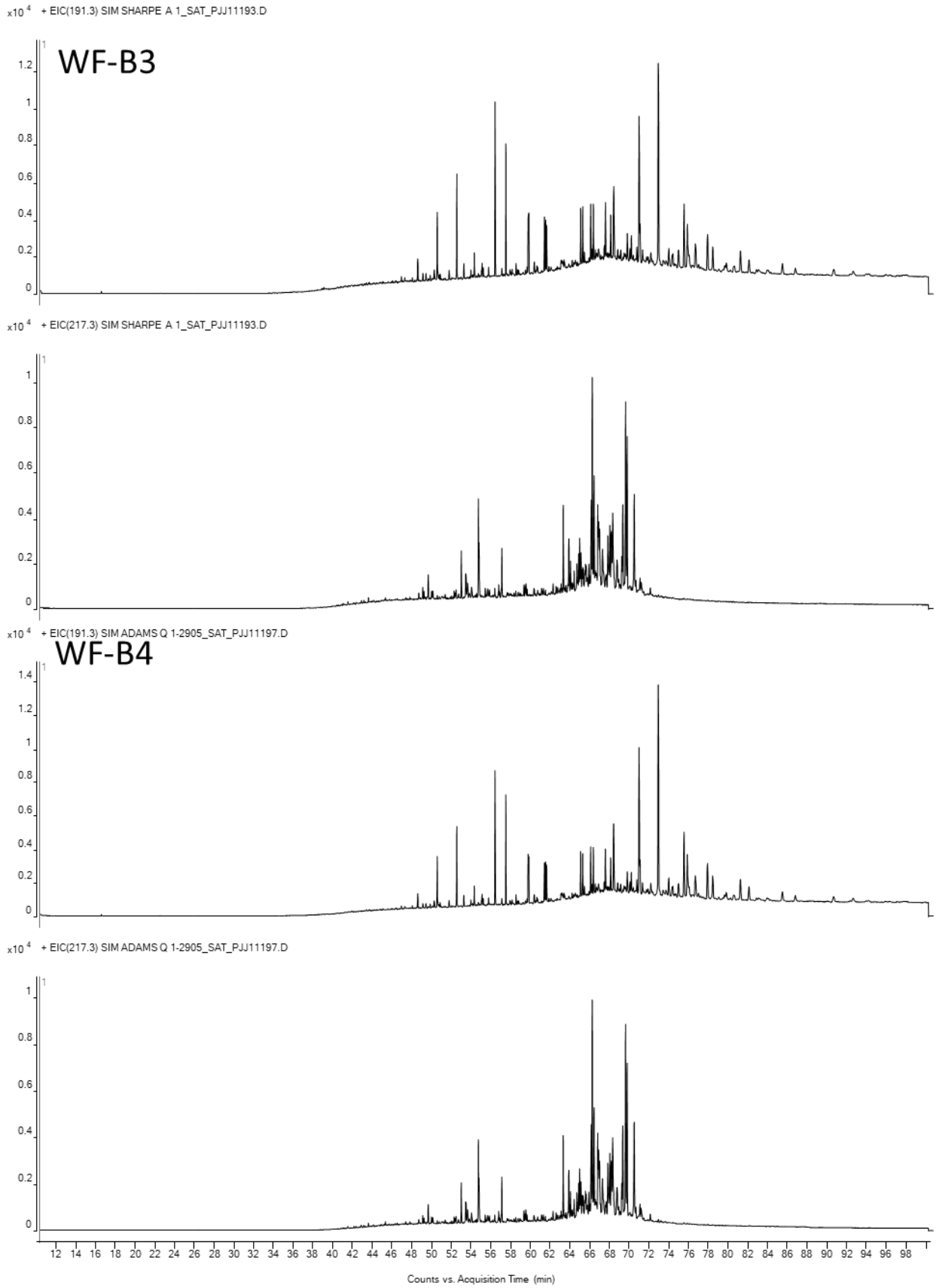
x10 4 + EIC(191.3) SIM SHARPE A 1_SAT_PJJ11193.D
WF-B3
x10 4 + EIC(217.3) SIM SHARPE A 1_SAT_PJJ11193.D
x10 4 + EIC(191.3) SIM ADAMS Q 1-2905_SAT_PJJ11197.D
WF-B4
x10 4 + EIC(217.3) SIM ADAMS Q 1-2905_SAT_PJJ11197.D
Counts vs. Acquisition Time (min)

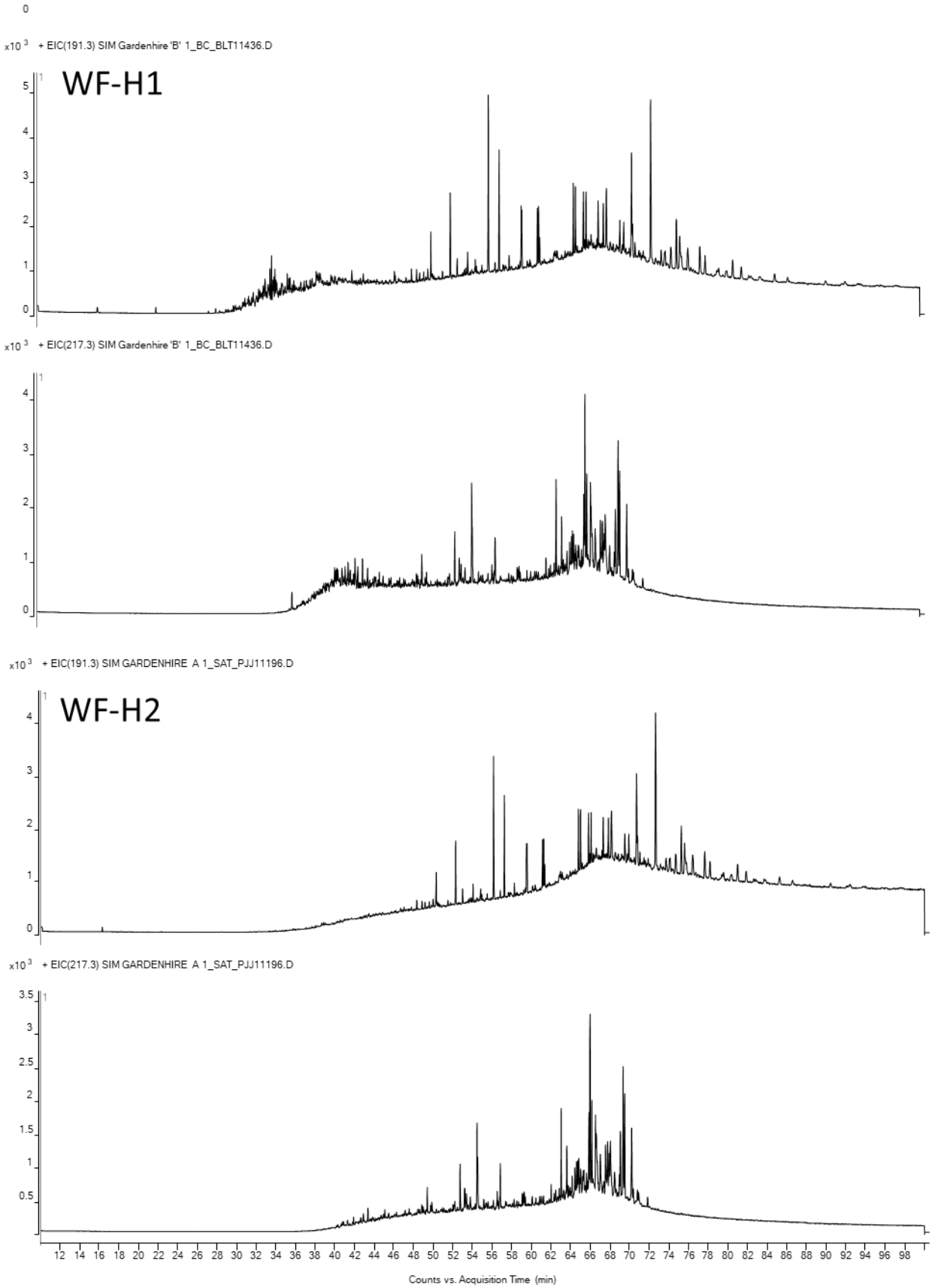
0
x10 3 + EIC(191.3) SIM Gardenhire 'B' 1_BC_BLT11436.D
WF-H1
x10 3 + EIC(217.3) SIM Gardenhire 'B' 1_BC_BLT11436.D
x10 3 + EIC(191.3) SIM GARDENHIRE A 1_SAT_PJJ11196.D
WF-H2
x10 3 + EIC(217.3) SIM GARDENHIRE A 1_SAT_PJJ11196.D
Counts vs. Acquisition Time (min)

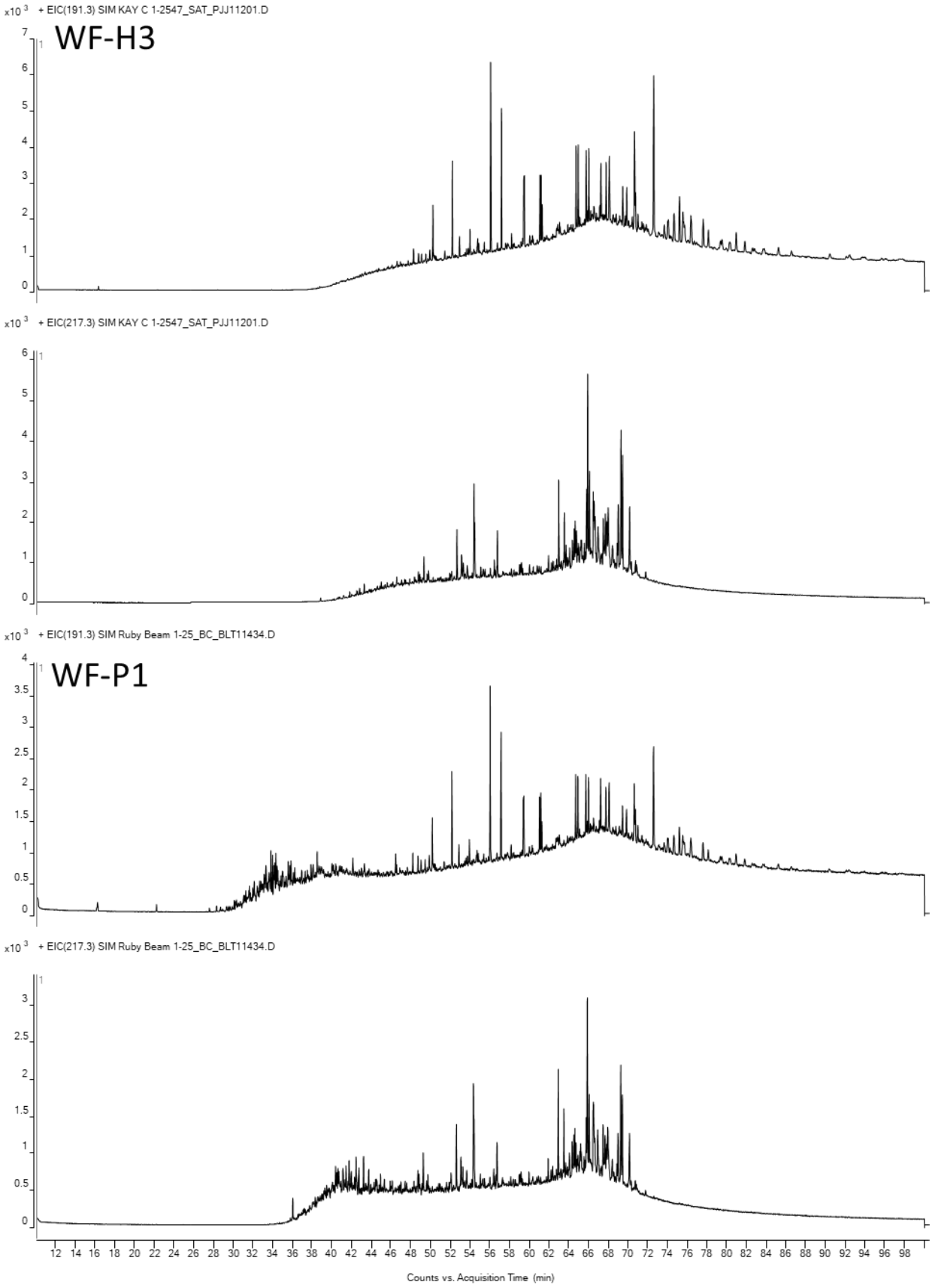
x10 3 + EIC(191.3) SIM KAY C 1-2547_SAT_PJJ11201.D
WF-H3
x10 3 + EIC(217.3) SIM KAY C 1-2547_SAT_PJJ11201.D
x10 3 + EIC(191.3) SIM Ruby Beam 1-25_BC_BLT11434.D
WF-P1
x10 3 + EIC(217.3) SIM Ruby Beam 1-25_BC_BLT11434.D
Counts vs. Acquisition Time (min)

E. Aromatic GCMS Chromatograms

Chromatograms of phenanthrenes (m/z 178+192+206) and dibenzothiophenes (m/z 184+198+212)

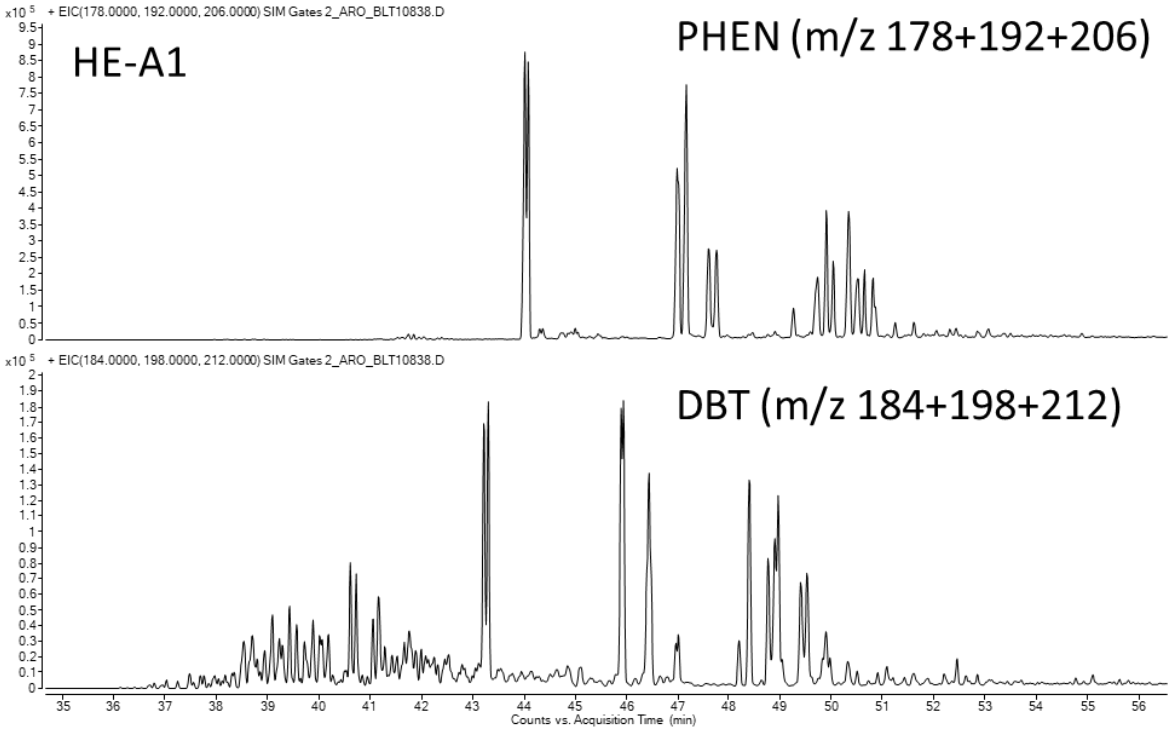

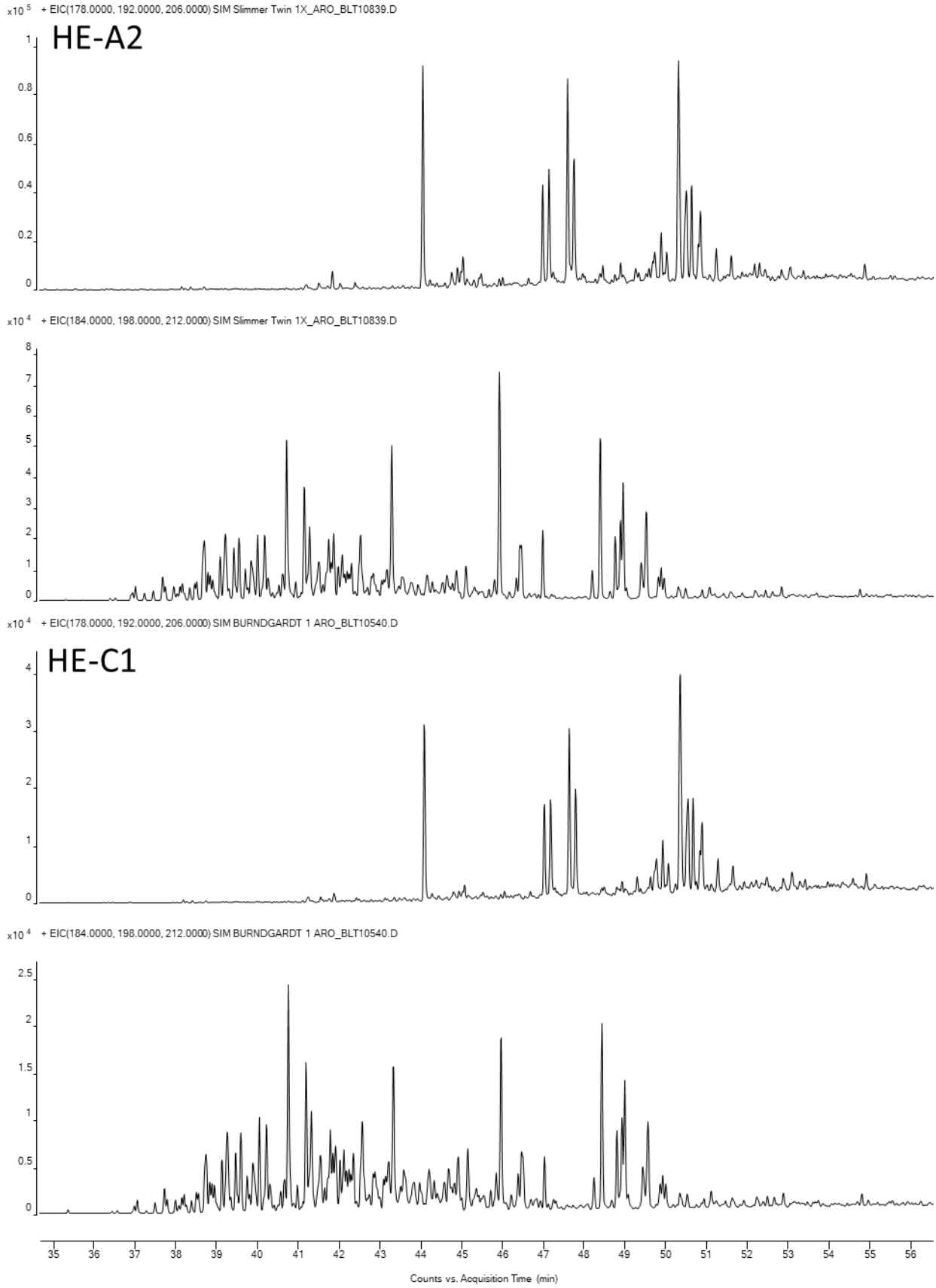
x10 5 + EIC(178.0000, 192.0000, 206.0000) SIM Slimmer Twin 1X_ARO_BLT10839.D
HE-A2
x10 4 + EIC(184.0000, 198.0000, 212.0000) SIM Slimmer Twin 1X_ARO_BLT10839.D
x10 4 + EIC(178.0000, 192.0000, 206.0000) SIM BURNDGARDT 1 ARO_BLT10540.D
HE-C1
x10 4 + EIC(184.0000, 198.0000, 212.0000) SIM BURNDGARDT 1 ARO_BLT10540.D
Counts vs. Acquisition Time (min)

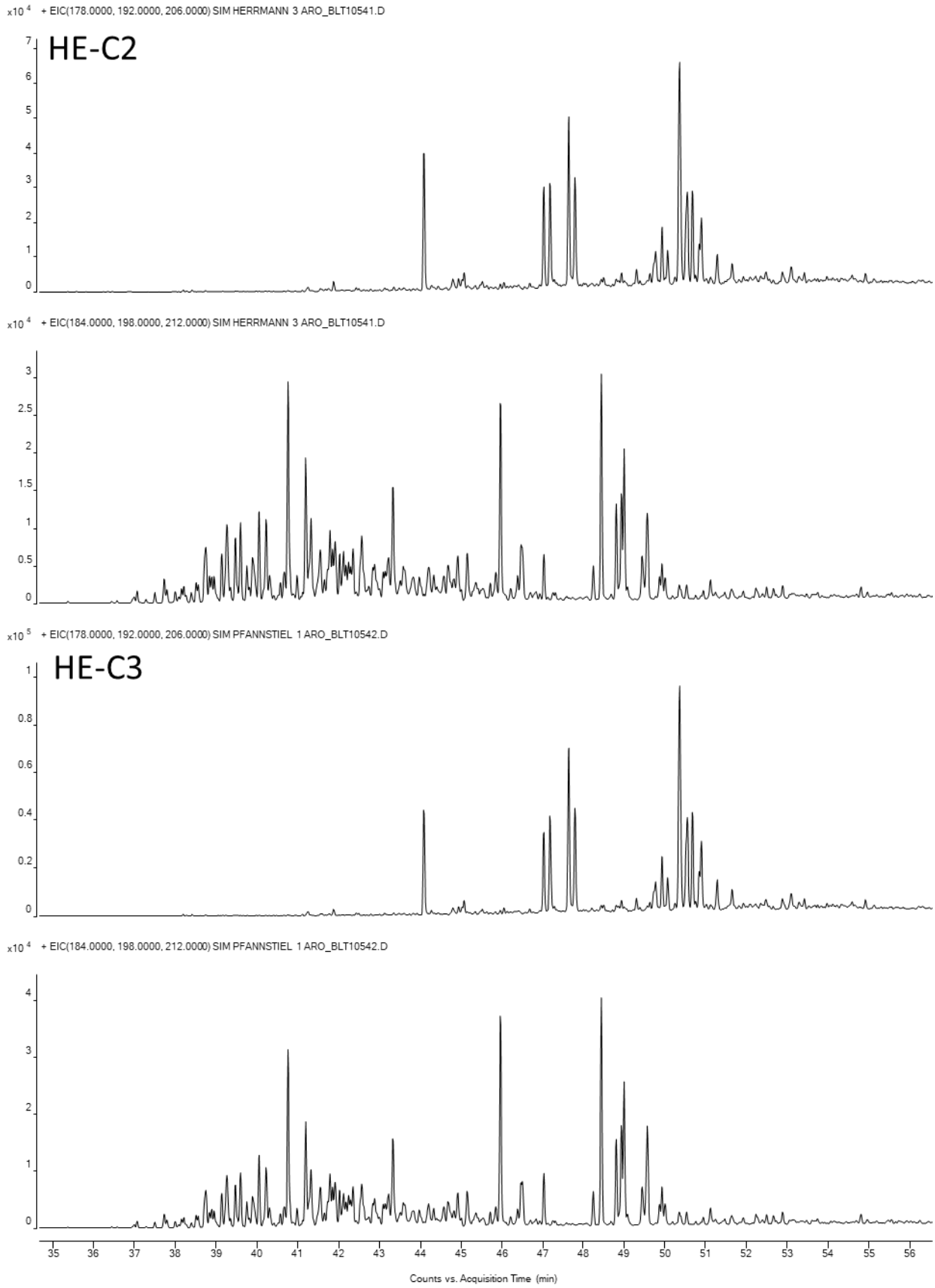
x10 4 + EIC(178.0000, 192.0000, 206.0000) SIM HERRMANN 3 ARO_BLT10541.D
HE-C2
x10 4 + EIC(184.0000, 198.0000, 212.0000) SIM HERRMANN 3 ARO_BLT10541.D
x10 5 + EIC(178.0000, 192.0000, 206.0000) SIM PFANNSTIEL 1 ARO_BLT10542.D
HE-C3
x10 4 + EIC(184.0000, 198.0000, 212.0000) SIM PFANNSTIEL 1 ARO_BLT10542.D
Counts vs. Acquisition Time (min)

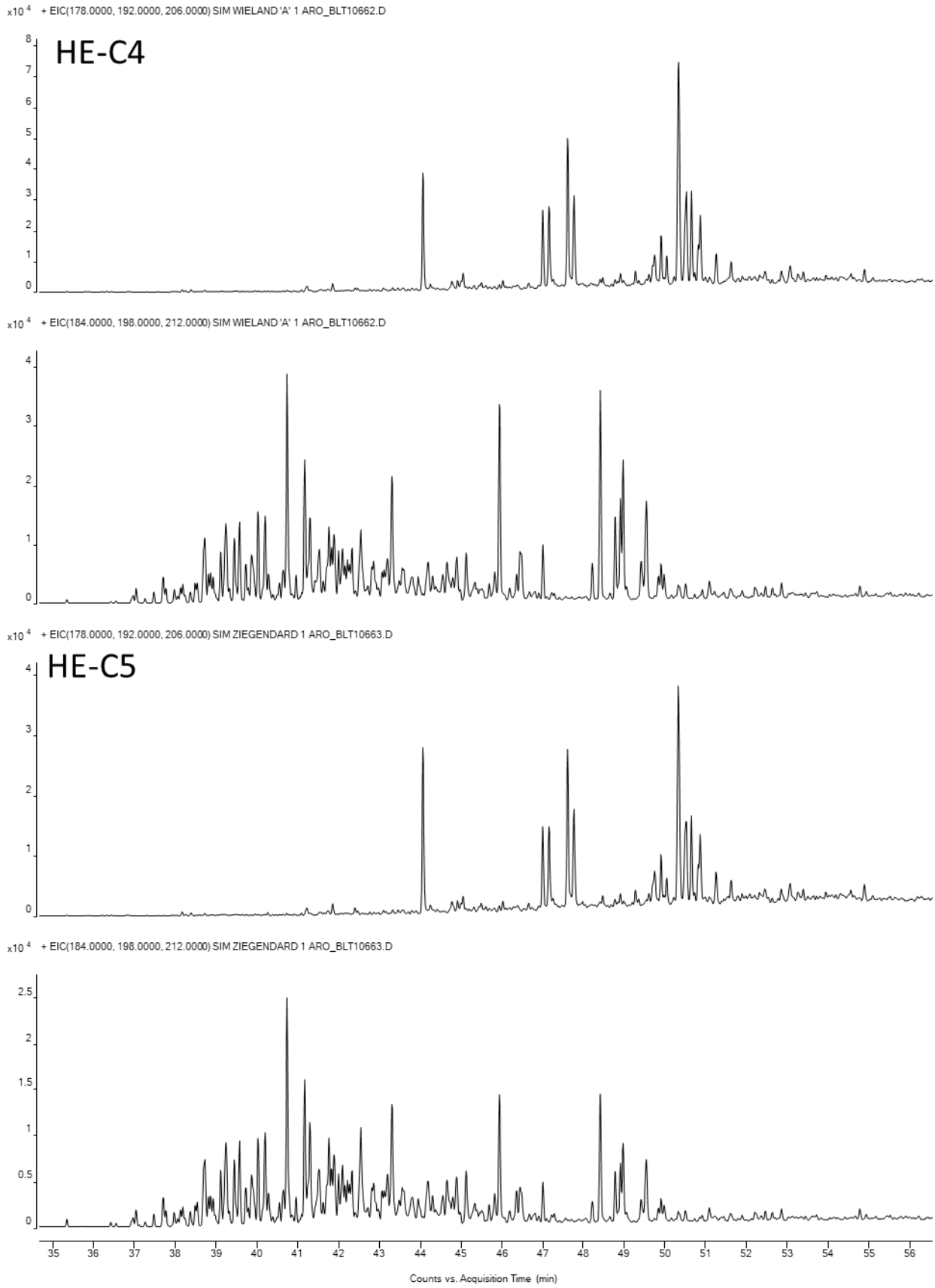
x10 4 + EIC(178.0000, 192.0000, 206.0000) SIM WIELAND 'A' 1 ARO_BLT10662.D
HE-C4
x10 4 + EIC(184.0000, 198.0000, 212.0000) SIM WIELAND 'A' 1 ARO_BLT10662.D
x10 4 + EIC(178.0000, 192.0000, 206.0000) SIM ZIEGENDARD 1 ARO_BLT10663.D
HE-C5
x10 4 + EIC(184.0000, 198.0000, 212.0000) SIM ZIEGENDARD 1 ARO_BLT10663.D
Counts vs. Acquisition Time (min)

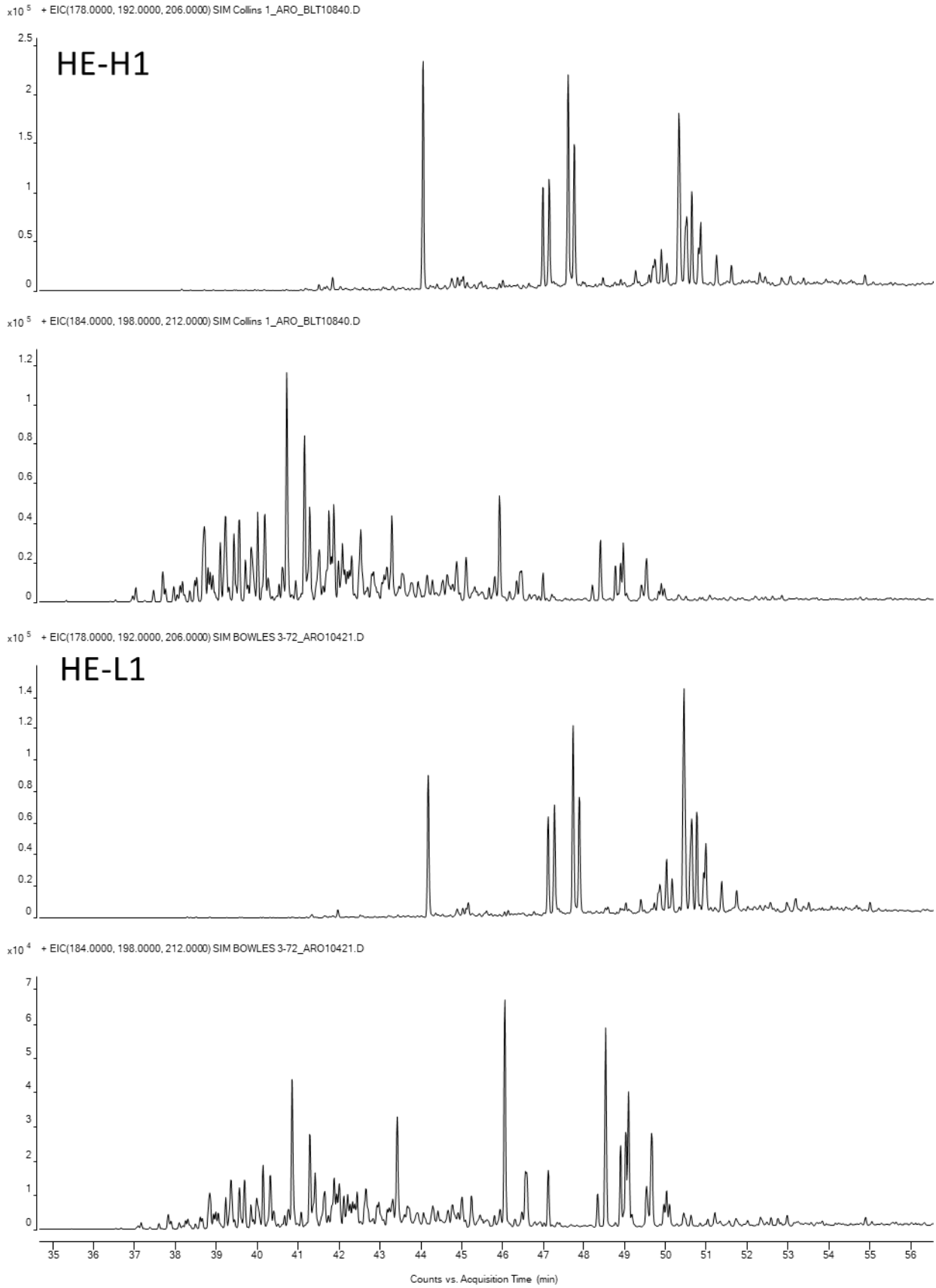
x10 5 + EIC(178.0000, 192.0000, 206.0000) SIM Collins 1_ARO_BLT10840.D
HE-H1
x10 5 + EIC(184.0000, 198.0000, 212.0000) SIM Collins 1_ARO_BLT10840.D
x10 5 + EIC(178.0000, 192.0000, 206.0000) SIM BOWLES 3-72_ARO10421.D
HE-L1
x10 4 + EIC(184.0000, 198.0000, 212.0000) SIM BOWLES 3-72_ARO10421.D
Counts vs. Acquisition Time (min)

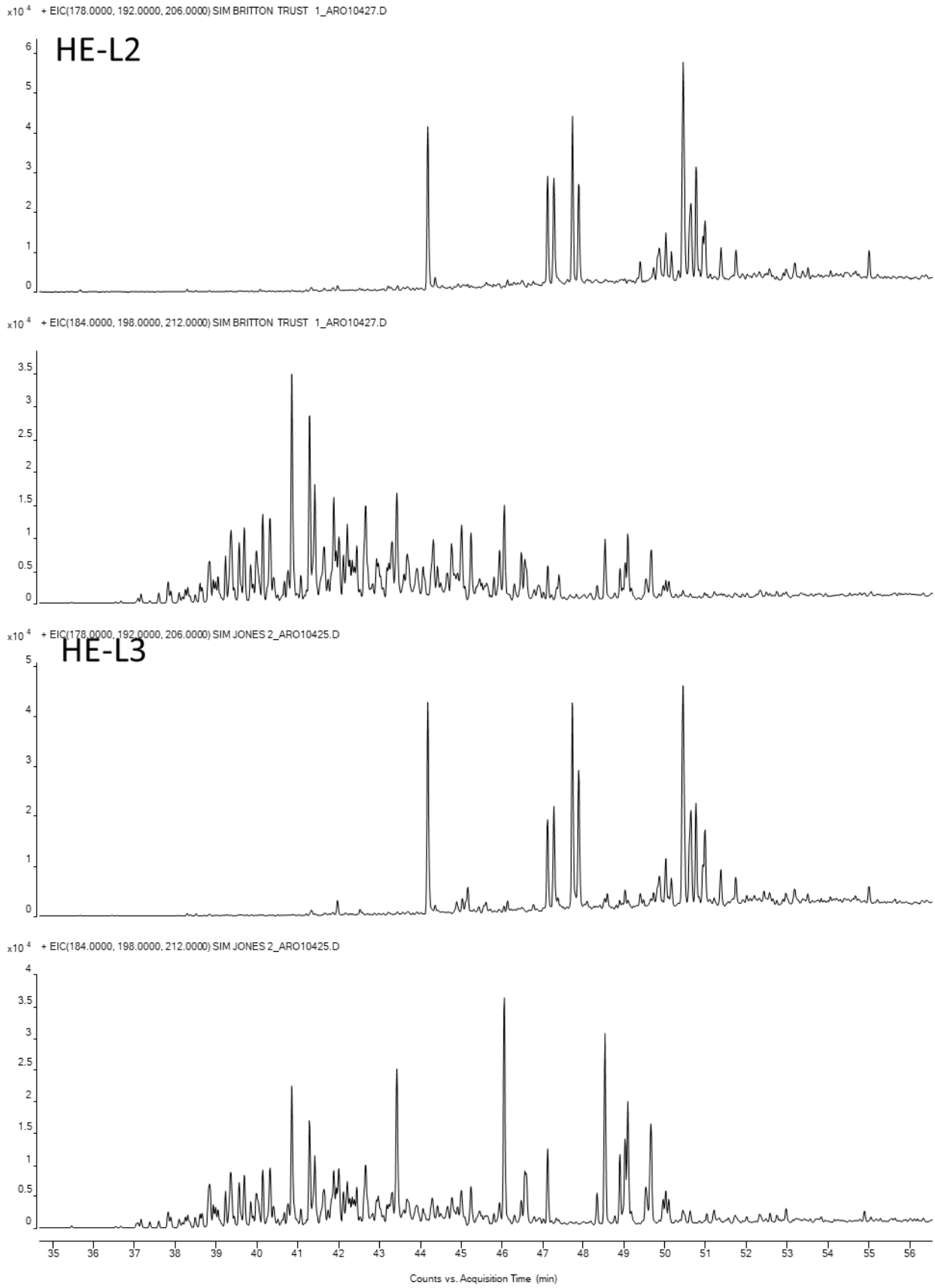
x10 4 + EIC(178.0000, 192.0000, 206.0000) SIM BRITTON TRUST 1_ARO10427.D
HE-L2
x10 4 + EIC(184.0000, 198.0000, 212.0000) SIM BRITTON TRUST 1_ARO10427.D
x10 4 + EIC(178.0000, 192.0000, 206.0000) SIM JONES 2_ARO10425.D
HE-L3
x10 4 + EIC(184.0000, 198.0000, 212.0000) SIM JONES 2_ARO10425.D
Counts vs. Acquisition Time (min)

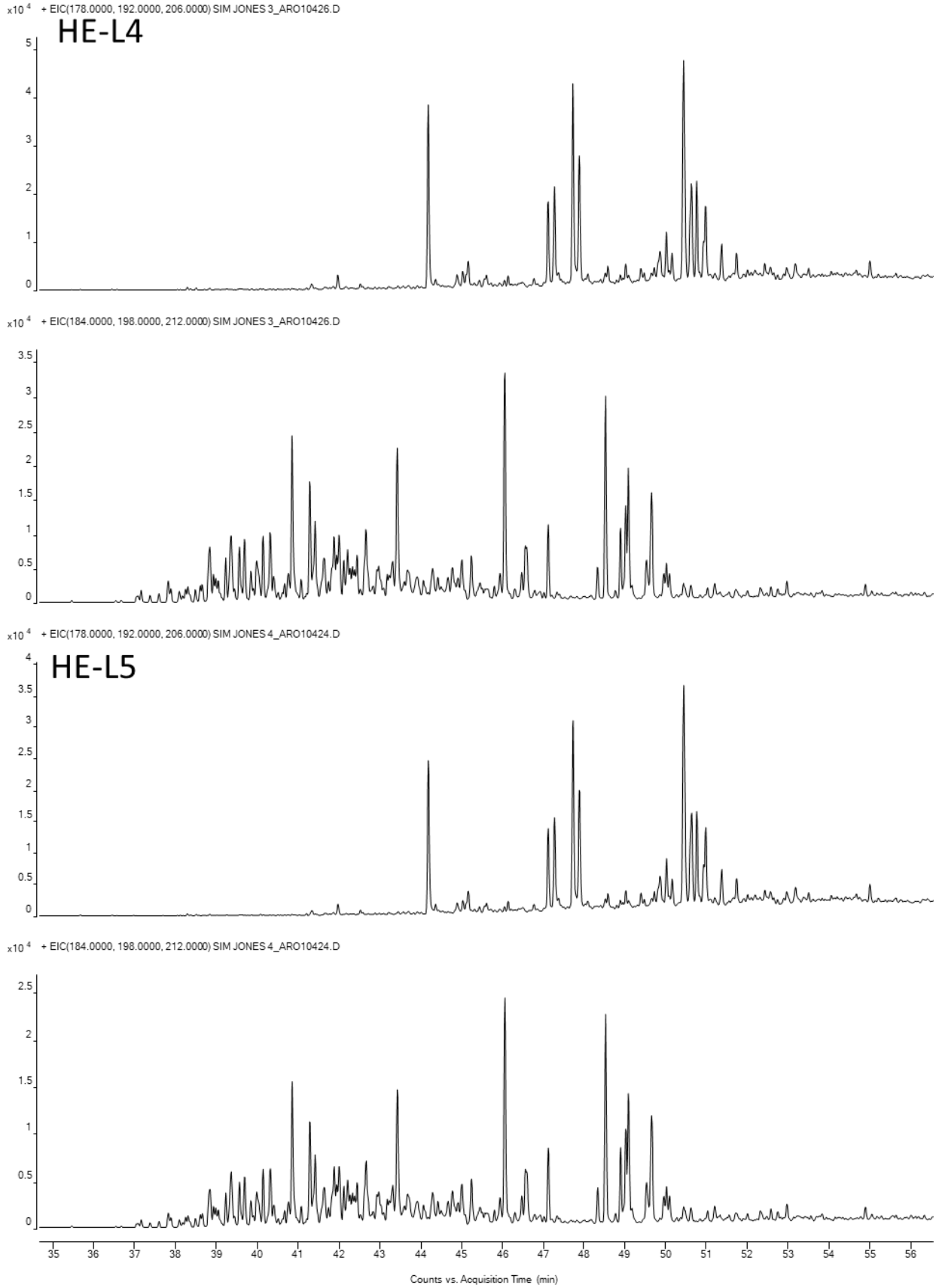
x10 4 + EIC(178.0000, 192.0000, 206.0000) SIM JONES 3_ARO10426.D
HE-L4
x10 4 + EIC(184.0000, 198.0000, 212.0000) SIM JONES 3_ARO10426.D
x10 4 + EIC(178.0000, 192.0000, 206.0000) SIM JONES 4_ARO10424.D
HE-L5
x10 4 + EIC(184.0000, 198.0000, 212.0000) SIM JONES 4_ARO10424.D
Counts vs. Acquisition Time (min)

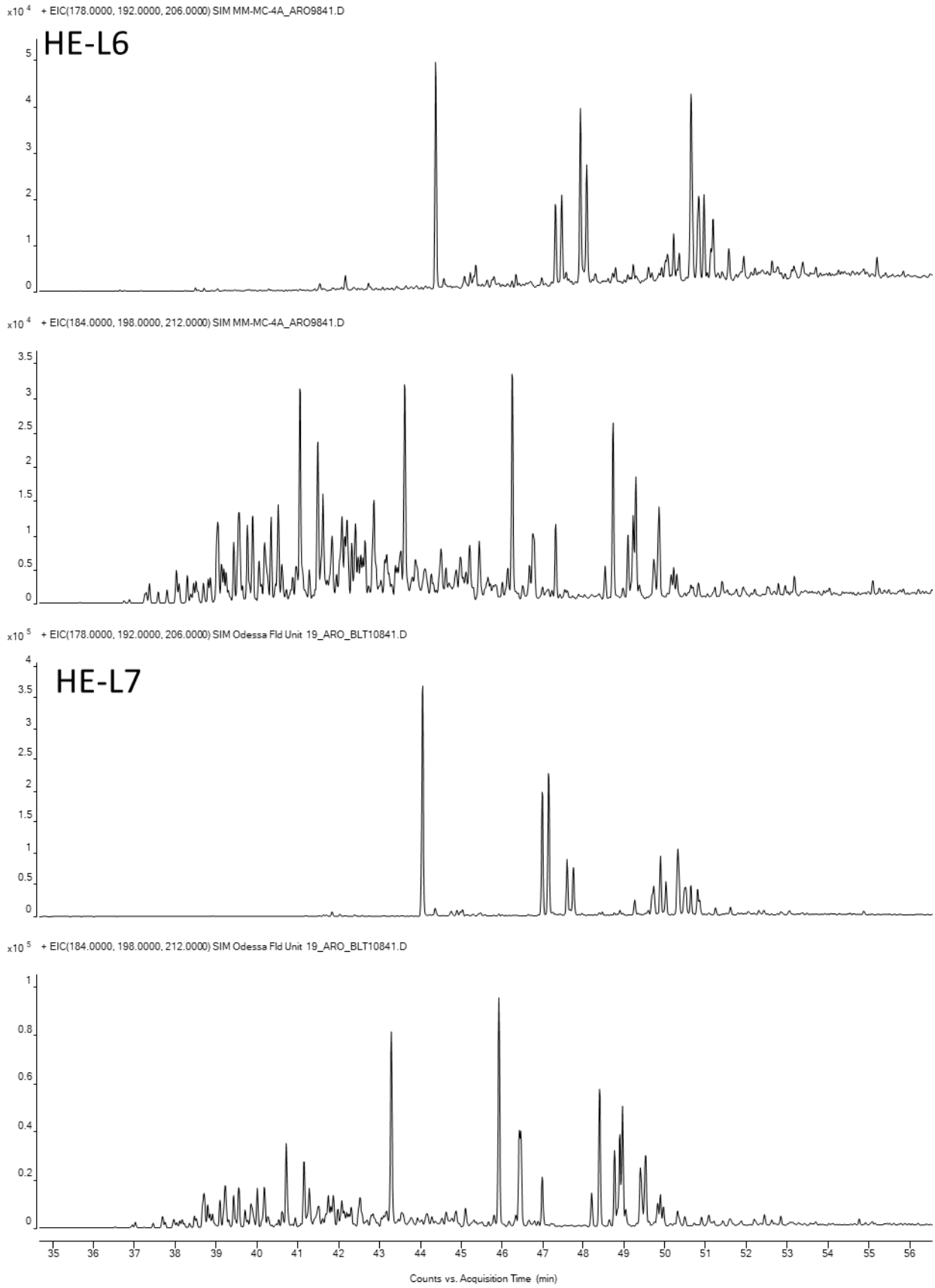
x10 4 + EIC(178.0000, 192.0000, 206.0000) SIM MM-MC-4A_ARO9841.D
HE-L6
x10 4 + EIC(184.0000, 198.0000, 212.0000) SIM MM-MC-4A_ARO9841.D
x10 5 + EIC(178.0000, 192.0000, 206.0000) SIM Odessa Fld Unit 19_ARO_BLT10841.D
HE-L7
x10 5 + EIC(184.0000, 198.0000, 212.0000) SIM Odessa Fld Unit 19_ARO_BLT10841.D
Counts vs. Acquisition Time (min)

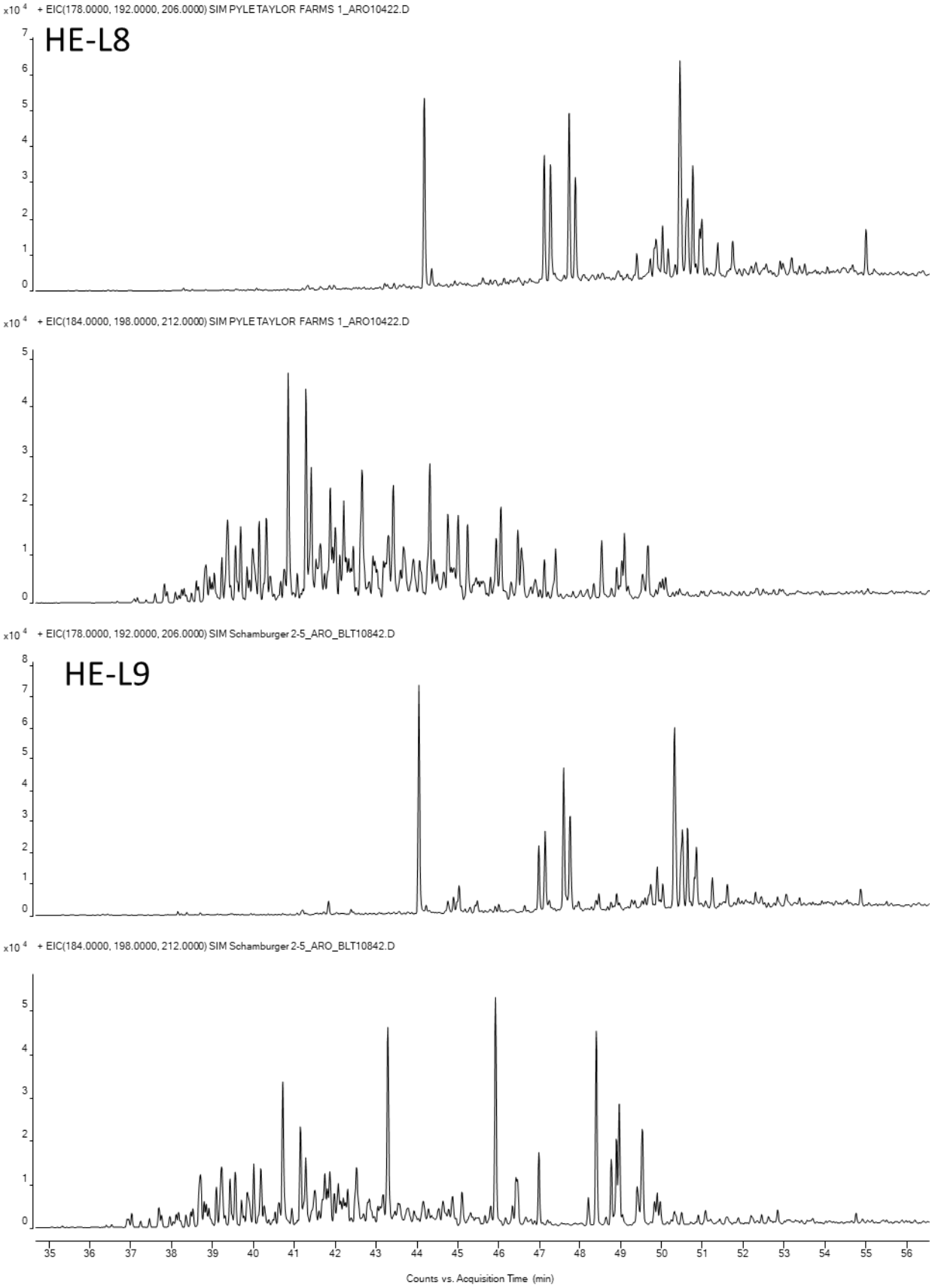
x10 4 + EIC(178.0000, 192.0000, 206.0000) SIM PYLE TAYLOR FARMS 1_ARO10422.D
HE-L8
x10 4 + EIC(184.0000, 198.0000, 212.0000) SIM PYLE TAYLOR FARMS 1_ARO10422.D
x10 4 + EIC(178.0000, 192.0000, 206.0000) SIM Schamburger 2-5_ARO_BLT10842.D
HE-L9
x10 4 + EIC(184.0000, 198.0000, 212.0000) SIM Schamburger 2-5_ARO_BLT10842.D
Counts vs. Acquisition Time (min)

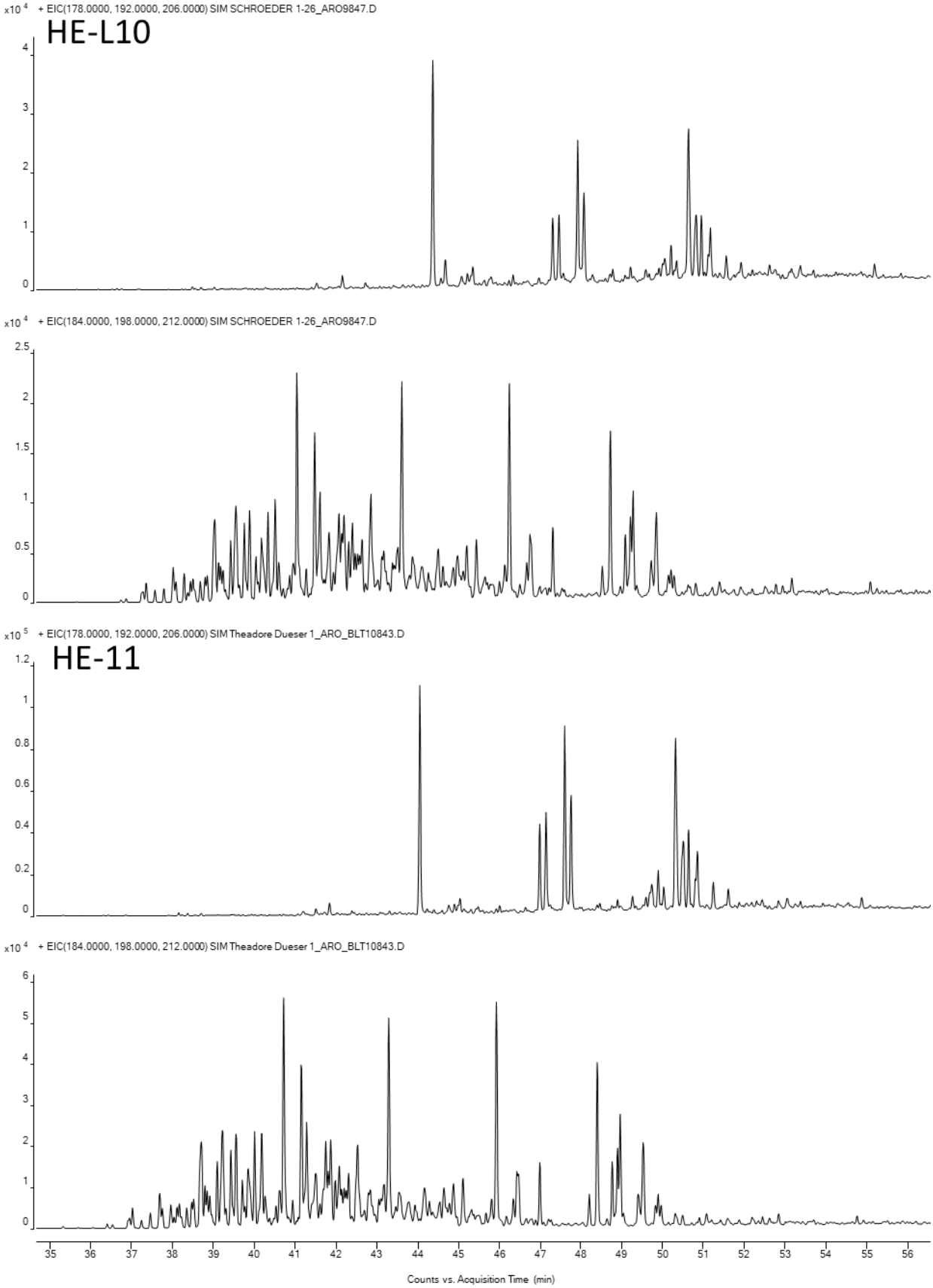
x10 4 + EIC(178.0000, 192.0000, 206.0000) SIM SCHROEDER 1-26_ARO9847.D
HE-L10
x10 4 + EIC(184.0000, 198.0000, 212.0000) SIM SCHROEDER 1-26_ARO9847.D
x10 5 + EIC(178.0000, 192.0000, 206.0000) SIM Theadore Dueser 1_ARO_BLT10843.D
HE-11
x10 4 + EIC(184.0000, 198.0000, 212.0000) SIM Theadore Dueser 1_ARO_BLT10843.D
Counts vs. Acquisition Time (min)

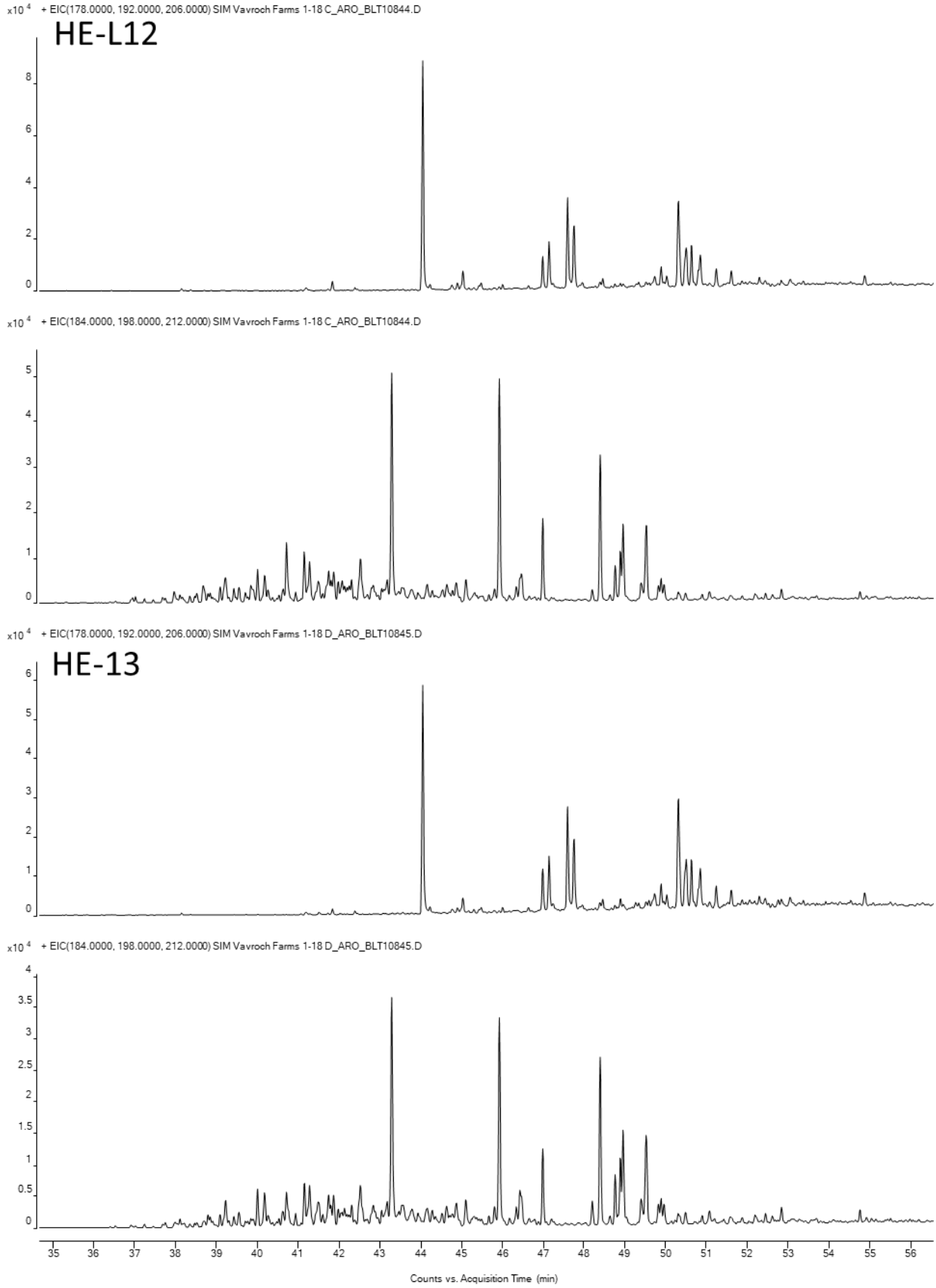
x10 4 + EIC(178.0000, 192.0000, 206.0000) SIM Vavroch Farms 1-18 C_ARO_BLT10844.D
HE-L12
x10 4 + EIC(184.0000, 198.0000, 212.0000) SIM Vavroch Farms 1-18 C_ARO_BLT10844.D
x10 4 + EIC(178.0000, 192.0000, 206.0000) SIM Vavroch Farms 1-18 D_ARO_BLT10845.D
HE-13
x10 4 + EIC(184.0000, 198.0000, 212.0000) SIM Vavroch Farms 1-18 D_ARO_BLT10845.D
Counts vs. Acquisition Time (min)

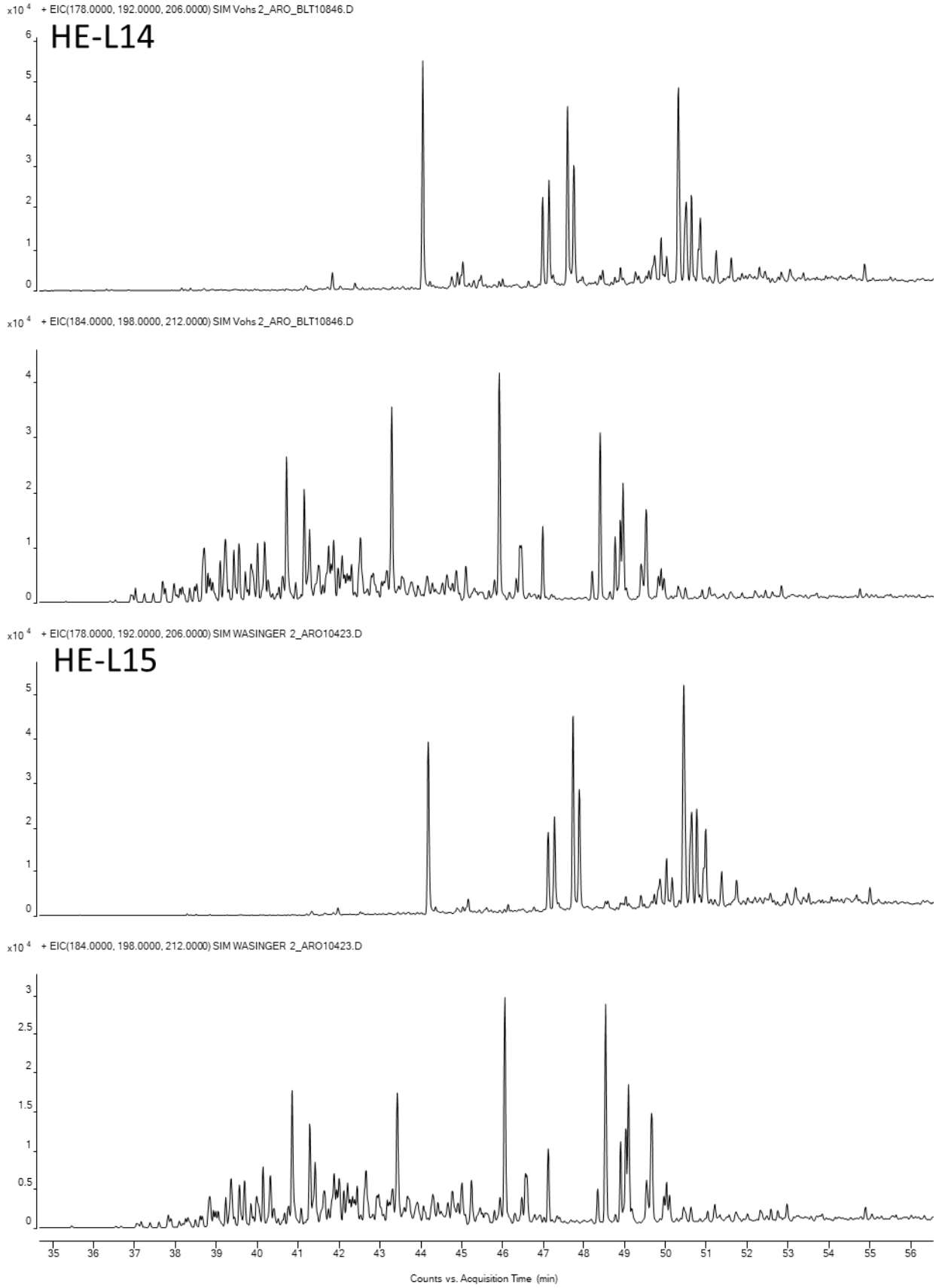
x10 4 + EIC(178.0000, 192.0000, 206.0000) SIM Vohs 2_ARO_BLT10846.D
HE-L14
x10 4 + EIC(184.0000, 198.0000, 212.0000) SIM Vohs 2_ARO_BLT10846.D
x10 4 + EIC(178.0000, 192.0000, 206.0000) SIM WASINGER 2_ARO10423.D
HE-L15
x10 4 + EIC(184.0000, 198.0000, 212.0000) SIM WASINGER 2_ARO10423.D
Counts vs. Acquisition Time (min)

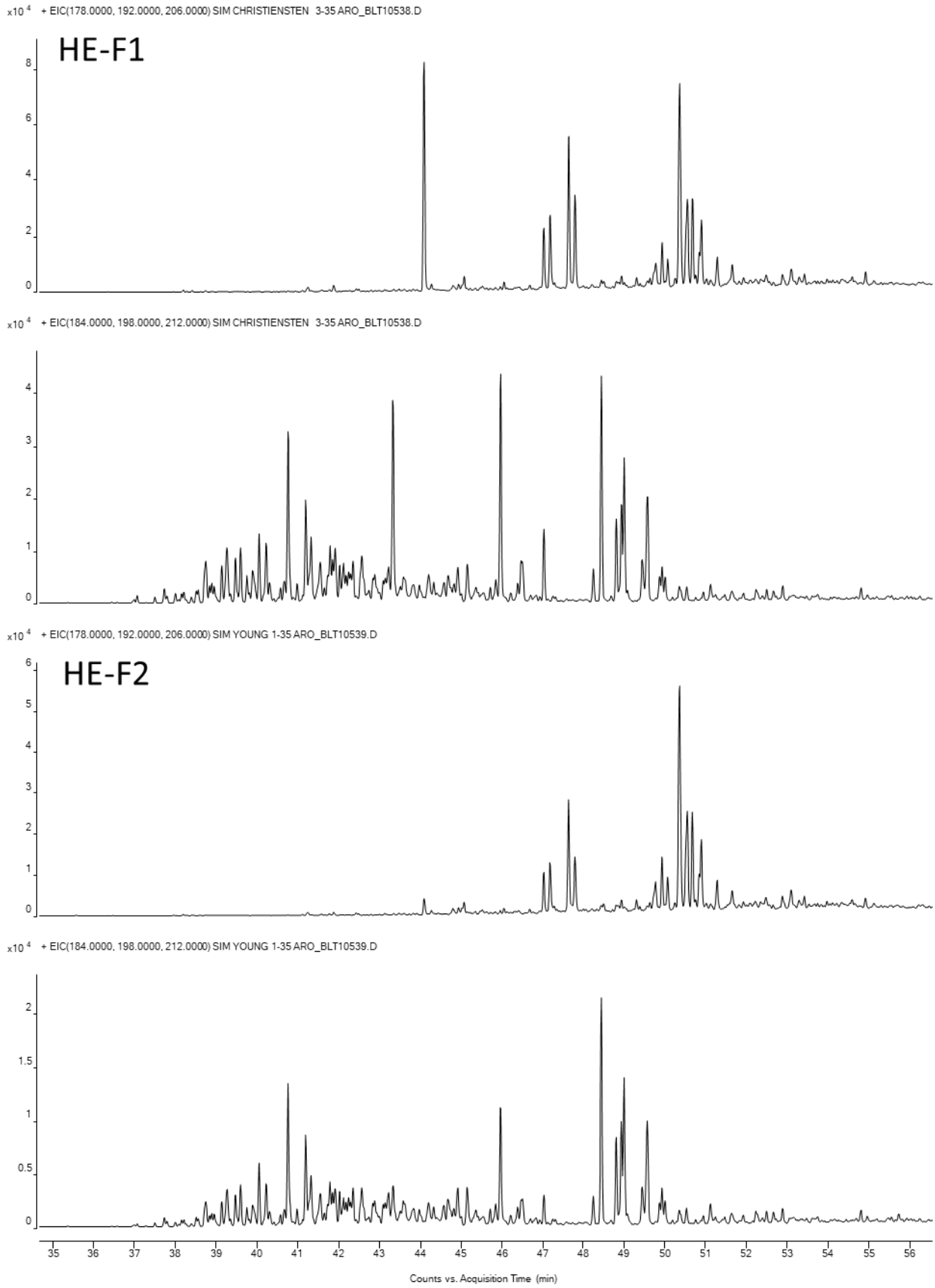
x10 4 + EIC(178.0000, 192.0000, 206.0000) SIM CHRISTIENSTEN 3-35 ARO_BLT10538.D
HE-F1
x10 4 + EIC(184.0000, 198.0000, 212.0000) SIM CHRISTIENSTEN 3-35 ARO_BLT10538.D
x10 4 + EIC(178.0000, 192.0000, 206.0000) SIM YOUNG 1-35 ARO_BLT10539.D
HE-F2
x10 4 + EIC(184.0000, 198.0000, 212.0000) SIM YOUNG 1-35 ARO_BLT10539.D
Counts vs. Acquisition Time (min)

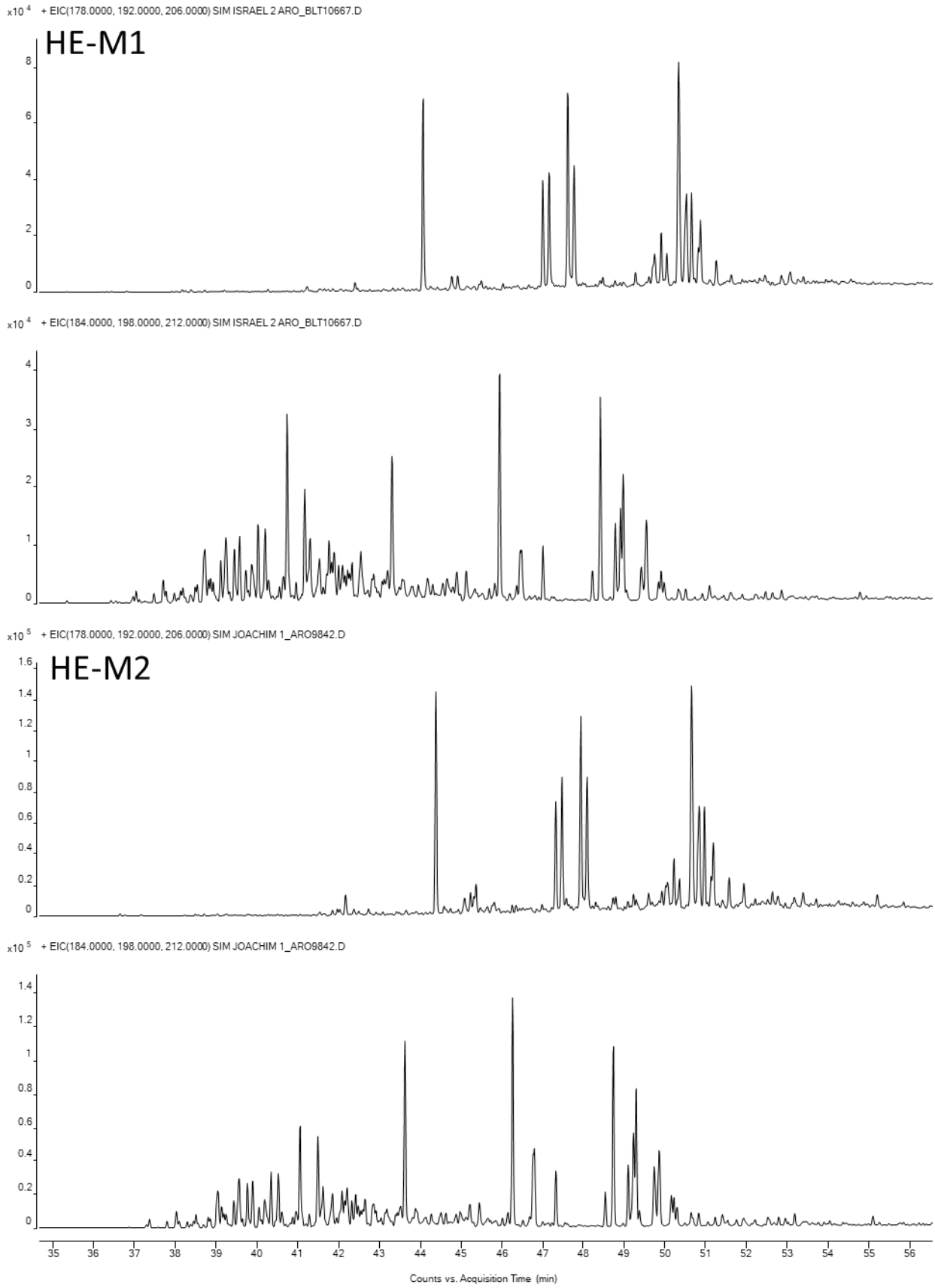
x10 4 + EIC(178.0000, 192.0000, 206.0000) SIM ISRAEL 2 ARO_BLT10667.D
HE-M1
x10 4 + EIC(184.0000, 198.0000, 212.0000) SIM ISRAEL 2 ARO_BLT10667.D
x10 5 + EIC(178.0000, 192.0000, 206.0000) SIM JOACHIM 1_ARO9842.D
HE-M2
x10 5 + EIC(184.0000, 198.0000, 212.0000) SIM JOACHIM 1_ARO9842.D
Counts vs. Acquisition Time (min)

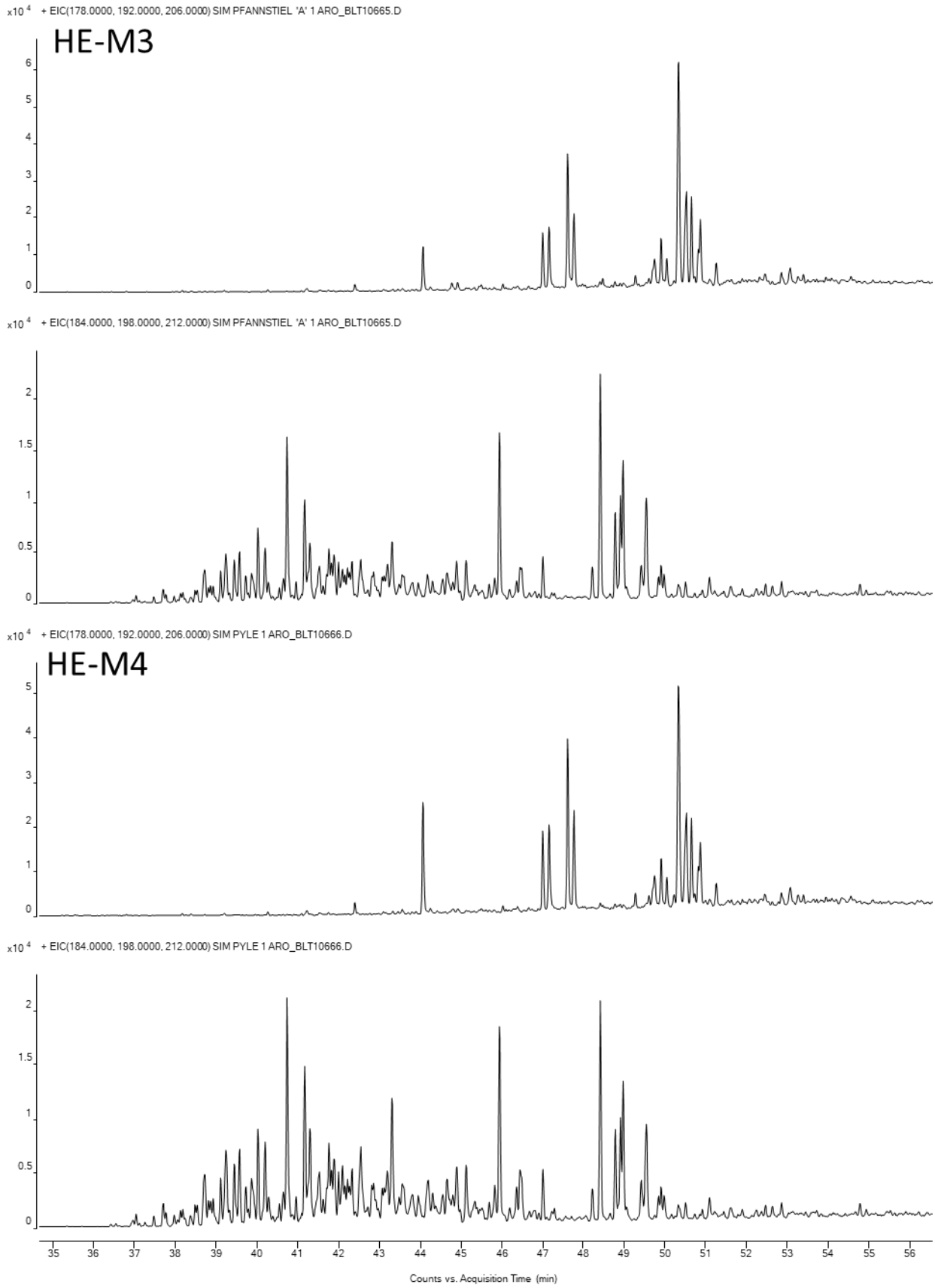
x10 4 + EIC(178.0000, 192.0000, 206.0000) SIM PFANNSTIEL 'A' 1 ARO_BLT10665.D
HE-M3
x10 4 + EIC(184.0000, 198.0000, 212.0000) SIM PFANNSTIEL 'A' 1 ARO_BLT10665.D
x10 4 + EIC(178.0000, 192.0000, 206.0000) SIM PYLE 1 ARO_BLT10666.D
HE-M4
x10 4 + EIC(184.0000, 198.0000, 212.0000) SIM PYLE 1 ARO_BLT10666.D
35 36 37 38 39 40 41 42 43 44 45 46 47 48 49 50 51 52 53 54 55 56
Counts vs. Acquisition Time (min)

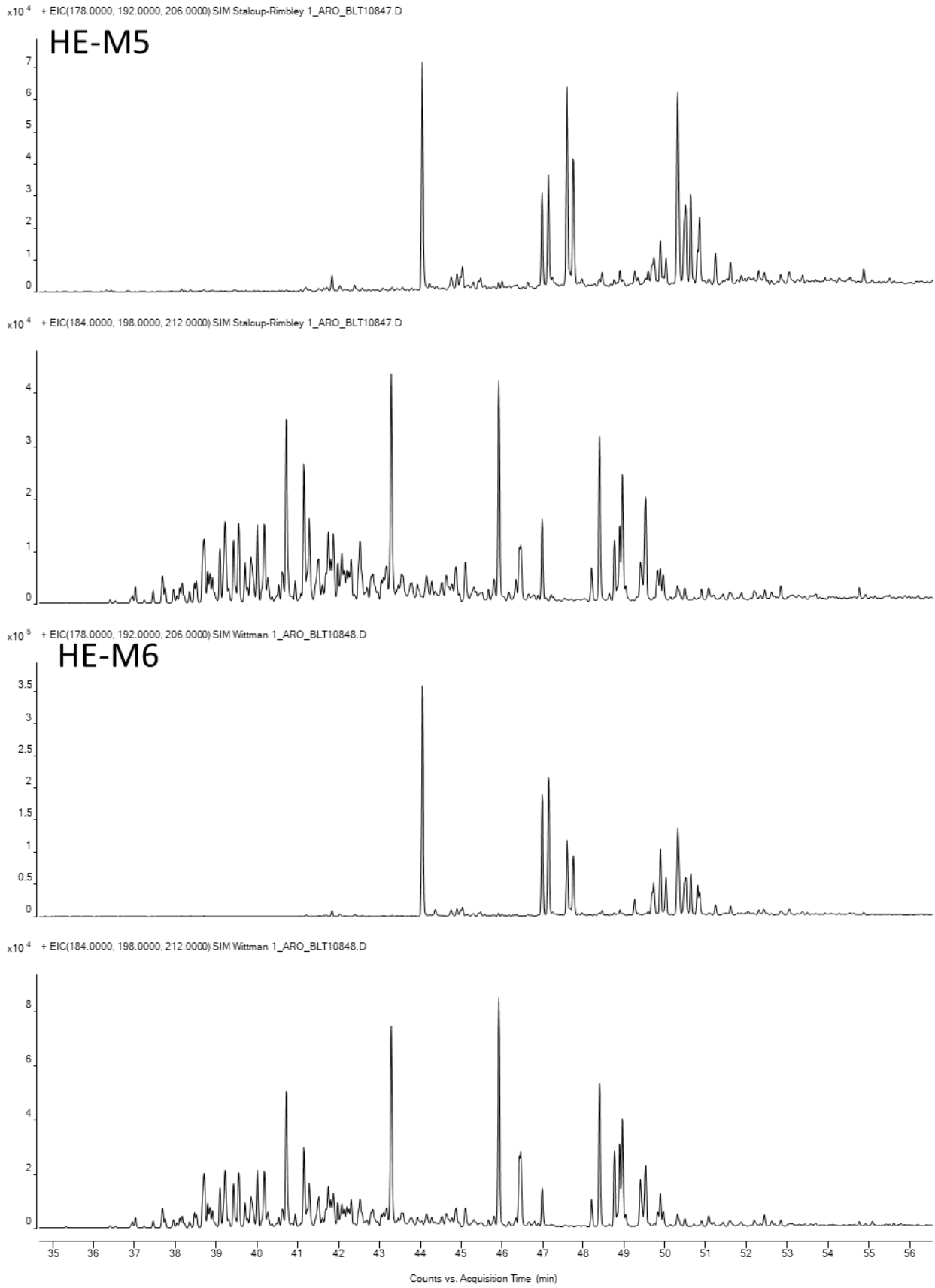
x10 4 + EIC(178.0000, 192.0000, 206.0000) SIM Stalcup-Rimbley 1_ARO_BLT10847.D
HE-M5
x10 4 + EIC(184.0000, 198.0000, 212.0000) SIM Stalcup-Rimbley 1_ARO_BLT10847.D
x10 5 + EIC(178.0000, 192.0000, 206.0000) SIM Wittman 1_ARO_BLT10848.D
HE-M6
x10 4 + EIC(184.0000, 198.0000, 212.0000) SIM Wittman 1_ARO_BLT10848.D
Counts vs. Acquisition Time (min)

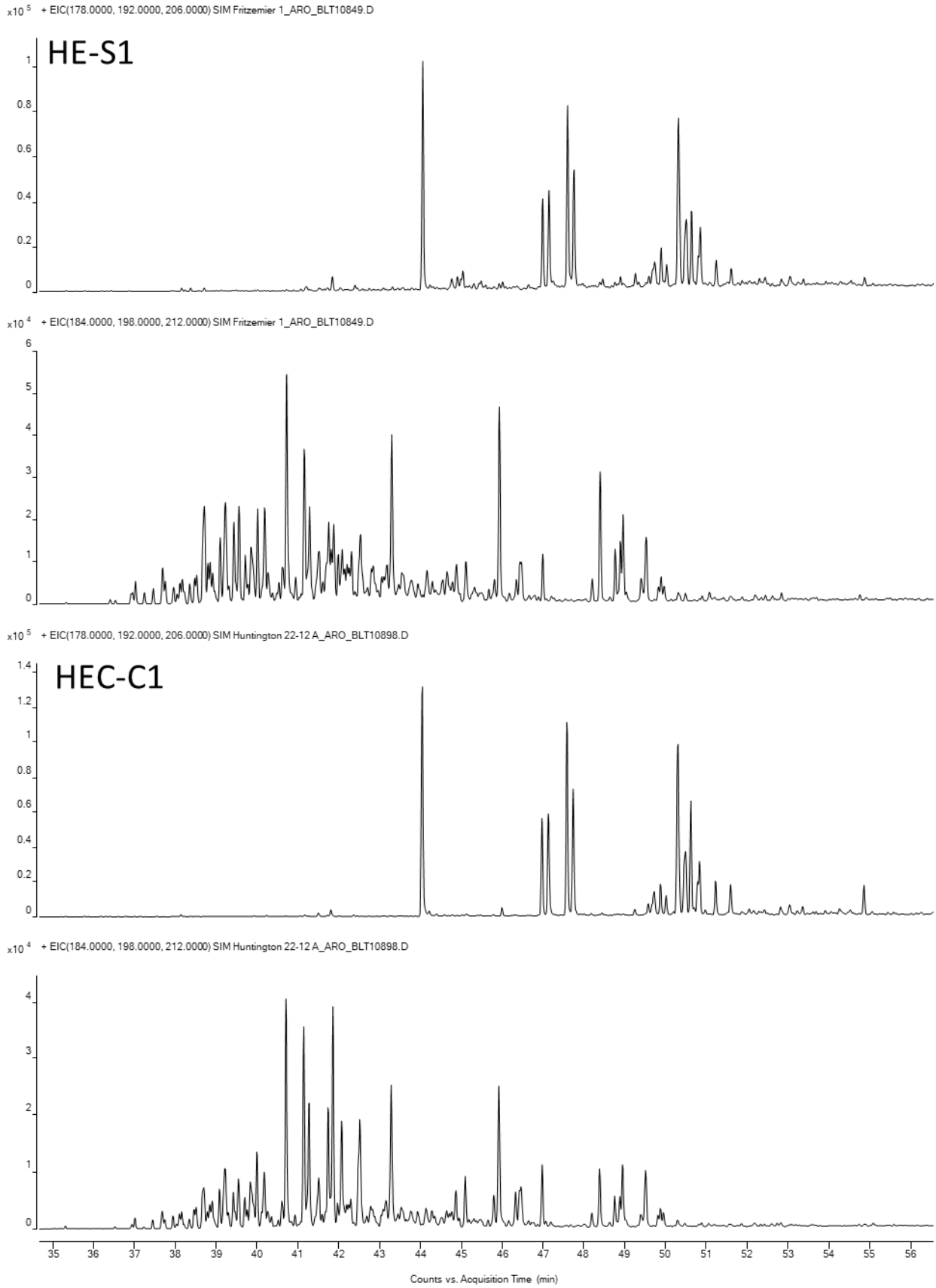
x10 5 + EIC(178.0000, 192.0000, 206.0000) SIM Fritzemier 1_ARO_BLT10849.D
HE-S1
x10 4 + EIC(184.0000, 198.0000, 212.0000) SIM Fritzemier 1_ARO_BLT10849.D
x10 5 + EIC(178.0000, 192.0000, 206.0000) SIM Huntington 22-12 A_ARO_BLT10898.D
HEC-C1
x10 4 + EIC(184.0000, 198.0000, 212.0000) SIM Huntington 22-12 A_ARO_BLT10898.D
Counts vs. Acquisition Time (min)

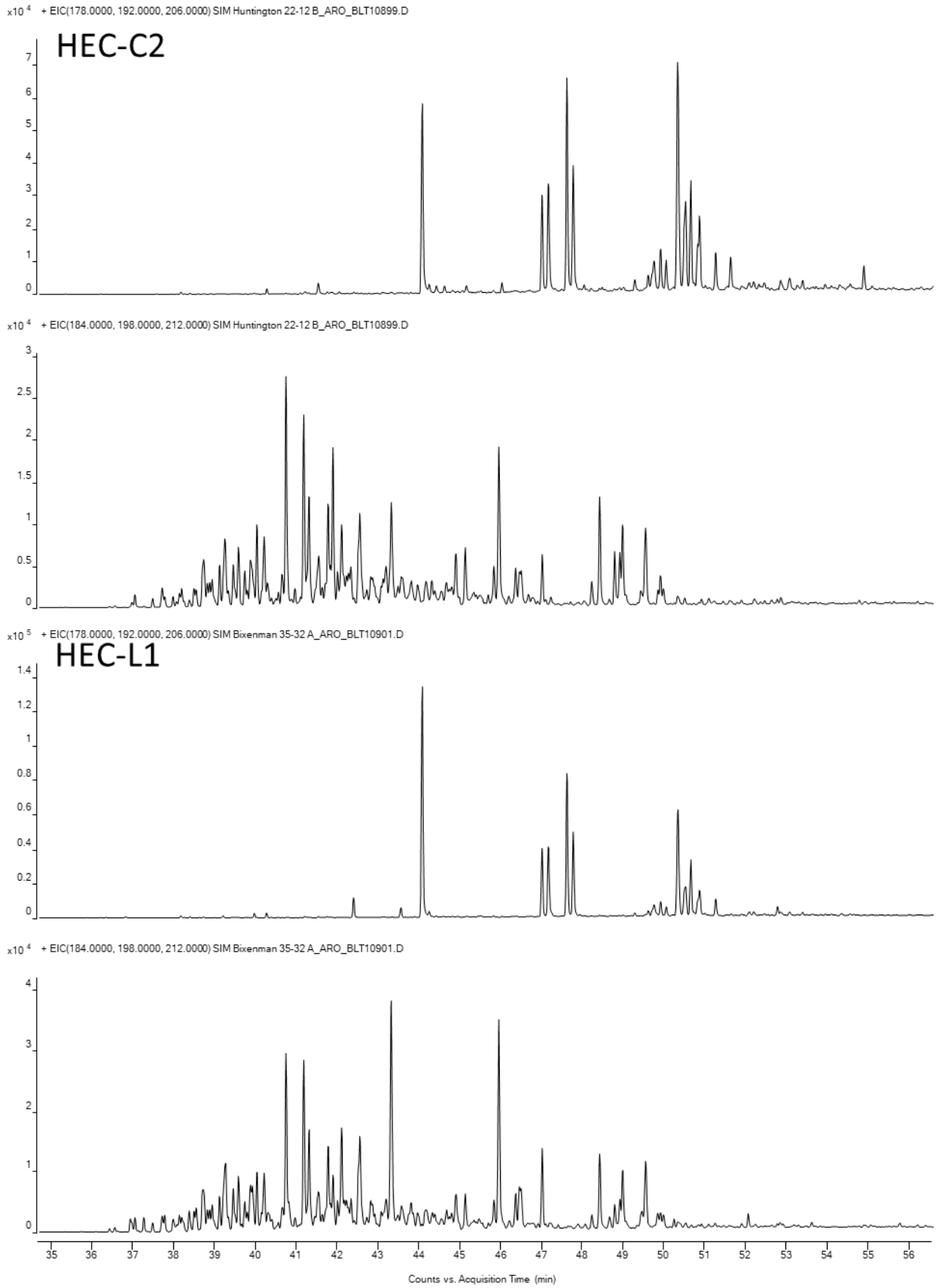
x10 4 + EIC(178.0000, 192.0000, 206.0000) SIM Huntington 22-12 B_ARO_BLT10899.D
HEC-C2
x10 4 + EIC(184.0000, 198.0000, 212.0000) SIM Huntington 22-12 B_ARO_BLT10899.D
x10 5 + EIC(178.0000, 192.0000, 206.0000) SIM Bixenman 35-32 A_ARO_BLT10901.D
HEC-L1
x10 4 + EIC(184.0000, 198.0000, 212.0000) SIM Bixenman 35-32 A_ARO_BLT10901.D
Counts vs. Acquisition Time (min)

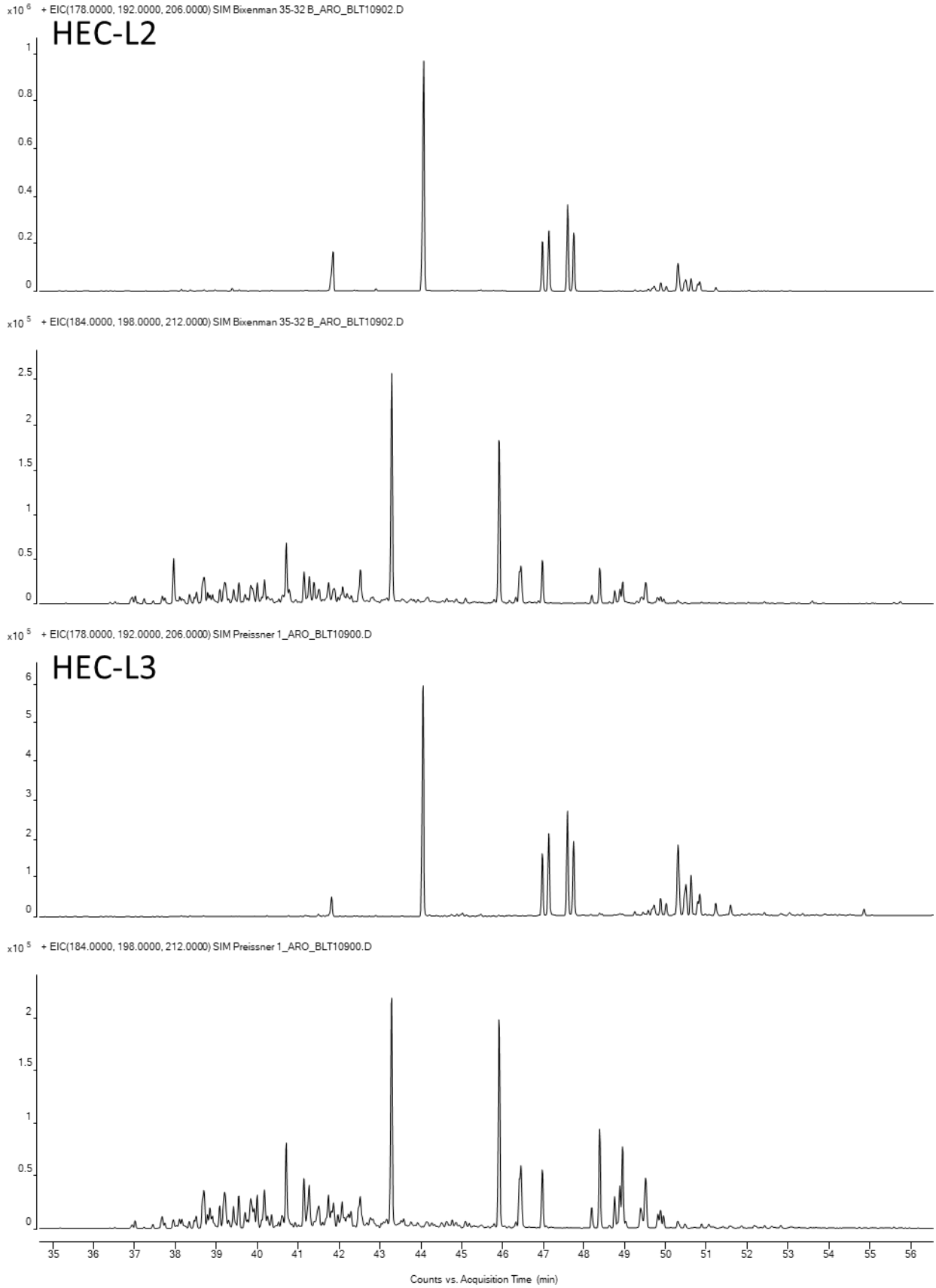
x10 6 + EIC(178.0000, 192.0000, 206.0000) SIM Bixenman 35-32 B_ARO_BLT10902.D
HEC-L2
x10 5 + EIC(184.0000, 198.0000, 212.0000) SIM Bixenman 35-32 B_ARO_BLT10902.D
x10 5 + EIC(178.0000, 192.0000, 206.0000) SIM Preissner 1_ARO_BLT10900.D
HEC-L3
x10 5 + EIC(184.0000, 198.0000, 212.0000) SIM Preissner 1_ARO_BLT10900.D
Counts vs. Acquisition Time (min)

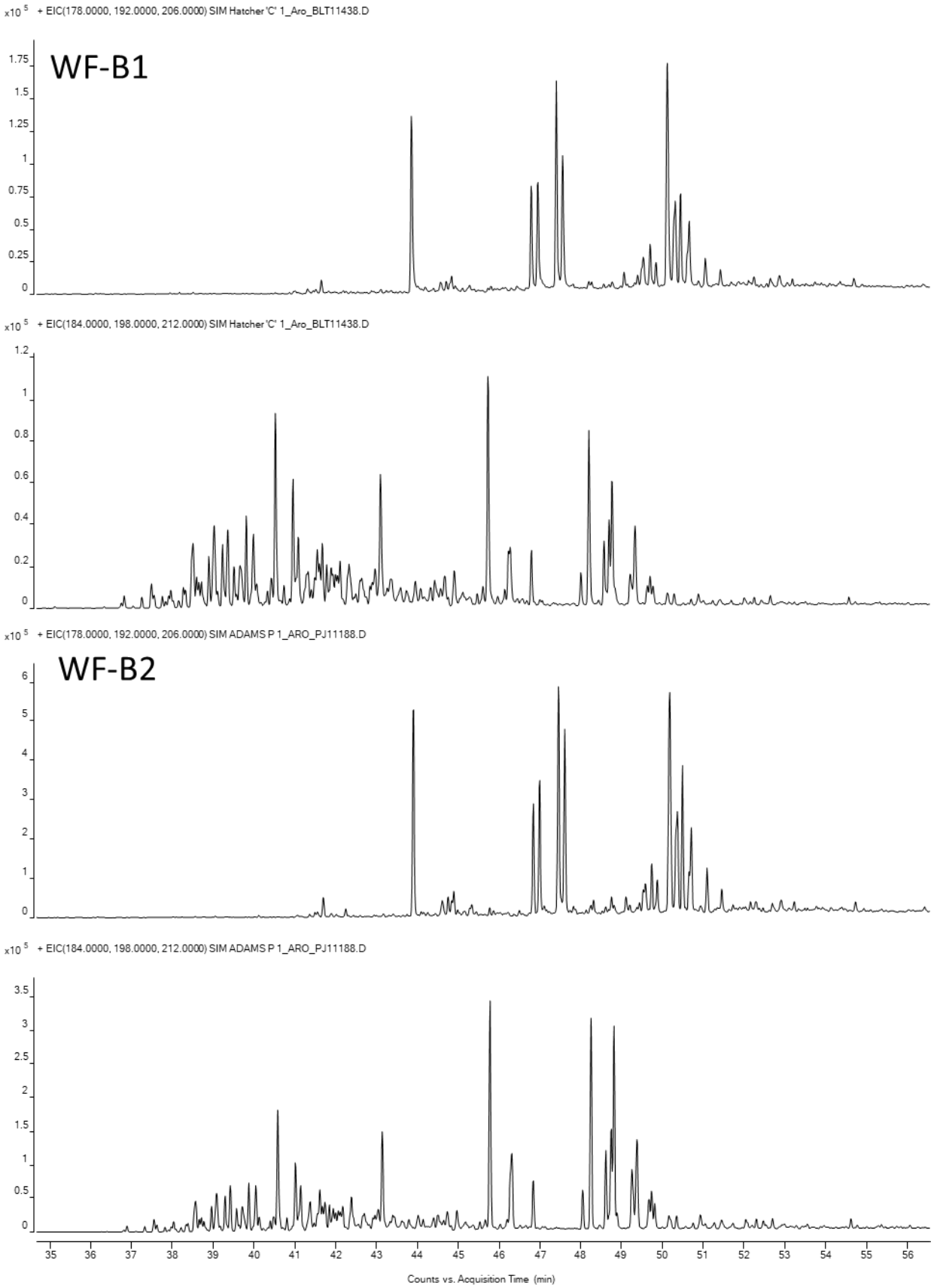
x10 5 + EIC(178.0000, 192.0000, 206.0000) SIM Hatcher 'C' 1_Aro_BLT11438.D
WF-B1
x10 5 + EIC(184.0000, 198.0000, 212.0000) SIM Hatcher 'C' 1_Aro_BLT11438.D
x10 5 + EIC(178.0000, 192.0000, 206.0000) SIM ADAMS P 1_ARO_PJ11188.D
WF-B2
x10 5 + EIC(184.0000, 198.0000, 212.0000) SIM ADAMS P 1_ARO_PJ11188.D
Counts vs. Acquisition Time (min)

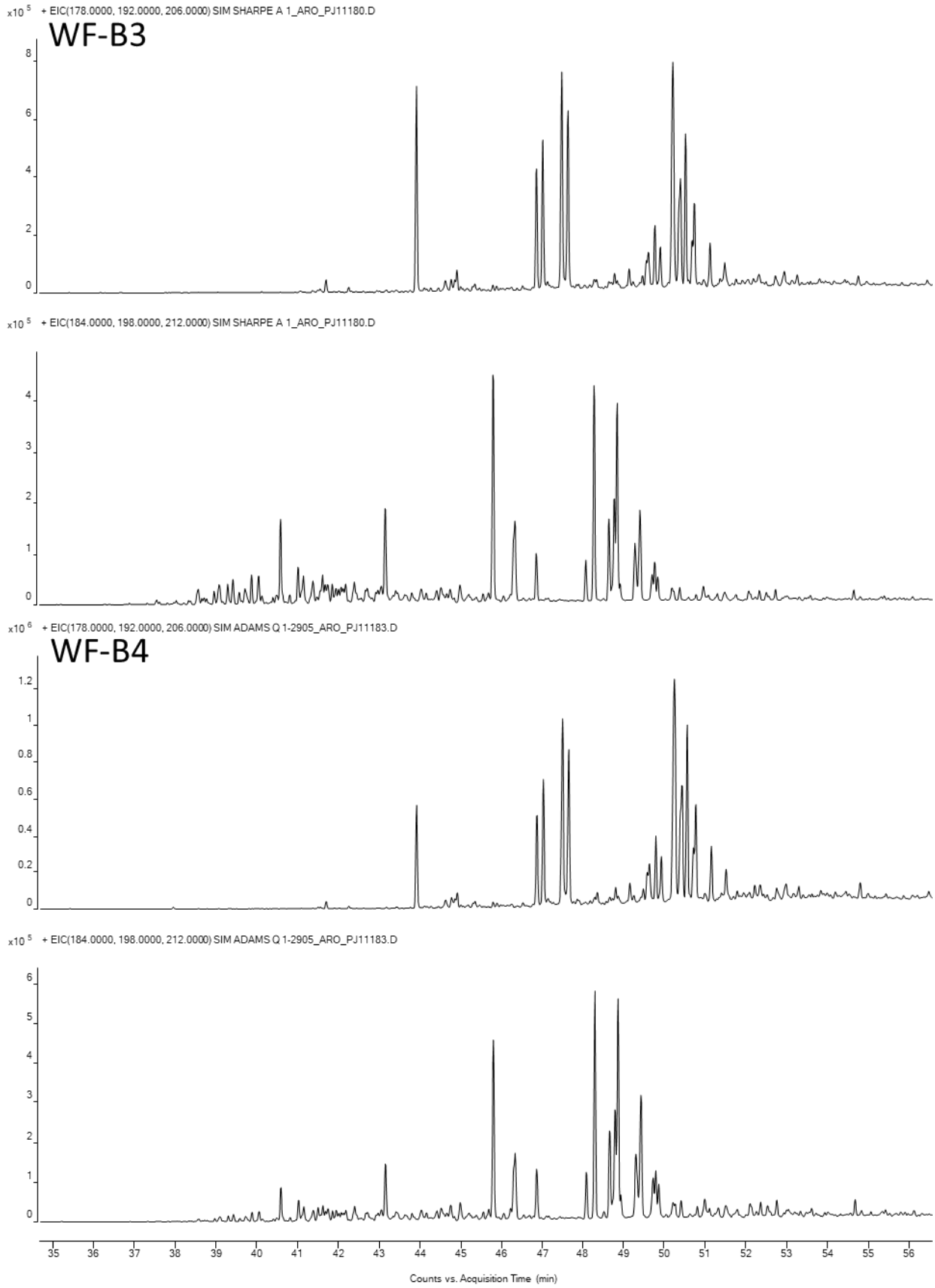
x10 5 + EIC(178.0000, 192.0000, 206.0000) SIM SHARPE A 1_ARO_PJ11180.D
WF-B3
x10 5 + EIC(184.0000, 198.0000, 212.0000) SIM SHARPE A 1_ARO_PJ11180.D
x10 6 + EIC(178.0000, 192.0000, 206.0000) SIM ADAMS Q 1-2905_ARO_PJ11183.D
WF-B4
x10 5 + EIC(184.0000, 198.0000, 212.0000) SIM ADAMS Q 1-2905_ARO_PJ11183.D
Counts vs. Acquisition Time (min)

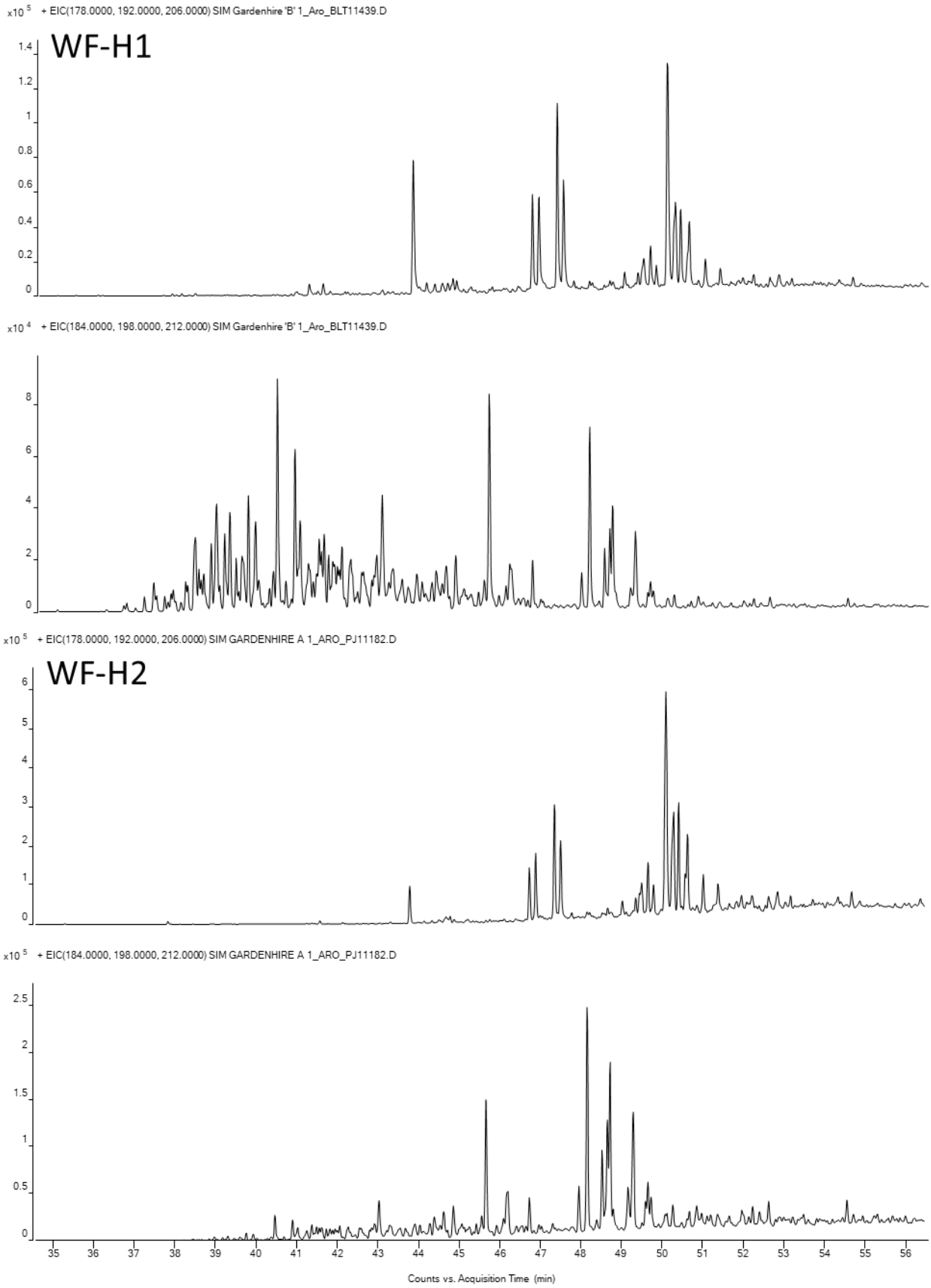
x10 5 + EIC(178.0000, 192.0000, 206.0000) SIM Gardenhire 'B' 1_Aro_BLT11439.D
WF-H1
x10 4 + EIC(184.0000, 198.0000, 212.0000) SIM Gardenhire 'B' 1_Aro_BLT11439.D
x10 5 + EIC(178.0000, 192.0000, 206.0000) SIM GARDENHIRE A 1_ARO_PJ11182.D
WF-H2
x10 5 + EIC(184.0000, 198.0000, 212.0000) SIM GARDENHIRE A 1_ARO_PJ11182.D
Counts vs. Acquisition Time (min)

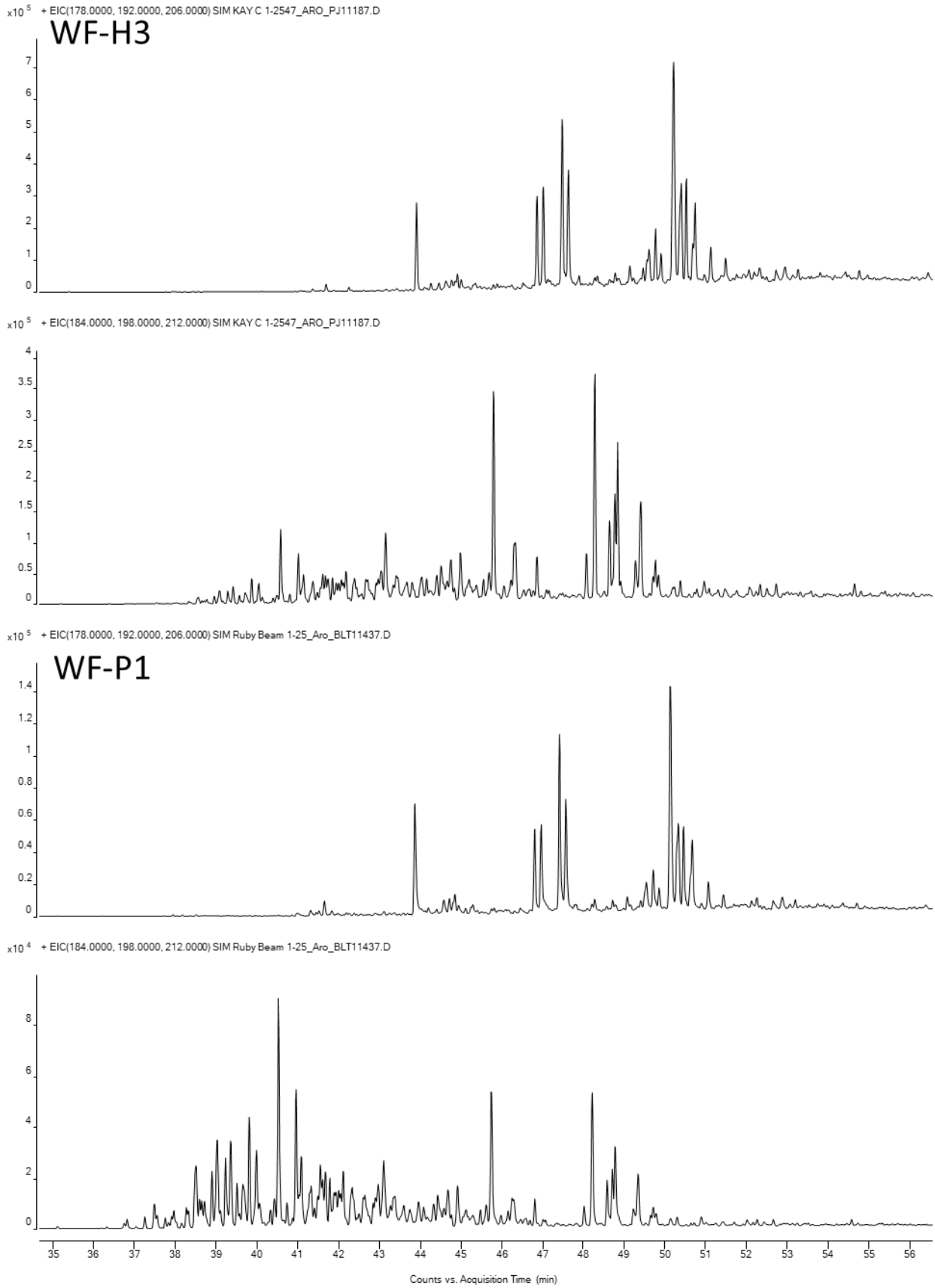
x10 5 + EIC(178.0000, 192.0000, 206.0000) SIM KAY C 1-2547_ARO_PJ11187.D
WF-H3
x10 5 + EIC(184.0000, 198.0000, 212.0000) SIM KAY C 1-2547_ARO_PJ11187.D
x10 5 + EIC(178.0000, 192.0000, 206.0000) SIM Ruby Beam 1-25_Aro_BLT11437.D
WF-P1
x10 4 + EIC(184.0000, 198.0000, 212.0000) SIM Ruby Beam 1-25_Aro_BLT11437.D
Counts vs. Acquisition Time (min)

F. Low Polarity Compound GCMS Chromatograms

Chromatogram of carbazoles (m/z 167+217)

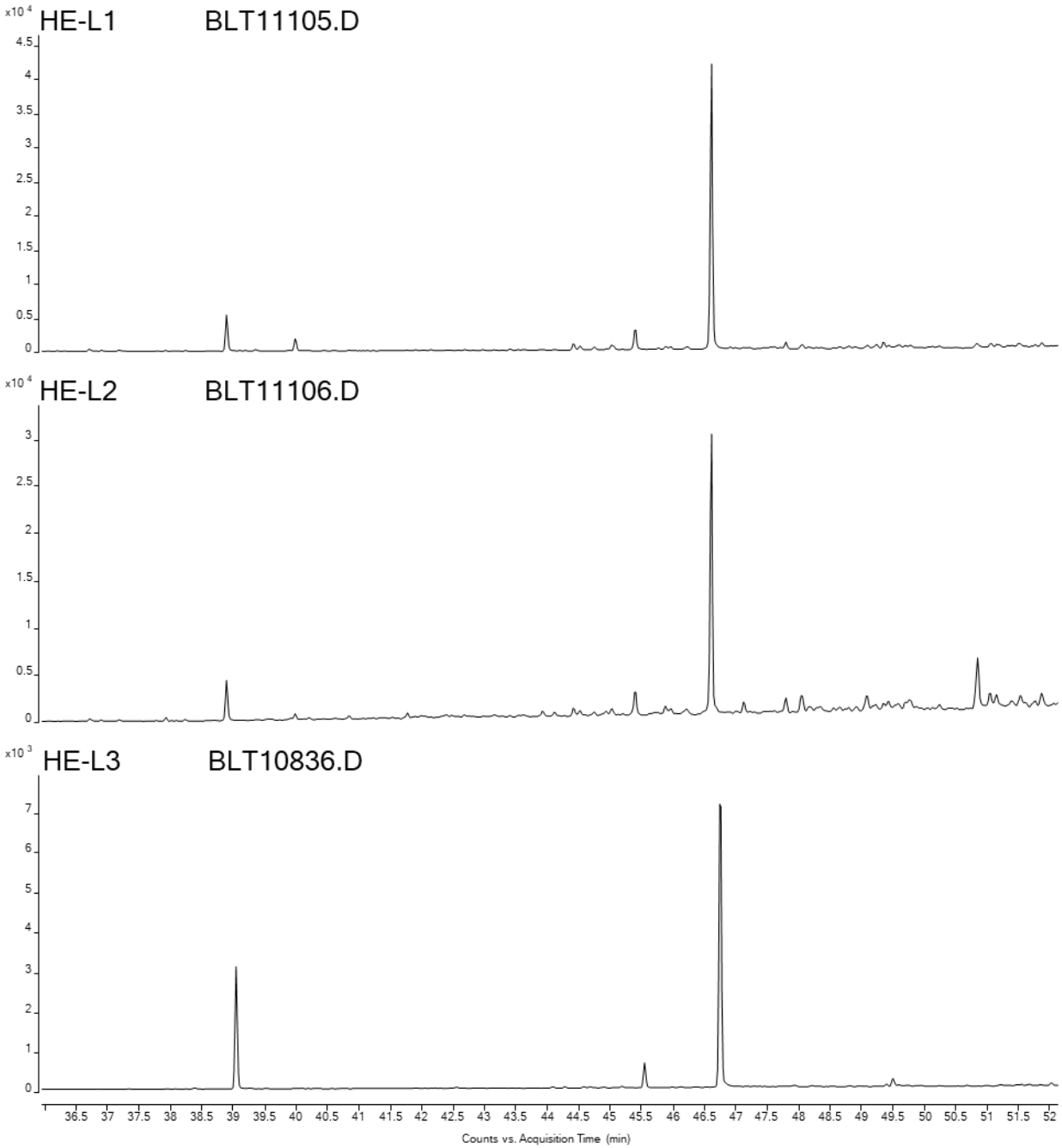

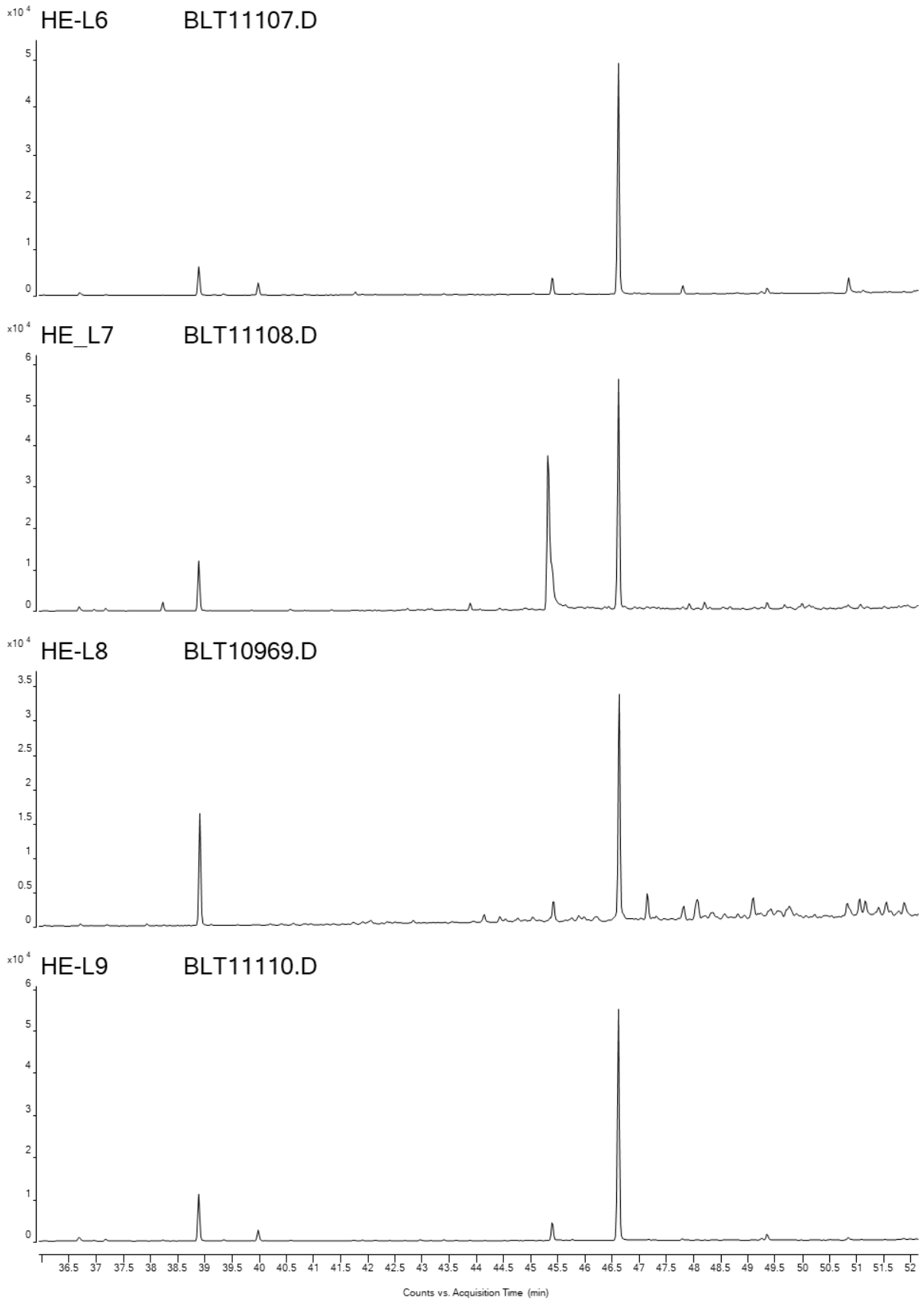
x10 4
HE-L6
BLT11107.D
x10 4
HE_L7
BLT11108.D
x10 4
HE-L8
BLT10969.D
x10 4
HE-L9
BLT11110.D
36.5 37 37.5 38 38.5 39 39.5 40 40.5 41 41.5 42 42.5 43 43.5 44 44.5 45 45.5 46 46.5 47 47.5 48 48.5 49 49.5 50 50.5 51 51.5 52
Counts vs. Acquisition Time (min)

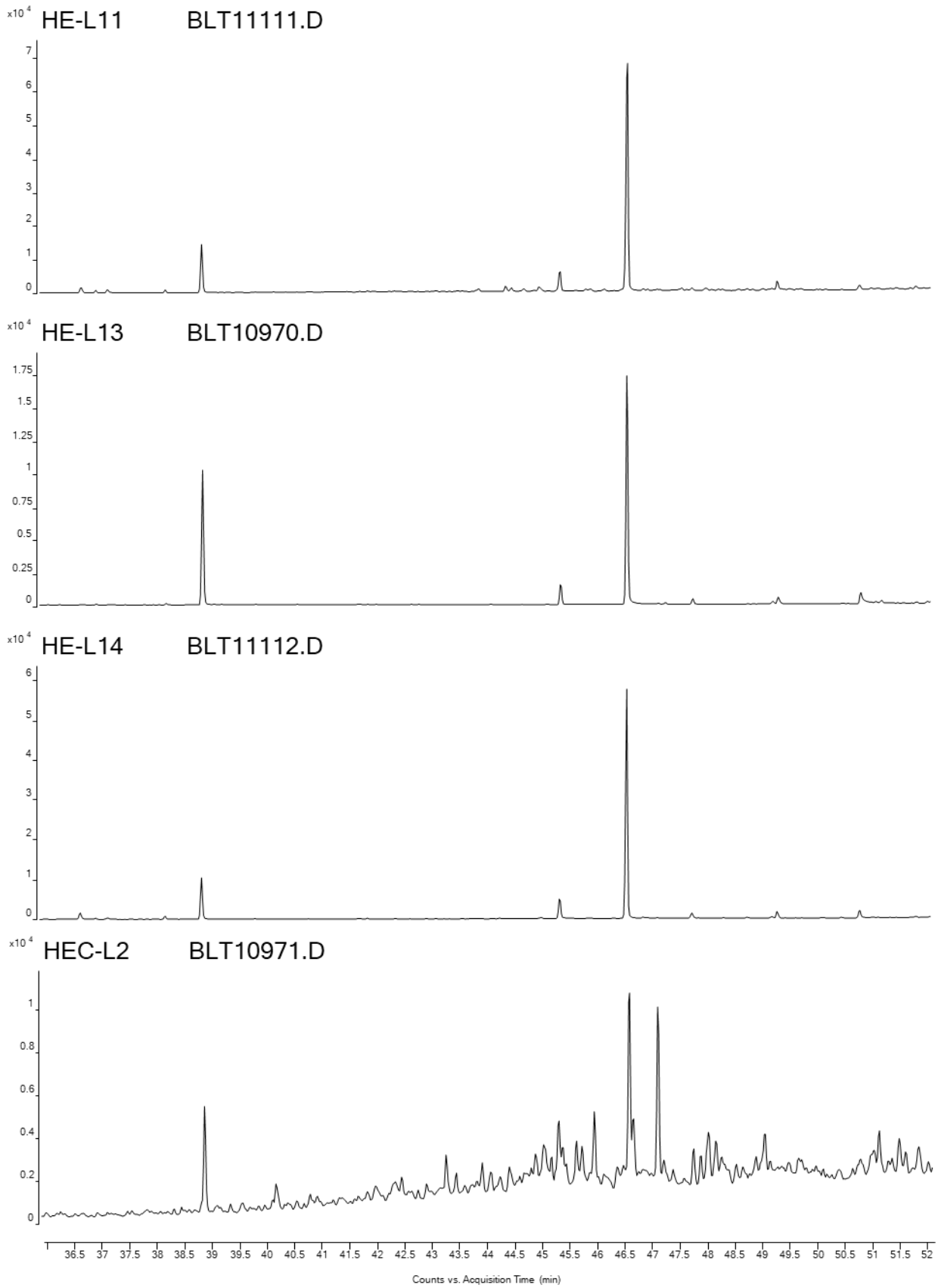
x10 4
HE-L11
BLT11111.D
x10 4
HE-L13
BLT10970.D
x10 4
HE-L14
BLT11112.D
x10 4
HEC-L2
BLT10971.D
Counts vs. Acquisition Time (min)

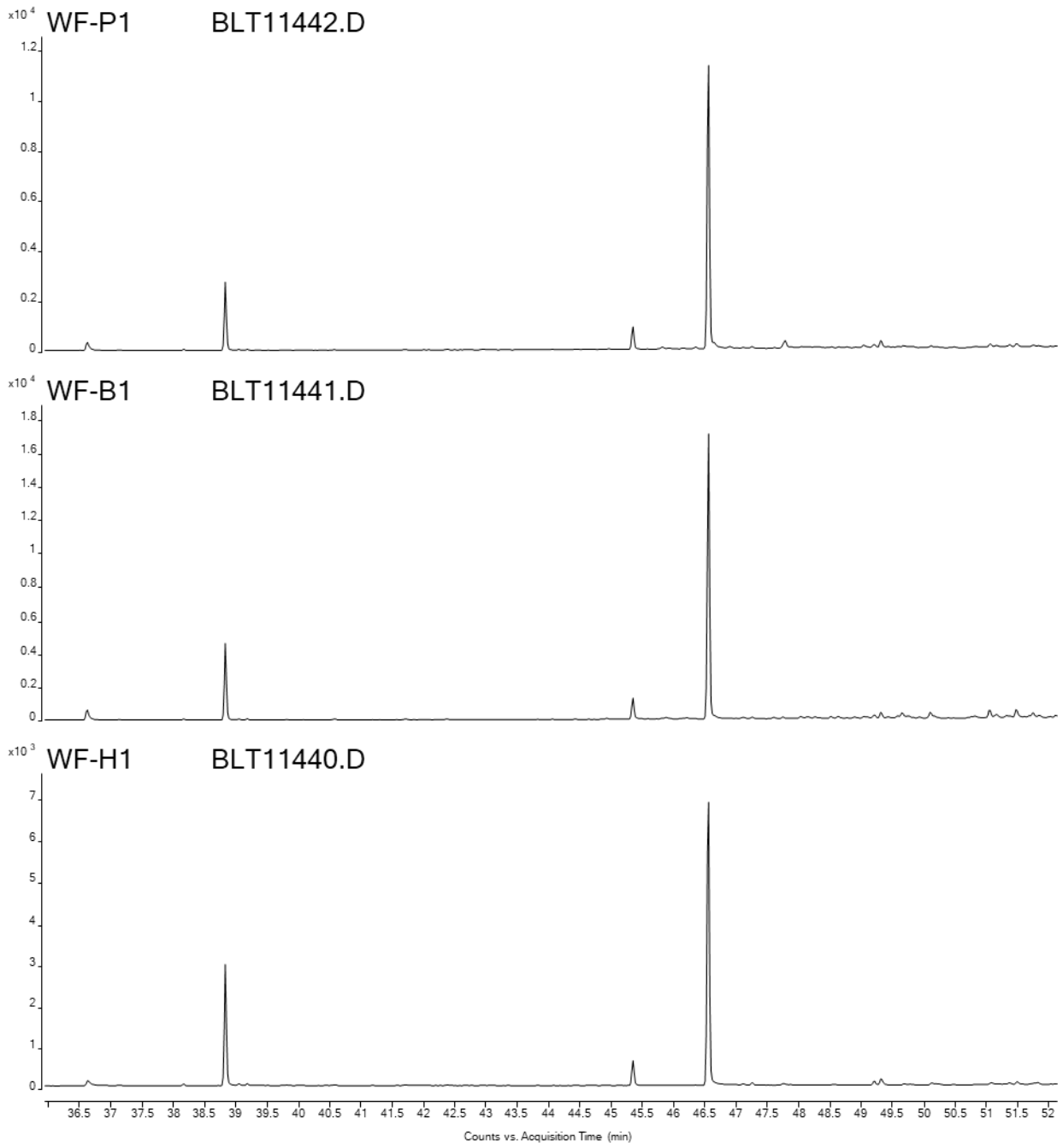
x10 4
WF-P1
BLT11442.D
x10 4
WF-B1
BLT11441.D
x10 3
WF-H1
BLT11440.D
Counts vs. Acquisition Time (min)